Università degli Studi di Bari
Dipartimento di Fisica
Dottorato di Ricerca in Fisica – XIII Ciclo

QUANTUM TIME EVOLUTION: FREE AND CONTROLLED DYNAMICS

Paolo Facchi

October, 2000

to Mimma

Preface

Unstable systems decay according to an exponential law. Such a law has been experimentally verified with very high accuracy on many quantum mechanical systems. Yet, its logical status is both subtle and delicate, because the temporal behavior of quantum systems is governed by unitary evolutions. The seminal work by Gamow [1928] on the exponential law, as well as its derivation by Weisskopf and Wigner [1930a] are based on the assumption that a pole near the real axis of the complex energy plane dominates the temporal evolution of the quantum system. This assumption leads to a spectrum of the Breit-Wigner type (Breit and Wigner [1936]) and to the Fermi Golden Rule (Fermi [1932]; Fermi [1950]). However, it is well known that a purely exponential decay law can neither be expected for very short (Mandelstam and Tamm [1945]; Fock and Krylov [1947]) nor for very long (Hellund [1953]; Namiki and Mugibayashi [1953]; Khalfin [1957]; Khalfin [1958]) times. The domain of validity of the exponential law is limited: the long-time power tails and the short-time quadratic behavior are unavoidable consequences of very general mathematical properties of the Schrödinger equation (Nakazato, Namiki and Pascazio [1996]).

This thesis is divided in two parts. In the first part we investigate in detail the quantum time evolution and frame it in a coherent theoretical scheme. Particular attention is devoted to the role of the form factor of the interaction, which is strictly related to the physical size of the system. It determines the analytical structure of the complex energy plane and the characteristic features of the temporal behavior.

It is known that the time evolution of an unstable system can be divided in three distinct regions: an initial quadratic region, characterized by its concavity τ_{Z}, an approximately exponential region and an inverse power-law tail at large times. We clarify, by investigating some solvable models and realistic decaying systems, that the duration of the initial quadratic region is in general much shorter than τ_{Z} and is indeed proportional to the physical size of the system. Moreover, we find that this region is nothing but the first of a series of damped oscillations over the dominant exponential contribution. They are caused by a peculiar interference effect between the contribution of a pole and that of a cut in the complex energy plane. These oscillations manifest themselves again at the transition between the exponential regime and the large-time inverse-power tail. We finally introduce an energy rescaling procedure, strictly related to the "$\lambda^2 t$" rescaling invented by Van Hove [1955], that enables one to understand in great detail how the characteristic time scales of the decay behave as a function of the coupling constant, in the small coupling limit.

All these results (endeavor to) give an answer to the following question: why is the exponential law valid with very good experimental accuracy for most unstable atoms and nuclei and why do its theoretically predicted deviations seem to escape the experimental investigation? Moreover, they give suggestions about the experimental conditions that are necessary to observe them. We stress that the only direct experimental evidence of the nonexponential behavior of a decaying system at short times is rather recent (Wilkinson, Bharucha, Fischer, Madison, Morrow, Niu, Sundaram and Raizen [1997]) and that the inverse-power law tails have

never been observed (Norman, Gazes, Crane and Bennett [1988]; Cho, Kasari and Yamaguchi [1993]).

One of the most puzzling features of quantum mechanics is the role of the observer, who can strongly influence the evolution of the system under investigation. This effect is perhaps nowhere more dramatic than in the phenomenon called "quantum Zeno paradox" (Misra and Sudarshan [1977]) leading to seemingly paradoxical consequences. The paradox states that a system that is continuously observed, in order to ascertain if it is decayed, does not decay at all. In other words, a watched pot never boils. Nowadays the name "quantum Zeno effect" seems more appropriate: repeated observations "slow down" the evolution. This effect is strictly related to the short-time deviations from the exponential law, in particular to the initial vanishing decay rate. Therefore, observation of the former is an indirect evidence of the initial quadratic behavior.

In the second part of this thesis we study the possibility of controlling the evolution by "observing" the quantum system. We will find that in the case of decaying systems, as opposed to oscillating ones, new physical phenomena occur (quantum "Heraclitus" effect): if the system is observed frequently, but not too frequently, the decay is enhanced, rather then hindered. Of course, by increasing the frequency of observations, a quantum Zeno effect is eventually obtained. This richer behavior is ultimately due to the above-mentioned onset of a time scale different from τ_Z in systems with a finite extension, i.e. a finite form factor.

Our general philosophy is that there is nothing "magic" in all these phenomena: they are simply the consequence of a dynamical evolution, that can be explained in terms of the Schrödinger equation, without making use of the "collapse postulate," as implied by the projection operators. The evolution is modified as a consequence of the new dynamical features introduced by the coupling with an external agent that (through its interaction) "looks" closely at the system. Only when this interaction can be effectively described in terms of an effective projection operator we recover the original formulation of quantum Zeno. This idea will constitute the "backbone" of the whole work. When this concept is fully elaborated, one can realize that a broader definition of Zeno effect is required, that takes into account the very concept of continuous measurement, performed for example by a quantum field or by the environment. The novel theoretical scheme we introduce enables one to look at the quantum time evolution from a different perspective and comprises, in a more general framework, all the examples of Zeno effects considered in the literature.

Contents

Chapter 1

Introduction and summary

We start off with a bird's eye view of the subjects analyzed in this thesis. This work is divided in two parts. In the first part (chapters 2-6) we investigate the characteristic features of the temporal behavior of quantum mechanical oscillating and unstable systems. In the second part (chapters 7-12) we study the possibility of controlling the dynamics of the system by coupling it with an external agent. The *leitmotif* of the whole work is the role of the form factor of the interaction and the consequent analytical properties of the propagator in the complex energy plane.

In chapter 2 we consider some theorems that yield bounds on the temporal behavior at short and long times, implying deviations from the exponential decay law. We will see that for a generic quantum system the dynamics cannot be purely Markovian, yielding an exponential decay, due to a quantal regeneration effect that gives rise to a survived component of the state at a given time from the decay components at earlier times. At short times the condition of finite energy dispersion, i.e., a spectral density which vanishes sufficiently fast at large energies, implies a vanishing decay rate at $t = 0$. The regeneration effect strongly manifests itself for a spatially confined system. Such a system, having a discrete energy spectrum, never fully decays and indeed keeps rebounding from the walls, repopulating almost completely the initial state at finite time intervals (quantum Poincaré recurrence). Therefore a truly unstable system, i.e. a system that definitely moves away from the initial state, necessarily must be endowed with a continuous spectrum. But, in this case too, the physical requirement of the existence of a finite ground state energy implies that the decay cannot be exponential at large times, this being another manifestation of the regeneration phenomenon.

In chapter 3 we construct some simple models that exhibit the characteristic features outlined in the previous chapter. We first summarize the oscillatory properties of a two-level system and then generalize to a many-level system with a constant energy level density and a constant coupling. In this case the energy uncertainty is infinite and indeed the decay is purely exponential up to a time inversely proportional to the level spacing. On the other hand, the spectrum is discrete and the recurrence phenomenon occurs at later times. By considering the continuum limit version of this model we get a discrete state coupled to a flat-band continuum, yielding a purely exponential behavior at all times. The two-level model and the flat-band model will serve as references throughout the whole work. They represent two extreme cases, yielding simple oscillations and exponential decay, respectively.

In chapter 4 we introduce some nonperturbative techniques that enable us to study in great detail the temporal behavior of a generic quantum system. We will see that the temporal evolution of the survival amplitude is strictly related to the analytical properties of its Fourier-Laplace transform, the resolvent, in the complex energy plane. In particular, we will see that

a truly unstable system has a propagator which is analytic in the complex energy plane except for a cut along the real axis, which corresponds to the continuous spectrum of the Hamiltonian. Therefore it can be expressed by a dispersion relation in terms of the discontinuity across the cut. By using Dyson's resummation it is possible to write the propagator in terms of the self-energy function, whose analytical properties are strictly related to those of the propagator. The exponential decay, as anticipated above, is due to the presence of a simple pole close to the cut in the second Riemann sheet. All corrections are ascribable to the cut and/or other (distant) poles contributions. We will see that at short times the latter sum up with the exponential yielding a quadratic behavior, while at large times, when the pole contribution has become exponentially small, the cut becomes dominant and yields an inverse power law tail. In addition, there is an interference term between the pole and the cut contributions, yielding damped oscillations over the exponential decay. From this perspective, the initial quadratic region is nothing but the first of this series of oscillations.

An important result introduced in chapter 4 is the off-diagonal decomposition of the total Hamiltonian in terms of the initial state. It reduces the self-energy function to a second-order contribution and enables one to write the Hamiltonian in the Lee form, as explained in chapter 5. Using this formulation, the role of the form factor of the interaction becomes fundamental. As already emphasized, a flat form factor gives rise to a purely exponential decay, i.e. to a propagator with a simple pole (Weisskopf-Wigner approximation). As a further improvement we consider a propagator with two poles, which derives from a Lorentzian form factor: it yields the initial quadratic behavior together with the damped oscillations and eventually the exponential decay. On the other hand, it reduces to the oscillating two-level system (with two real poles) and to the flat-band system (with only one complex pole) for limiting values of the parameters. Moreover, one can think of the two-pole model as a "reduction" of the real system, with improved and richer characteristics than the Weisskopf-Wigner reduction. The second part of the chapter is finally devoted to the study of the temporal evolution of a real (and richer) system, such as the hydrogen atom. In the rotating wave approximation the Hamiltonian is indeed in the Lee form and the form factor can be exactly evaluated. This model displays all the general properties introduced earlier, such as a branch cut and a pole in the second Riemann sheet, and enables us to compute the temporal evolution of a realistic system with all its characteristic regions and time scales.

In chapter 6 we finally introduce a technique that enables one to evaluate, for a truly unstable system, all corrections to the exponential decay in the limit of small coupling. We will deal with a limiting procedure introduced by Van Hove [1955] in order to rigorously derive a Markovian master equation from the Schrödinger equation. In particular, we will use the analogous of Van Hove's "$\lambda^2 t$" limit in the complex energy plane and rigorously derive the Weisskopf-Wigner single-pole approximation. Moreover we evaluate all corrections to the exponential decay law for Hamiltonians which are not of the Lee type, when the coupling constant is small, but finite.

We stress that the only direct experimental evidence of the nonexponential behavior of a decaying system at short times is rather recent (Wilkinson, Bharucha, Fischer, Madison, Morrow, Niu, Sundaram and Raizen [1997]) and that the inverse power law tail has never been observed (Norman, Gazes, Crane and Bennett [1988]; Cho, Kasari and Yamaguchi [1993]). On the other hand, the temporal behavior of quantum mechanical systems can be strongly influenced by the action of an external agent. Moreover, this influence is strictly related to the deviations from the exponential law, in particular at short times. Therefore such an influence yields an indirect proof of these deviations.

The second part of this work is devoted to the possibility of modifying the undisturbed

evolution of a quantum system by coupling it to another system or apparatus. A good example is the quantum Zeno effect (Misra and Sudarshan [1977]), where the quantum mechanical evolution of a given (not necessarily unstable) state is slowed down (or even halted) by performing a series of measurements that ascertain whether the system is still in its initial state. This peculiar effect is historically associated and usually ascribed to what we could call a "pulsed" quantum mechanical observation on the system. However, it can also be obtained by performing a "continuous" observation of the quantum state, e.g. by means of an intense field (Mihokova, Pascazio and Schulman [1997]; Schulman [1998]; Facchi and Pascazio [2000a]).

In chapter 7 we introduce the quantum Zeno effect and its relation with the short-time quadratic behavior of the survival probability. We consider the effect of repeated instantaneous measurements on the initial state in the limit of infinite frequency, according to the formulation of Misra and Sudarshan: the system is forced to remain in the subspace defined by the measuring projections. We then analyze the more realistic case of a finite period between successive measurements and exhibit the possibility of increasing, rather then slowing down, the decay rate of a truly unstable system, i.e. the possibility of an "inverse" quantum Zeno effect. In particular, we prove a theorem that states the relation between the emergence of a Zeno–inverse Zeno transition and the value of the wave function renormalization. We then clarify a subtle difference (related to "repopulation" effects) from the original formulation by Misra and Sudarshan, by illustrating an application of pulsed measurements to an oscillating system. In particular we find that the quantum Zeno effect is present even when repopulation effects take place. This motivates us to formulate a more general framework for the Zeno effects. An important step in this direction is the understanding that the quantum Zeno effect does not necessarily require the use of von Neumann's projections, and it is possible to give a dynamical explanation (Pascazio and Namiki [1994]), that involves only the Schrödinger equation and a Hamiltonian yielding a generalized spectral decomposition. As a consequence, it becomes straightforward to consider the case of continuous measurement, as opposed to pulsed measurements, by coupling the system with a (quantum) apparatus via a time-independent interaction. In this case too, even if repopulation phenomena (in amplitude and/or probability) take place, a quantum Zeno and, possibly, an inverse quantum Zeno effects occur. The coupling constant in the continuous case plays the role of the frequency of measurements in the pulsed version. In fact, it is possible to prove an adiabatic theorem, which is the counterpart of Misra and Sudarshan's theorem, for a purely dynamical evolution. It states that by coupling a quantum system with an apparatus and by increasing the coupling constant, the Hilbert space of the system is split into subspaces which are eigenspaces of the interaction Hamiltonian and a superselection rule arises between different sectors. Therefore, any possible interference between different subspaces is destroyed and the system is forced to evolve within each sector, whence if it starts in one sector it cannot leave it. By using this result we can finally formulate the Zeno effects in a broader framework (Facchi and Pascazio [2001]), which includes all possible cases considered in the literature.

In chapter 8 we will study the effect of pulsed and continuous observations in a quantum optical example, the down-conversion process. This can be viewed as the decay of a pump photon into a couple of down-converted photons of lower energy, or, alternatively, when the pump is described classically, as the decay of the vacuum state, which is unstable. Interesting features of this system are its simplicity, which yields a solvable model, and its richness, for, by changing the parameters, it is possible to obtain Zeno, inverse Zeno and even an oscillatory behavior. Last, but not least, we mention its possible experimental implementation.

In chapter 9 we use again a down-conversion process in order to elucidate a subtle relation between the quantum Zeno effect and the classical stabilization induced by parametric

resonance. We will study a periodic system, implemented by alternating slices of nonlinear and linear crystals, and interpret the stabilization condition within the theoretical scheme of the quantum Zeno effect given above. On the other hand, the Heisenberg equations of motion are exactly the same equations obtained for a classical inverted pendulum, giving rise to parametric-resonance stability. In other words, rather surprisingly, the core of the Zeno region consists of a region of operator stability which has a purely classical origin.

Another interesting system, which is suitable for experimental verification, is studied in chapter 10. We consider a three-level system (such as an atom or a molecule), initially prepared in an excited state. The decay will be (approximately) exponential and characterized by a certain lifetime. But if one shines on the system an intense laser field, tuned at the transition frequency of the other two levels, the lifetime of the initial state is modified and depends on the intensity of the laser. A continuous observation is performed by the laser field and an inverse Zeno effect is obtained. This is a realistic implementation of a continuous (Rabi) observation. By using the asymptotic properties of the electromagnetic form factors, we can compute the behavior of the modified lifetime as a function of the intensity of the laser.

The deviations from exponential law in quantum mechanics, given by the regeneration effects, bear a close relation with localization phenomena and the quantum suppression of classical chaos. Indeed, all these effects are ultimately due to quantum mechanical interference effects, contained in the off-diagonal elements of the density matrix. The effectiveness of the quantum Zeno effects is related to the ability of destroying this coherence. In chapter 11 we consider the kicked rotator, a classical chaotic system which exhibits momentum localization and consequent suppression of chaos. We show that by performing perfect measurements (or equivalently a generalized spectral decomposition) of the momentum variable after each kick, the localization is completely destroyed, a master equation is obtained and the evolution becomes completely chaotic, yielding a diffusive behavior of the energy variable. This is a clear manifestation of an inverse quantum Zeno effect. Moreover, quantum chaos is obtained, even when the classical system has a regular behavior. This is due to the measurement-induced exponential behavior of the occupation probability and yields a completely randomized classical map in the semiclassical limit.

Finally, in chapter 12 we look at the modified (Zeno) dynamics from a different (but fruitful) perspective. In the previous chapters the Zeno subspaces are always held fixed during the evolution. Moreover, we stressed that the coherence between different sectors is destroyed due to a superselection rule and the system is forced to remain in its initial sector. By contrast, we now consider a situation in which the Zeno subspace changes, by changing the projections. As a consequence, the system is forced to remain in a continuously varying sector and therefore to follow an externally imposed trajectory. We call this effect "dynamical" quantum Zeno effect. In this case we show that the coherence is completely preserved and results in a quantal Berry phase. In principle, we can construct any geometrical phase, without any additional dynamical contribution. We exhibit a specific experimental setup in which this effect can be seen for a neutron spin and model this situation in terms of a nonhermitian Hamiltonian. We will see that the degree of preserved coherence is related to a condition for adiabaticity, very close to the original formulation of the geometrical phase given in the seminal paper by Berry [1984].

Part I

FREE DYNAMICS

Chapter 2

The exponential decay law in quantum mechanics

2.1 The exponential decay law: a heuristic derivation

The simplest way to obtain the exponential decay probability of an unstable system is to follow a heuristic approach. This derivation is usually called the "classical" theory of decay. It is essentially based on the assumption that the unstable system has a given decay probability per unit time Γ, which is constant and does not depend on the total number of unstable systems or on their past history. Let $N(t)$ be the number of undecayed systems at time t. For sufficiently large $N(t)$, the number of systems that will decay in the interval $(t, t+dt)$ is

$$-dN = N\Gamma dt \qquad \Rightarrow \qquad \frac{dN}{dt} = -\Gamma N, \tag{2.1}$$

which yields

$$N(t) = N_0 e^{-\Gamma t}, \tag{2.2}$$

where $N_0 = N(0)$ is the number of systems at $t = 0$. One defines the *survival probability* at time t as

$$P(t) = \frac{N(t)}{N_0} = e^{-\Gamma t}, \tag{2.3}$$

where the $N_0 \to \infty$ limit is implicitly assumed. The (positive) quantity Γ is the *decay rate* and is nothing but the inverse *lifetime* τ. Indeed the probability that the system survives up to a time in the interval $(t, t+dt)$ is just the survival probability $P(t)$ at time t times the decay probability Γdt in the interval dt, whence the lifetime τ is

$$\tau = \int_0^\infty t e^{-\Gamma t} \Gamma dt = \frac{1}{\Gamma}. \tag{2.4}$$

Note that the law (2.3) has the peculiar property

$$\frac{P'(t)}{P(t)} = -\Gamma = \text{const} \tag{2.5}$$

and at short times $P(t)$ decreases linearly with time

$$P(t) \sim 1 - \Gamma t, \qquad \text{for} \quad t \to 0. \tag{2.6}$$

Notice that the assumptions underpinning the above derivation are delicate. Indeed the essential ingredients of a Markovian stochastic process, in which memory effects are completely absent, are apparent. The survival probability (2.3) satisfies the semigroup law

$$P(t+t') = P(t)P(t'), \tag{2.7}$$

namely the probability is invariant under time translation, modulo a scale factor. This property is ultimately due to the assumption of a constant decay rate [see Eq. (2.5)], which excludes the possibility that cooperative effects take place.

2.2 Quantum survival amplitude and probability

The derivation of the exponential decay law in quantum mechanics is the result of a series of approximations, sometimes very subtle, which eventually yield the Fermi Golden Rule. Let us define the fundamental quantities we will use in this work, their mutual relations and their links with the physics of the decay problem in quantum mechanics.

Consider a quantum system Q represented by the state $|\psi(t)\rangle$. Let $|a\rangle$ be the initial state at $t = 0$, viz., $|\psi(0)\rangle = |a\rangle$. The dynamical evolution of Q in the Schrödinger picture is governed by the unitary operator $U(t) = \exp(-iHt)$, where we considered a time-independent Hamiltonian H. We define the *survival amplitude* at time t

$$\mathcal{A}(t) = \langle a|U(t)|a\rangle = \langle a|e^{-iHt}|a\rangle \tag{2.8}$$

and the *survival probability* at time t

$$P(t) = |\mathcal{A}(t)|^2 = |\langle a|e^{-iHt}|a\rangle|^2. \tag{2.9}$$

2.2.1 The regeneration effect

We write the state at time t in the following form

$$|\psi(t)\rangle = \exp(-iHt)|a\rangle = \mathcal{A}(t)|a\rangle + |\psi_d(t)\rangle \tag{2.10}$$

where

$$|\psi_d(t)\rangle = P_d|\psi(t)\rangle = (1-P_a)|\psi(t)\rangle, \qquad P_a = |a\rangle\langle a|, \quad P_d = 1 - P_a. \tag{2.11}$$

Notice that $|\psi_d(t)\rangle$ represents the decay products and is orthogonal to the initial state $|a\rangle$.

$$\langle a|\psi_d(t)\rangle = 0. \tag{2.12}$$

In other words, we have decomposed the Hilbert space $\mathcal{H} = \mathcal{H}_a \oplus \mathcal{H}_d$ as a direct sum of the (one-dimensional) space of the survived system $\mathcal{H}_a = P_a\mathcal{H}$ and its orthogonal complement $\mathcal{H}_d = P_d\mathcal{H}$, which contains the decay products. The system, under its unitary evolution, decays by evolving from $\mathcal{H}_a$ into $\mathcal{H}_d$.

By applying the unitary operator $\exp(-iHt')$ to both sides of Eq. (2.10) and taking the inner product with the initial state $\langle a|$, we get

$$\begin{aligned} \mathcal{A}(t+t') &= \mathcal{A}(t)\mathcal{A}(t') + \mathcal{R}(t',t), \\ \mathcal{R}(t',t) &= \langle a|\exp(-iHt')|\psi_d(t)\rangle \end{aligned} \tag{2.13}$$

This equation, first derived by Ersak [1969], sheds light on the physics of the decay problem. The additional term $\mathcal{R}(t',t)$ in the r.h.s of Ersak's equation provides a "regeneration" contribution to the survival amplitude. The decayed components of the state at a given time give rise to a surviving component at later times. It is just this regeneration effect which prevents the occurrence of a purely exponential decay. Indeed, if $\mathcal{R}(t',t) = 0$, the survival probability would satisfy the "classical" equation (2.7) that necessarily implies an exponential form.

2.2.2 Spectral density function representation

Consider a complete set of eigenstates $\{|\nu\rangle\}$ of the Hamiltonian H

$$H|\nu\rangle = E_\nu|\nu\rangle, \tag{2.14}$$

$$\sum_\nu |\nu\rangle\langle\nu| = 1. \tag{2.15}$$

By plugging the closure relation (2.15) into Eq. (2.8), the survival amplitude can be written in the following form

$$\mathcal{A}(t) = \langle a|U(t)|a\rangle = \sum_\nu \langle a|e^{-iHt}|\nu\rangle\langle\nu|a\rangle = \int dE\; e^{-iEt}\varpi_a(E), \tag{2.16}$$

where

$$\varpi_a(E) = \sum_\nu |\langle\nu|a\rangle|^2\delta(E-E_\nu) = \langle a|\delta(E-H)|a\rangle \tag{2.17}$$

is the *spectral density function* of the initial state $|a\rangle$.

Let us examine the properties of $\varpi_a(E)$. It is a nonnegative function with support on the spectrum of H. Therefore, being integrable and nonnegative, it is an absolutely integrable function. Indeed, by using Eq. (2.17),

$$\int dE\; |\varpi_a(E)| = \int dE\; \varpi_a(E) = \sum_\nu |\langle\nu|a\rangle|^2 = \langle a|a\rangle = 1. \tag{2.18}$$

Notice that if the spectrum contains a continuous part σ_c, the sum in Eq. (2.17) contains actually an integration over that part. Indeed ν is a shorthand notation for a collective index, namely $\{|\nu\rangle = |E', s\rangle\}$, where E' is the energy and s are other (possible) quantum numbers that are degenerate with respect to the energy. We get

$$\begin{aligned}
\varpi_a(E) &= \sum_\nu |\langle\nu|a\rangle|^2\delta(E-E_\nu) \\
&= \int_{\sigma_c} dE' \sum_s |\langle E', s|a\rangle|^2\delta(E-E') + \sum_n\sum_s |\langle E_n, s|a\rangle|^2\delta(E-E_n) \\
&= \left(\sum_s |\langle E, s|a\rangle|^2\right)\chi_{\sigma_c}(E) + \sum_n \left(\sum_s |\langle E_n, s|a\rangle|^2\right)\delta(E-E_n),
\end{aligned} \tag{2.19}$$

where $\chi_{\sigma_c}(E)$ is the characteristic function of the set σ_c [$\chi_{\sigma_c}(E) = 1$ for $E \in \sigma_c$ and 0 otherwise]. Therefore the spectral density is an ordinary function over the continuous spectrum σ_c and has delta-like singularities over the discrete spectrum.

2.3 Short-time behavior

A naive expansion of Eq. (2.9) yields

$$\begin{aligned}
P(t) &= \langle a|e^{-iHt}|a\rangle\langle a|e^{+iHt}|a\rangle \sim \sum_{n=0}^{\infty}\frac{(-i)^n}{n!}t^n\langle a|H^n|a\rangle \sum_{m=0}^{\infty}\frac{(i)^m}{m!}t^m\langle a|H^m|a\rangle \\
&\sim \sum_{n=0}^{\infty}\frac{(-1)^n}{(2n)!}\,c_{2n}\,t^{2n},
\end{aligned} \tag{2.20}$$

where

$$c_{2n} = \sum_{k=0}^{2n} (-1)^k \left(\begin{array}{c} 2n \\ k \end{array} \right) \langle a|H^k|a\rangle \langle a|H^{2n-k}|a\rangle. \tag{2.21}$$

Note that Eq. (2.20) is a symmetric function of t as a consequence of the invariance of the theory under time reversal. For small enough times it is sufficient to expand up to order t^2, obtaining

$$P(t) = 1 - t^2 \left(\langle a|H^2|a\rangle - \langle a|H|a\rangle^2 \right) + \mathrm{O}(t^4) = 1 - t^2 \left(\triangle E\right)^2 + \mathrm{O}(t^4), \tag{2.22}$$

which, being a quadratic function of t, implies that the decay rate vanishes for $t \to 0$, at variance with Eq. (2.5). Notice that if the state $|a\rangle$ is an eigenstate of H the evolution is trivially given by $P(t) = 1$, $\forall t$.

The asymptotic expansion (2.20) is meaningful if one requires that the state $|a\rangle$ is normalizable and all moments of H over the state $|a\rangle$ are finite. If the moments are finite up to some order N we get an asymptotic series to N terms.

If the first two moments of the Hamiltonian are finite, the survival probability for short times reads

$$P(t) \sim 1 - \frac{t^2}{\tau_{\mathrm{Z}}^2} \sim \exp\left(-\frac{t^2}{\tau_{\mathrm{Z}}^2} \right) \quad \text{for} \quad t \to 0, \tag{2.23}$$

where

$$\tau_{\mathrm{Z}} \equiv 1/\Delta E \tag{2.24}$$

is called the *Zeno time* [1] and determines the convexity of the survival probability at $t = 0$. An accurate estimate of the Zeno time for a truly unstable system is usually a difficult and delicate problem. A quantitative evaluation of τ_{Z} is important, for it enables one to find a characteristic temporal scale for the short-time behavior of the survival probability. We will see that for generic systems the asymptotic expansion (2.23) is valid for times much shorter than τ_{Z}.

Notice that the quantum survival probability represents the probability that a system, prepared at time $t = 0$ in state $|a\rangle$, is found in the same state *at* time t. In other words, it represents the experimental probability (namely the frequency for a very large number of identically prepared systems) of finding the system in the initial state when one lets it evolve *undisturbed* for a time t and then measures it exactly at time t. As we will see in the second part of this work, the survival probability of a system that is measured *throughout* the time interval $(0, t)$ is completely different from that considered in this section and this effect is ultimately ascribable to the nonexponential behavior of the "undisturbed" survival probability.

Moreover, notice that the hypotheses in the derivation of Eq. (2.23) are in general not valid in quantum field theory, where the energy uncertainty is in general infinite. In this case, as we will see, the survival probability at short times can exhibit a different behavior (Bernardini, Maiani and Testa [1993]; Facchi and Pascazio [1999b]).

2.3.1 Vanishing decay rate

We now want to show under what rigorous conditions the survival probability deviates from the exponential law at the beginning of the decay process. We look therefore for the conditions

[1] This time is named after the Greek philosopher Zeno from Elea, for its role in a peculiar quantum phenomenon called *quantum Zeno effect*. See Chap. 7

leading to $\dot{P}(0) = 0$. From the Fourier representation (2.16), or from the very definition (2.8), we see immediately that the survival amplitude must satisfy the reality condition

$$\mathcal{A}(t)^* = \mathcal{A}(-t). \tag{2.25}$$

Therefore the survival probability satisfies the relation $P(t) = P(-t)$ (time reversal invariance). On the other hand, $\varpi_a(E)$ is an absolutely integrable function due to Eq. (2.18), whence $\mathcal{A}(t)$ is continuous. Notice that if $P(t)$ is differentiable then one gets $\dot{P}(t) = -\dot{P}(-t)$ and in particular

$$\dot{P}(0^+) = -\dot{P}(0^-). \tag{2.26}$$

Therefore the time derivative of the survival probability is in general a discontinuous function at $t = 0$, unless it vanishes there.

Now suppose that the expectation value of $|H|$ in the state $|a\rangle$ exists and is finite (Nakazato and Pascazio [1995]),

$$\langle a|\ |H|\ |a\rangle = \int dE\ |E|\ \varpi_a(E) < \infty, \tag{2.27}$$

i.e., $E\varpi_a(E)$ is an absolutely integrable function. From this it follows that the survival amplitude $\mathcal{A}(t)$ is differentiable for all t, and the derivative

$$\dot{\mathcal{A}}(t) = -i \int dE\ e^{-iEt} E\ \varpi_a(E) \tag{2.28}$$

is continuous. From Eq. (2.25), the time derivative of the survival probability reads

$$\dot{P}(t) = \dot{\mathcal{A}}(t)\mathcal{A}(t)^* + \mathcal{A}(t)\dot{\mathcal{A}}(t)^* = \dot{\mathcal{A}}(t)\mathcal{A}(-t) - \mathcal{A}(t)\dot{\mathcal{A}}(-t), \tag{2.29}$$

and in particular

$$\dot{P}(0^+) = \dot{P}(0^-) = 0 \tag{2.30}$$

by virtue of the continuity of $\mathcal{A}$ and $\dot{\mathcal{A}}$.

Therefore the only condition of finiteness of $\langle |H| \rangle$ (with $|a\rangle$ normalizable) is sufficient to assert that the survival probability must deviate from the exponential decay at sufficiently small times and the decay rate must vanish at $t = 0$.

Notice that if one requires the physical condition of lower boundeness of the Hamiltonian, in order to have a stable ground state, the above condition translates into the finiteness of the expectation value of the energy $\langle H \rangle$ (Chiu, Sudarshan and Misra [1977]). Indeed in this case we can assume, without loss of generality, that the spectrum of H is confined in the positive semiaxis. Therefore, if the expectation value of energy is finite, we get

$$\langle a|H|a\rangle = \int_0^\infty dE\ E\ \varpi_a(E) = \int_0^\infty dE\ |E|\ \varpi_a(E) = \langle a|\ |H|\ |a\rangle < \infty, \tag{2.31}$$

and Eq. (2.30) follows again. In other words, for a physical system, i.e. a system with a lower bounded Hamiltonian and finite energy, the decay rate necessarily vanishes at $t = 0$ and the survival probability cannot be exponential at short times.

2.3.2 Fleming's unitary bound

Let us consider Heisenberg's uncertainty relation between a time-independent observable A and a time-independent Hamiltonian H

$$\triangle A\ \triangle E \geq \frac{1}{2}\,|\langle [A, H] \rangle| = \frac{1}{2}\left|\frac{d}{dt}\langle A \rangle\right| \tag{2.32}$$

where

$$\triangle A = \sqrt{\langle A^2\rangle - \langle A\rangle^2}, \qquad \triangle E = \sqrt{\langle H^2\rangle - \langle H\rangle^2}. \tag{2.33}$$

Equation (2.32) is used in the literature to prove the uncertainty relation between time and energy. See Messiah [1961], Sec. VII-13. By specializing the observable A to the projection operator over the initial state $|a\rangle$, namely

$$A = P_a = |a\rangle\langle a|, \qquad |\psi(0)\rangle = |a\rangle, \tag{2.34}$$

one easily obtains

$$\langle A\rangle = P(t), \qquad \triangle A = \sqrt{P(t) - P(t)^2}. \tag{2.35}$$

Whence Eq. (2.32) reads

$$\left|\frac{dP}{dt}\right| \leq 2\triangle E\sqrt{P - P^2}. \tag{2.36}$$

This is an inequality that clearly restricts the rate of change of the survival probability of a quantum system. This relation can be integrated to give a lower bound on the survival probability. Indeed one can write

$$\left|\int_1^{P(t)} \frac{dP}{\sqrt{P(1-P)}}\right| \leq \int_0^t \frac{1}{\sqrt{P(1-P)}}\left|\frac{dP}{dt}\right| dt \leq 2\triangle E\, t, \tag{2.37}$$

and, by setting $P = \cos^2\xi$, Eq. (2.37) is easily integrated to yield

$$\arccos\sqrt{P(t)} \leq \triangle E\, t, \qquad t \leq \frac{\pi}{2\triangle E}. \tag{2.38}$$

By noting that $\triangle E = 1/\tau_{\rm Z}$, we finally get Fleming's unitary bound on the survival probability at short times (Fleming [1973])

$$P(t) \geq \cos^2\left(\frac{t}{\tau_{\rm Z}}\right), \qquad t \leq \frac{\pi}{2}\tau_{\rm Z}. \tag{2.39}$$

Notice that the equality holds for a degenerate two level system oscillating with Rabi frequency $1/\tau_{\rm Z}$. Moreover note that the quantity $\triangle E$ is assumed to be finite, i.e., $\tau_{\rm Z} > 0$. An infinite $\triangle E$ would mean that the initial state $|a\rangle$ is not in the domain of definition of H and, strictly speaking, in this case there would be no Schrödinger equation.

2.4 Large-time behavior

We examine now the properties of the survival amplitude for large times. We will see that if the spectrum of the Hamiltonian is discrete, i.e. if the system is constrained in a limited spatial region, the regeneration described in Sec. 2.2.1 is such that the system never decays completely. If, on the other hand the spectrum is continuous, the initial state is eventually fully depleted, but $\mathcal{A}(t)$ cannot be a pure exponential if the energy spectrum is bounded from below.

2.4.1 Discrete spectrum: quantum recurrence

If the system is enclosed in a finite volume, the energy spectrum is discrete and the survival amplitude (2.16) never relaxes toward zero, but has an oscillatory behavior. The system periodically goes back as close as one wishes to the initial state and exhibits a recurrence phenomenon.

When the spectrum is discrete the spectral density ϖ_a has delta-like singularities in correspondence of the energy levels of the system. The survival amplitude (2.16) reads

$$\mathcal{A}(t) = \langle a|U(t)|a\rangle = \sum_r \langle a|e^{-iHt}|r\rangle\langle r|a\rangle = \sum_r |\langle r|a\rangle|^2 \, e^{-iE_r t}. \tag{2.40}$$

Note that the sum in Eq. (2.40) is at most over a countable set of terms. Suppose that the energies E_r have commensurable ratios. In this case Eq. (2.40) is nothing but a Fourier series and $\mathcal{A}(t)$ is exactly periodic with frequency equal to the greatest common divisor of the E_r's. On the other hand, if some energy levels don't have a commensurable ratio the survival amplitude is no longer strictly periodic. In this case the system never goes back to the initial state in a finite time, but it returns to a neighborhood of that state and the motion is quasi-periodic. A similar recurrence theorem holds in classical mechanics and is due to Poincaré (for a modern formulation see Arnold [1989], Sec. III.16). The quantum version is due to Bocchieri and Loinger [1957].

By letting $c_r = \langle r|a\rangle$, the state at time t has the following form

$$|\psi(t)\rangle = e^{-iHt}|a\rangle = \sum_{r=1}^{\infty} c_r e^{-iE_r t}|r\rangle. \tag{2.41}$$

Therefore the distance between the state $|\psi(t)\rangle$ and the initial state $|\psi(0)\rangle$ is

$$\begin{aligned} \mathcal{D}(t) &\equiv \|\psi(t) - \psi(0)\|^2 = \langle \psi(t) - \psi(0)|\psi(t) - \psi(0)\rangle \\ &= 2\sum_{r=1}^{\infty} |c_r|^2 \left[1 - \cos(E_r t)\right] = 4\sum_{r=1}^{\infty} |c_r|^2 \sin^2\left(\frac{E_r t}{2}\right). \end{aligned} \tag{2.42}$$

But if the state is normalizable, we get

$$\|\psi(t)\|^2 = \sum_{r=1}^{\infty} |c_r|^2 = 1, \tag{2.43}$$

whence, for any positive number ε, there exists an integer ν such that

$$\sum_{r=\nu+1}^{\infty} |c_r|^2 < \frac{\varepsilon}{8}. \tag{2.44}$$

By using this equation we can write

$$4\sum_{r=\nu+1}^{\infty} |c_r|^2 \sin^2\left(\frac{E_r t}{2}\right) \leq 4\sum_{r=\nu+1}^{\infty} |c_r|^2 < \frac{\varepsilon}{2} \tag{2.45}$$

and it follows that

$$\mathcal{D}(t) < f(t) + \frac{\varepsilon}{2}, \qquad f(t) \equiv 4\sum_{r=1}^{\nu} |c_r|^2 \sin^2\left(\frac{E_r t}{2}\right). \tag{2.46}$$

Note that $f(t)$ is a sum of a finite number of continuous periodic functions, whence it is a quasi-periodic function (Bohr [1932]). Therefore for any $\varepsilon > 0$, a relatively dense set $\{T\}_{\tau(\varepsilon)}$ exists [2] such that for any T one gets

$$|f(T) - f(0)| = f(T) < \frac{\varepsilon}{2}. \tag{2.47}$$

[2] A set S of real numbers is said relatively dense (on the real line) if there exists a positive real number σ such that every interval of size σ contains at the least one element of S. For example the set of relative numbers is relatively dense (but not dense) on the real line. Physically, $\tau = \inf\sigma$ is the *recurrence time*.

Therefore the inequality

$$\mathcal{D}(T) = \|\psi(T) - \psi(0)\|^2 < \varepsilon \tag{2.48}$$

holds in a relatively dense set of the real line.

In conclusion, we proved that for a spatially confined system, the evolution is quasi-periodic and the system returns to a neighborhood of the initial state in a finite time.

2.4.2 Continuous spectrum: truly unstable system

Let us now assume that the Hamiltonian H has only a continuous spectrum. In this case the energy density $\varpi_a(E)$ is an ordinary function of energy E with no delta singularities. Therefore, by Eq. (2.16), the survival probability is the Fourier transform of the energy density, as first stressed by Fock and Krylov [1947]. Assume now on physical grounds that the energy spectrum is lower bounded in order to have a stable ground state. It follows that the spectral density vanishes for $E < E_g$, where $E_g > -\infty$ is the ground-state energy, and we can write

$$\varpi_a(E) = \theta(E - E_g)\varpi_a(E), \tag{2.49}$$

with θ the unit step function. Whence Eq. (2.16) reads

$$\mathcal{A}(t) = \int_{E_g}^{\infty} dE\ \varpi_a(E)e^{-iEt}. \tag{2.50}$$

Remember from Eq. (2.18) that $\varpi_a(E)$ is an absolutely integrable function. Whence, due to Riemann-Lebesgue's lemma, $\mathcal{A}(t)$ vanishes at infinity

$$\lim_{t\to\infty} \mathcal{A}(t) = \lim_{t\to\infty} \int_{E_g}^{\infty} dE\ \varpi_a(E)e^{-iEt} = 0 \tag{2.51}$$

and we can say that the state $|a\rangle$ is a *truly unstable* state.

A theorem on Fourier trasforms due to Paley and Wiener [1934] states that if the function $\varpi_a(E)$ vanishes identically for $E < E_g$, with $E_g > -\infty$, then its Fourier trasform $\mathcal{A}(t)$ must satisfy the inequality

$$\int_{-\infty}^{\infty} \frac{|\log|\mathcal{A}(t)||}{1+t^2} dt < \infty. \tag{2.52}$$

Therefore, the survival probability cannot be an exponential, for the integral (2.52) would diverge as $\log t$ for $t \to \infty$. At large time the decay must be slower, for example a power law.

Notice that this is a very general result: the only condition required is the existence of a finite value E_g. The use of Paley-Wiener's theorem in this context is due to Khalfin [1957]; Khalfin [1958].

Chapter 3

Simple solvable models

3.1 Introduction

In the previous chapter we analyzed some mathematical properties of the time evolution of the survival probability for a quantum system. At short times, the decay follows a quadratic law and has a lower bound given by Fleming's theorem (2.39). At large times, the decay cannot be an exponential, as a consequence of Paley-Wiener's theorem (2.52). In order to understand better the features of the survival probability, a detailed analysis is needed, based on some subtle properties of the resolvent. Before proceeding in this analysis we want to examine the emergence of an exponential decay law in some quantum mechanical models. We will examine three simple solvable models: a two-level system, a many-level discrete system with a flat spectrum and its continuum version. These examples will enable us to understand the physical role of the mathematical hypotheses of the previous chapter.

3.2 Two-level systems and Bloch vector

We start by considering a two-level system undergoing Rabi oscillations. This is the simplest nontrivial quantum mechanical example, for it involves 2×2 matrices and very simple algebra. One can think of an atom shined by a laser field whose frequency resonates with one of the atomic transitions, or a neutron spin in a magnetic field.

The two-level Hamiltonian reads

$$\begin{aligned} H &= \omega_a |a\rangle\langle a| + \omega_b |b\rangle\langle b| + \lambda(|a\rangle\langle b| + |b\rangle\langle a|) = \begin{pmatrix} \omega_a & \lambda \\ \lambda & \omega_b \end{pmatrix}, \\ &= \omega_m + \frac{\triangle\omega}{2}\sigma_3 + \lambda\sigma_1 = \omega_m + \begin{pmatrix} \frac{\triangle\omega}{2} & \lambda \\ \lambda & -\frac{\triangle\omega}{2} \end{pmatrix}, \end{aligned} \tag{3.1}$$

where $\omega_a > \omega_b$, λ is the coupling constant, σ_j $(j = 1, 2, 3)$ the Pauli matrices,

$$\omega_m = \frac{\omega_a + \omega_b}{2}, \qquad \triangle\omega = \omega_a - \omega_b, \tag{3.2}$$

and

$$|a\rangle = \begin{pmatrix} 1 \\ 0 \end{pmatrix}, \quad |b\rangle = \begin{pmatrix} 0 \\ 1 \end{pmatrix} \tag{3.3}$$

are eigenstates of σ_3. We will use the above notation interchangeably. Let the initial state be

$$|\psi(0)\rangle = |a\rangle = \begin{pmatrix} 1 \\ 0 \end{pmatrix}, \tag{3.4}$$

so that the evolution yields

$$|\psi(t)\rangle = e^{-iHt}|a\rangle = e^{-i\omega_m t}\left[\left(\cos\Omega t - i\frac{\triangle\omega}{2\Omega}\sin\Omega t\right)|a\rangle \; - \; i\frac{\lambda}{\Omega}\sin\Omega t\;|b\rangle\right], \tag{3.5}$$

where

$$\Omega = \sqrt{\left(\frac{\triangle\omega}{2}\right)^2 + \lambda^2} \tag{3.6}$$

is the Rabi frequency of the oscillations. The survival amplitude and probability read

$$\begin{aligned} \mathcal{A}(t) &= \langle a|\psi(t)\rangle = e^{-i\omega_m t}\left(\cos\Omega t - i\frac{\triangle\omega}{2\Omega}\sin\Omega t\right), \\ P(t) &= |\mathcal{A}(t)|^2 = 1 - \frac{\lambda^2}{\Omega^2}\sin^2(\Omega t), \end{aligned} \tag{3.7}$$

and the oscillations are in general not complete, i.e., the initial state is never fully depleted. It is well known that when the two unperturbed levels become degenerate, i.e., $\triangle\omega = 0$, the Rabi frequency becomes $\Omega = \lambda$ and the oscillations become complete.

For future convenience, let us derive the above results by alternative methods. As a general procedure, valid for a generic many-level system, we can write the state of the system at time t as

$$|\psi(t)\rangle = \mathcal{A}(t)|a\rangle + b(t)|b\rangle = \begin{pmatrix} \mathcal{A}(t) \\ b(t) \end{pmatrix}, \tag{3.8}$$

where $|\mathcal{A}(t)|^2 + |b(t)|^2 = 1$. By using the Schrödinger equation we get

$$i\dot{\mathcal{A}} = \omega_a\mathcal{A} + \lambda b, \tag{3.9}$$

$$i\dot{b} = \omega_b b + \lambda\mathcal{A}, \tag{3.10}$$

which yield again Eq. (3.7).

On the other hand we can also find the spectral density. It is straightforward to determine the eigenvalues and the eigenstates of the total Hamiltonian H

$$E_{1,2} = \omega_m \pm \Omega, \tag{3.11}$$

$$|E_{1,2}\rangle = \pm\sqrt{\frac{1}{2}\left(1 \pm \frac{\triangle\omega}{2\Omega}\right)}\,|a\rangle + \sqrt{\frac{1}{2}\left(1 \mp \frac{\triangle\omega}{2\Omega}\right)}\,|b\rangle = \begin{pmatrix} \pm\sqrt{\frac{1}{2}\left(1 \pm \frac{\triangle\omega}{2\Omega}\right)} \\ \sqrt{\frac{1}{2}\left(1 \mp \frac{\triangle\omega}{2\Omega}\right)} \end{pmatrix}, \tag{3.12}$$

whence we can write the spectral density

$$\begin{aligned} \varpi_a(E) &= |\langle E_1|a\rangle|^2\delta(E - E_1) + |\langle E_2|a\rangle|^2\delta(E - E_2) \\ &= \frac{1}{2}\left(1 + \frac{\triangle\omega}{2\Omega}\right)\delta(E - \omega_m - \Omega) + \frac{1}{2}\left(1 - \frac{\triangle\omega}{2\Omega}\right)\delta(E - \omega_m + \Omega), \end{aligned} \tag{3.13}$$

which consists of two delta functions with different weights, at the energies of the total Hamiltonian (symmetric with respect to ω_m). The survival amplitude (3.7) is immediately obtained by a Fourier transform.

Note that $\langle a|H^2|a\rangle = \omega_a^2 + \lambda^2$ and $\langle a|H|a\rangle = \omega_a$. Therefore the Zeno time reads

$$\tau_{\rm Z} = 1/\triangle E = 1/\lambda, \tag{3.14}$$

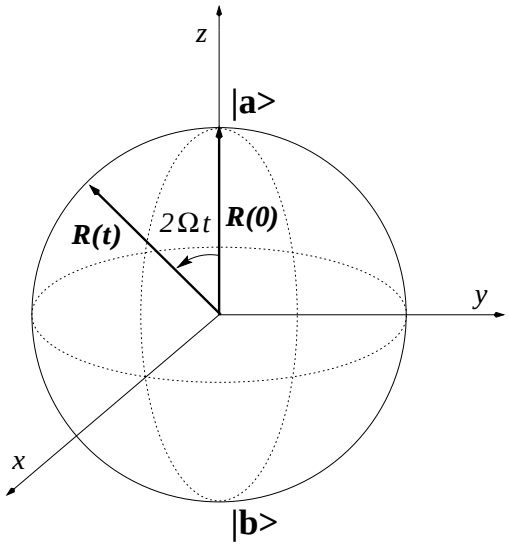

Figure 3.1: The Poincaré sphere and the Bloch vector.

and does not depends on ω_a and ω_b. Moreover, for this model, all the Hamiltonian moments are finite, the expansion (2.20) is valid and converges exactly to (3.7). Note also that Fleming's unitary bound (2.39) is trivially valid in this case and in fact, as anticipated, becomes an equality for the degenerate case $\triangle\omega = 0$.

In the following, we shall often make use of the rotating coordinates introduced by Bloch [1946] and Rabi, Ramsey and Schwinger [1954], and of well-known computational techniques due to Feynman, Vernon and Hellwarth [1957]. In terms of the polarization (Bloch) vector

$$\boldsymbol{R}(t) = \langle\psi_t|\boldsymbol{\sigma}|\psi_t\rangle = (R_1, R_2, R_3)^T, \tag{3.15}$$

where ^{T} denotes the transposed matrix, the Schrödinger equation, when $\omega_a = \omega_b = 0$, reads

$$\dot{\boldsymbol{R}}(t) = 2\boldsymbol{\Omega} \times \boldsymbol{R}(t), \tag{3.16}$$

where

$$\boldsymbol{\Omega} = (\Omega, 0, 0)^T, \tag{3.17}$$

with the Rabi frequency $\Omega = \lambda$. The norm of the Bloch vector is preserved: $\|\boldsymbol{R}(t)\| = 1, \forall t$. See Fig. 3.1.

The density matrix of a two-level system is expressed in terms of the Bloch vector according to the formula

$$\rho = \begin{pmatrix} \rho_{aa} & \rho_{ab} \\ \rho_{ba} & \rho_{bb} \end{pmatrix} = \frac{1}{2}(\mathbf{1} + \boldsymbol{R}\cdot\boldsymbol{\sigma}), \tag{3.18}$$

so that

$$\rho_{aa} = \frac{1}{2}(1 + R_3) = P_a, \qquad \rho_{bb} = \frac{1}{2}(1 - R_3) = P_b, \qquad \rho_{ab} = \frac{1}{2}(R_1 - iR_2), \tag{3.19}$$

where $P_a \equiv \rho_{aa}$ ($P_b \equiv \rho_{bb}$) is the probability that the system is in level $|a\rangle$ ($|b\rangle$) and $\rho_{ba} = \rho^*_{ab}$. Notice that $\mathrm{Tr}\rho = P_a + P_b = 1$ (normalization) and $\mathrm{Tr}(\rho\boldsymbol{\sigma}) = \boldsymbol{R}$. Viceversa, the Bloch vector is readily expressed in terms of the density matrix:

$$\begin{aligned} R_1 &= \rho_{ab} + \rho_{ba}, \\ R_2 &= i(\rho_{ab} - \rho_{ba}), \\ R_3 &= \rho_{aa} - \rho_{bb} = P_a - P_b. \end{aligned} \tag{3.20}$$

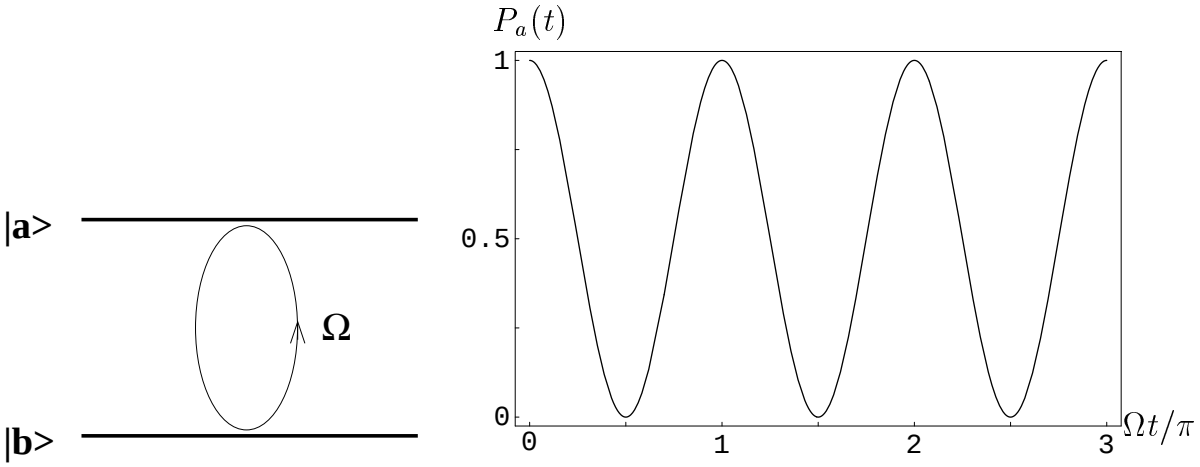

Figure 3.2: Rabi oscillations in a two-level system.

The level configuration and the dynamics of the oscillations are shown in Fig. 3.2. Observe that the probability goes back to its initial value after a time $T_{\rm P} = \pi/\Omega$: this is a very simple instance of Poincaré recurrence time.

3.3 Many-level system

We now consider a many-level system which exhibits an exponential decay at early times. Let us improve the two-level model (3.1). Consider the Hamiltonian

$$H = \omega_a |a\rangle\langle a| + \sum_n \omega_n |n\rangle\langle n| + \lambda \sum_n (|a\rangle\langle n| + |n\rangle\langle a|), \tag{3.21}$$

which couples state $|a\rangle$ with many states $|n\rangle$. Assume the orthonormality conditions

$$\langle a|a\rangle = 1, \quad \langle a|n\rangle = 0, \quad \langle n|n'\rangle = \delta_{n,n'} \quad \forall n, n'. \tag{3.22}$$

The state of the system at time t reads

$$|\psi(t)\rangle = \mathcal{A}(t)|a\rangle + \sum_n b_n(t)|n\rangle, \tag{3.23}$$

with $|\mathcal{A}(t)|^2 + \sum_n |b_n(t)|^2 = 1$. Let us choose, as usual, the initial state $|\psi(0)\rangle = |a\rangle$, i.e., $\mathcal{A}(0) = 1$. By using the Schrödinger equation $i\partial_t|\psi\rangle = H|\psi\rangle$ one gets

$$i\dot{\mathcal{A}} = \omega_a \mathcal{A} + \lambda \sum_n b_n, \tag{3.24}$$

$$i\dot{b}_n = \omega_n b_n + \lambda \mathcal{A}. \tag{3.25}$$

Equation (3.25) is easily integrated with the initial condition $b_n(0) = 0$

$$b_n(t) = -i\lambda \int_0^t dt_1 e^{-i\omega_n(t-t_1)} \mathcal{A}(t_1). \tag{3.26}$$

By substituting Eq. (3.26) into Eq. (3.24) one gets

$$\dot{\mathcal{A}}(t) = -i\omega_a \mathcal{A}(t) - \lambda^2 \int_0^t dt_1 \mathcal{A}(t_1) \sum_n e^{-i\omega_n(t-t_1)}. \tag{3.27}$$

Assume now that the levels are uniformly spaced between $-\infty$ e $+\infty$ (constant level density $\rho = 1/\delta\omega$):

$$\omega_n = n\,\delta\omega, \qquad \text{with} \quad n = 0, \pm 1, \pm 2, \ldots \ (\delta\omega = \text{const}). \tag{3.28}$$

By making use of Poisson's formula

$$\sum_{n=-\infty}^{+\infty} e^{-inx} = 2\pi \sum_{n=-\infty}^{+\infty} \delta(x - 2\pi n), \tag{3.29}$$

we can write

$$\sum_{n=-\infty}^{+\infty} e^{-i\omega_n t} = \sum_{n=-\infty}^{+\infty} e^{-in\delta\omega t} = \frac{2\pi}{\delta\omega} \sum_{n=-\infty}^{+\infty} \delta\left(t - \frac{2\pi n}{\delta\omega}\right), \tag{3.30}$$

and Eq. (3.27) yields

$$\begin{aligned} \dot{\mathcal{A}}(t) &= -i\omega_a \mathcal{A}(t) - \lambda^2 \int_0^t dt_1 \mathcal{A}(t_1) \frac{2\pi}{\delta\omega} \sum_{n=-\infty}^{+\infty} \delta\left(t - t_1 - \frac{2\pi n}{\delta\omega}\right) \\ &= -i\omega_a \mathcal{A}(t) - \frac{2\pi\lambda^2}{\delta\omega} \sum_{n=-\infty}^{+\infty} \mathcal{A}\left(t - \frac{2\pi n}{\delta\omega}\right) \int_0^t dt_1 \delta\left(t - t_1 - \frac{2\pi n}{\delta\omega}\right). \end{aligned} \tag{3.31}$$

By integrating we get

$$\int_0^t dt_1 \delta\left(t - t_1 - \frac{2\pi n}{\delta\omega}\right) = \begin{cases} 0 & \text{per} \quad n < 0 \\ \frac{1}{2}\theta(t) & \text{per} \quad n = 0 \\ \theta\left(t - \frac{2\pi n}{\delta\omega}\right) & \text{per} \quad n > 0 \end{cases}, \tag{3.32}$$

where we defined $\int_0^{t_0} \delta(t)dt = 1/2$ $(t_0 > 0)$. Therefore Eq. (3.31) reads

$$\dot{\mathcal{A}}(t) = -\left(i\omega_a + \frac{\gamma}{2}\right) \mathcal{A}(t) - \gamma \sum_{n=1}^{\infty} \mathcal{A}(t - nT)\ \theta(t - nT), \tag{3.33}$$

where

$$\gamma = 2\pi\lambda^2/\delta\omega = 2\pi\lambda^2\rho, \qquad T = 2\pi/\delta\omega = 2\pi\rho. \tag{3.34}$$

The differential equation (3.33) can be integrated recursively, starting from $t = 0$. For example in the interval $0 \le t < T$ only the first term survives

$$\dot{\mathcal{A}}(t) = -\left(i\omega_a + \frac{\gamma}{2}\right) \mathcal{A}(t), \tag{3.35}$$

whose integral, with the initial condition $\mathcal{A}(0) = 1$, reads

$$\mathcal{A}(t) = \exp\left[-\left(i\omega_a + \frac{\gamma}{2}\right) t\right] \quad (0 \le t < T), \tag{3.36}$$

and yields a purely exponential decay. In general, by writing

$$\mathcal{A}(t) = e^{-\left(i\omega_a + \frac{\gamma}{2}\right)t} + \sum_{n=1}^{\infty} e^{-\left(i\omega_a + \frac{\gamma}{2}\right)(t - nT)} f_n(t - nT)\ \theta(t - nT) \tag{3.37}$$

we get, by differentiation,

$$\dot{\mathcal{A}}(t) = -\left(i\omega_a + \frac{\gamma}{2}\right) \mathcal{A}(t) + \sum_{n=1}^{\infty} e^{-\left(i\omega_a + \frac{\gamma}{2}\right)(t - nT)} \dot{f}_n(t - nT)\ \theta(t - nT), \tag{3.38}$$

where we let $f_n(0) = 0$ for every n, in order to get rid of the terms proportional to $\delta(t - nT)$ which are absent in the original differential equation (3.33). By comparing Eq. (3.38) and Eq. (3.33) one obtains

$$\sum_{n=1}^{\infty} e^{-\left(i\omega_a+\frac{\gamma}{2}\right)(t-nT)} \dot{f}_n(t-nT)\,\theta(t-nT) = -\gamma \sum_{n=1}^{\infty} \mathcal{A}(t-nT)\,\theta(t-nT). \tag{3.39}$$

By plugging Eq. (3.37) into the above equation, after a straightforward algebraic manipulation, we get

$$\begin{aligned}\sum_{n=1}^{\infty} e^{-\left(i\omega_a+\frac{\gamma}{2}\right)(t-nT)} \dot{f}_n(t-nT)\,\theta(t-nT) &= -\gamma \sum_{n=1}^{\infty} e^{-\left(i\omega_a+\frac{\gamma}{2}\right)(t-nT)}\theta(t-nT) \\ &\quad -\gamma \sum_{n=2}^{\infty} e^{-\left(i\omega_a+\frac{\gamma}{2}\right)(t-nT)}\theta(t-nT) \sum_{m=1}^{n-1} f_m(t-nT)\end{aligned} \tag{3.40}$$

and by comparing the l.h.s. with the r.h.s. we finally get the following recursive relations

$$\dot{f}_1(t) = -\gamma, \qquad \dot{f}_n(t) = -\gamma - \gamma \sum_{m=1}^{n-1} f_m(t), \quad (n \geq 2). \tag{3.41}$$

By using the initial condition $f_1(0) = f_n(0) = 0$, we can easily integrate the differential equations (3.41) and obtain

$$f_1(t) = -\gamma t, \qquad f_n(t) = -\gamma t + (n-1) \sum_{m=2}^{n-1} \frac{(-\gamma t)^m}{m!} + \frac{(-\gamma t)^n}{n!}, \quad (n \geq 2). \tag{3.42}$$

As a result the survival amplitude has the form given by Eq. (3.37), with $f_n(t)$ a polynomial of order n given by (3.42). For example, by explicitly writing the first three terms, we get

$$\begin{aligned}\mathcal{A}(t) &= \exp\left[-\left(i\omega_a + \frac{\gamma}{2}\right) t\right] \\ &\quad -\gamma\,(t-T)\exp\left[-\left(i\omega_a + \frac{\gamma}{2}\right)(t-T)\right]\theta(t-T) \\ &\quad + \left[-\gamma\,(t-2T) + \frac{\gamma^2}{2}(t-2T)^2\right]\exp\left[-\left(i\omega_a + \frac{\gamma}{2}\right)(t-2T)\right]\theta(t-2T) \\ &\quad + \sum_{n=3}^{\infty} \text{terms proportional to } \theta(t-nT).\end{aligned} \tag{3.43}$$

Notice that the exponential decay law *exactly* holds for a time interval $T = 2\pi/\delta\omega = 2\pi\rho$, that becomes larger and larger by increasing the level density ρ.

3.3.1 Spectral density

We seek now the eigenstates and the eigenvalues of the total Hamiltonian (3.21), namely we solve the time-independent Schrödinger equation

$$H|\nu\rangle = E_\nu|\nu\rangle. \tag{3.44}$$

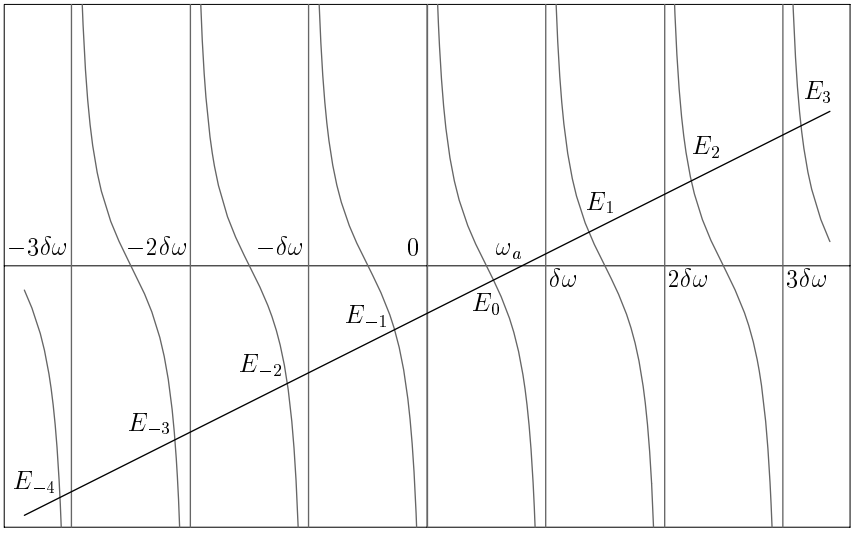

Figure 3.3: Graphic determination of the eigenvalues.

By using the definition (3.21) and by projecting Eq. (3.44) over $\langle a|$ and $\langle n|$ we get

$$\omega_a \langle a|\nu\rangle + \lambda \sum_n \langle n|\nu\rangle = E_\nu \langle a|\nu\rangle, \tag{3.45}$$

$$\omega_n \langle n|\nu\rangle + \lambda \langle a|\nu\rangle = E_\nu \langle n|\nu\rangle. \tag{3.46}$$

Incidentally note that Eqs. (3.45)-(3.46) have the same structure of Eqs. (3.25)-(3.24) after substituting $i\partial_t$ with E_ν. Equation (3.46) gives

$$\langle n|\nu\rangle = \langle a|\nu\rangle \frac{\lambda}{E_\nu - \omega_n}, \tag{3.47}$$

where we assumed that $E_\nu \neq \omega_n$. In fact, we will see that this condition is always satisfied. By plugging Eq. (3.47) into Eq. (3.45) we get the eigenvalue equation

$$E_\nu - \omega_a = \lambda^2 \sum_n \frac{1}{E_\nu - \omega_n}. \tag{3.48}$$

By using the definition (3.28) and the formula (Gradshteyn and Ryzhik [1994], 1.421 3)

$$\sum_{n=-\infty}^{+\infty} \frac{1}{x-n} = \pi \cot(\pi x), \tag{3.49}$$

Eq. (3.48) reads

$$E_\nu - \omega_a = \frac{\lambda^2 \pi}{\delta\omega} \cot\left(\frac{\pi E_\nu}{\delta\omega}\right). \tag{3.50}$$

Therefore the eigenvalues are given by the intersection between the line $y = x - \omega_a$ and the curve $(\lambda^2\pi/\delta\omega)\cot(\pi x/\delta\omega)$ as shown in Fig. 3.3. It is apparent that the eigenvalues E_ν are interspersed among (and never coincide with) the unperturbed eigenvalues ω_n, i.e., $\omega_n < E_\nu < \omega_{n+1}$.

By making use of Eq. (3.47) and of the normalization condition for the state $|\nu\rangle$ we get

$$1 = |\langle a|\nu\rangle|^2 + \sum_n |\langle n|\nu\rangle|^2 = |\langle a|\nu\rangle|^2 \left(1 + \lambda^2 \sum_n \frac{1}{(E_\nu - \omega_n)^2}\right). \tag{3.51}$$

We can easily evaluate the sum in the previous equation by differentiation of formula (3.49)

$$\sum_{n=-\infty}^{+\infty} \frac{1}{(x-n)^2} = \pi^2(1+\cot^2 \pi x), \tag{3.52}$$

from which one obtains

$$\sum_n \frac{1}{(E_\nu - \omega_n)^2} = \frac{\pi^2}{\delta\omega^2}\left[1+\cot^2\left(\frac{\pi E_\nu}{\delta\omega}\right)\right]. \tag{3.53}$$

By the eigenvalue equation (3.50) we finally get

$$\sum_n \frac{1}{(E_\nu - \omega_n)^2} = \frac{\pi^2}{\delta\omega^2} + \left(\frac{E_\nu - \omega_a}{\lambda^2}\right)^2, \tag{3.54}$$

whence

$$|\langle a|\nu\rangle|^2 = \frac{\lambda^2}{(E_\nu-\omega_a)^2 + (\lambda^2\pi/\delta\omega)^2 + \lambda^2} = \delta\omega \frac{\gamma/2\pi}{(E_\nu-\omega_a)^2 + (\gamma/2)^2 + \lambda^2}, \tag{3.55}$$

where the definition (3.34) was used. By plugging Eq. (3.55) into Eq. (2.17), the spectral density function reads

$$\varpi_a(E) = \sum_\nu \delta(E-E_\nu)\ \delta\omega \frac{\gamma/2\pi}{(E_\nu-\omega_a)^2 + (\gamma/2)^2 + \lambda^2}, \tag{3.56}$$

which is nothing but a Lorentzian function of width $\sqrt{\gamma^2+4\lambda^2}$ sampled at the eigenenergies E_ν. As noted above the E_ν's are interspersed among the ω_n's, whence the level density is approximately $\rho = 1/\delta\omega$, for there is a state inside any energy interval (ω_n, ω_{n+1}) of size $\delta\omega$ (see Fig. 3.3).

Some comments are now in order. First of all, note that the condition on the mean energy value $\langle a|H|a\rangle = \omega_a < \infty$ is satisfied, but the Hamiltonian (3.21) is not lower bounded and the spectral density (3.56) extends between $-\infty$ and $+\infty$. In fact, the condition on $\langle|H|\rangle$ is not satisfied, for

$$\langle a|\ |H|\ |a\rangle = \int dE\ |E|\ \varpi_a(E) = \sum_\nu \delta\omega \frac{\gamma}{2\pi} \frac{|E_\nu|}{(E_\nu-\omega_a)^2 + (\gamma/2)^2 + \lambda^2} = \infty, \tag{3.57}$$

is divergent, being a positive series with terms of order $1/\nu$. Therefore the time derivative of the survival probability at the origin is discontinuous and nonvanishing, $\dot{P}(0^\pm) = \pm\gamma$, with a decay rate $\gamma > 0$.

On the other hand, the spectrum is discrete, whence $|a\rangle$ is not a truly unstable state and Eq. (2.51) does not hold. In fact, as noted above, the exponential law holds only for a time interval $T = 2\pi\rho$. The last sum in the survival amplitude (3.37) modifies the exponential decay, which is eventually superseded, and the initial state is repopulated accordingly to the recurrence theorem proved in Sec. 2.4.1. See Fig. 3.4. In our case the Poincaré time is obviously proportional to the density ρ and becomes larger and larger by decreasing the level spacing $\delta\omega$, i.e., by enlarging the box volume.

In order to obtain a purely exponential decay for all times, only the first term in the survival amplitude (3.37) must contribute. To this end, since the other terms are proportional to $\theta(t-nT)$, with $T = 2\pi\rho$, the level density $\rho = 1/\delta\omega$ should be increased, by keeping the decay rate $\gamma = 2\pi\lambda^2\rho$ constant. In the $\rho \to \infty$ limit, i.e. by letting the box volume become infinite, the initial state $|a\rangle$ will decay into a flat continuum of states and we expect a purely exponential decay.

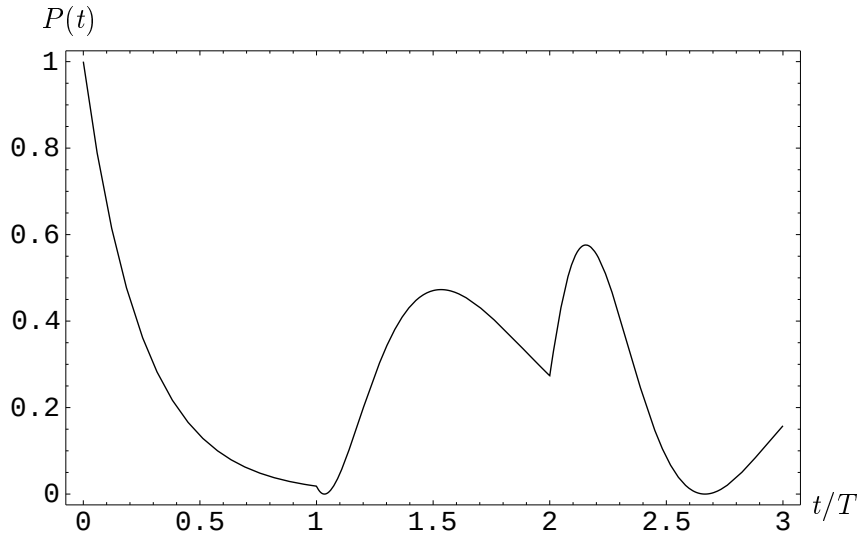

Figure 3.4: Time evolution of the survival probability $P(t) = |\mathcal{A}(t)|^2$. We chose $\omega_a = 0$ and $\gamma = 4/T$.

3.4 Continuum limit

By performing the $\delta\omega \to 0$ limit in Eq. (3.28) we get a continuous spectrum. We now want to examine in detail the rescaling and limiting procedure of the Hamiltonian (3.21).

First, consider the rescaled states $|\omega_n\rangle = (\delta\omega)^{-1/2}|n\rangle$. The orthonormality condition (3.22) becomes

$$\langle\omega_n|\omega_{n'}\rangle = \frac{\delta_{n,n'}}{\delta\omega} \longrightarrow \langle\omega|\omega'\rangle = \delta(\omega - \omega'). \tag{3.58}$$

In this limit the Hamiltonian (3.21) becomes

$$\begin{aligned} H &= \omega_a|a\rangle\langle a| + \sum_n \delta\omega\ \omega_n|\omega_n\rangle\langle\omega_n| + \frac{\lambda}{\delta\omega^{1/2}}\sum_n \delta\omega(|a\rangle\langle\omega_n| + |\omega_n\rangle\langle a|) \\ &\longrightarrow \omega_a|a\rangle\langle a| + \int d\omega\ \omega|\omega\rangle\langle\omega| + \tilde{\lambda}\int d\omega(|a\rangle\langle\omega| + |\omega\rangle\langle a|), \end{aligned} \tag{3.59}$$

where we are forced to keep $\tilde{\lambda} = \lambda/\delta\omega^{1/2}$ finite, in order to avoid an explosive interaction term in the $\delta\omega \to 0$ limit. But this is exactly what we required in the final discussion of the last section in order to get a finite decay rate (3.34). In other words, this is a natural ingredient of the continuum limit.

Notice that in the rescaling procedure the quantity $\delta\omega$ plays the role of infinitesimal integration interval and a Riemann integral is built up in the limit

$$\sum_n f_n\delta\omega \longrightarrow \int f(\omega)d\omega. \tag{3.60}$$

Now the procedure is straightforward: the receipt is simply to substitute sums with integrals. The state of the system at time t reads

$$|\psi(t)\rangle = \mathcal{A}(t)|a\rangle + \int d\omega\ b(\omega,t)|\omega\rangle, \tag{3.61}$$

where $|\mathcal{A}(t)|^2 + \int d\omega |b(\omega,t)|^2 = 1$. The equations (3.24)-(3.25) become

$$i\dot{\mathcal{A}}(t) = \omega_a \mathcal{A}(t) + \tilde{\lambda} \int_{-\infty}^{\infty} d\omega\, b(\omega,t), \tag{3.62}$$

$$i\dot{b}(\omega,t) = \omega b(\omega,t) + \tilde{\lambda}\mathcal{A}(t). \tag{3.63}$$

Equation (3.63) with the initial condition $b(\omega,0) = 0$ is integrated to give

$$b(\omega,t) = -i\tilde{\lambda} \int_0^t dt_1 e^{-i\omega(t-t_1)} \mathcal{A}(t_1), \tag{3.64}$$

and Eq. (3.62) reads

$$\dot{\mathcal{A}}(t) = -i\omega_a \mathcal{A}(t) - \tilde{\lambda}^2 \int_0^t dt_1 \mathcal{A}(t_1) \int_{-\infty}^{\infty} d\omega\, e^{-i\omega(t-t_1)}. \tag{3.65}$$

By using again the prescription $\int_0^{t_0} \delta(t)dt = 1/2$ $(t_0 > 0)$ [see Eq. (3.32)], we easily obtain

$$\begin{aligned} \dot{\mathcal{A}}(t) &= -i\omega_a \mathcal{A}(t) - \tilde{\lambda}^2 \int_0^t dt_1 \mathcal{A}(t_1) 2\pi\delta(t-t_1) \\ &= -\left(\frac{\gamma}{2} + i\omega_a\right) \mathcal{A}(t), \\ &\qquad \text{with} \quad \gamma = 2\pi\tilde{\lambda}^2 = \lim_{\substack{\lambda\to 0 \\ \rho\to\infty}} 2\pi\lambda^2\rho. \end{aligned} \tag{3.66}$$

The solution is a pure exponential decay at all times

$$\mathcal{A}(t) = \exp\left[-\left(\frac{\gamma}{2} + i\omega_a\right) t\right]. \tag{3.67}$$

Let us now evaluate the spectral density. By noting that

$$\omega_n < E_\nu < \omega_{n+1} \longrightarrow \omega \le E_\nu \le \omega, \qquad \text{for} \quad \delta\omega \to 0, \tag{3.68}$$

i.e., $E_\nu = \omega$ in the limit, and that we must require $\lambda \to 0$, the spectral density (3.56) becomes

$$\varpi_a(E) = \int d\omega\, \delta(E-\omega)\, \frac{\gamma}{2\pi} \frac{1}{(\omega-\omega_a)^2 + (\gamma/2)^2} = \frac{\gamma}{2\pi} \frac{1}{(E-\omega_a)^2 + (\gamma/2)^2}, \tag{3.69}$$

which, as expected, is a Lorentzian function, the Fourier transform of the exponential.

Note that we could obtain the eigenstates of H and the spectral density directly from the continuum Hamiltonian (3.59), by following a procedure analogous to that followed in Sec. 3.3.1. In fact this is a very instructive derivation (Fano [1961]), for it must deal with the singularity arising from the inversion of the continuum-limit version of Eq. (3.46). [Loosely speaking, in the continuum limit the energies E_ν coincide with the unperturbed energies ω_n, as shown by Eq. (3.68), and one has to apply distributions theory.]

The comments made after Eq. (3.56) for the discrete case are also valid for its continuum version. The expectation value $\langle H \rangle = \omega_a$ is finite, but the spectrum is not lower bounded, and $\langle |H| \rangle$ is infinite. Whence the decay rate does not vanish at $t = 0$. On the other hand in the continuum limit, the state $|a\rangle$ becomes a truly unstable state, and no recurrence phenomena take place. Moreover Paley-Wiener's inequality (2.52) does not hold, for the spectrum is not lower bounded, and the exponential decay holds at all times. Some long-living resonances can be well approximated by a Breit-Wigner distribution (3.69) and the effectiveness of Paley-Wiener's

theorem is more and more reduced by increasing the available energy $E_a - E_g$ ($E_a = \omega_a =$ initial state energy). On the other hand, a near-threshold unstable system exhibits deviations from exponential decay for not extremely long times.

The main conclusion of the above analysis is that the discrete-spectrum Hamiltonian (3.21) yields *exactly* the same dynamics of the continuum-spectrum Hamiltonian (3.59) for a time interval $T = 2\pi/\delta\omega$ inversely proportional to the level spacing, i.e. directly proportional to some power of the box length. Therefore a system enclosed in a sufficiently large box (namely, every physical system in a lab) is "practically" a truly unstable system up to times T. This is the physical definition of "infinite" volume.

Chapter 4

Nonperturbative analysis

4.1 Introduction

In order to understand in detail the temporal behavior of quantum systems, it is necessary to introduce nonperturbative techniques, that take into account the role of the interaction at all orders in the coupling constant. In section 2.4.1 we have seen that a spatially confined quantum system exhibits a recurrence phenomenon and has a finite Poincaré time, whence, in order to get a truly unstable system, one needs a continuous energy spectrum. In this case, by perturbation theory, one can calculate an exponential decay with constant decay rate γ, given by the Fermi Golden Rule. But the perturbative result $P(t) \simeq \exp(-\gamma t)$ is not completely satisfactory, for its derivation is valid in a region shorter than the lifetime, where the decay probability is approximately unity. On the other hand, one always observes an exponential decay rate at times much larger than the lifetime. Therefore one is led to ask what are the theoretical reasons of such a well established experimental law. In this chapter, by using a nonperturbative approach, we will tackle this problem and will understand that, for a small coupling constant, the decay is very well approximated by an exponential for times much larger than the lifetime, before the deviations at large times given by Paley-Wiener's theorem (2.52) become effective. We will derive the exponential decay law (with a decay rate given by the Fermi Golden Rule) and the corrections at short and long times. We will see that there is a profound link between the properties of the temporal evolution operator and the analytical properties of its Fourier-Laplace transform, the resolvent operator, in the complex energy plane. In particular, we will see that the resolvent has a branch cut along the continuous spectrum of the total Hamiltonian H and that the exponential decay law is due to the presence of a pole (close to the cut in the second Riemann sheet of the complex energy plane) which dominates the temporal behavior at intermediate times. All corrections are only due to the branch cut and become effective at short and long times.

4.2 The resolvent

We introduce the resolvent of the Hamiltonian and its perturbative expansion and set up the notation to tackle the problem of quantum decay with nonperturbative techniques. We will see in the next section that the resolvent is related to the temporal evolution operator by a Fourier-Laplace transform. The use of the resolvent in the study of some nonperturbative properties of quantum systems was first introduced by Kato [1949]. We will use the same notation of Messiah [1961], Vol. II, Cap. XVI.

The resolvent of an operator H is the function of the complex variable E defined as

$$G(E) = \frac{1}{E - H}. \tag{4.1}$$

The resolvent G is a bounded operator for every complex value of E with the exception of the eigenvalues of H. Notice that if H is hermitian, its eigenvalues are real. Let $\triangle(E)$ be the distance between E and the closest eigenvalue of H . The norm of the resolvent satisfies the relation

$$\|G(E)\| = \frac{1}{\triangle(E)}. \tag{4.2}$$

Consider a Hamiltonian H with a purely discrete spectrum of distinct eigenvalues

$$E_0(= E_g), E_1, \ldots, E_j, \ldots .$$

Assume, on physical ground, that the spectrum is lower bounded. Let P_j be the projection operator on the subspace belonging to E_j:

$$HP_j = E_j P_j. \tag{4.3}$$

The following relations of orthogonality and closeness hold

$$P_j P_k = \delta_{jk} P_j, \quad \sum_j P_j = 1. \tag{4.4}$$

From Eq. (4.1) one gets

$$G(E)P_j = \frac{P_j}{E - E_j}, \tag{4.5}$$

whence

$$G(E) = \sum_j \frac{P_j}{E - E_j}. \tag{4.6}$$

An eigenvalue of H is therefore a simple pole of G and one gets

$$P_j = \frac{1}{2\pi i} \oint_{\Gamma_j} G(E) dE, \tag{4.7}$$

where Γ_j is a closed anticlockwise contour in the complex E plane around point E_j and does not contain any other eigenvalue of H. The projection P_j is therefore the residue of G at the pole E_j. In general, if the contour Γ encloses a (countable) set S of eigenvalues E_s, one gets

$$P_\Gamma = \sum_{s \in S} P_s = \frac{1}{2\pi i} \oint_\Gamma G(E) dE. \tag{4.8}$$

It is easy to prove that

$$(E - H)G = G(E - H) = 1, \tag{4.9}$$

whence, from Eq. (4.8),

$$HP_\Gamma = \frac{1}{2\pi i} \oint_\Gamma E G(E) dE. \tag{4.10}$$

Let us write, as usual, the Hamiltonian operator as a sum of two terms $H = H_0 + H_{\rm int}$, where H_0 is the free Hamiltonian and $H_{\rm int}$ the interaction one. We can define

$$G(E) = \frac{1}{E - H_0 - H_{\rm int}}, \quad G_0(E) = \frac{1}{E - H_0} \tag{4.11}$$

and it is easy to prove that G satisfies the identity

$$G(E) = G_0(E)\left(1 + H_{\rm int}G(E)\right), \tag{4.12}$$

whose iteration yields

$$\begin{aligned} G &= G_0 + G_0H_{\rm int}G_0 + G_0H_{\rm int}G_0H_{\rm int}G_0 + \cdots \\ &= G_0\sum_{n=0}^{\infty}\left(H_{\rm int}G_0\right)^n. \end{aligned} \tag{4.13}$$

Explicitly,

$$\begin{aligned} G(E) &= \frac{1}{E-H_0} + \frac{1}{E-H_0}H_{\rm int}\frac{1}{E-H_0} \\ &\quad + \frac{1}{E-H_0}H_{\rm int}\frac{1}{E-H_0}H_{\rm int}\frac{1}{E-H_0} + \cdots. \end{aligned} \tag{4.14}$$

From the property (4.2), the series (4.13)-(4.14) converges absolutely for $\|H_{\rm int}\| < \|G_0\|^{-1} = \triangle_0(E)$, where $\triangle_0(E)$ is the distance between E and the closest eigenvalue of H_0 . By using this approach, we can therefore put forward rigorous statements about the convergence conditions of the perturbative expansion.

4.3 Fourier-Laplace transform

Our main interest in the resolvent is due to its link with the temporal evolution operator $U(t) = \exp(-iHt)$. The following operatorial relations hold

$$U(t) = \frac{i}{2\pi}\int_\Gamma e^{-iEt}\frac{1}{E-H}dE = \frac{i}{2\pi}\int_\Gamma e^{-iEt}G(E)dE, \tag{4.15}$$

$$G(E) = -i\int_0^{\eta\,\infty} e^{iEt}e^{-iHt}dt = -i\int_0^{\eta\,\infty} e^{iEt}U(t)dt, \tag{4.16}$$

where E is a complex variable, Γ a clockwise contour around all singularities of the resolvent, i.e., around the spectrum of H, and $\eta = \text{sign}(\text{Im}E)$.

For $t > 0$, the integral (4.16) converges for $\text{Im}E > 0$ ($\eta = +1$) and $G(E)$ can be written as a Fourier-Laplace transform

$$U(t)\theta(t) = \frac{i}{2\pi}\int_B dE\; e^{-iEt}\frac{1}{E-H} = \frac{i}{2\pi}\int_B dE\; e^{-iEt}G(E), \tag{4.17}$$

$$G(E) = -i\int_0^{\infty} dt\; e^{iEt}e^{-iHt} = -i\int_0^{\infty} dt\; e^{iEt}U(t)dt, \tag{4.18}$$

where the Bromwich path B is a horizontal line $\text{Im}E = \text{const} > 0$ in the half plane of convergence of the Fourier-Laplace transform (4.18) (upper half-plane). The link with Eqs. (4.15)-(4.16) is apparent: the Bromwich path B is above all the singularities of the resolvent (they are all real. See fig. 4.1). For $t > 0$, we can close the contour in the lower half plane $\text{Im}E < 0$ such that all singularities are enclosed. On the other hand, for $t < 0$ the contour is closed in the upper plane $\text{Im}E > 0$, where there are no singularities and the result is null. Therefore, the integration of the Fourier-Laplace transform (4.18) goes from 0 to $+\infty$, for the evolution operator vanishes for negative times.

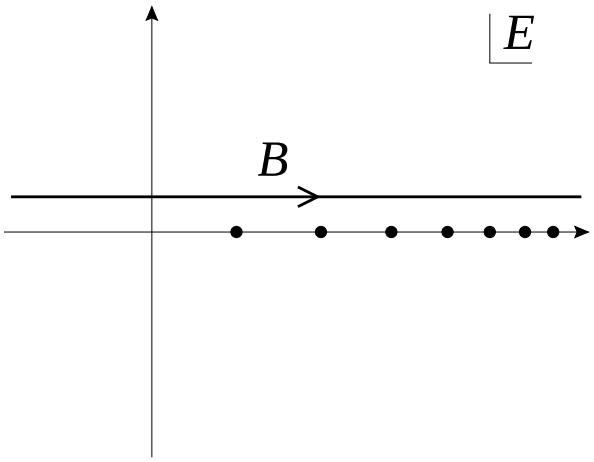

Figure 4.1: Singularities of $G_0(E)$ or $G(E)$ for a discrete spectrum and integration path B.

We now show that the resolvent identity (4.12) and its perturbative expansion correspond in the time domain to an integral equation for the time evolution operator and to Dyson's expansion, respectively. Remember that the ordinary product of two transforms corresponds to a convolution product in the time domain, namely

$$\widetilde{f}(E)\,\widetilde{g}(E) \longleftrightarrow \int_0^t d\tau\; f(t-\tau)g(\tau), \tag{4.19}$$

where $\widetilde{f}(E)$ e $\widetilde{g}(E)$ are the Fourier-Laplace transforms of $f(t)$ e $g(t)$. By using Eq. (4.19), Eq. (4.12) becomes

$$U(t) = U_0(t) - i\int_0^t d\tau U_0(t-\tau)H_{\rm int}U(\tau), \tag{4.20}$$

where $U_0(t) = \exp(-iH_0t)$. By multiplying to the left with $U_0^\dagger(t) = U_0(-t)$ and inserting the unity $1 = U_0(\tau)U_0^\dagger(\tau)$ between $H_{\rm int}$ and $U(\tau)$ one gets

$$U_0^\dagger(t)U(t) = 1 - i\int_0^t d\tau U_0^\dagger(\tau)H_{\rm int}U_0(\tau)U_0^\dagger(\tau)U(\tau), \tag{4.21}$$

whence

$$U_{\rm I}(t) = 1 - i\int_0^t d\tau H_{\rm int}(\tau)U_{\rm I}(\tau), \tag{4.22}$$

where $H_{\rm int}(t) = e^{iH_0t}H_{\rm int}e^{-iH_0t}$ and $U_{\rm I}(t) = e^{iH_0t}e^{-iHt}$. This is the usual integral equation for the time evolution operator in the interaction picture, yielding Dyson's perturbative expansion

$$\begin{aligned} U_{\rm I}(t) &= \sum_{n=0}^{\infty}(-i)^n\int_0^t dt_1\int_0^{t_1}dt_2...\int_0^{t_{n-1}}dt_nH_{\rm int}(t_1)H_{\rm int}(t_2)...H_{\rm int}(t_n) \\ &= T\exp\left(-i\int_0^t d\tau\; H_{\rm int}(\tau)\right), \end{aligned} \tag{4.23}$$

with T the time ordering operator.

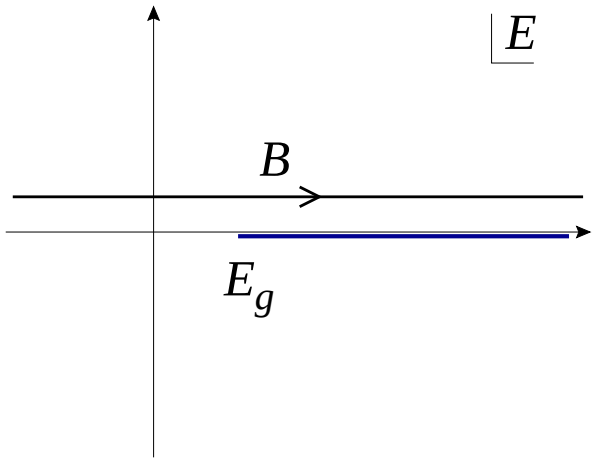

Figure 4.2: Singularities of $G_a(E)$ for a continuous spectrum. The branch cut is placed on the spectrum of H.

4.4 Dyson resummation

Consider a Hamiltonian $H = H_0 + H_{\rm int}$. Let $\{|n\rangle\}$ be a complete orthonormal set of eigenvectors of the free Hamiltonian H_0. One gets

$$H_0|n\rangle = E_n|n\rangle, \qquad 1 = \sum_n |n\rangle\langle n|. \tag{4.24}$$

At $t = 0$, the system is represented by the state $|a\rangle$, which is not an eigenstate of the total Hamiltonian. (In this case the evolution is a trivial phase.) We assume, for simplicity, that $|a\rangle$ is an eigenstate of H_0. This is not a restrictive assumption and it is natural. On the other hand, notice that we can always define a free Hamiltonian, whose eigenstate is $|a\rangle$.

We have seen in the previous section that the unitary operators $U_0(t) = e^{-iH_0 t}$ and $U(t) = e^{-iHt}$ are related to the resolvents by Fourier-Laplace transforms for $t > 0$

$$\begin{aligned} U_0(t) &= \frac{i}{2\pi}\int_B dE\; e^{-iEt} G_0(E), \qquad G_0(E) = \frac{1}{E - H_0}\;, \\ U(t) &= \frac{i}{2\pi}\int_B dE\; e^{-iEt} G(E), \qquad G(E) = \frac{1}{E - H}\;, \end{aligned} \tag{4.25}$$

where the Bromwich path B is shown in Fig. 4.1. If we consider a system enclosed in a box of volume V, then H_0 and H have a discrete spectrum, whence the singularities of $G_0(E)$ and $G(E)$ are simple poles placed on the real axis from the ground-state energies $E_g^{(0)}$ and E_g up to $+\infty$. The survival amplitude reads

$$\mathcal{A}(t) = \langle a|U(t)|a\rangle = \frac{i}{2\pi}\int_B dE\; e^{-iEt} G_a(E), \qquad G_a(E) \equiv \langle a|G(E)|a\rangle. \tag{4.26}$$

By inserting a complete set $\{|\lambda\rangle\}$ of eigenstates of the total Hamiltonian H

$$H|\lambda\rangle = E_\lambda|\lambda\rangle, \qquad \sum_\lambda |\lambda\rangle\langle\lambda| = 1, \tag{4.27}$$

one gets

$$G_a(E) = \sum_\lambda \langle a|\lambda\rangle\langle\lambda|\frac{1}{E - H}|a\rangle = \sum_\lambda \frac{|\langle a|\lambda\rangle|^2}{E - E_\lambda}, \tag{4.28}$$

where the positions of the poles of the propagator are apparent. Consider now the $V \to \infty$ limit: the discrete energy spectrum becomes continuous and the poles of $G_a(E)$ shrink into a continuous line. Therefore there is a branching point at E_g and a cut $[E_g, +\infty)$. By inserting the unity $\int dE\delta(E - E_\lambda) = 1$, Eq. (4.28) reads

$$G_a(E) = \int_{-\infty}^{\infty} dE' \sum_\lambda \frac{|\langle a|\lambda\rangle|^2}{E - E'}\delta(E' - E_\lambda) = \int_{E_g}^{\infty} dE' \frac{\varpi_a(E')}{E - E'}, \tag{4.29}$$

where

$$\varpi_a(E) = \sum_\lambda |\langle a|\lambda\rangle|^2 \delta(E - E_\lambda) \geq 0, \tag{4.30}$$

is the spectral density function. Therefore the propagator $G_a(E)$ is an analytic function in the whole cut E plane (see Fig. 4.2).

4.4.1 Diagrammatics

By taking the expectation value on $|a\rangle$ of the perturbative expansion (4.13) one gets

$$\begin{aligned} G_a(E) &= G_a^0(E) + G_a^0 V_{aa} G_a^0 + \sum_n G_a^0 V_{an} G_n^0 V_{na} G_a^0 \\ &\quad + \sum_{n,n'} G_a^0 V_{an} G_n^0 V_{nn'} G_{n'}^0 V_{n'a} G_a^0 + \cdots, \end{aligned} \tag{4.31}$$

where

$$G_n^0(E) \equiv \langle n|G_0(E)|n\rangle = \frac{1}{E - E_n} \quad \text{and} \quad V_{nn'} \equiv \langle n|H_{\text{int}}|n'\rangle. \tag{4.32}$$

Equation (4.31) can be represented by the diagram in Fig. 4.3a. The complete propagator $G_a(E)$ is represented by a bold line and the free propagator $G_a^0(E)$ by a thin line. The interaction $V_{nn'}$ corresponds to an X and the free propagator of the decayed states $G_n^0(E)$ corresponds to three parallel lines.

We are searching for a closed expression of the expansion (4.31). To this end we put together all diagrams in Fig. 4.3a according to the number of thin lines $G_a^0(E)$, i.e., to the power of the pole at $E = E_a$.

$$\begin{aligned} G_a(E) &= G_a^0 + G_a^0 V_{aa} G_a^0 + \sum_{n\neq a} G_a^0 V_{an} G_n^0 V_{na} G_a^0 + \sum_{n,n'\neq a} G_a^0 V_{an} G_n^0 V_{nn'} G_{n'}^0 V_{n'a} G_a^0 \\ &\quad + G_a^0 V_{aa} G_a^0 V_{aa} G_a^0 + \sum_{n\neq a} G_a^0 V_{an} G_n^0 V_{na} G_a^0 V_{aa} G_a^0 + \sum_{n\neq a} G_a^0 V_{aa} G_a^0 V_{an} G_n^0 V_{na} G_a^0 \\ &\quad + G_a^0 V_{aa} G_a^0 V_{aa} G_a^0 V_{aa} G_a^0 \\ &\quad + \cdots \\ &= G_a^0 + G_a^0 \left[V_{aa} + \sum_{n\neq a} V_{an} G_n^0 V_{na} + \sum_{n,n'\neq a} V_{an} G_n^0 V_{nn'} G_{n'}^0 V_{n'a} + \cdots \right] G_a^0 \\ &\quad + G_a^0 \left[V_{aa} + \sum_{n\neq a} V_{an} G_n^0 V_{na} + \cdots \right] G_a^0 \left[V_{aa} + \sum_{n\neq a} V_{an} G_n^0 V_{na} + \cdots \right] G_a^0 \\ &\quad + G_a^0 \Big[V_{aa} + \cdots \Big] G_a^0 \Big[V_{aa} + \cdots \Big] G_a^0 \Big[V_{aa} + \cdots \Big] G_a^0 \\ &\quad + \cdots . \end{aligned} \tag{4.33}$$

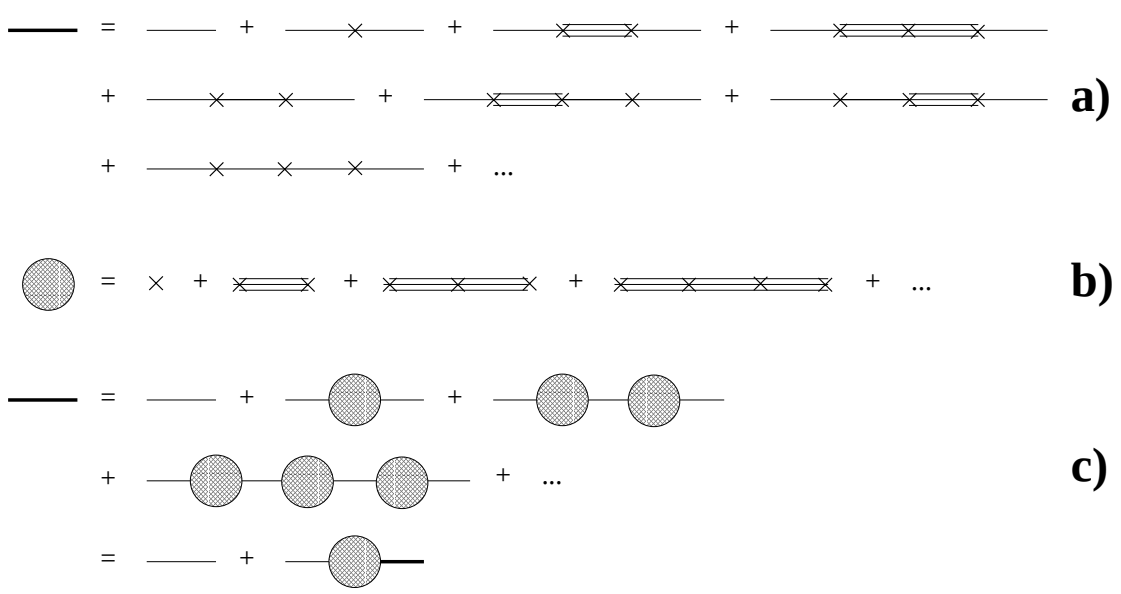

Figure 4.3: Diagrammatic representation of Eqs. (4.31)-(4.35): a) total propagator $G_a(E)$, Eq. (4.31); b) self-energy function $\Sigma_a(E)$, Eq. (4.34); c) Dyson resummation of a), Eq. (4.35).

By resumming, we get the *self-energy* function

$$\begin{aligned}\Sigma_a(E) &= V_{aa} + \sum_{n\neq a} V_{an} G_n^0(E) V_{na} + \sum_{n,n'\neq a} V_{an} G_n^0(E) V_{nn'} G_{n'}^0(E) V_{n'a} + \cdots \\ &= V_{aa} + \sum_{n\neq a} V_{an} \frac{1}{E-E_n} V_{na} + \sum_{n,n'\neq a} V_{an} \frac{1}{E-E_n} V_{nn'} \frac{1}{E-E_{n'}} V_{n'a} + \cdots \end{aligned} \quad (4.34)$$

which represents all possible intermediate states of the total propagator $G_a(E)$ that do not contain the free propagator $G_a^0(E) = 1/(E-E_a)$ and the pole in $E = E_a$. Represent $\Sigma_a(E)$ with a blob in Fig. 4.3b. We can now express $G_a(E)$ in terms of $\Sigma_a(E)$, as in Fig. 4.3c, namely

$$\begin{aligned} G_a(E) &= G_a^0(E) + G_a^0(E)\, \Sigma_a(E)\, G_a^0(E) \\ &\quad + G_a^0(E)\, \Sigma_a(E)\, G_a^0(E)\, \Sigma_a(E)\, G_a^0(E) + \cdots \\ &= G_a^0(E) + G_a^0(E)\, \Sigma_a(E)\, G_a(E). \end{aligned} \quad (4.35)$$

The above equation is a purely algebraic one and is immediately solved

$$G_a(E) = \frac{1}{G_a^0(E)^{-1} - \Sigma_a(E)} = \frac{1}{E - E_a - \Sigma_a(E)}, \quad (4.36)$$

where the link between the total propagator $G_a(E)$ and the self-energy function $\Sigma_a(E)$ is apparent.

Note that the analytical properties of the self-energy function derive from the properties of the propagator we outlined after Eq. (4.30). Indeed $\Sigma_a(E)$ has obviously the same branch cut of $G_a(E)$ in $[E_g, +\infty)$. Moreover $\Sigma_a(E)$ is an analytic function in the cut E plane, for a pole of $\Sigma_a(E)$ corresponds to a zero of $G_a(E)$. But, by taking the real and imaginary part of Eq. (4.29), it is easy to show that the propagator never vanishes in the cut plane. Therefore the self-energy function can be written in the same form as the propagator (4.29):

$$\Sigma_a(E) = \int_{E_g}^{\infty} dE' \, \frac{\kappa_a(E')}{E - E'} \, , \quad (4.37)$$

with a (positive: see Eq. (4.60) below) spectral density function $\kappa_a(E) \geq 0$.

4.4.2 Operator derivation

Consider the operator identity (4.9) when the total Hamiltonian is written as a sum $H = H_0 + H_{\rm int}$

$$(E - H_0 - H_{\rm int})\, G(E) = 1. \tag{4.38}$$

Introduce a (not necessarily one dimensional) orthogonal projection P_a, which commutes with H_0, i.e.

$$[H_0, P_a] = 0. \tag{4.39}$$

The projection P_a represents the subspace $\mathcal{H}_a$ of the initial "undecayed" states and is spanned by a subset of eigenvectors of the free Hamiltonian H_0. Of course, when $\mathcal{H}_a$ is one dimensional P_a reduces to $P_a = |a\rangle\langle a|$ and $H_0 P_a = E_a P_a$. The orthogonal subspace $\mathcal{H}_d = \mathcal{H}_a^{\perp}$ contains the decay products and is represented by the projection $P_d = 1 - P_a$. Note that the total Hilbert space $\mathcal{H}$ is decomposed in a direct sum $\mathcal{H} = \mathcal{H}_a \oplus \mathcal{H}_d$

Multiplying Eq. (4.38) by P_a or P_d to the left and by P_a to the right and by inserting the identity $1 = P_a + P_d$ just before $G(E)$ in the l.h.s. one gets (Cohen-Tannoudji, Dupont-Roc and Grynberg [1998])

$$(E - P_a H P_a)\; P_a G(E) P_a - P_a H_{\rm int} P_d\; P_d G(E) P_a = P_a, \tag{4.40}$$

$$-P_d H_{\rm int} P_a\; P_a G(E) P_a + (E - P_d H P_d)\; P_d G(E) P_a = 0, \tag{4.41}$$

which are two coupled linear equations for $P_a G(E) P_a$ and $P_d G(E) P_a$. Equation (4.41) can be immediately solved

$$P_d G(E) P_a = \frac{P_d}{E - P_d H P_d} H_{\rm int} P_a\; P_a G(E) P_a \tag{4.42}$$

and, substituting into Eq. (4.40), one gets

$$\left(E - P_a H_0 P_a - P_a H_{\rm int} P_a - P_a H_{\rm int} \frac{P_d}{E - P_d H P_d} H_{\rm int} P_a \right)\; P_a G(E) P_a = P_a. \tag{4.43}$$

By introducing the *level shift operator* (Goldberger and Watson [1964])

$$R(E) = H_{\rm int} + H_{\rm int} \frac{P_d}{E - P_d H P_d} H_{\rm int} \tag{4.44}$$

into Eq. (4.43) and solving, we finally get the restricted propagator to the initial subspace $\mathcal{H}_a$

$$P_a G(E) P_a = \frac{P_a}{E - P_a H_0 P_a - P_a R(E) P_a}. \tag{4.45}$$

This is the operator version of Eq. (4.36). It generalizes Eq. (4.36) for a generic orthogonal projection P_a and reduces to it when $P_a = |a\rangle\langle a|$ is one dimensional. Indeed, in this case one gets

$$P_a G(E) P_a = \frac{P_a}{E - E_a - \langle a|R(E)|a\rangle}. \tag{4.46}$$

On the other hand, a perturbative expansion of the level shift operator (4.44) reads

$$\begin{aligned} R(E) &= H_{\rm int} + H_{\rm int} \frac{P_d}{E - H_0} H_{\rm int} + H_{\rm int} \frac{P_d}{E - H_0} H_{\rm int} \frac{P_d}{E - H_0} H_{\rm int} + \cdots \\ &= H_{\rm int} + H_{\rm int} \frac{P_d}{E - H_0} R(E). \end{aligned} \tag{4.47}$$

It is apparent that $R(E)$ contains as intermediate states only the decayed ones, given by the projector P_d, and by taking the expectation value in the initial state $|a\rangle$ one obtains again Eq. (4.34). Therefore we can write

$$\Sigma_a(E) = \langle a|R(E)|a\rangle, \tag{4.48}$$

i.e., the self-energy function $\Sigma_a(E)$ is the expectation value in the initial state $|a\rangle$ of the level shift operator $R(E)$.

4.5 Off-diagonal decomposition

In the previous section we found that the total propagator $G_a(E)$ can be written as in Eq. (4.36) in terms of the self-energy function $\Sigma_a(E)$, which is in turn given by the perturbative expansion (4.34) or equivalently by the expectation value (4.48) of the level shift operator.

Consider, as usual, a Hamiltonian $H = H_0 + H_{\rm int}$ split in a free part H_0 and an interaction part $H_{\rm int}$. Choose the initial state $|a\rangle$ and consider the orthogonal projections

$$P_a = |a\rangle\langle a|, \qquad P_d = 1 - P_a \tag{4.49}$$

Now decompose the total Hamiltonian as (Peres [1980b])

$$H = H_0^a + H_{\rm int}^a, \tag{4.50}$$

where

$$H_0^a = P_a H P_a + P_d H P_d \qquad \text{and} \quad H_{\rm int}^a = P_a H P_d + P_d H P_a. \tag{4.51}$$

Notice that, if $|a\rangle$ is an eigenstate of H_0 with eigenvalue E_a, it is also an eigenstate of the new free Hamiltonian H_0^a, for we get

$$H_0^a|a\rangle = \left(E_a + \langle a|H_{\rm int}|a\rangle\right)|a\rangle. \tag{4.52}$$

The interesting feature of the decomposition (4.50) is that all diagonal contributions of the interaction $H_{\rm int}$ have been absorbed in the free Hamiltonian H_0^a, and only the off-diagonal terms with respect to the eigenstates of H_0 are contained in the new interaction $H_{\rm int}^a$. This is apparent by rewriting H_0^a and $H_{\rm int}^a$ in the following form

$$\begin{aligned} H_0^a &= H_0 + P_a H_{\rm int} P_a + P_d H_{\rm int} P_d, \\ H_{\rm int}^a &= P_a H_{\rm int} P_d + P_d H_{\rm int} P_a = H_{\rm int} - P_a H_{\rm int} P_a - P_d H_{\rm int} P_d. \end{aligned} \tag{4.53}$$

Moreover, notice that the only nonvanishing off-diagonal elements of $H_{\rm int}^a$ are those between $|a\rangle$ and $|n\rangle$ with $n \neq a$. In terms of matrix elements

$$\langle a|H_{\rm int}^a|a\rangle = \langle n|H_{\rm int}^a|n'\rangle = 0, \qquad \text{for} \quad n, n' \neq a. \tag{4.54}$$

Reconsider now the analysis of the previous section in terms of the new decomposition (4.50). The level shift operator (4.44) reads

$$R(E) = H_{\rm int}^a + H_{\rm int}^a \frac{P_d}{E - P_d H_0^a P_d} H_{\rm int}^a = H_{\rm int}^a + H_{\rm int}^a \frac{P_d}{E - H_0^a} H_{\rm int}^a, \tag{4.55}$$

i.e., the perturbative expansion (4.47) reduces *exactly* to the sum of the first two terms only. Therefore the self-energy function consists only of its second order contribution

$$\Sigma_a(E) = \langle a|R(E)|a\rangle = \langle a|H_{\rm int}^a \frac{P_d}{E - H_0^a} H_{\rm int}^a|a\rangle = \sum_{\tilde{n}\neq\tilde{a}} \frac{|\langle a|H_{\rm int}^a|\tilde{n}\rangle|^2}{E - \tilde{E}_n}, \tag{4.56}$$

where $|\tilde{n}\rangle$ are the eigenvectors of H_0^a with energies $\tilde{E}_n$, namely

$$H_0^a|\tilde{n}\rangle = \tilde{E}_n|\tilde{n}\rangle, \tag{4.57}$$

with, as noted above, $|\tilde{a}\rangle = |a\rangle$ and $\tilde{E}_a = E_a + \langle a|H_{\rm int}|a\rangle$. Incidentally, notice that (4.54) translates immediately into the new basis (Dirac [1958], Chap. 13; Messiah [1961], Chap. XXI)

$$\langle\tilde{a}|H_{\rm int}^a|\tilde{a}\rangle = \langle\tilde{n}|H_{\rm int}^a|\tilde{n}'\rangle = 0, \qquad \text{for} \quad \tilde{n},\tilde{n}' \neq \tilde{a}, \tag{4.58}$$

as it is apparent already in the far r.h.s. of Eq. (4.56).

Henceforth, if not otherwise stated, we will always consider the total Hamiltonian decomposed in a free and an interaction part as in Eq. (4.50) and we will consequently drop all superscripts a and all tildes.

A final comment is now in order. From Eq. (4.56) and Eq. (4.58) we get

$$\Sigma_a(E) = \sum_n \frac{|\langle a|H_{\rm int}|n\rangle|^2}{E - E_n} = \int_{E_g}^{\infty} dE' \, \frac{\kappa_a(E')}{E - E'}, \tag{4.59}$$

with

$$\kappa_a(E) = \sum_n |\langle a|H_{\rm int}|n\rangle|^2 \, \delta(E - E_n) = \langle a|H_{\rm int}\delta(E - H_0)H_{\rm int}|a\rangle \geq 0. \tag{4.60}$$

Thus we obtain again Eq. (4.37) and, as a byproduct, the definition of $\kappa_a(E)$ in terms of the initial state $|a\rangle$ and the Hamiltonian and the positivity condition mentioned after Eq. (4.37). By plugging the definitions (4.51) into Eq. (4.60) we get the alternative form

$$\kappa_a(E) = \langle a|HP_d \, \delta(E - P_dHP_d) \, P_dH|a\rangle. \tag{4.61}$$

Incidentally, notice that κ_a (whence Σ_a) are small quantities of order $\mathrm{O}(\lambda^2)$, λ being the coupling constant.

4.6 Analytical continuation of the propagator

Equation (4.59), together with Eq. (4.36), states that $G_a(E)$ has a branching point at $E = E_g$, a branch cut extending to $E = +\infty$ and no other singularities on the first Riemann sheet. However, it can happen that some singularities show up on the second sheet. The analytical properties of the propagator and its continuation into the second Riemann sheet were first studied by Peierls [1991], Sec. 5.3; Araki, Munakata, Kawaguchi and Goto [1957] and Schwinger [1960].

4.6.1 Analytical continuation of the self-energy function

We can evaluate the self-energy function across the cut by letting $E \to E \pm i0^+$ with E real. We get

$$\Sigma_a(E\pm i0^+) = \int_{E_g}^{\infty} dE' \frac{\kappa_a(E')}{E - E' + i0^+} = \mathrm{P}\int_{E_g}^{\infty} dE' \frac{\kappa_a(E')}{E - E'} \mp i\pi \int_{E_g}^{\infty} dE' \kappa_a(E')\delta(E - E'), \tag{4.62}$$

where P denotes the principal value. Therefore we can write

$$\Sigma_a(E \pm i0^+) = \Delta_a(E) \mp \frac{i}{2}\Gamma_a(E) \tag{4.63}$$

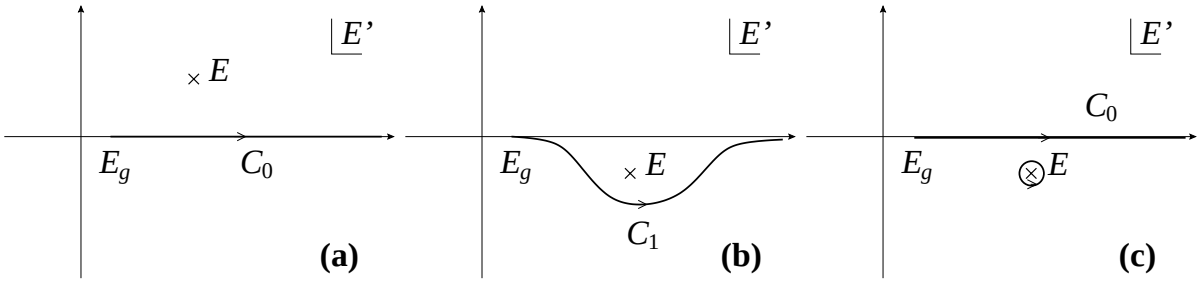

Figure 4.4: Integration path in the complex E' plane (a) for $\mathrm{Im}E > 0$ and (b) for $\mathrm{Im}E < 0$. The initial contour C_0 is placed on the real axis and starts from the ground state energy E_g. The new contour C_1 is deformed in order to keep $E' = E$ above it. (c) The contour C_1 can be deformed again into the initial contour C_0 and a small circle around the pole.

where

$$\Gamma_a(E) = 2\pi\kappa_a(E) \geq 0, \qquad \Delta_a(E) = \mathrm{P}\int_{-\infty}^{+\infty} \frac{dE'}{2\pi}\, \frac{\Gamma_a(E')}{E - E'} \tag{4.64}$$

are reciprocal Hilbert transforms. It is apparent that the discontinuity is purely imaginary and reads

$$\Sigma_a(E + i0^+) - \Sigma_a(E - i0^+) = -i\Gamma_a(E) = -2\pi i\kappa_a(E) \tag{4.65}$$

Notice that, in general, $\Sigma_a(E^*) = \Sigma_a(E)^*$.

Remember that the Fourier-Laplace transform $G_a(E)$ of the survival amplitude (4.26) is defined for $\mathrm{Im}E > 0$, in order to assure the convergence of Eq. (4.16) for $t > 0$. Therefore, the pole at $E' = E$ in the integral (4.59) is placed above the integration path in the complex E' plane. During the continuation process into the second Riemann sheet through the cut, the integration path must be modified so that the pole is always above it, as shown in Fig. 4.4. After the whole process, on the second Riemann sheet the self-energy function (4.59) will get an additional term

$$\Sigma_a(E) \longrightarrow \Sigma_{a\mathrm{II}}(E) = \int_{E_g}^{\infty} dE' \frac{\kappa_a(E')}{E - E'} - 2\pi i\kappa_a(E) = \Sigma_a(E) - 2\pi i\kappa_a(E)\ , \qquad E \in \mathbb{C}. \tag{4.66}$$

Note that the new term has in general a nonvanishing imaginary part and obviously represents the analytical continuation of the discontinuity of the self-energy function across the cut.

4.6.2 The pole in the second Riemann sheet

From Eq. (4.36), a pole E_{pole} of $G_a(E)$ on the second sheet must satisfy the equation

$$E_{\mathrm{pole}} = E_a + \Sigma_{a\mathrm{II}}(E_{\mathrm{pole}}), \tag{4.67}$$

where $\Sigma_{a\mathrm{II}}(E)$ is the determination (4.66) of the self-energy function in the second sheet. By setting

$$E_{\mathrm{pole}} = E_a + \Delta E - i\frac{\gamma}{2}, \tag{4.68}$$

one gets

$$\Delta E - i\frac{\gamma}{2} = \left[\Sigma_a(E) - 2\pi i\kappa_a(E)\right]_{E=E_a+\Delta E-i\frac{\gamma}{2}}, \tag{4.69}$$

whose imaginary and real part read

$$\frac{\gamma}{2}\left[1+\int_{E_g}^{\infty} dE \frac{\kappa_a(E)}{|E_a - E + \Delta E - i\frac{\gamma}{2}|^2}\right] = 2\pi \mathrm{Re}\Big[\kappa_a(E)\Big]_{E=E_a+\Delta E-i\frac{\gamma}{2}}, \tag{4.70}$$

$$\Delta E = \int_{E_g}^{\infty} dE \frac{(E_a - E + \Delta E)\kappa_a(E)}{|E_a - E + \Delta E - i\frac{\gamma}{2}|^2} + 2\pi \mathrm{Im}\Big[\kappa_a(E)\Big]_{E=E_a+\Delta E-i\frac{\gamma}{2}}. \tag{4.71}$$

By noting that

$$\lim_{\gamma\to 0} \frac{\gamma}{E^2+\frac{\gamma^2}{4}} = 2\pi\delta(E), \qquad \lim_{\gamma\to 0} \frac{E}{E^2+\frac{\gamma^2}{4}} = \frac{\mathrm{P}}{E}, \tag{4.72}$$

where P denotes the principal value, and remembering that $\kappa_a(E) = \mathrm{O}(\lambda^2)$, with λ coupling constant, we can solve perturbatively (for small λ) the above equations

$$\gamma = 2\pi\kappa_a(E_a) + \mathrm{O}(\lambda^4) = 2\pi \sum_n |\langle n|H_{\mathrm{int}}|a\rangle|^2 \,\delta(E_a - E_n) + \mathrm{O}(\lambda^4), \tag{4.73}$$

$$\Delta E = \mathrm{P}\int_{E_g}^{\infty} dE \frac{\kappa_a(E)}{E_a - E} + \mathrm{O}(\lambda^4) = \mathrm{P}\sum_n \frac{|\langle n|H_{\mathrm{int}}|a\rangle|^2}{E_a - E_n} + \mathrm{O}(\lambda^4), \tag{4.74}$$

which are respectively the Fermi Golden Rule (Fermi [1932]; Fermi [1950]; Fermi [1960]) and the level shift.

The procedure just shown (Nakazato, Namiki and Pascazio [1996]) is general (and historical), but involves limiting procedure like (4.72). It is also difficult to implement at higher orders in λ. For a general (and more practical) procedure, we note that $\Sigma_a(E)$ is $\mathrm{O}(\lambda^2)$, so that the pole can be found perturbatively: by expanding $\Sigma_{a\mathrm{II}}(E)$ around $E = E_a$ we get a power series

$$\Sigma_{a\mathrm{II}}(E) = \Sigma_{a\mathrm{II}}(E_a - i0^+) + \Sigma'_{a\mathrm{II}}(E_a - i0^+)\,(E - E_a) + \ldots, \tag{4.75}$$

whose radius of convergence is $R_c = E_a - E_g$ because of the branching point at $E = E_g$. The circle of convergence lies half on the first Riemann sheet and half on the second sheet, as shown in Fig. 4.5. For sufficiently small λ, the pole is well inside the convergence circle, because $|E_{\mathrm{pole}} - E_a| \sim \lambda^2 E_a \ll R_c$, and we can rewrite Eq. (4.67) as

$$E_{\mathrm{pole}} = E_a + \Sigma_a(E_a + i0^+) + \Sigma'_a(E_a + i0^+)(E_{\mathrm{pole}} - E_a) + \ldots, \tag{4.76}$$

where we used the fact that $\Sigma_{a\mathrm{II}}(E)$ is the analytical continuation of $\Sigma_a(E)$ below the branch cut, whence $\Sigma_{a\mathrm{II}}(E_a - i0^+) = \Sigma_a(E_a + i0^+)$. We can now iteratively solve Eq. (4.76) to obtain

$$E_{\mathrm{pole}} = E_a + \Sigma_a(E_a + i0^+) + \Sigma'_a(E_a + i0^+)\Sigma_a(E_a + i0^+) + \mathrm{O}(\lambda^6). \tag{4.77}$$

From Eq. (4.77) and Eq. (4.63) we get

$$\gamma = -2\,\mathrm{Im}\Big[\Sigma_a(E_a + i0^+)\Big] + \mathrm{O}(\lambda^4) = \Gamma_a(E_a) + \mathrm{O}(\lambda^4), \tag{4.78}$$

$$\Delta E = \mathrm{Re}\Big[\Sigma_a(E_a + i0^+)\Big] + \mathrm{O}(\lambda^4) = \Delta_a(E_a) + \mathrm{O}(\lambda^4), \tag{4.79}$$

which, by using the definition (4.64), yield again Eqs. (4.73)-(4.74). Therefore, for small coupling, there is a simple pole with negative imaginary part, placed in the second Riemann sheet in a neighborhood of $E = E_a$ of radius $\mathrm{O}(\lambda^2)$.

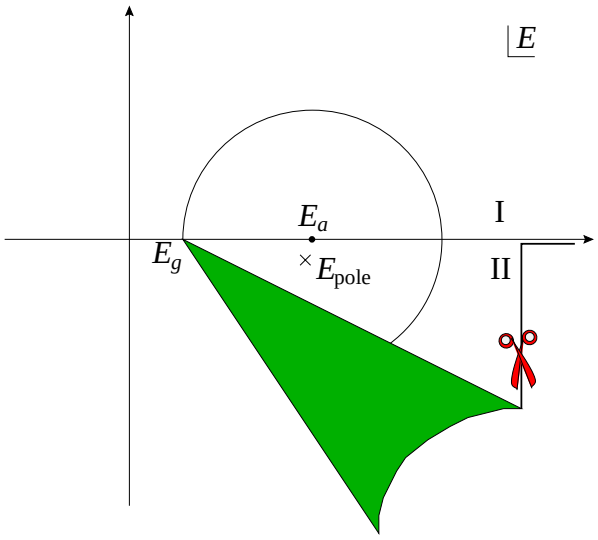

Figure 4.5: Cut and pole in the complex E-plane and convergence circle for the expansion of $\Sigma_a(E)$ around $E = E_a$. I and II are the first and second Riemann sheets, respectively. The pole is on the second Riemann sheet, at a distance $\mathrm{O}(\lambda^2)$ from E_a.

4.6.3 Lorentzian spectral density and Weisskopf-Wigner approximation

We now investigate the relationship between the propagator $G_a(E)$, and hence the self-energy function $\Sigma_a(E)$, and the spectral density function $\varpi_a(E)$. As we have seen, they yield two different representations of the survival amplitude $\mathcal{A}(t)$: Eq. (4.26) and Eq. (2.16), respectively. The link between this two representations is given by the dispersion relation (4.29), which expresses the propagator in terms of an integral over its discontinuity, the spectral density. In other words

$$G_a(E + i0^+) - G_a(E - i0^+) = -2i\pi\varpi_a(E), \qquad E \in \mathbb{R}. \tag{4.80}$$

By using the analytical property of the resolvent $G_a(E^*) = G_a(E)^*$ we get the relation we seek

$$\varpi_a(E) = \frac{i}{2\pi}[G_a(E + i0^+) - G_a(E + i0^+)^*] = -\frac{1}{\pi}\,\mathrm{Im}\Big[G_a(E + i0^+)\Big]. \tag{4.81}$$

The spectral density (4.81) can be given an interesting form in terms of the real and imaginary part of the self-energy function (4.63). One can write

$$\begin{aligned} \varpi_a(E) &= -\frac{1}{\pi}\,\mathrm{Im}\left[\frac{1}{E - E_a - \Delta_a(E) + i\frac{\Gamma_a(E)}{2}}\right] \\ &= \frac{\Gamma_a(E)}{2\pi}\,\frac{1}{\Big(E - E_a - \Delta_a(E)\Big)^2 + \Big(\frac{\Gamma_a(E)}{2}\Big)^2}\,, \end{aligned} \tag{4.82}$$

which has a Lorentzian form, with energy-dependent coefficients. It is apparent that if the two coefficients are slowly varying functions of energy within the peak of the Lorentzian, the decay is well approximated by an exponential law. A purely exponential decay is obtained by assuming constant coefficients (evaluated at E_a), namely

$$\varpi_a(E) = \frac{\Gamma_a(E_a)}{2\pi}\,\frac{1}{\Big(E - E_a - \Delta_a(E_a)\Big)^2 + \Big(\frac{\Gamma_a(E_a)}{2}\Big)^2}\,, \tag{4.83}$$

which is the Breit-Wigner spectrum (Breit and Wigner [1936]).

More generally, in order to obtain a purely exponential decay, one neglects all branch cut and/or other distant poles contributions, and considers only the dominant pole contribution. In other words, one does not look at the rich analytical structure of the propagator and retains only its pole singularity. In this case the self-energy function becomes a constant (equal to its value at the pole), namely

$$G_a(E) = \frac{1}{E - E_a - \Sigma_a(E)} \longrightarrow G_a^{\rm WW}(E) = \frac{1}{E - E_a - \Sigma_{a\rm II}(E_{\rm pole})} = \frac{1}{E - E_{\rm pole}}, \qquad (4.84)$$

where in the last equality we used the pole equation (4.67). This is the celebrated Weisskopf-Wigner approximation (Weisskopf and Wigner [1930a]; Weisskopf and Wigner [1930b]) and yields a purely exponential behavior, $\mathcal{A}(t) = \exp(-iE_{\rm pole}t)$, without short- and long-time corrections. From Eq. (4.84) we immediately get the spectral density function

$$\varpi_a^{\rm WW}(E) = \frac{\gamma}{2\pi} \frac{1}{\Big(E - E_a - \Delta E\Big)^2 + \Big(\frac{\gamma}{2}\Big)^2}\ , \qquad (4.85)$$

which reduces to (4.83) if one retains only the second-order contribution of the perturbation expansion of the pole coordinates (4.78)-(4.79).

4.7 Temporal behavior of the survival amplitude

In order to analyze the temporal behavior of the survival amplitude it is rather convenient to deform the Bromwich path B in a new contour $C = h + c$, where h is the so-called Hankel contour, running from $E = E_g - i\infty$ on the first Riemann sheet, going around the branch point $E = E_g$ and returning back to $E = E_g - i\infty$ on the second sheet, and c is a small circle around the pole $E_{\rm pole}$ on the second Riemann sheet (see Fig. 4.6). From Eq. (4.26) one gets

$$\begin{aligned} \mathcal{A}(t) &= Ze^{-i(E_a+\Delta E)t-\frac{\gamma}{2}t} + \frac{i}{2\pi}\int_h e^{-iEt}G_a(E)dE \\ &\equiv \mathcal{A}_{\rm pole}(t) + \mathcal{A}_{\rm cut}(t), \end{aligned} \qquad (4.86)$$

where

$$Z = \left[\frac{dG_a^{-1}(E)}{dE}\right]^{-1}_{E=E_{\rm pole}} = \frac{1}{1 - \Sigma'_{a\rm II}(E_{\rm pole})} \qquad (4.87)$$

is the residue at the pole. The simple pole yields therefore an exponential decay, but this law is modified by the cut contribution. As we will see, at early times the latter sums up with the exponential and gives a quadratic behavior, while at large times, when the pole contribution becomes exponentially small, the cut becomes dominant and yields an inverse power law tail. Notice that the integral over h is of order

$$\frac{i}{2\pi}\int_{E_g-i\infty}^{E_g} dE\ e^{-iEt}[G_a(E) - G_{a\rm II}(E)] = {\rm O}(\lambda^2), \qquad (4.88)$$

for $[G_a(E) - G_{a\rm II}(E)] \propto [\Sigma_a(E) - \Sigma_{a\rm II}(E)] = {\rm O}(\lambda^2)$. Therefore at intermediate times the decay is exponential with a correction of order ${\rm O}(\lambda^2)$.

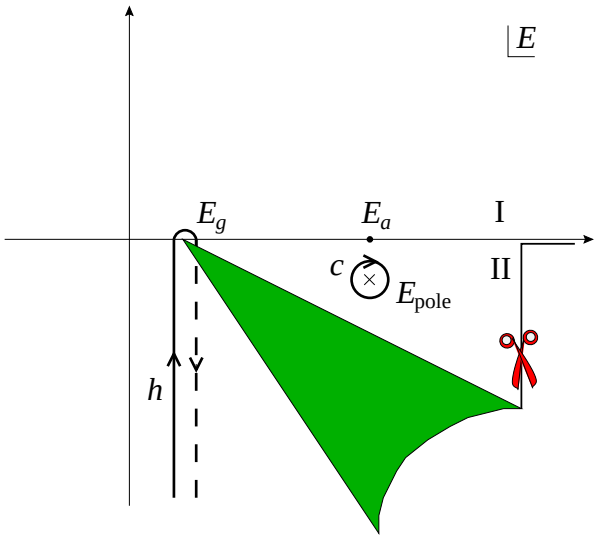

Figure 4.6: The deformed integration path C, sum of the Hankel contour h and the small circle c. The contour h originates in $E_g - i\infty$ on the first Riemann sheet, goes around the branching point E_g and returns back to $E_g - i\infty$ on the second sheet. The circle c runs clockwise around the pole E_{pole} on the second sheet.

4.7.1 Small times

Now we study in detail the temporal behavior of the survival amplitude $\mathcal{A}(t)$ for $t \to 0$. By changing the integration variable $\eta = Et$, Eq. (4.26) becomes

$$\mathcal{A}(t) = \frac{i}{2\pi} \int_B d\eta \, \frac{e^{-i\eta}}{f(\eta, t)}, \tag{4.89}$$

where, from Eq. (4.36), $f(\eta, t)$ reads

$$f(\eta, t) = \eta - E_a t - t \, \Sigma_a \left(\frac{\eta}{t} \right). \tag{4.90}$$

From the above equation it is apparent that the temporal behavior of the survival amplitude at short times is determined by the behavior of the self-energy function in the complex E plane in the neighborhood of $E = \eta/t = \infty$. From a physical perspective this is related to the time-energy uncertainty relations: at short times the system is allowed to explore intermediate states with large energies E. (Remember also the role of the time-energy uncertainty relation in the derivation of Fleming's unitary bound in Sec. 2.3.2.) Let us analyze the behavior of $\Sigma_a(1/u) = \langle a|R(1/u)|a\rangle$ in a neighborhood of the origin $u = 0$. By expanding (4.44), with $E = 1/u$, we get

$$R\left(\frac{1}{u}\right) = H_{\text{int}} + u H_{\text{int}} \frac{P_d}{1 - u P_d H P_d} H_{\text{int}} = H_{\text{int}} + u H_{\text{int}} P_d H_{\text{int}} + \mathrm{O}(u^2), \tag{4.91}$$

whence

$$\Sigma_a\left(\frac{1}{u}\right) = u \langle a|H_{\text{int}} P_d H_{\text{int}}|a\rangle + \mathrm{O}(u^2) = u \langle a|H_{\text{int}}^2|a\rangle + \mathrm{O}(u^2), \tag{4.92}$$

where we used Eq. (4.58), which gives $P_a H_{\text{int}} P_d H_{\text{int}} P_a = P_a H_{\text{int}}^2 P_a$. Notice now that, being $|a\rangle$ an eigenstate of the free Hamiltonian H_0 and being H_{int} completely off-diagonal, one gets

$$\langle a|H_{\text{int}}^2|a\rangle = \langle a|H^2|a\rangle - \langle a|H|a\rangle^2 = (\triangle H)^2 = \tau_{\text{Z}}^{-2}, \tag{4.93}$$

i.e., the Zeno time depends only on the off-diagonal part of the Hamiltonian. By using Eq. (4.93), Eq. (4.92) finally becomes

$$\Sigma_a\left(\frac{1}{u}\right) = \frac{u}{\tau_{\rm Z}^2} + {\rm O}(u^2), \tag{4.94}$$

whence the function $f(\eta, t)$ for $t \to 0$ reads

$$f(\eta, t) = \eta - E_a t - \frac{1}{\eta}\frac{t^2}{\tau_{\rm Z}^2} + {\rm O}(t^3). \tag{4.95}$$

Therefore the survival amplitude at small times has the asymptotic expansion

$$\mathcal{A}(t) \sim \frac{i}{2\pi}\int_B d\eta\, \frac{\eta e^{-i\eta}}{\eta^2 - E_a t\eta - t^2/\tau_{\rm Z}^2} = \frac{i}{2\pi}\int_B d\eta\, \frac{\eta e^{-i\eta}}{(\eta - t\eta_1)(\eta - t\eta_2)}, \tag{4.96}$$

where

$$\eta_{1,2} = \frac{E_a}{2} \pm \sqrt{\left(\frac{E_a}{2}\right)^2 + \frac{1}{\tau_{\rm Z}^2}}. \tag{4.97}$$

By closing the Bromwich path in Eq. (4.96) with a large semicircle in the lower half plane, the integral reduces to the sum of the residues at the real poles $t\eta_{1,2}$:

$$\mathcal{A}(t) \sim \left(\frac{\eta_1}{\eta_1 - \eta_2}e^{-i\eta_1 t} - \frac{\eta_2}{\eta_1 - \eta_2}e^{-i\eta_2 t}\right). \tag{4.98}$$

Therefore the survival probability at small times reads

$$P(t) = |\mathcal{A}(t)|^2 \sim \frac{\eta_1^2 + \eta_2^2 - 2\eta_1\eta_2\cos[t(\eta_1 - \eta_2)]}{(\eta_1 - \eta_2)^2} \sim 1 + \eta_1\eta_2 t^2 = 1 - \frac{t^2}{\tau_{\rm Z}^2}, \tag{4.99}$$

in agreement with the expansion (2.23). Notice that at short times the behavior is governed by two "effective" poles which replace the global contribution of the cut and the pole on the second sheet. We will come back to this point later.

4.7.2 Large times

We look now at the temporal behavior of the survival amplitude at large times. In order to evaluate the cut contribution at large times, change the integration variable in the integral in Eq. (4.86), and get $[x = i(E - E_g)t]$

$$\mathcal{A}_{\rm cut}(t) = \frac{e^{-iE_g t}}{2\pi}\int_0^\infty dx\, e^{-x}\left(\frac{1}{g(x,t)} - \frac{1}{g(xe^{-2\pi i}, t)}\right), \tag{4.100}$$

where $g(x,t) = ix + t(E_a - E_g) + t\Sigma_a(E_g - ix/t)$ and the second term represents the contribution of the second Riemann sheet (it is easy to show that the branching point contribution vanishes). One obtains

$$\mathcal{A}_{\rm cut}(t) = \frac{e^{-iE_g t}}{2\pi}\int_0^\infty dx\, e^{-x}\left(\frac{1}{tE_{ag} + t\Sigma_a(E_g - i\frac{x}{t}) + ix} - \frac{1}{tE_{ag} + t\Sigma_{a\rm II}(E_g - i\frac{x}{t}) + ix}\right), \tag{4.101}$$

where we let $E_{ag} = E_a - E_g$. Let us evaluate the difference between the two terms by using Eq. (4.66)

$$\mathcal{A}_{\rm cut}(t) = \frac{-ie^{-iE_g t}}{t}\int_0^\infty dx\, e^{-x}\frac{\kappa_a\left(E_g - i\frac{x}{t}\right)}{\left(E_{ag} + \Sigma_a(E_g - i\frac{x}{t}) + i\frac{x}{t}\right)\left(E_{ag} + \Sigma_{a\rm II}(E_g - i\frac{x}{t}) + i\frac{x}{t}\right)}. \quad (4.102)$$

Notice that, from Eq. (4.37), $\kappa_a(E)$ must vanish sufficiently fast at the ends of the integration domain in order to assure the convergence of the integral $\forall E$, namely

$$\kappa_a(E) \sim E_{ag}\begin{cases} C_0\left(\frac{E-E_g}{E_{ag}}\right)^\delta & \text{for} \quad E \to E_g, \quad \delta > 0, \\ C_\infty\left(\frac{E}{E_{ag}}\right)^{-\delta'} & \text{for} \quad E \to \infty, \quad \delta' > 0, \end{cases} \quad (4.103)$$

where we introduced the constant E_{ag} for dimensional reason, whence C_0 e C_∞ are adimensional. From a physical perspective Eqs. (4.103) have the following meaning: there is an energy scale E_0 (E_∞) such that the first (second) equation is valid for $E < E_0$ ($E > E_\infty$). Such energy scales depend, obviously, on the model under investigation.

The dominant contribution to the integral (4.102) comes from the region $x \lesssim 1$ due to the negative exponential. For sufficiently large times such that $x \lesssim 1 \ll (E_0 - E_g)t$, i.e. for $t \gg (E_0 - E_g)^{-1}$, we can evaluate the integral by using the approximation (4.103) for the numerator and letting $x/t = 0$ in the denominator. We get (Goldberger and Watson [1964]; Nakazato, Namiki and Pascazio [1996])

$$\begin{aligned} \mathcal{A}_{\rm cut}(t) &\sim \frac{-ie^{-iE_g t}}{t}\int_0^\infty dx\, e^{-x}\frac{E_{ag}C_0\left(-i\frac{x}{E_{ag}t}\right)^\delta}{(E_{ag} + \Sigma_a(E_g))^2} \\ &= C_0(-i)^{\delta+1}\Gamma(\delta+1)\left(\frac{E_{ag}}{E_{ag} + \Sigma_a(E_g)}\right)^2\frac{e^{-iE_g t}}{(E_{ag}t)^{\delta+1}} \\ &\equiv C\frac{e^{-iE_g t}}{(E_{ag}t)^{\delta+1}} \end{aligned} \quad (4.104)$$

where $\Gamma(t) = \int_0^\infty dx e^{-x}x^{t-1}$ is the Euler function, C a constant, and Eq. (4.66) and the first of Eqs. (4.103) were used in order to write

$$\Sigma_a(E_g) = \Sigma_{a\rm II}(E_g). \quad (4.105)$$

Therefore we proved that the survival amplitude has an inverse-power law contribution, $t^{-(1+\delta)}$, at sufficiently large times. This contribution will eventually supersede the exponential contribution in Eq. (4.86).

Let us summarize our results. The survival amplitude $\mathcal{A}(t) = \langle a|U(t)|a\rangle$ at large times has the asymptotic behavior

$$\mathcal{A}(t) \sim Ze^{-\frac{\gamma}{2}t - i(E_a + \Delta E)t} + C\frac{e^{-iE_g t}}{(E_{ag}t)^{1+\delta}}, \quad (4.106)$$

whence, the survival probability reads

$$P(t) \sim \mathcal{Z}e^{-\gamma t} + \frac{\mathcal{C}}{(E_{ag}t)^{2(1+\delta)}} + \frac{2\sqrt{\mathcal{C}\mathcal{Z}}}{(E_{ag}t)^{1+\delta}}e^{-\frac{\gamma}{2}t}\cos[(E_{ag} + \Delta E)t - \xi], \quad (4.107)$$

where we set $\mathcal{Z} = |Z|^2$, $\mathcal{C} = |C|^2$ and $\xi = \mathrm{Arg}(Z) - \mathrm{Arg}(C)$. Notice that together with the exponential, $\exp(-\gamma t)$, and the inverse-power term, $(E_{ag}t)^{-2(1+\delta)}$, there is an interference

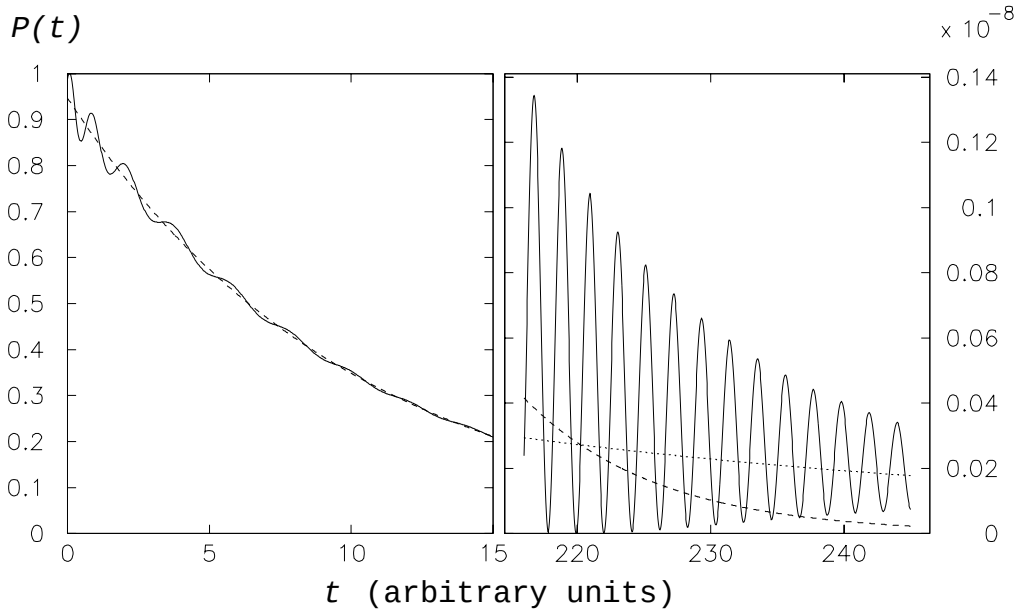

Figure 4.7: Temporal behavior of the survival probability $P(t)$. All characteristics are greatly exaggerated by a convenient choice of the parameters. The frequency of the oscillations reaches its asymptotic value after a few oscillations. Notice that different scales have been used for the two graphs. The dashed line is the exponential and the dotted line the power law. Notice the transition between the two laws at large times.

term between the pole and the cut contribution (Facchi and Pascazio [1998]). This term yields damped oscillations (of frequency approximately equal to the distance between the pole and the branching cut, because $\Delta E = O(\lambda^2)$) over the exponential decay. This interference effect is important for intermediate times, and becomes dominant at the transition between the exponential and the inverse-power law. Therefore, the short time behavior, yielding a vanishing decay rate, is nothing but the first of a series of oscillations. The temporal behavior of the survival probability is sketched in Fig. 4.7. Notice the transition from exponential decay to the inverse-power law for large times.

Chapter 5

Lee model and form factors

5.1 Introduction

We will now study the temporal evolution in greater detail, by making use of a quantum field theoretical framework, and discuss the primary role played by the form factors of the interaction.

5.2 The Lee Hamiltonian

Consider the total Hamiltonian H and the initial state $|a\rangle$. As we saw in Sec. 4.5 we can write the total Hilbert space as a direct sum $\mathcal{H} = \mathcal{H}_a \oplus \mathcal{H}_d$, with $\mathcal{H}_a = P_a\mathcal{H}$ and $\mathcal{H}_d = P_d\mathcal{H}$, find an orthonormal basis $\{|n\rangle\}$ in $\mathcal{H}_d$

$$\langle a|a\rangle = 1, \quad \langle a|n\rangle = 0, \quad \langle n|n'\rangle = \delta_{nn'} \tag{5.1}$$

and split the total Hamiltonian in the free and interaction part (4.51), which satisfy the relations

$$\begin{aligned} H_0|a\rangle = \omega_a|a\rangle, \qquad & H_0|n\rangle = \omega_n|n\rangle, \\ \langle a|H_{\rm int}|a\rangle = \langle n|H_{\rm int}|n'\rangle = 0, \qquad & \forall n, n'. \end{aligned} \tag{5.2}$$

The interaction Hamiltonian $H_{\rm int}$ is completely off-diagonal and has nonvanishing matrix elements only between $\mathcal{H}_a$ and $\mathcal{H}_d$, namely

$$\langle a|H_{\rm int}|n\rangle = \langle n|H_{\rm int}|a\rangle^* = g_n. \tag{5.3}$$

Equations (5.1)-(5.3) completely determine the free and interaction Hamiltonians in terms of the chosen basis. Indeed we get

$$H = H_0 + H_{\rm int}, \tag{5.4}$$

where

$$H_0 = \omega_a|a\rangle\langle a| + \sum_n \omega_n|n\rangle\langle n|, \qquad H_{\rm int} = \sum_n g_n \left(|a\rangle\langle n| + g_n^*|n\rangle\langle a|\right). \tag{5.5}$$

This is called the *Lee Hamiltonian* and was first introduced by Lee [1954] as a solvable quantum field model for studying the renormalization problem.

As before, we take as initial state $|\psi(0)\rangle = |a\rangle$. The interaction of this normalizable state with the states $|n\rangle$ (the formal sum in the above equation usually represents an integral over a

continuum of states) is responsible for its decay and depends on the *form factor* g_n. Note that the many-level Hamiltonian (3.21) is of the Lee type with $g_n = \lambda = \text{const}$.

As we saw in the previous chapter, the propagator can be expressed as

$$G_a(E) = \frac{1}{E - \omega_a - \Sigma_a(E)}, \tag{5.6}$$

where the self-energy function $\Sigma_a(E)$ consists only of a second order contribution and is related to the form factor g_n by the equation

$$\Sigma_a(E) = \sum_n \frac{|\langle a|H_{\text{int}}|n\rangle|^2}{E - \omega_n} = \int d\omega \, \frac{\kappa_a(\omega)}{E - \omega}, \tag{5.7}$$

with

$$\kappa_a(E) = \sum_n |\langle a|H_{\text{int}}|n\rangle|^2 \, \delta(E - \omega_n) = \sum_n |g_n|^2 \delta(E - \omega_n). \tag{5.8}$$

A comment is now in order. If one is simply interested in the survival amplitude [or, equivalently, in the expression of the propagator (5.6)] and not in the details of the interactions g_n between $|a\rangle$ and different states $|n\rangle$ with the same energy $\omega_n = \omega$, one can simply replace this set of states with a single, representative, state $|\omega\rangle$ and the Hamiltonian (5.5) can be replaced by the following equivalent one

$$H = H_0 + H_{\text{int}} = \omega_a |a\rangle\langle a| + \int d\omega \, \omega |\omega\rangle\langle\omega| + \int d\omega \, g(\omega)(|a\rangle\langle\omega| + |\omega\rangle\langle a|), \tag{5.9}$$

with the form factor $g(\omega) = \sqrt{\kappa_a(\omega)}$ and with

$$|a\rangle\langle a| + \int d\omega \, |\omega\rangle\langle\omega| = 1. \tag{5.10}$$

In terms of the Hamiltonian (5.9) the self-energy function simply reads

$$\Sigma_a(E) = \int d\omega \, \frac{|\langle a|H_{\text{int}}|\omega\rangle|^2}{E - \omega} = \int d\omega \, \frac{g^2(\omega)}{E - \omega}. \tag{5.11}$$

As usual the survival amplitude is given by the inverse Fourier-Laplace transform of the propagator

$$\mathcal{A}(t) = \frac{i}{2\pi} \int_{\text{B}} dE \, e^{-iEt} G_a(E) = \frac{i}{2\pi} \int_{\text{B}} dE \, \frac{e^{-iEt}}{E - \omega_a - \Sigma_a(E)}, \tag{5.12}$$

the Bromwich path B being a horizontal line $\text{Im}E = \text{const} > 0$ in the half plane of convergence of the Fourier-Laplace transform (upper half plane).

5.3 Two-pole model

We consider now a particular case: let the form factor be Lorentzian

$$g(\omega) = \frac{\lambda}{\sqrt{\pi}} \sqrt{\frac{\Lambda}{\omega^2 + \Lambda^2}}. \tag{5.13}$$

This describes, for instance, an atom-field coupling in a cavity with high finesse mirrors (Lang, Scully and Lamb [1973]; Ley and Loudon [1987]; Gea-Banacloche, Lu, Pedrotti, Prasad, Scully and Wodkiewicz [1990]). (Notice that the Hamiltonian in this case is not lower bounded and

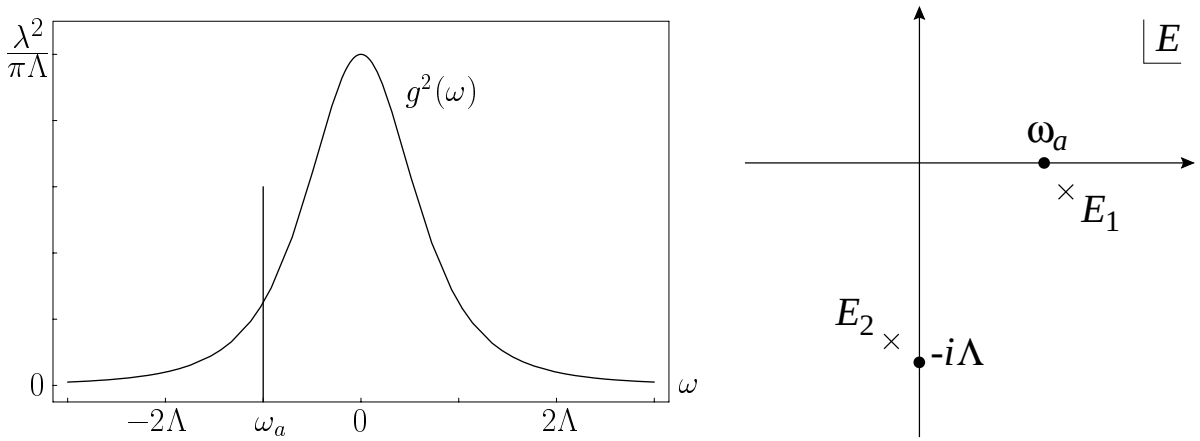

Figure 5.1: (a) Form factor $g^2(\omega)$ and initial state energy ω_a. (b) Poles of the propagator in the complex E-plane.

we expect no deviations from exponential behavior at very large times.) In this case one easily obtains (for $\mathrm{Im}E > 0$)

$$\Sigma_a(E) = \frac{\lambda^2}{E + i\Lambda} = \lambda^2 \frac{E}{E^2 + \Lambda^2} - i\lambda^2 \frac{\Lambda}{E^2 + \Lambda^2} = \Delta_a(E) - \frac{i}{2}\Gamma_a(E), \tag{5.14}$$

whence the propagator

$$G_a(E) = \frac{E + i\Lambda}{(E - \omega_a)(E + i\Lambda) - \lambda^2} \tag{5.15}$$

has two poles in the lower half energy plane (see Fig. 5.1). Their values are

$$E_1 = \omega_a + \Delta - i\frac{\gamma}{2}, \quad E_2 = -\Delta - i\left(\Lambda - \frac{\gamma}{2}\right), \tag{5.16}$$

where

$$\begin{cases} \Delta = -\frac{\omega_a}{2} + \frac{\omega_a}{2}\sqrt{\frac{\sqrt{v^4 + 4\omega_a^2\Lambda^2} + v^2}{2\omega_a^2}} \\ \\ \gamma = \Lambda - \sqrt{\frac{\sqrt{v^4 + 4\omega_a^2\Lambda^2} - v^2}{2}} \end{cases}, \quad \text{with} \quad v^2 = \omega_a^2 + 4\lambda^2 - \Lambda^2. \tag{5.17}$$

(Notice that v^2 can be negative.) The propagator and the survival amplitude read

$$\begin{aligned} G_a(E) &= \frac{E_1 + i\Lambda}{E_1 - E_2}\frac{1}{E - E_1} - \frac{E_2 + i\Lambda}{E_1 - E_2}\frac{1}{E - E_2} \\ &= \frac{1 - \mathcal{R}}{E - (\omega_a + \Delta) + i\gamma/2} + \frac{\mathcal{R}}{E + \Delta + i(\Lambda - \gamma/2)} \end{aligned} \tag{5.18}$$

and

$$\mathcal{A}(t) = (1 - \mathcal{R})e^{-i(\omega_a + \Delta)t}e^{-\gamma t/2} + \mathcal{R}e^{i\Delta t}e^{-(\Lambda - \gamma/2)t}, \tag{5.19}$$

respectively, where

$$1 - \mathcal{R} = \mathrm{Res}[G_a(E_1)] = \frac{1}{1 - \Sigma_a'(E_1)} = \frac{\omega_a + \Delta + i(\Lambda - \gamma/2)}{\omega_a + 2\Delta + i(\Lambda - \gamma)} \tag{5.20}$$

is the residue of the pole E_1 of the propagator. The survival probability reads

$$P(t) = \mathcal{Z}\exp(-\gamma t) + 2\mathrm{Re}[\mathcal{R}^*(1-\mathcal{R})e^{-i(\omega_a+2\Delta)t}]\exp(-\Lambda t) + |\mathcal{R}|^2\exp[-(2\Lambda-\gamma)t], \quad (5.21)$$

where $\mathcal{Z} = |1-\mathcal{R}|^2$ is the wave function renormalization

$$\mathcal{Z} = \frac{(\omega_a+\Delta)^2 + (\Lambda-\gamma/2)^2}{(\omega_a+2\Delta)^2 + (\Lambda-\gamma)^2} \ . \quad (5.22)$$

On the other hand, by substituting the expression of the self-energy function (5.14) into Eq. (4.82) the spectral density function reads

$$\varpi_a(E) = \frac{\lambda^2}{\pi}\ \frac{\frac{\Lambda}{E^2+\Lambda^2}}{\left(E-\omega_a-\lambda^2\frac{E}{E^2+\Lambda^2}\right)^2 + \left(\lambda^2\frac{\Lambda}{E^2+\Lambda^2}\right)^2} \ . \quad (5.23)$$

Small coupling

It is interesting to consider some limits of the model investigated. Consider the weak coupling limit $\lambda \ll \omega_a, \Lambda$. One obtains from Eq. (5.17)

$$\begin{aligned} \Delta &= \frac{\lambda^2}{\omega_a^2+\Lambda^2}\omega_a + \mathrm{O}(\lambda^4) = \mathrm{P}\int d\omega \frac{g^2(\omega)}{\omega_a-\omega} + \mathrm{O}(\lambda^4), \\ \gamma &= 2\Lambda\frac{\lambda^2}{\omega_a^2+\Lambda^2} + \mathrm{O}(\lambda^4) = 2\pi g^2(\omega_a) + \mathrm{O}(\lambda^4). \end{aligned} \quad (5.24)$$

Notice that the latter formula is the Fermi Golden Rule and that E_1 is the "dominant" pole. Indeed, the second exponential in Eq. (5.19) is damped very quickly, on a time scale Λ^{-1} much faster than γ^{-1}, whence, after a short initial quadratic (Zeno) region of duration Λ^{-1}, the decay becomes purely exponential with decay rate γ. Note that the corrections are of order λ^2

$$\mathcal{R} = \frac{\lambda^2}{\omega_a^2+\Lambda^2}\frac{\omega_a - i\Lambda}{\omega_a+i\Lambda} + \mathrm{O}(\lambda^4) \quad (5.25)$$

and the Zeno time is $\tau_{\mathrm{Z}} = \lambda^{-1} \gg \Lambda^{-1}$, i.e. the initial quadratic (Zeno) region is much shorter than the Zeno time: in general, the Zeno time does *not* yield a correct estimate of the duration of the Zeno region. The approximation $P(t) \simeq 1 - t^2/\tau_{\mathrm{Z}}^2$ holds for times $t < \Lambda^{-1} \ll \tau_{\mathrm{Z}}$.

Large bandwidth

In the limit of large bandwidth $\Lambda \gg \omega_a, \lambda$, from Eq. (5.17) one gets $\gamma = 2\lambda^2/\Lambda + \mathrm{O}(\Lambda^{-2})$ and in order to have a non trivial result with a finite decay rate, we let

$$\Lambda \to \infty, \quad \lambda \to \infty, \qquad \text{with} \quad \frac{\lambda^2}{\Lambda} = \frac{\gamma}{2} = \text{const.} \quad (5.26)$$

In this limit the continuum has a flat band, $g(\omega) = \sqrt{\gamma/2\pi}$ =const, and we expect to recover the results of Sec. 3.4. Indeed, in this case one gets $\mathcal{R} = 0$ and $\Delta = 0$, whence

$$G_a(E) = \frac{1}{E-\omega_a+i\gamma/2}, \quad (5.27)$$

so that the survival amplitude and probability read

$$\mathcal{A}(t) = \exp\left(-i\omega_a t - \frac{\gamma}{2}t\right) \quad \text{and} \quad P(t) = \exp(-\gamma t). \quad (5.28)$$

In this case the propagator (5.27) has only a simple pole and the survival probability (5.28) is purely exponential.

Narrow bandwidth

In the limit of narrow bandwidth $\Lambda \ll \omega_a, \lambda$, the form factor becomes

$$g^2(\omega) = \lambda^2 \delta(\omega) \tag{5.29}$$

and the continuum is "concentrated" in $\omega = 0$. Therefore the continuum behaves as a second discrete level and one obtains Rabi oscillations. In fact one gets

$$\gamma = 0, \quad \Delta = -\frac{\omega_a}{2} + \Omega, \quad \mathcal{R} = \frac{1}{2}\left(1 - \frac{\omega_a}{2\Omega}\right), \tag{5.30}$$

where

$$\Omega = \sqrt{\lambda^2 + \frac{\omega_a^2}{4}} \tag{5.31}$$

is the usual Rabi frequency of a two-level system with energy difference ω_a and coupling λ. By (5.30) the survival amplitude and probability read

$$\begin{aligned} \mathcal{A}(t) &= \frac{1}{2}\left(1 + \frac{\omega_a}{2\Omega}\right) e^{-i\left(\frac{\omega_a}{2} + \Omega\right)t} + \frac{1}{2}\left(1 - \frac{\omega_a}{2\Omega}\right) e^{-i\left(\frac{\omega_a}{2} - \Omega\right)t}, \\ P(t) &= 1 - \frac{\lambda^2}{\Omega^2} \sin^2(\Omega t)\,. \end{aligned} \tag{5.32}$$

In this case, if $\omega_a = 0$, the survival probability (5.32) oscillates between 1 and 0. On the other hand, if $\omega_a \neq 0$ the initial state never decays completely.

Incidentally, notice that the Zeno time is still $\tau_{\mathrm{Z}} = \lambda^{-1}$ and yields now a good estimate of the duration of the Zeno region. This is, so to say, a "coincidence" due to the oscillatory features of the system. (Remember that for $\omega_a = 0$ Fleming's unitary bound (2.39) becomes an equality and that τ_{Z} depends only on the off-diagonal part of the total Hamiltonian.)

Strong coupling

Another interesting case is that of strong coupling, $\lambda \to \infty$. This is a typical case in which the strong coupling provokes violent oscillations before the system reaches the asymptotic regime. In the limit $\lambda \gg \Lambda, \omega_a$, we get

$$\Delta = \lambda - \frac{\omega_a}{2} + \mathrm{O}(\lambda^{-1}), \quad \gamma = -i\frac{\Lambda}{2} + \mathrm{O}(\lambda^{-1}), \quad \mathcal{R} = \frac{1}{2} - \frac{\omega_a + i\Lambda}{4\lambda} + \mathrm{O}(\lambda^{-3}), \tag{5.33}$$

whence the survival amplitude reads

$$\mathcal{A}(t) \simeq \exp\left(-i\frac{\omega_a}{2}t - \frac{\Lambda}{2}t\right)\left[\left(\frac{1}{2} + \frac{\omega_a + i\Lambda}{4\lambda}\right) e^{-i\lambda t} + \left(\frac{1}{2} - \frac{\omega_a + i\Lambda}{4\lambda}\right) e^{i\lambda t}\right], \tag{5.34}$$

which yields fast oscillations of frequency λ damped at a rate $\Lambda \ll \lambda$.

5.3.1 Two-pole reduction

We show that the two-pole model is the first improvement, after the Weisskopf-Wigner single pole, in the approximation of a generic realistic model. First note that, according to the Weisskopf-Wigner approximation, an exponential decay is obtained by considering a constant self-energy function $\Sigma_a = -i\gamma/2$, i.e. a resolvent with a single pole with negative imaginary part. On the other hand, as we noted in Sec. 4.7.1, the initial quadratic behavior of the survival

amplitude is governed by two effective poles of the resolvent, which ultimately derive from the behavior (4.94) of the self-energy function at infinity

$$\Sigma_a(E) \sim \frac{1}{\tau_{\rm Z}^2 E}, \qquad \text{for} \quad E \to \infty. \tag{5.35}$$

If one wants to capture this short time behavior maintaining the exponential law at later times, and is not interested in the large-time power-law deviations, one can proceed in the following way. The requirement for having an exponential decay, with decay rate γ for $t \to \infty$ translates in the behavior of the self-energy function for $E \to 0$, namely in the requirement of having a Weisskopf-Wigner constant self-energy function with negative imaginary part

$$\Sigma_a(0) = -ib. \tag{5.36}$$

The simplest form of the self-energy function satisfying both requirements (5.35) and (5.36) is

$$\Sigma_a(E) = \frac{1}{\tau_{\rm Z}^2 E + i/b} = \frac{1/\tau_{\rm Z}^2}{E + i/b\tau_{\rm Z}^2} \tag{5.37}$$

By letting $\tau_{\rm Z} = 1/\lambda$ and $1/b\tau_Z^2 = \Lambda$, this becomes exactly the self-energy function of the two-pole model (5.14). Therefore the two-pole model is the simplest approximation which yields the short quadratic behavior together with the exponential one.

Note that the process outlined above can be iterated to find better approximations of the real $\Sigma_a(E)$ by adding other poles and/or zeros. But notice also that this approach does not yield the inverse power-law tail. Indeed the latter is essentially due to the nonanalytic behavior of the self energy function at the branching point, a feature that cannot be captured by an olomorphic function.

5.4 An equivalence method

We apply now a method of equivalence to the Lee Hamiltonian (5.9), which enables us to look at the Zeno region from a different perspective. The Hamiltonian (5.9) describes the decay of a discrete state $|a\rangle$ into the continuum of states $|\omega\rangle$ with a given form factor $g(\omega)$. According to Eq. (4.94) and Eq. (5.11), the Zeno time is related to the integral of the squared form factor by the simple relation

$$\frac{1}{\tau_{\rm Z}^2} = \int d\omega \; g^2(\omega). \tag{5.38}$$

On the other hand, for a two-level system the Zeno time is just the inverse off-diagonal element of the Hamiltonian, namely $\tau_{\rm Z} = 1/\lambda$ [and, of course, this is in agreement with the above equation, as shown by Eq. (5.29)]. We seek now an equivalent decay model, that shares with the two-level model this nice property. To this end, let us add a new "intermediate" discrete state $|b\rangle$ to the Lee model. Consider then the Rabi oscillation λ of the two-level system $|a\rangle$, $|b\rangle$ and let the initial state $|a\rangle$ decay only *through* state $|b\rangle$, i.e. couple $|b\rangle$ to a continuum with form factor $g_b(\omega)$. In other words, the Hamiltonian (5.9) is substituted by the following one

$$H = \omega_a|a\rangle\langle a| + \omega_b|b\rangle\langle b| + \int d\omega \; \omega|\omega\rangle\langle\omega| + \lambda\left(|a\rangle\langle b| + |b\rangle\langle a|\right) + \int d\omega \; g_b(\omega)(|b\rangle\langle\omega| + |\omega\rangle\langle b|). \tag{5.39}$$

We require that this Hamiltonian is equivalent to the original one in describing the decay of the initial state $|a\rangle$. To this end, notice that the part of Hamiltonian describing the decay of state $|b\rangle$ (and neglecting the coupling with $|a\rangle$) is just a Lee Hamiltonian and gives

$$G_b(E) = \frac{1}{E - \omega_b - \Sigma_b(E)}, \qquad \Sigma_b(E) = \int d\omega \; \frac{g_b^2(\omega)}{E - \omega}. \tag{5.40}$$

On the other hand, state $|a\rangle$ couples only to state $|b\rangle$ with a coupling λ. Therefore the evolution of state $|a\rangle$ is just a Rabi oscillation between state $|b\rangle$ dressed by the continuum $|\omega\rangle$ and state $|a\rangle$, namely

$$G_a = G_a^0 + G_a^0 \lambda G_b \lambda G_a \ , \tag{5.41}$$

whence

$$G_a(E) = \frac{1}{E - \omega_a - \lambda^2 G_b(E)} \ . \tag{5.42}$$

Therefore, in the modified model, the self-energy function of the initial state $|a\rangle$ is nothing but the coupling λ^2 times the dressed propagator $G_b(E)$

$$\Sigma_a(E) = \lambda^2 G_b(E) = \frac{\lambda^2}{E - \omega_b - \Sigma_b(E)}. \tag{5.43}$$

Equation (5.43) is the equivalence relation sought. One has to choose the auxiliary form factor $g_b(\omega)$ in Eq. (5.39) as a function of the original one $g(\omega)$, in order to satisfy this relation and get an equivalent description of the decay. Our interest in this equivalence is due to the asymptotic behavior of formula (5.43)

$$\Sigma_a(E) \sim \frac{\lambda^2}{E} = \frac{1}{\tau_Z^2 E}, \qquad \text{for} \quad E \to \infty \ , \tag{5.44}$$

which explicitly shows the relation between the coupling λ and the Zeno time τ_Z. In the equivalent model, therefore, the initial quadratic behavior is singled out from the remaining part of the decay: the Zeno region, i.e., the first oscillation, is nothing but the initial unperturbed Rabi oscillation between states $|a\rangle$ and $|b\rangle$ (which initially "represents" the original continuum in its globality). After the initial stage of the decay, the coupling $g_b(\omega)$ between $|b\rangle$ and $|\omega\rangle$ (namely the details of the original continuum) comes into play and modifies the initial Rabi oscillation with its characteristic time scale. This explains from a different perspective the difference, already stressed in previous sections, between the Zeno time and the duration of the initial quadratic region.

As an example, we recover the self-energy function (5.14) of the two-pole model, by requiring that Σ_b be the constant

$$\Sigma_b(E) = -\omega_b - i\Lambda \ , \tag{5.45}$$

which implies that

$$g_b(\omega) = \sqrt{\frac{\Lambda}{\pi}} \qquad \text{and} \quad \omega_b = 0. \tag{5.46}$$

In other words, the auxiliary state $|b\rangle$ is placed at the mean energy of the original continuum $g(\omega)$ and decays into a flat-band continuum with decay rate $\gamma_b = 2\Lambda$: the decay into a Lorentzian continuum is exactly equivalent to a Rabi coupling with a level that in turn exponentially decays into a flat continuum.

A final comment is now in order. One can draw a clear picture of the two-pole reduction, discussed in the previous section, just by looking at the construction of the equivalent model. The first approximation of a real decay, the Weisskopf-Wigner approximation, is represented by the simple exponential decay of level $|b\rangle$ with its time scale γ_b^{-1}. The two-pole approximation superimposes an oscillating dynamics with time scale λ^{-1} to the latter, yielding the initial Zeno region. By complicating the model with the addition of other dynamical elements with their characteristic scales, one can construct a better approximation of the real decay law.

5.5 The decay of a two-level atom

It is interesting and instructive to apply the techniques and considerations sketched above to a *real* physical system. For this purpose we shall look at the properties of the hydrogen atom in the electromagnetic field.

Consider the Hamiltonian of a two-level atom interacting with the photon field (Cohen-Tannoudji, Dupont-Roc and Grynberg [1998])

$$\begin{aligned} H &= H_a + H_f + H_{\rm int} \\ &= \omega_0 |2\rangle\langle 2| + \sum_{\boldsymbol{k},\lambda} \omega_k a^\dagger_{\boldsymbol{k}\lambda} a_{\boldsymbol{k}\lambda} + \sum_{\boldsymbol{k},\lambda} \left(\phi_{\boldsymbol{k}\lambda} a^\dagger_{\boldsymbol{k}\lambda} |1\rangle\langle 2| + \phi^*_{\boldsymbol{k}\lambda} a_{\boldsymbol{k}\lambda} |2\rangle\langle 1| \right). \end{aligned} \tag{5.47}$$

We considered only the linear part of the interaction in the rotating wave approximation and neglected the atom translational degree of freedom. $a_{\boldsymbol{k}\lambda}$ is the annihilation operator of a photon with momentum $\boldsymbol{k}$ (energy $\omega_k = |\boldsymbol{k}|$) and polarization $\lambda = 1, 2$ and satisfying the usual commutation relations

$$[a_{\boldsymbol{k}\lambda}, a^\dagger_{\boldsymbol{k}'\lambda'}] = \delta_{\lambda\lambda'} \delta^3(\boldsymbol{k} - \boldsymbol{k}'). \tag{5.48}$$

The quantities $\phi_{\boldsymbol{k}\lambda}$ are the matrix elements of the interaction Hamiltonian between the states

$$|1; 1_{\boldsymbol{k}\lambda}\rangle \equiv |1\rangle \otimes |\boldsymbol{k}, \lambda\rangle, \quad |2; 0\rangle \equiv |2\rangle \otimes |0\rangle, \tag{5.49}$$

where the first ket refers to the atom and the second to the photon.

Note that the rotating wave Hamiltonian (5.47) is in fact a Lee Hamiltonian (5.5), and therefore the self-energy function is exact at the second order in the coupling constant.

5.5.1 Matrix elements

The matrix elements of the interaction Hamiltonian are

$$\phi_{\boldsymbol{k}\lambda} = \frac{e}{m_e \sqrt{2\epsilon_0 V \omega}} \, \boldsymbol{\epsilon}^*_{\boldsymbol{k}\lambda} \cdot \langle 1| \exp(-i\boldsymbol{k}\cdot\boldsymbol{x}) \, \boldsymbol{p}|2\rangle \tag{5.50}$$

and in the dipole approximation read

$$\phi_{\boldsymbol{k}\lambda} = \frac{-ie\omega_0}{\sqrt{2\epsilon_0 V \omega}} \, \boldsymbol{\epsilon}^*_{\boldsymbol{k}\lambda} \cdot \boldsymbol{x}_{12}. \tag{5.51}$$

They were exactly evaluated by Moses [1972a]; Moses [1973] and Seke [1994a] in the energy-angular momentum basis for photons. Here we will derive them by using the atomic eigenfunction in the momentum representation (Facchi and Pascazio [1999b]). For concreteness we concentrate our attention on the 2P-1S transition of hydrogen: $|1\rangle \equiv |n_1 = 1, l_1 = 0, m_1 = 0\rangle$, $|2\rangle \equiv |n_2 = 2, l_2 = 1, m_2\rangle$.

We can write

$$\langle r_1| \exp(-i\boldsymbol{k}\cdot\boldsymbol{x})\boldsymbol{p}|r_2\rangle = \int d^3p \langle r_1| \exp(-i\boldsymbol{k}\cdot\boldsymbol{x})|\boldsymbol{p}\rangle\langle\boldsymbol{p}|\boldsymbol{p}|r_2\rangle. \tag{5.52}$$

By using the property of the momentum eigenstates $|\boldsymbol{p}\rangle$

$$\exp(-i\boldsymbol{k}\cdot\boldsymbol{x})|\boldsymbol{p}\rangle = |\boldsymbol{p} - \boldsymbol{k}\rangle, \tag{5.53}$$

Eq. (5.52) becomes

$$\langle r_1| \exp(-i\boldsymbol{k}\cdot\boldsymbol{x})\boldsymbol{p}|r_2\rangle = \int d^3p \, \widetilde{u}^*_{r_1}(\boldsymbol{p} - \boldsymbol{k}) \, \boldsymbol{p} \, \widetilde{u}_{r_2}(\boldsymbol{p}), \tag{5.54}$$

where $\widetilde{u}_r(\boldsymbol{p}) \equiv \langle \boldsymbol{p}|r\rangle$ is the atomic eigenfunction in the momentum representation.

For the ground state 1S one gets (a_0 is the Bohr radius)

$$\begin{aligned}\widetilde{u}_{100}(\boldsymbol{p}) &= \int d^3x \langle \boldsymbol{p}|\boldsymbol{x}\rangle\langle \boldsymbol{x}|100\rangle = \int \frac{d^3x}{(2\pi)^{3/2}} e^{-i\boldsymbol{p}\cdot\boldsymbol{x}} u_{100}(\boldsymbol{x}) \\ &= \int \frac{d^3x}{(2\pi)^{3/2}} e^{-i\boldsymbol{p}\cdot\boldsymbol{x}} \frac{1}{\sqrt{\pi a_0^3}} e^{-r/a_0} = \sqrt{\frac{8}{\pi^2 a_0^5}} \frac{1}{\left[(1/a_0)^2 + p^2\right]^2}, \end{aligned} \tag{5.55}$$

and for the 2P state one gets

$$\widetilde{u}_{21m_2}(\boldsymbol{p}) = \int \frac{d^3x}{(2\pi)^{3/2}} e^{-i\boldsymbol{p}\cdot\boldsymbol{x}} \frac{1}{\sqrt{2^5\pi a_0^5}}\, \boldsymbol{x}\cdot\boldsymbol{\xi}_{m_2} e^{-r/2a_0} = -i\sqrt{\frac{1}{\pi^2 a_0^7}} \frac{\boldsymbol{p}\cdot\boldsymbol{\xi}_{m_2}}{\left[(1/2a_0)^2 + p^2\right]^3}, \tag{5.56}$$

where the unit spherical vectors $\boldsymbol{\xi}_q$ are linear combinations of the unit orthogonal vectors $\boldsymbol{e}_x$, $\boldsymbol{e}_y$ and $\boldsymbol{e}_z$:

$$\boldsymbol{\xi}_0 = \boldsymbol{e}_z, \qquad \boldsymbol{\xi}_{\pm 1} = \mp \frac{\boldsymbol{e}_x \pm i\boldsymbol{e}_y}{\sqrt{2}}. \tag{5.57}$$

By plugging Eqs. (5.55) and (5.56) into Eq. (5.54) we obtain

$$\langle 100|\exp(-i\boldsymbol{k}\cdot\boldsymbol{x})\boldsymbol{p}|21m_2\rangle = -i\sqrt{\frac{2^3}{\pi^4 a_0^{12}}} \int d^3p \frac{1}{\left[(1/a_0)^2 + (\boldsymbol{p}-\boldsymbol{k})^2\right]^2}\, \boldsymbol{p}\, \frac{\boldsymbol{p}\cdot\boldsymbol{\xi}_{m_2}}{\left[(1/2a_0)^2 + p^2\right]^3}. \tag{5.58}$$

By utilizing spherical coordinates with the azimuth axes in the $\boldsymbol{k}$ direction, Eq. (5.58) transforms into

$$-i\sqrt{\frac{2}{\pi^4 a_0^{12}}}\, \boldsymbol{\xi}_{m_2} \int_{-1}^{1} d\eta (1-\eta^2) \int_{-\infty}^{\infty} dp \frac{p^4}{\left[p^2 - 2pk\eta + k^2 + (1/a_0)^2\right]^2 \left[p^2 + (1/2a_0)^2\right]^3}. \tag{5.59}$$

By calculating the residues in the complex p plane and integrating over η, a straightforward calculation finally gives

$$\langle 100|\exp(-i\boldsymbol{k}\cdot\boldsymbol{x})\boldsymbol{p}|21m_2\rangle = -i\frac{2^{9/2}}{3^4}\frac{1}{a_0}\frac{1}{\left[1 + (\omega_k/\Lambda_n)^2\right]^2}\, \boldsymbol{\xi}_{m_2}, \tag{5.60}$$

where (α is the fine structure constant and m_e the electron mass)

$$\Lambda_n = \frac{3}{2a_0} = \frac{3}{2}\alpha m_e \simeq 8.498 \cdot 10^{18}\text{rad/s} \tag{5.61}$$

is the *natural cutoff*, that characterizes the form factor, given by the finite extension of the atomic orbitals. By increasing ω_k above the frequency cutoff Λ_n, the matrix element (5.60) couples less and less the atom and the photons.

In conclusion, the exact matrix element (5.50) reads

$$\phi_{\boldsymbol{k}\lambda} = -i\lambda \left(\frac{3\Delta}{8\pi}\right)^{\frac{1}{2}} \boldsymbol{\epsilon}^*_{\boldsymbol{k}\lambda}\cdot\boldsymbol{\xi}_{m_2} \frac{1}{\omega^{\frac{1}{2}}\left[1 + (\omega_k/\Lambda_n)^2\right]^2}, \tag{5.62}$$

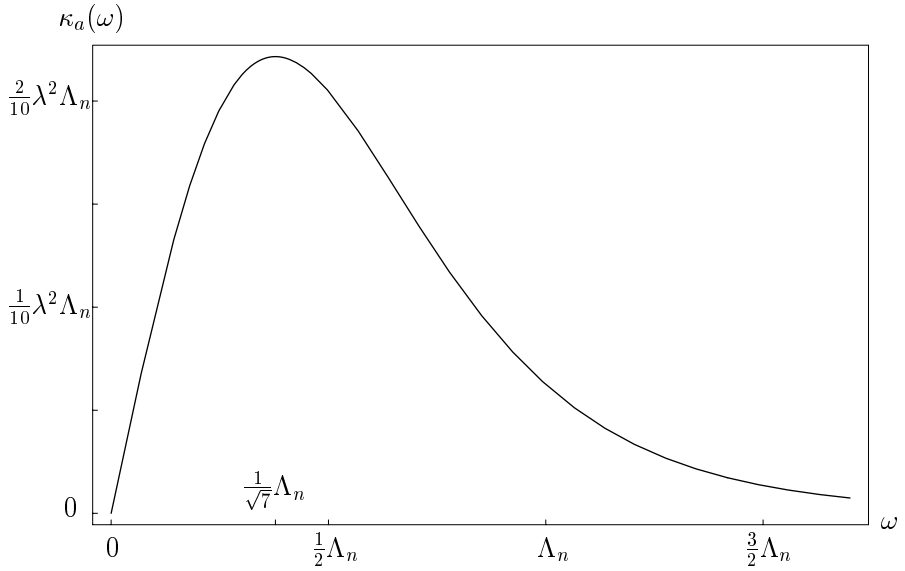

Figure 5.2: The spectral density $\kappa_a(\omega)$, for the 2P-1S transition. The maximum value is at $\omega = \Lambda_n/\sqrt{7}$. Horizontal axis in units Λ_n, vertical axis in units $\lambda^2\Lambda_n$.

where λ is the photon-atom coupling constant

$$\lambda = \left(\frac{2}{\pi}\right)^{\frac{1}{2}} \left(\frac{2}{3}\right)^{\frac{9}{2}} \alpha^{\frac{3}{2}} \simeq 8.022 \cdot 10^{-5}, \tag{5.63}$$

and $\Delta = 2\pi^3/V$ is the unit cell in $\boldsymbol{k}$ space, when the electromagnetic field is confined in a box of volume V. The spectral density

$$\kappa_a(\omega) = \sum_{\boldsymbol{k},\lambda} |\phi_{\boldsymbol{k}\lambda}|^2 \delta(\omega - \omega_k), \tag{5.64}$$

reads in the continuum limit ($V \to \infty$)

$$\kappa_a(\omega) = \lambda^2 \frac{\omega}{\left[1 + (\omega/\Lambda_n)^2\right]^4} \tag{5.65}$$

and is shown in Fig. 5.2. Notice again that the natural cutoff Λ_n is proportional to the inverse of the Bohr radius a_0, which measures the atomic size. Photons with wavelengths shorter than the atomic size couple less and less to the atom. This is apparent in Eq. (5.50), where for larger frequencies the imaginary exponential oscillates more and more inside the integration volume $v \simeq a_0^3$. An alternative description is given by Eqs. (5.54), (5.58): the two momentum eigenfunctions have an extension of order $1/a_0$ and are shifted by $|\boldsymbol{k}|$ (frequency of the emitted or absorbed photon): when $\omega = |\boldsymbol{k}| \gg a_0^{-1} (\simeq \text{cutoff})$, the integral (5.54) vanishes.

Note that for $\omega/\Lambda_n \ll 1$ in Eq. (5.62) the denominator behaves like $\omega^{1/2}$ and one obtains the matrix element in the dipole approximation

$$\phi_{\boldsymbol{k}\lambda} = \frac{-ie\omega_0}{\sqrt{2\epsilon_0 V\omega}}\, \boldsymbol{\epsilon}^*_{\boldsymbol{k}\lambda} \cdot \frac{2^{\frac{15}{2}}}{3^5} a_0\, \boldsymbol{\xi}_{m_2} = -i\lambda \left(\frac{3\Delta}{8\pi}\right)^{\frac{1}{2}} \frac{1}{\omega^{\frac{1}{2}}}\, \boldsymbol{\epsilon}^*_{\boldsymbol{k}\lambda} \cdot \boldsymbol{\xi}_{m_2}, \tag{5.66}$$

which yields a linear spectral density function

$$\kappa_a(\omega) = \lambda^2 \omega. \tag{5.67}$$

5.5.2 Analysis in the time and energy domain

The Hamiltonian (5.47) yields a conservation law. Indeed it is easy to prove that the *excitation number* operator

$$\mathcal{N} = |2\rangle\langle 2| + \sum_{\boldsymbol{k},\lambda} a^\dagger_{\boldsymbol{k}\lambda} a_{\boldsymbol{k}\lambda}, \tag{5.68}$$

commutes with the Hamiltonian (5.47):

$$[\mathcal{N}, H] = 0. \tag{5.69}$$

(This is of course a general property of Lee Hamiltonians.) Therefore the Hilbert space is naturally split into subspaces (Tamm-Dancoff sectors) which are invariant under the action of H, whence under the system evolution (Tamm [1945]; Dancoff [1950]). They are labeled by the eigenvalues of $\mathcal{N}$, whose restriction within each subspace is proportional to the unit operator. The Hilbert space is therefore written as a direct sum

$$\mathcal{H} = \bigoplus_{\mathcal{N}=0}^{\infty} \mathcal{H}_{\mathcal{N}}. \tag{5.70}$$

We will consider the evolution in the subspace $\mathcal{H}_1$ belonging to the eigenvalue $\mathcal{N} = 1$ (spontaneous decay). A state $|\psi\rangle$ belonging to $\mathcal{H}_1$ has the form

$$|\psi(t)\rangle = \mathcal{A}(t)|2;0\rangle + \sum_{\boldsymbol{k},\lambda} y_{\boldsymbol{k}\lambda}(t)|1;1_{\boldsymbol{k}\lambda}\rangle, \tag{5.71}$$

with

$$\langle\psi(t)|\psi(t)\rangle = |\mathcal{A}(t)|^2 + \sum_{\boldsymbol{k},\lambda} |y_{\boldsymbol{k},\lambda}(t)|^2 = 1, \qquad \forall t. \tag{5.72}$$

The Schrödinger equation reads

$$\begin{aligned} i\,\dot{\mathcal{A}}(t) &= \omega_0 \mathcal{A}(t) + \sum_{\boldsymbol{k},\lambda} \phi^*_{\boldsymbol{k}\lambda} y_{\boldsymbol{k}\lambda}(t), \\ i\,\dot{y}_{\boldsymbol{k}\lambda}(t) &= \omega_k y_{\boldsymbol{k}\lambda}(t) + \phi_{\boldsymbol{k}\lambda}\mathcal{A}(t), \end{aligned} \tag{5.73}$$

that can be Fourier-Laplace transformed, with the initial condition $\mathcal{A}(0) = 1$, $y_{\boldsymbol{k}\lambda}(0) = 0$, in the following equations

$$\begin{aligned} E\widetilde{\mathcal{A}}(E) &= \omega_0 \widetilde{\mathcal{A}}(E) + \sum_{\boldsymbol{k},\lambda} \phi^*_{\boldsymbol{k}\lambda} \widetilde{y}_{\boldsymbol{k}\lambda}(E) + 1, \\ E\widetilde{y}_{\boldsymbol{k}\lambda}(E) &= \omega_k \widetilde{y}_{\boldsymbol{k}\lambda}(E) + \phi_{\boldsymbol{k}\lambda}\widetilde{\mathcal{A}}(E). \end{aligned} \tag{5.74}$$

The above algebraic equations can be immediately solved to give the familiar expression for the propagator

$$G_a(E) = \widetilde{\mathcal{A}}(E) = \frac{1}{E - \omega_0 - \Sigma_a(E)}, \tag{5.75}$$

and

$$\widetilde{y}_{\boldsymbol{k}\lambda}(E) = \frac{\phi_{\boldsymbol{k}\lambda}}{E - \omega_k}\, G_a(E), \tag{5.76}$$

with the self-energy function

$$\Sigma_a(E) = \sum_{\boldsymbol{k},\lambda} \frac{|\phi_{\boldsymbol{k}\lambda}|^2}{E - \omega_k} = \int_0^\infty \frac{\kappa_a(\omega)}{E - \omega}, \tag{5.77}$$

where κ_a is given by Eq. (5.65). The survival amplitude is given by the inverse transform (5.12), which reads ($\varepsilon = E/\Lambda_n$)

$$\mathcal{A}(t) = \frac{i}{2\pi}\int_B d\varepsilon \frac{e^{-i\varepsilon\Lambda_n t}}{\varepsilon - \frac{\omega_0}{\Lambda_n} - \lambda^2\bar{\Sigma}(\varepsilon)}, \tag{5.78}$$

where

$$\bar{\Sigma}(\varepsilon) = \frac{1}{\lambda^2\Lambda_n}\Sigma_a(\varepsilon\Lambda_n) = \int_0^\infty dx \frac{x}{(1+x^2)^4}\frac{1}{\varepsilon - x}. \tag{5.79}$$

This is an exact result for the Hamiltonian under investigation. As we have seen, the dipole approximation would give a linear spectral density function (5.67), whence

$$\Sigma_a(E) = \lambda^2\int_0^\Lambda d\omega\,\frac{\omega}{E-\omega} = -\lambda^2\Lambda - \lambda^2 E\log\left(1 - \frac{\Lambda}{E}\right). \tag{5.80}$$

The artificial cutoff Λ, introduced in order to assure the convergence of the integral, provides the appearance of a nonphysical plasmon mode (Gaveau and Schulman [1995]), and the survival amplitude never decays fully (Facchi and Pascazio [1999b]).

The integral (5.79) can be analytically solved to yield

$$\begin{aligned}\bar{\Sigma}(\varepsilon) &= \frac{-15\pi + (88 - 96i\pi)\varepsilon + 45\pi\varepsilon^2 + 144\varepsilon^3}{96(\varepsilon^2+1)^4} \\ &\quad + \frac{15\pi\varepsilon^4 + 72\varepsilon^5 + 3\pi\varepsilon^6 + 16\varepsilon^7}{96(\varepsilon^2+1)^4} + \frac{\varepsilon}{(\varepsilon^2+1)^4}\log\varepsilon.\end{aligned} \tag{5.81}$$

$\bar{\Sigma}(\varepsilon)$ has a logarithmic branch cut in the complex ε plane and no singularities in the first Riemann sheet. Indeed the seemingly fourth order poles at $\varepsilon = \pm i$, are also fourth order zeros of the numerator and one gets

$$\bar{\Sigma}(\pm i) = \frac{-5\pi \mp 32i}{256}. \tag{5.82}$$

It is easy to verify that the discontinuity across the cut reads [$\bar{\kappa}_a(\eta) = \kappa_a(\eta\Lambda_n)/\lambda^2\Lambda_n$]

$$\bar{\Sigma}(\eta + i0^+) - \bar{\Sigma}(\eta - i0^+) = -2\pi i\bar{\kappa}_a(\eta) = -2\pi i\frac{\eta}{(\eta^2+1)^4}\theta(\eta), \tag{5.83}$$

whence

$$\bar{\Sigma}_{\rm II}(\varepsilon) = \bar{\Sigma}(\varepsilon) - 2\pi i\bar{\kappa}_a(\varepsilon) = \bar{\Sigma}(\varepsilon) - 2\pi i\frac{\varepsilon}{(\varepsilon^2+1)^4}, \tag{5.84}$$

in agreement with Eq. (4.66).

Pole coordinates

The exponential decay is governed by the pole on the second Riemann sheet, whose coordinates are given by

$$E_{\rm pole} = \omega_0 + \Delta E - i\frac{\gamma}{2}, \tag{5.85}$$

with

$$\begin{aligned}\gamma &= -2\,{\rm Im}\left[\Sigma\left(\omega_0 + i0^+\right)\right] + {\rm O}(\lambda^4) = 2\pi\kappa_a(\omega_0) + {\rm O}(\lambda^4) \\ &= 2\pi\lambda^2\frac{\omega_0}{\left[1 + \left(\frac{\alpha}{4}\right)^2\right]^4} + {\rm O}(\lambda^4) \simeq 6.2682\cdot 10^8{\rm s}^{-1}\end{aligned} \tag{5.86}$$

$$\begin{aligned}\Delta E &= {\rm Re}\left[\Sigma\left(\omega_0 + i0^+\right)\right] + {\rm O}(\lambda^4) = {\rm P}\int_0^\infty d\omega\frac{\kappa_a(\omega)}{\omega_0 - \omega} + {\rm O}(\lambda^4) \\ &= \lambda^2\Lambda_n\,{\rm P}\int_0^\infty dx\frac{x}{(1+x^2)^4}\frac{1}{\frac{\alpha}{4} - x} + {\rm O}(\lambda^4) \simeq -2.7380\cdot 10^{10}{\rm rad/s},\end{aligned} \tag{5.87}$$

where we used Eqs. (4.78)-(4.79) and the spectral density (5.65).

5.5.3 Temporal behavior

By deforming the integration path in the second Riemann sheet we can write the survival amplitude as the sum of two contributions

$$\mathcal{A}(t) = \mathcal{A}_{\rm pole}(t) + \mathcal{A}_{\rm cut}(t). \tag{5.88}$$

The first term, due to the pole, yields the exponential decay law

$$\mathcal{A}_{\rm pole}(t) = \mathrm{Res}\left\{ \frac{e^{-i\varepsilon\Lambda_n t}}{\varepsilon - \frac{\omega_0}{\Lambda_n} - \lambda^2\bar{\Sigma}(\varepsilon)}, \frac{E_{\rm pole}}{\Lambda_n} \right\} = \sqrt{\mathcal{Z}} e^{-\frac{\gamma}{2}t} e^{-i(\omega_0+\Delta E)t + i\zeta}, \tag{5.89}$$

where

$$\sqrt{\mathcal{Z}} e^{i\zeta} \equiv \frac{1}{1 - \lambda^2 \bar{\Sigma}'_{\rm II}(E_{\rm pole}/\Lambda_n)} \simeq (1 - 4.38\lambda^2) e^{-i1.00\lambda^2\pi}. \tag{5.90}$$

with $\sqrt{\mathcal{Z}}$ and ζ real numbers [their numerical values refer to the 2P-1S transition and are very small, for $\lambda^2 = \mathrm{O}(\alpha^3)$]. The second term, $\mathcal{A}_{\rm cut}$, due to the branch cut, contains all deviations from exponential decay. For short times it modifies the exponential law yielding a quadratic law, and for large times it eventually becomes dominant yielding an inverse power law. The interference between the two terms yields a damped oscillatory behavior over the exponential law.

Short times and Zeno time $\tau_{\rm Z}$

For short times the survival probability has a quadratic behavior

$$P(t) \sim 1 - \frac{t^2}{\tau_{\rm Z}^2}, \tag{5.91}$$

where the Zeno time $\tau_{\rm Z}$ is related to the asymptotic behavior of the self-energy function at large energies, as in Eq. (4.94). From the analytical expression of the self-energy function (5.81) and the definition (5.79) one easily gets for $\varepsilon \to \infty$

$$\bar{\Sigma}(\varepsilon) \sim \frac{1}{6\varepsilon} \qquad \Rightarrow \qquad \Sigma_a(E) \sim \frac{\lambda^2\Lambda_n^2}{6}\frac{1}{E}, \tag{5.92}$$

whence

$$\frac{1}{\tau_{\rm Z}^2} = \frac{\lambda^2}{6}\Lambda_n^2. \tag{5.93}$$

According to Eq. (4.93) this is nothing but the expectation value of $H_{\rm int}^2$ in the initial state $|2,0\rangle$. Indeed we get

$$\begin{aligned} \frac{1}{\tau_Z^2} &= \langle 2,0|H_{\rm int}^2|2,0\rangle = \sum_\lambda \int d^3k\, |\langle 2,0|H_{\rm int}|1,1_{\boldsymbol{k}\lambda}\rangle|^2 \\ &= \int_0^\infty d\omega\, \kappa_a(\omega) = \lambda^2\Lambda_n^2 \int_0^\infty dx \frac{x}{(1+x^2)^4} = \frac{\lambda^2}{6}\Lambda_n^2. \end{aligned} \tag{5.94}$$

By substituting the expressions for Λ_n and λ from Eqs. (5.61) and (5.63) into (5.93), the Zeno time reads (Facchi and Pascazio [1998])

$$\tau_{\rm Z} = \frac{\sqrt{6}}{\lambda}\frac{1}{\Lambda_n} = (3\pi)^{\frac{1}{2}} \left(\frac{3}{2}\right)^{\frac{7}{2}} \frac{1}{\alpha^{\frac{5}{2}} m_e} \simeq 3.593 \cdot 10^{-15}\mathrm{s}. \tag{5.95}$$

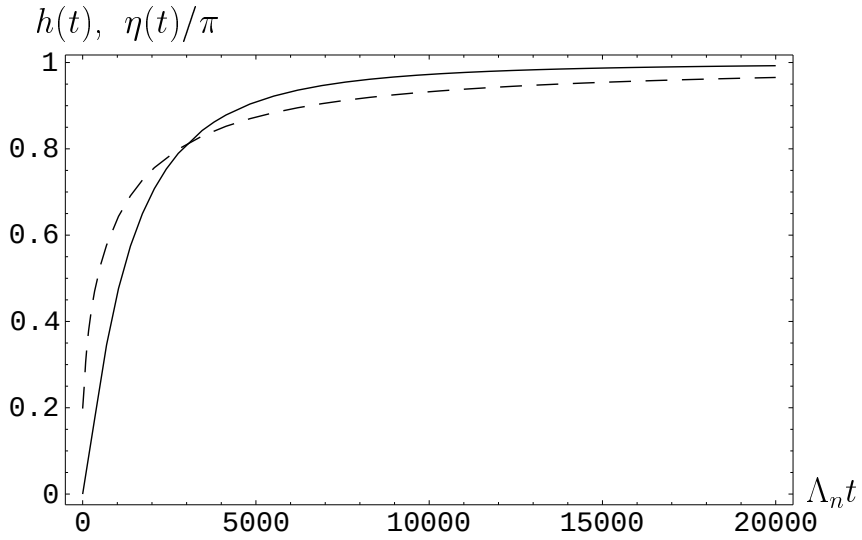

Figure 5.3: The functions $h(t)$ (solid line) and $\eta(t)/\pi$ (dashed line). The horizontal scale is in units Λ_n^{-1}. Notice that for $t \simeq 5000\Lambda_n^{-1}$ the curves have approximately reached their asymptotic values.

This is an accurate estimate of the value of $\tau_{\rm Z}$ for a physical unstable system. Notice that it is a time comparable with modern pulsed-laser time resolution. But, as stressed before, strictly speaking, $\tau_{\rm Z}$ is only the convexity of the survival probability at $t = 0$ and indeed, as we shall see soon, the quadratic expansion holds for times much shorter than $\tau_{\rm Z}$.

Large times and inverse power law

The exponent of the inverse power law is related to the asymptotic behavior of the spectral density function $\kappa_a(E)$ in the neighborhood of the ground energy E_g. From Eq. (5.65) we get ($E_g = 0$)

$$\kappa_a(\omega) \sim \lambda^2\omega, \qquad \text{for} \quad \omega \to 0. \tag{5.96}$$

Therefore Eq. (4.103) holds with $\delta = 1$ and the inverse power law will be quadratic $1/t^2$. Indeed, the asymptotics of $\mathcal{A}_{\rm cut}$ is given by Eq. (4.104) with $E_{ag} = \omega_0$ and $C_0 = \lambda^2$, namely

$$\mathcal{A}_{\rm cut}(t) \sim -\lambda^2 \left(\frac{\omega_0}{\omega_0 + \Sigma_a(0)}\right)^2 \frac{\Gamma(2)}{(\omega_0 t)^2} \tag{5.97}$$

From the analytical expression (5.81) one gets $\bar{\Sigma}(0) = -\frac{5}{32}\pi$, whence

$$\mathcal{A}_{\rm cut}(t) \sim -\lambda^2 \frac{\sqrt{\mathcal{C}}}{(\omega_0 t)^2}, \qquad \mathcal{C} \equiv \frac{1}{\left(1 - \frac{5}{8}\pi\frac{\lambda^2}{\alpha}\right)^4} = 1 + 1076.2\lambda^2 \tag{5.98}$$

(the numerical values refer to the 2P-1S hydrogen transition). This quadratic power tail is well known in the literature (Knight and Milonni [1976]; Davidovich and Nussenzveig [1980]; Hillery [1981]; Seke and Herfort [1989]; Seke [1992]; Facchi and Pascazio [1998]).

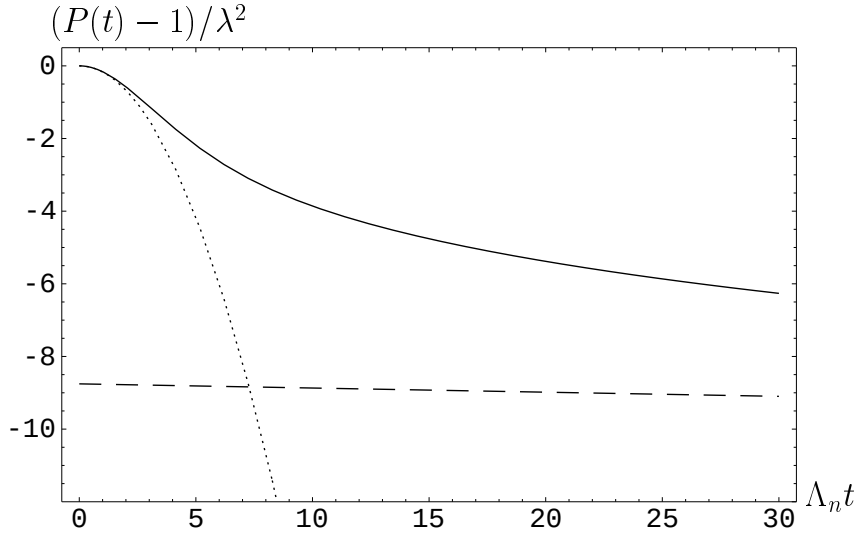

Figure 5.4: Short time behavior of the survival probability. The behavior of $P(t)-1$ (solid line), the pole contribution (dashed line) and the quadratic behavior (5.102) (dotted line) are shown. The horizontal scale is in units Λ_n^{-1}, the vertical scale in units λ^2.

Oscillations

Summarizing, the general expression (valid $\forall t \geq 0$) for the survival amplitude $\mathcal{A}(t)$ is

$$\mathcal{A}(t) = \sqrt{\mathcal{Z}} e^{-\frac{\gamma}{2}t} e^{-i(\omega_0+\Delta E)t+i\zeta} + \lambda^2 \frac{\sqrt{\mathcal{C}}}{(\omega_0 t)^2} h(t) e^{i\eta(t)}, \tag{5.99}$$

where $h(t)$ and $\eta(t)$ are real functions satisfying

$$\begin{aligned} &\lim_{t\to 0} \frac{h(t)}{(\omega_0 t)^2} = \frac{\sqrt{1+\mathcal{Z}-2\sqrt{\mathcal{Z}}\cos\zeta}}{\lambda^2\sqrt{\mathcal{C}}} \qquad \lim_{t\to\infty} h(t) = 1, \\ &\eta(0) = \arctan\left(\frac{\sqrt{\mathcal{Z}}\sin\zeta}{\sqrt{\mathcal{Z}}\cos\zeta - 1}\right) \qquad \lim_{t\to\infty} \eta(t) = \pi, \end{aligned} \tag{5.100}$$

and are plotted in Fig. 5.3. The survival probability reads

$$P(t) = \mathcal{Z} e^{-\gamma t} + \lambda^4 \frac{\mathcal{C}}{(\omega_0 t)^4} h^2(t) + 2\lambda^2 \frac{\sqrt{\mathcal{C}\mathcal{Z}}}{(\omega_0 t)^2} e^{-\frac{\gamma}{2}t} h(t) \cos\left[(\omega_0+\Delta E)t + \eta(t) - \zeta\right]. \tag{5.101}$$

The temporal behavior of the survival probability is shown in Figs. 5.4 and 5.5. For short and large times Eq. (5.101) has the asymptotic expansions

$$P(t) \sim 1 - \frac{t^2}{\tau_{\rm Z}^2}, \quad \text{for} \quad t \ll \tau_{\rm Z} \tag{5.102}$$

$$P(t) \sim \mathcal{Z} e^{-\gamma t} - 2\lambda^2 \frac{\sqrt{\mathcal{C}\mathcal{Z}}}{(\omega_0 t)^2} e^{-\frac{\gamma}{2}t} \cos\left[(\omega_0+\Delta E)t - \zeta\right] + \lambda^4 \frac{\mathcal{C}}{(\omega_0 t)^4}, \quad \text{for} \quad t \gg \Lambda_n^{-1}, \tag{5.103}$$

respectively. Notice that the "long-time" expansion (5.103) is already valid for rather short times $t \gg \Lambda_n^{-1} \simeq 10^{-19}$s, much shorter than the Zeno time $\tau_{\rm Z} \simeq 10^{-15}$s. Notice also that the

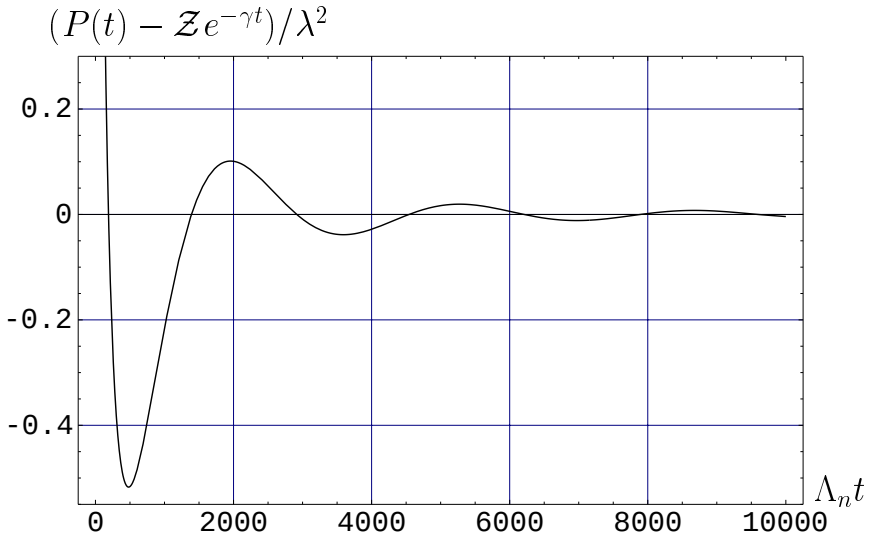

Figure 5.5: Temporal behavior of the survival probability. In order to emphasize the presence of oscillations [of order $\mathrm{O}(\alpha^3)$], the dominant exponential contribution was subtracted. We utilize the same scales of the previous figure: horizontal = Λ_n^{-1}, vertical = λ^2. The first oscillation (out of scale) is much shorter and wider than the following ones: see previous figure.

first oscillation is much shorter than the other ones. In fact, the system relaxes towards the asymptotic expression (5.103) within 2 or 3 oscillations (see Figs. 5.3 and 5.5).

The transition to a power law occurs when the two addenda in Eq. (5.99) are comparable, namely

$$\sqrt{\mathcal{Z}}e^{-\frac{\gamma}{2}\tau_{\mathrm{pow}}} = \lambda^2 \frac{\sqrt{\mathcal{C}}}{(\omega_0\tau_{\mathrm{pow}})^2} h(\tau_{\mathrm{pow}}) \quad \Rightarrow \quad (\omega_0\tau_{\mathrm{pow}})^2 e^{-\frac{\gamma}{2}\tau_{\mathrm{pow}}} \simeq \lambda^2, \tag{5.104}$$

i.e., for $\tau_{\mathrm{pow}} \simeq 98\ \tau_{\mathrm{E}}$.

In figures 5.4 and 5.5, it is apparent that the deviations from the exponential are very small and difficult to observe experimentally. In addition, there is the problem of the initial state preparation: the first half oscillation has a duration of about $200\Lambda_n^{-1} \simeq 2.3 \cdot 10^{-17}$s, so that a sharp initial state preparation, even by modern pulsed-laser techniques, appears difficult. On the other hand, the problem of sharply defining the initial moment of excitation might be circumvented: close scrutiny of Eqs. (5.99)-(5.103) suggests that experimental observation of the probability oscillations would not only provide a direct evidence of the cut contribution $\mathcal{A}_{\mathrm{cut}}$ to the survival amplitude, but also an indirect, yet convincing, proof of the presence of the Zeno region.

Chapter 6

Van Hove's limit

6.1 Introduction

The deviations from a purely exponential behavior in a decay process will now be analyzed in relation to Van Hove's "$\lambda^2 t$" limiting procedure. Our attention will be focused on the effects that arise when the coupling constant is small but nonvanishing. We first consider the two-level atom model studied in Sec. 5.5, then gradually extend our analysis to a more general framework. We estimate all deviations from exponential behavior at leading orders in the coupling constant.

We have seen in chapters 4 and 5 that the quantum mechanical derivation of the exponential law is based on the sensible idea that the temporal evolution of a quantum system is dominated by a pole near the real axis of the complex energy plane (Weisskopf-Wigner approximation). This yields an irreversible evolution, characterized by a master equation and exponential decay (Gardiner [1990]; van Kampen [1992]). An important contribution to this issue was given by Van Hove [1955], who rigorously showed that it is possible to obtain a master equation (leading to exponential behavior) for a quantum mechanical system endowed with many (infinite) degrees of freedom, by making use of the so-called "$\lambda^2 t$" limit. The crucial idea is to consider the limit

$$\lambda \to 0 \quad \text{keeping} \quad \tilde{t} = \lambda^2 t \quad \text{finite } (\lambda\text{-independent constant}), \tag{6.1}$$

where λ is the coupling constant and t time. One then looks at the evolution of the quantum system as a function of the rescaled time $\tilde{t}$. There has recently been a renewed interest in the physical literature for this time-scale transformation and its subtle mathematical features: see Accardi, Kozyrev and Volovich [1997] and Accardi, Lu and Volovich [2000].

We look in particular at the rescaling procedure from the perspective of the complex energy plane (Facchi and Pascazio [1999c]), rather than in terms of the time variable. This enables us to pin down the different sources of non-exponential behavior. Our analysis is extended to a general field-theoretical framework: general estimates are given of all deviations from the exponential law (both at short and long times) at leading orders in the coupling constant.

6.2 Two-level atom in the rotating-wave approximation

In section 5.5 we studied the decay of a two-level atom in the quantized radiation field. Let us summarize our results, emphasizing the role of the coupling constant λ.

At short and long times the survival probability reads

$$P(t) \sim 1 - \frac{t^2}{\tau_{\rm Z}^2} \qquad (t \ll \tau_{\rm Z}), \tag{6.2}$$

$$P(t) \sim \mathcal{Z} e^{-\gamma t} + \lambda^4 \frac{\mathcal{C}}{(\omega_0 t)^4} - 2\lambda^2 \frac{\sqrt{\mathcal{C}\mathcal{Z}}}{(\omega_0 t)^2} e^{-\frac{\gamma}{2}t} \cos\left[(\omega_0 + \Delta E)t - \zeta\right] \qquad (t \gg \Lambda_n^{-1}), \tag{6.3}$$

where

$$\tau_{\rm Z} = \frac{\sqrt{6}}{\lambda \Lambda_n} \simeq 3.593 \cdot 10^{-15}{\rm s}, \tag{6.4}$$

$$\gamma = 2\pi\lambda^2 \kappa_a(\omega_0) + {\rm O}(\lambda^4) = 2\pi\lambda^2 \omega_0 + {\rm O}(\lambda^4) \simeq 6.268 \cdot 10^8 {\rm s}^{-1}, \tag{6.5}$$

$$\Delta E = \lambda^2 {\rm P} \int_0^\infty d\omega \, \frac{\kappa_a(\omega)}{\omega_0 - \omega} + {\rm O}(\lambda^4) \simeq -0.5\lambda^2 \Lambda_n, \tag{6.6}$$

$$\sqrt{\mathcal{Z}} e^{i\zeta} \simeq (1 - 4.38\lambda^2) e^{-i1.00\pi\lambda^2} = 1 + {\rm O}(\lambda^2), \tag{6.7}$$

$$\sqrt{\mathcal{C}} \simeq 1 + 538\lambda^2 = 1 + {\rm O}(\lambda^2). \tag{6.8}$$

The second formula gives the Fermi Golden Rule, yielding the lifetime

$$\tau_{\rm E} = \gamma^{-1} \simeq 1.595 \cdot 10^{-9}{\rm s}, \tag{6.9}$$

and the third formula the second order correction to the energy level ω_0. The exact expressions for the quantities (6.5)-(6.8) are given in the previous chapter.

6.2.1 Van Hove's limit

Let us look at Van Hove's "$\lambda^2 t$" limiting procedure applied to the above model. Before proceeding to a detailed analysis, it is worth putting forward a few preliminary remarks: we shall scrutinize (in terms of the coupling constant) the mechanisms that make the nonexponential contributions in (6.2)-(6.3) vanish. To this end, observe first that as $\lambda \to 0$ the Zeno time (6.4) diverges, while the *rescaled* Zeno time vanishes

$$\tilde{\tau}_{\rm Z} \equiv \lambda^2 \tau_{\rm Z} = \lambda \frac{\sqrt{6}}{\Lambda_n} = {\rm O}(\lambda). \tag{6.10}$$

On the other hand, the rescaled lifetime (6.9) remains constant [see (6.5)]:

$$\tilde{\tau}_{\rm E} \equiv \lambda^2 \tau_{\rm E} = \frac{1}{2\pi\omega_0} = {\rm O}(1). \tag{6.11}$$

Moreover, the transition to a power law occurs when the first two terms in the right hand side of (6.3) are comparable, so that

$$(\omega_0 t)^2 e^{-\frac{\gamma}{2}t} \simeq \lambda^2, \tag{6.12}$$

because both $\mathcal{C}$ and $\mathcal{Z}$ are $\simeq 1$. In the limit of small λ, (6.12) yields $t = \tau_{\rm pow}$, with

$$2\log(\omega_0 \tau_{\rm pow}) - \frac{\gamma}{2}\tau_{\rm pow} \simeq 2\log\lambda, \tag{6.13}$$

namely, by (6.5),

$$\frac{\tau_{\rm pow}}{\tau_{\rm E}} \simeq 4\log\frac{1}{\lambda} + 4\log\frac{\tau_{\rm pow}}{2\pi\lambda^2\tau_{\rm E}} = 12\log\frac{1}{\lambda} + 4\log\frac{\tau_{\rm pow}}{\tau_{\rm E}} + 4\log\frac{1}{2\pi}. \tag{6.14}$$

Therefore, when time is rescaled,

$$\tilde{\tau}_{\rm pow} \equiv \lambda^2 \tau_{\rm pow} = 12\tilde{\tau}_{\rm E} \log\frac{1}{\lambda} + {\rm O}\left(\log\log\frac{1}{\lambda}\right) = {\rm O}\left(\log\frac{1}{\lambda}\right). \tag{6.15}$$

Finally, the power contributions are $\sim {\rm O}(\lambda^{3\alpha})\ \tilde{t}^{-\alpha}\ (\alpha = 2, 4)$, the period of the oscillations [last term in (6.3)] behaves like λ^2/ω_0 and the quantities (6.7)-(6.8) become both unity.

In conclusion, only the exponential law survives in the limit (6.1), with the correct normalization factor ($\mathcal{Z} = 1$), and one is able to derive a purely exponential behavior (Markovian dynamics) from the quantum mechanical Schrödinger equation (unitary dynamics). It is important to notice that, in order to obtain the exponential law, a normalizable state (such as a wave packet) must be taken as initial state. Our initial state $|2;0\rangle$ is indeed normalizable.

6.2.2 The limit in the complex energy plane

Let us now proceed to a more formal analysis in the complex energy domain. In the rotating-wave approximation the self-energy function $\Sigma^{(2)}(E)$ consists only of a second order diagram and can be evaluated exactly:

$$\Sigma_a(E) = \lambda^2 \Sigma^{(2)}(E) \equiv \lambda^2 \int_0^\infty d\omega\ \frac{\kappa_a(\omega)}{E-\omega}, \tag{6.16}$$

where the spectral density $\kappa_a(E)$ is given (for the 2P-1S transition) by (5.65) and the self-energy function Σ is computed in (5.81). In the complex E-plane $\Sigma^{(2)}(E)$ has a branch cut running from 0 to ∞, a branching point in the origin and no singularity on the first Riemann sheet. Dyson's resummation yields

$$G_a(E) = \frac{1}{E - \omega_0 - \lambda^2 \Sigma^{(2)}(E)}, \tag{6.17}$$

and we obtain for the survival amplitude (in the interaction representation)

$$\begin{aligned} \mathcal{A}(t) &\equiv \langle 2;0|e^{iH_0 t} U(t)|2;0\rangle = \frac{i}{2\pi}\int_{\rm B} dE\ e^{-iEt} G_a(E+\omega_0) \\ &= \frac{i}{2\pi}\int_{\rm B} dE \frac{e^{-iEt}}{E - \lambda^2\Sigma^{(2)}(E+\omega_0)}. \end{aligned} \tag{6.18}$$

In Van Hove's limit one looks at the evolution of the system over time intervals of order $t = \tilde{t}/\lambda^2$ ($\tilde{t}$ independent of λ), in the limit of small λ. Our purpose is to see how this limit works in the complex-energy plane, i.e. what is the limiting form of the propagator. To this end, by rescaling time $\tilde{t} \equiv \lambda^2 t$, we can write

$$\mathcal{A}\left(\frac{\tilde{t}}{\lambda^2}\right) = \frac{i}{2\pi}\int_{\rm B} d\tilde{E} \frac{e^{-i\tilde{E}\tilde{t}}}{\tilde{E} - \Sigma^{(2)}(\lambda^2\tilde{E} + \omega_0)}, \tag{6.19}$$

where we are naturally led to introduce the rescaled energy $\widetilde{E} \equiv E/\lambda^2$. Taking the Van Hove limit we get

$$\widetilde{\mathcal{A}}(\tilde{t}) \equiv \lim_{\lambda\to 0} \mathcal{A}\left(\frac{\tilde{t}}{\lambda^2}\right) = \frac{i}{2\pi}\int_{\rm B} d\tilde{E}\ e^{-i\tilde{E}\tilde{t}} \widetilde{G}_a(\tilde{E}), \tag{6.20}$$

where the propagator in the rescaled energy reads

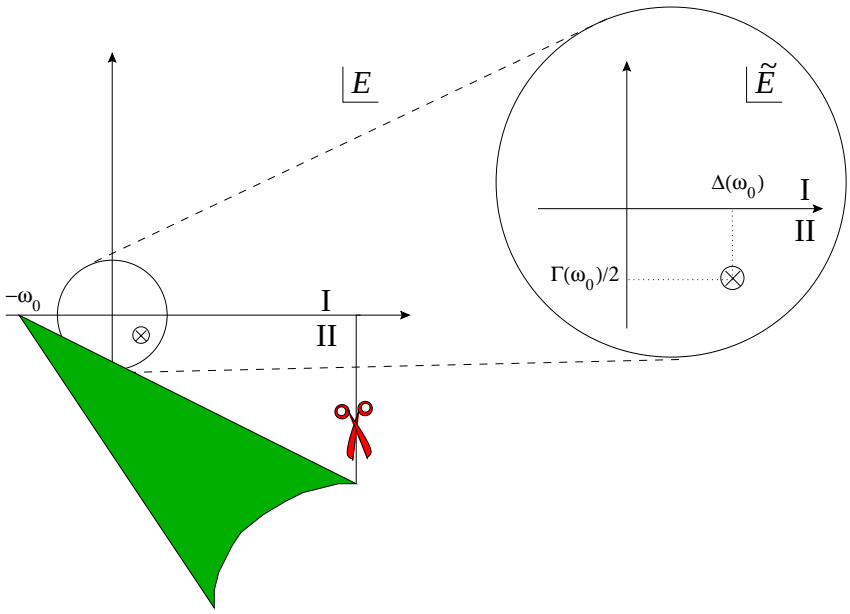

Figure 6.1: Singularities of the propagator (6.18) in the complex-E plane. The first Riemann sheet (I) is singularity free. The logarithmic cut is due to $\Sigma^{(2)}(E)$ and the pole is located on the second Riemann sheet (II). In the complex-$\tilde{E}$ plane, the pole has coordinates (6.23)-(6.24).

$$\widetilde{G}_a(\tilde{E}) \equiv \lim_{\lambda\to 0} \frac{1}{\tilde{E} - \Sigma^{(2)}(\lambda^2\tilde{E} + \omega_0)} = \frac{1}{\tilde{E} - \Sigma^{(2)}(\omega_0 + i0^+)}, \tag{6.21}$$

the term $+i0^+$ being due to the fact that $\mathrm{Im}\tilde{E} > 0$. The self-energy function in the $\lambda \to 0$ limit becomes

$$\Sigma^{(2)}(\omega_0 + i0^+) = \int_0^\infty d\omega \frac{\kappa_a(\omega)}{\omega_0 - \omega + i0^+} = \Delta(\omega_0) - \frac{i}{2}\Gamma(\omega_0) \tag{6.22}$$

where

$$\Delta(\omega_0) \equiv \mathrm{P}\int_0^\infty d\omega \frac{\kappa_a(\omega)}{\omega_0 - \omega}, \tag{6.23}$$

$$\Gamma(\omega_0) \equiv 2\pi\kappa_a(\omega), \tag{6.24}$$

which yields a purely exponential decay (Weisskopf-Wigner approximation and Fermi Golden Rule). In figure 6.1 we endeavoured to clarify the role played by the time-energy rescaling in the complex-E plane.

One can get a more detailed understanding of the mechanisms that underpin the limiting procedure by looking at higher order terms in the coupling constant. The pole of the original propagator (6.17) satisfies the equation

$$E_{\mathrm{pole}} - \lambda^2\Sigma^{(2)}(E_{\mathrm{pole}} + \omega_0) = 0, \tag{6.25}$$

which can be solved by using the technique outlined in Sec. 4.6.2, namely by expanding the self-energy function around $E = 0$ in power series

$$\Sigma^{(2)}(E + \omega_0) = \Sigma^{(2)}(\omega_0) + E\Sigma^{(2)\prime}(\omega_0) + \frac{E^2}{2}\Sigma^{(2)\prime\prime}(\omega_0) + \ldots, \tag{6.26}$$

whose radius of convergence is ω_0, due to the branching point of $\Sigma^{(2)}$ in the origin. We get (iteratively)

$$E_{\mathrm{pole}} = \lambda^2\Sigma^{(2)}(\omega_0) + \lambda^4\Sigma^{(2)\prime}(\omega_0)\Sigma^{(2)}(\omega_0) + \mathrm{O}(\lambda^6), \tag{6.27}$$

which, due to (6.22), becomes

$$E_{\rm pole} \equiv \Delta E - \frac{i}{2}\gamma = \lambda^2\Delta(\omega_0) - i\frac{\lambda^2}{2}\Gamma(\omega_0) + {\rm O}(\lambda^4). \tag{6.28}$$

In the rescaled energy (6.28) reads

$$\tilde{E}_{\rm pole} = \frac{E_{\rm pole}}{\lambda^2} = \Delta(\omega_0) - \frac{i}{2}\Gamma(\omega_0) + {\rm O}(\lambda^2) \stackrel{\lambda\to 0}{\longrightarrow} \Delta(\omega_0) - \frac{i}{2}\Gamma(\omega_0), \tag{6.29}$$

which is the same as (6.22). This is again the Fermi Golden Rule.

6.3 N-level atom with counter-rotating terms

Before proceeding to a general analysis it is interesting to see how the above model is modified by the presence of the other atomic levels and the inclusion of counter-rotating terms in the interaction Hamiltonian. This will enable us to pin down other salient features of the $\lambda^2 t$ limit. The Hamiltonian is

$$H = H_0' + \lambda V', \tag{6.30}$$

where

$$H_0' \equiv \sum_\nu \omega_\nu b_\nu^\dagger b_\nu + \sum_\beta \int_0^\infty d\omega\, \omega a_{\omega\beta}^\dagger a_{\omega\beta}, \tag{6.31}$$

$$V' = \sum_{\mu,\nu}\sum_\beta \int_0^\infty d\omega \left[\varphi_\beta^{\mu\nu}(\omega) b_\mu^\dagger b_\nu a_{\omega\beta}^\dagger + \varphi_\beta^{\mu\nu *}(\omega) b_\nu^\dagger b_\mu a_{\omega\beta}\right], \tag{6.32}$$

where ν runs over all the atomic states and $b_\nu^\dagger, b_\nu$ and $a_{\omega\beta}^\dagger, a_{\omega\beta}$ satisfy anticommutation and commutation relations, respectively. [The Hamiltonian of a two-level atom in the rotating-wave approximation is recovered if we set $\omega_2 = \omega_0,\ \omega_1 = 0$ and neglect the counter-rotating terms.] Starting from the initial state $|\mu;0\rangle$, Dyson's resummation yields

$$G_\mu(E) = \frac{1}{E - \omega_\mu - \Sigma_\mu(E)} \tag{6.33}$$

and the 1-particle irreducible self-energy function takes the form

$$\Sigma_\mu(E) = \lambda^2\Sigma(E) = \lambda^2\Sigma^{(2)}(E) + \lambda^4\Sigma^{(4)}(E) + \ldots, \tag{6.34}$$

with

$$\Sigma^{(2)}(E) \equiv \sum_{\nu,\beta}\int_0^\infty d\omega \frac{|\varphi_\beta^{\nu\mu}(\omega)|^2}{E - \omega_\nu - \omega}. \tag{6.35}$$

Both $\Sigma^{(2)}$ and $\Sigma^{(4)}$ are shown as Feynman diagrams in Fig. 6.2. In the Van Hove limit one obtains

$$\Sigma(\lambda^2\tilde{E} + \omega_\mu) \stackrel{\lambda\to 0}{\longrightarrow} \Sigma^{(2)}(\lambda^2\tilde{E} + \omega_\mu)\Big|_{\lambda=0} = \Sigma^{(2)}(\omega_\mu + i0^+). \tag{6.36}$$

The propagator in the rescaled energy takes now the form

$$\widetilde{G}_\mu(\tilde{E}) = \lim_{\lambda\to 0}\frac{1}{\tilde{E} - \Sigma^{(2)}(\lambda^2\tilde{E} + \omega_\mu) + {\rm O}(\lambda^2)} = \frac{1}{\tilde{E} - \Sigma^{(2)}(\omega_\mu + i0^+)}, \tag{6.37}$$

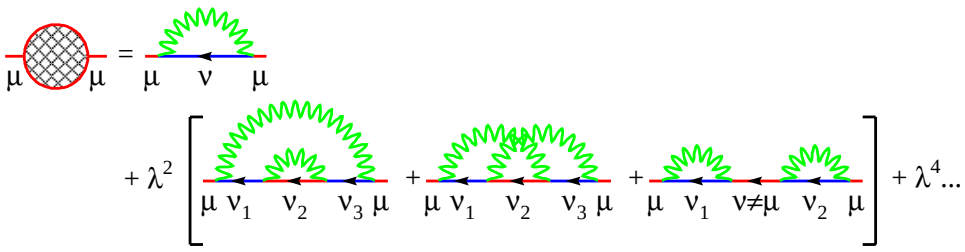

Figure 6.2: Graphic representation of (6.34): $\Sigma^{(2)}$ and $\Sigma^{(4)}$ are in the first and second line, respectively.

where

$$\Sigma^{(2)}(\omega_\mu + i0^+) = \sum_{\nu,\beta} \int_0^\infty d\omega \frac{|\varphi_\beta^{\nu\mu}(\omega)|^2}{\omega_\mu - \omega_\nu - \omega + i0^+}. \tag{6.38}$$

The last two equations correspond to (6.21)-(6.22): the propagator reduces to that of a generalized rotating-wave approximation.

We see that the Van Hove limit works by following two logical steps. First, it constrains the evolution in a Tamm-Dancoff sector: the system can only "explore" those states that are directly related to the initial state $|\mu\rangle$ by the interaction V'. In other words, in this limit, the excitation number $\mathcal{N}_\mu \equiv b_\mu^\dagger b_\mu + \sum_{\beta,\omega} a_{\omega\beta}^\dagger a_{\omega\beta}$ becomes a conserved quantity (even though the original Hamiltonian contains counter-rotating terms), the Hamiltonian dynamics effectively becomes of the Lee type and, as a consequence, the self-energy function consists only of a second order contribution that can be evaluated exactly. Second, it reduces this second order contribution, which depends on energy as in (6.35), to a constant (its value in the energy ω_μ of the initial state), like in (6.36). Hence the analytical properties of the propagator, which had branch-cut singularities, reduce to those of a single complex pole, whose imaginary part (responsible for exponential decay) yields the Fermi Golden Rule, evaluated at second order of perturbation theory.

Notice that it is the latter step (and not the former one) which is strictly necessary to obtain a dissipative behavior: Indeed, as we have seen in Sec. 4.6.3, substitution of the pole value in the total self-energy function yields exponential decay, including all higher-order corrections to the Fermi Golden Rule. On the other hand, the first step is very important when one is interested in computing the leading order corrections to the exponential behavior. To this purpose one can solve the problem in a restricted Tamm-Duncoff sector of the total Hilbert space (i.e., in an eigenspace of $\mathcal{N}_\mu$ — in our case, $\mathcal{N}_\mu = 1$) and exactly evaluate the evolution of the system with its deviations from exponential law.

Let us add a final remark. As is well known, a nondispersive propagator yields a Markovian evolution. Let us briefly sketch how this occurs in the present model. From (6.33), antitransforming,

$$\frac{i}{2\pi}\int_B dE\, e^{-iEt}\,[E\, G_\mu(E+\omega_\mu) - 1] = \frac{i}{2\pi}\int_B dE\, e^{-iEt}\lambda^2\Sigma(E+\omega_\mu)\, G_\mu(E+\omega_\mu), \tag{6.39}$$

we obtain (for $t > 0$)

$$i\dot{\mathcal{A}}(t) = \lambda^2 \int_0^t d\tau\, \sigma(t-\tau)\, \mathcal{A}(\tau), \tag{6.40}$$

where $\mathcal{A}(t)$ is the survival amplitude and

$$\sigma(t) \equiv \frac{1}{2\pi}\int_B dE\, e^{-iEt}\Sigma(E+\omega_\mu) = \frac{e^{i\omega_\mu t}}{2\pi}\int_B dE\, e^{-iEt}\Sigma(E). \tag{6.41}$$

Equation (6.40) is clearly nonlocal in time and all memory effects are contained in $\sigma(t)$, the inverse transform of the self-energy function. If such a self-energy function is a complex constant (energy independent), $\Sigma(E) = C$, then $\sigma(t) = C\delta(t)$ and equation (6.40) becomes

$$i\dot{\mathcal{A}}(t) = \lambda^2 C\mathcal{A}(t), \tag{6.42}$$

describing a Markovian behavior, without memory effects (Gardiner [1990]; van Kampen [1992]). In particular, the Van Hove limit is equivalent to set $C = \Sigma^{(2)}(\omega_\mu + i0^+)$ and the Weisskopf-Wigner approximation is $C = \Sigma^{(2)}(\omega_\mu + i0^+) + \mathrm{O}(\lambda^2)$.

In conclusion, in the Van Hove limit, the evolution of the survival amplitude, which was nonlocal in time due to the dispersive character of the propagator (the self-energy function depended on E) becomes local and Markovian (only the value of the self-energy function in ω_μ determines the evolution).

6.4 General framework

We can now further generalize our analysis: consider the Hamiltonian

$$H = H_0 + \lambda V \tag{6.43}$$

and suppose that the initial state $|a\rangle$ has the following properties

$$H_0|a\rangle = E_a|a\rangle, \qquad \langle a|V|a\rangle = 0, \qquad \langle a|a\rangle = 1. \tag{6.44}$$

The survival amplitude (in the interaction representation) of state $|a\rangle$ reads

$$\mathcal{A}(t) = \langle a|e^{iH_0 t}U(t)|a\rangle = \frac{i}{2\pi}\int_{\mathrm{B}} dE\, e^{-iEt}G_a(E+E_a) = \frac{i}{2\pi}\int_{\mathrm{B}} dE\, \frac{e^{-iEt}}{E - \lambda^2\Sigma(E+E_a)}, \tag{6.45}$$

where $\lambda^2\Sigma(E)$ is the 1-particle irreducible self-energy function, that can be expressed by a perturbation expansion

$$\Sigma_a(E) = \lambda^2\Sigma(E) = \lambda^2\Sigma^{(2)}(E) + \lambda^4\Sigma^{(4)}(E) + \cdots . \tag{6.46}$$

The second order contribution has the general form

$$\Sigma^{(2)}(E) \equiv \langle a|VP_d\frac{1}{E-H_0}P_dV|a\rangle = \sum_{n\neq a}|\langle a|V|n\rangle|^2\,\frac{1}{E-E_n} = \int_0^\infty \frac{dE'}{2\pi}\,\frac{\Gamma(E')}{E-E'}, \tag{6.47}$$

where $P_d = 1 - |a\rangle\langle a|$ is the projector over the decayed states, $\{|n\rangle\}$ is a complete set of eingenstates of H_0 ($H_0|n\rangle = E_n|n\rangle$ and we set $E_0 = 0$) and

$$\Gamma(E) \equiv 2\pi\sum_{n\neq a}|\langle a|V|n\rangle|^2\,\delta(E-E_n). \tag{6.48}$$

Notice that $\Gamma(E) \geq 0$ for $E > 0$ and is zero otherwise. In the Van Hove limit we get

$$\widetilde{\mathcal{A}}(\tilde{t}) \equiv \lim_{\lambda\to 0}\mathcal{A}\left(\frac{\tilde{t}}{\lambda^2}\right) = \frac{i}{2\pi}\int_{\mathrm{B}} d\tilde{E}\, e^{-i\tilde{E}\tilde{t}}\widetilde{G}_a(\tilde{E}), \tag{6.49}$$

where the resulting propagator in the rescaled energy $\tilde{E} = E/\lambda^2$ reads

$$\widetilde{G}_a(\tilde{E}) = \frac{1}{\tilde{E} - \Sigma^{(2)}(E_a + i0^+)}. \tag{6.50}$$

To obtain this result we used

$$\Sigma(\lambda^2\tilde{E}+E_a) \stackrel{\lambda\to 0}{\longrightarrow} \Sigma^{(2)}(\lambda^2\tilde{E}+E_a)\Big|_{\lambda=0} = \Sigma^{(2)}(E_a+i0^+) \tag{6.51}$$

(Weisskopf-Wigner approximation and Fermi Golden Rule).

Just above the positive real axis we can write

$$\Sigma^{(2)}(E+i0^+) = \Delta(E) - \frac{i}{2}\Gamma(E), \tag{6.52}$$

where

$$\Delta(E) = \mathrm{P}\int_0^\infty \frac{dE'}{2\pi}\frac{\Gamma(E')}{E-E'}. \tag{6.53}$$

Let $\Gamma(E)$ be sommable in $(0,+\infty)$. Furthermore by assuming as in Eq. (4.103) the near-threshold behavior

$$\Gamma(E) \propto E^{\eta-1} \quad \text{for} \quad E\to 0, \tag{6.54}$$

for some $\eta > 1$, one gets the following asymptotic behavior at short and long times:

$$P(t) \;\sim\; 1-\frac{t^2}{\tau_{\mathrm{Z}}^2} \qquad (t\ll\tau_{\mathrm{Z}}), \tag{6.55}$$

$$P(t) \;\sim\; |Z|^2 e^{-t/\tau_{\mathrm{E}}} + \lambda^4\frac{|C|^2}{(E_a t)^{2\eta}} + 2\lambda^2\frac{|CZ|}{(E_a t)^{\eta}}e^{-t/2\tau_{\mathrm{E}}}\cos\left[(E_a+\Delta E)t-\xi\right] \qquad (t\gg\tau_{\mathrm{Z}}), \tag{6.56}$$

where

$$\tau_{\mathrm{Z}} = \frac{1}{\lambda}\left[\int_0^\infty \frac{dE}{2\pi}\Gamma(E)\right]^{-1/2}, \tag{6.57}$$

$$\tau_{\mathrm{E}} = \frac{1}{\lambda^2\Gamma(E_a)} + \mathrm{O}(1), \tag{6.58}$$

$$\Delta E = \lambda^2\Delta(E_a) + \mathrm{O}(\lambda^4), \tag{6.59}$$

$$\xi = \mathrm{Arg}Z - \mathrm{Arg}C, \tag{6.60}$$

$$Z = 1+\mathrm{O}(\lambda^2), \tag{6.61}$$

$$C = 1+\mathrm{O}(\lambda^2). \tag{6.62}$$

The transition to a power law occurs when the first two terms in the r.h.s. of (6.56) are comparable, namely for $t=\tau_{\mathrm{pow}}$, where τ_{pow} is the solution of the equation

$$\frac{\tau_{\mathrm{pow}}}{\tau_{\mathrm{E}}} = 4(\eta+1)\log\frac{1}{\lambda} + 2\eta\log\frac{E_a}{\Gamma(E_a)} + \log\left|\frac{Z}{C}\right| + \eta\log\frac{\tau_{\mathrm{pow}}}{\tau_{\mathrm{E}}}, \tag{6.63}$$

i.e., for $\lambda\to 0$

$$\tau_{\mathrm{pow}} = 4\tau_{\mathrm{E}}(\eta+1)\log\lambda^{-1} + \mathrm{O}\left(\log\log\lambda^{-1}\right). \tag{6.64}$$

Let us now look at the temporal behavior for a small but *finite* value of λ, using Van Hove's technique. In the rescaled time, $\tilde{t}=\lambda^2 t$, the Zeno region vanishes

$$\tilde{\tau}_{\mathrm{Z}} \equiv \lambda^2\tau_{\mathrm{Z}} = \lambda\left[\int_0^\infty \frac{dE}{2\pi}\Gamma(E)\right]^{-1/2} = \mathrm{O}(\lambda) \tag{6.65}$$

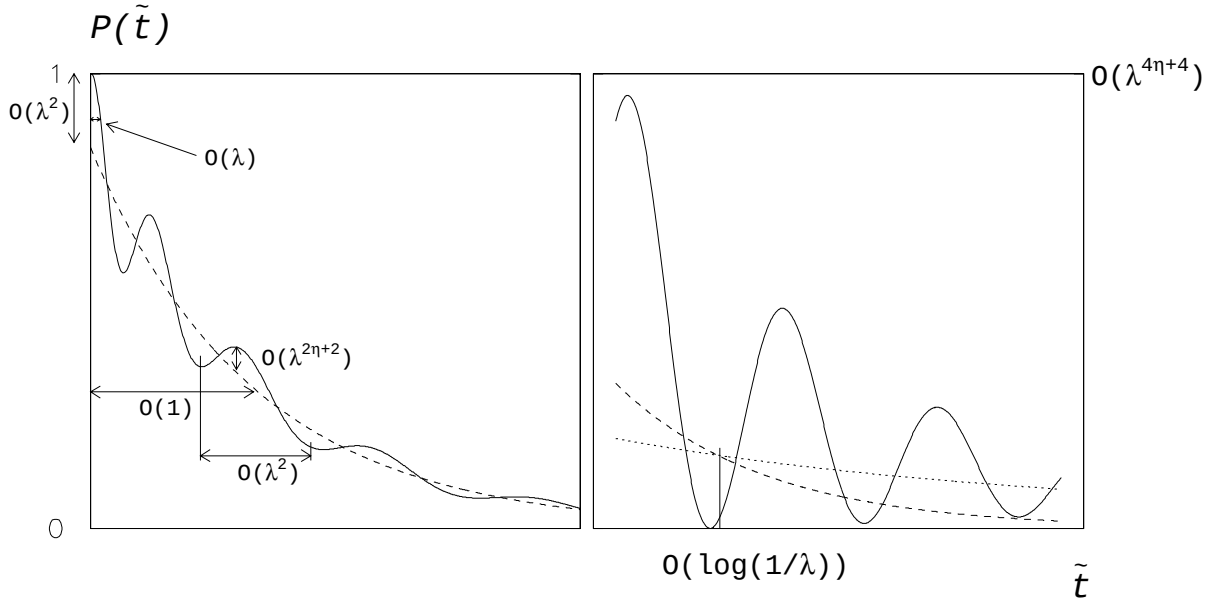

Figure 6.3: Essential features (not in scale!) of the survival probability as a function of the rescaled time $\tilde{t}$. The Zeno time is $\mathrm{O}(\lambda)$, the lifetime $\mathrm{O}(1)$, during the whole evolution there are oscillations of amplitude $\mathrm{O}(\lambda^{2\eta+2})$ and the transition to a power law occurs after a time $\mathrm{O}(\log(1/\lambda))$ [see (6.65)-(6.68)]. From (6.61), the normalization factor becomes unity like $1-\mathrm{O}(\lambda^2)$. The dashed line is the exponential and the dotted line the power law.

and Eq. (6.56) becomes valid at *shorter and shorter* (rescaled) times and reads

$$P(\tilde{t}) \sim |Z|^2 e^{-\tilde{t}/\tilde{\tau}_{\mathrm{E}}} + \lambda^{4(\eta+1)} \frac{|C|^2}{(E_a \tilde{t})^{2\eta}} + 2\lambda^{2(\eta+1)} \frac{|CZ|}{(E_a t)^{\eta}} e^{-\tilde{t}/2\tilde{\tau}_{\mathrm{E}}} \cos\left(\frac{E_a + \Delta E}{\lambda^2}\tilde{t} - \xi\right), \quad (6.66)$$

where

$$\tilde{\tau}_{\mathrm{E}} \equiv \lambda^2 \tau_{\mathrm{E}} = \frac{1}{\Gamma(E_a)} = \mathrm{O}(1), \quad (6.67)$$

$$\tilde{\tau}_{\mathrm{pow}} \equiv \lambda^2 \tau_{\mathrm{pow}} \simeq 4\tilde{\tau}_{\mathrm{E}}(\eta+1)\log\frac{1}{\lambda} = \mathrm{O}\left(\log\frac{1}{\lambda}\right). \quad (6.68)$$

Figure 6.3 displays the main features of the temporal behavior of the survival probability. The typical values of the physical constants yield very small deviations from the exponential law. For this reason, we displayed in Fig. 6.3 the survival probability by greatly exaggerating its most salient features.

The Van Hove limit performs several actions at once: It makes the initial quadratic (quantum Zeno) region vanish, it "squeezes" out the oscillations and it "pushes" the power law to infinity, leaving only a clean exponential law at all times, with the right normalization. All this is not surprising, being implied by the Weisskopf-Wigner approximation. However, the concomitance of these features is so remarkable that one cannot but wonder at the effectiveness of this limiting procedure.

Part II

CONTROLLED DYNAMICS

Chapter 7

Quantum Zeno and inverse quantum Zeno effect

7.1 Introduction

In this chapter we shall investigate the main features of the so-called quantum Zeno effect (von Neumann [1932]; Beskow and Nilsson [1967]; Khalfin [1968]; Misra and Sudarshan [1977]), named after the Greek philosopher Zeno from Elea, famous for his paradoxical argumentations against motion. One of Zeno's paradoxes is the object of the present investigation: A sped arrow never reaches its target, because at every instant of time, if we look at the arrow, we see that it occupies a portion of space equal to its own size. At any given moment the arrow is therefore immobile, and by summing up many such "immobilities" it is clearly impossible, according to Zeno, to obtain motion. It is amusing that some quantum mechanical states, under particular conditions, behave in a way that is reminiscent of this paradox. In very few words, the evolution of a quantum mechanical state can be slowed down (or even halted in some limit) when very frequent measurements are performed on the system, in order to check whether it is still in its initial state: Zeno's quantum arrow (the wave function) does not move, if it is continuously observed.

The interest in the quantum Zeno effect (QZE) has been revived, during the last decade, mainly because of some interesting proposals that made it liable to *experimental* investigation. Unlike previous studies, confined to a purely academic level, the investigation of the last few years has focused on practical experiments, possible applications, as well as theoretical implications and interpretative issues. The quantum Zeno effect has been mainly investigated for oscillating systems (Cook [1988]; Itano, Heinzen, Bollinger and Wineland [1990]; Pascazio, Namiki, Badurek and Rauch [1993]; Kwiat, Weinfurter, Herzog, Zeilinger and Kasevich [1995]), whose Poincaré time is finite. However, the discussion cannot be limited to oscillating systems: new and somewhat unexpected phenomena are disclosed when one considers unstable systems, whose Poincaré time is infinite (Bernardini, Maiani and Testa [1993]; Facchi and Pascazio [1998]; Maiani and Testa [1998]; Joichi, Matsumoto and Yoshimura [1998]; Alvarez-Estrada and Sánchez-Gómez [1999]). In this case the analysis becomes more complicated and requires a quantum field theoretical framework.

In this chapter, we introduce the fundamentals of the quantum Zeno and "inverse" quantum Zeno effect (IZE), by making use of elementary quantum mechanical techniques. We shall first use the seminal formulation of QZE in terms of projection operators: this is the usual approach and makes use of what we might call a "pulsed" observation of the quantum state (Mihokova, Pascazio and Schulman [1997]; Schulman [1998]). We then explain that it is not necessary to

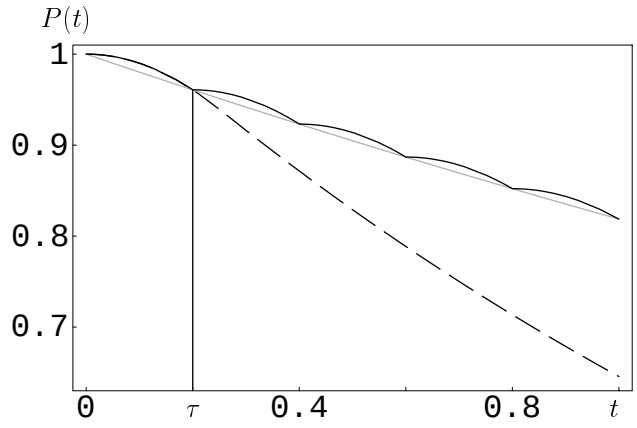

Figure 7.1: Evolution with frequent "pulsed" measurements: quantum Zeno effect. The dashed (full) line is the survival probability without (with) measurements.

use projection operators and nonunitary dynamics: a fully dynamical explanation of the QZE is possible, involving Hamiltonians and no projectors (Petrosky, Tasaki and Prigogine [1990]; Pascazio and Namiki [1994]). Then we introduce the notion of "continuous" observation of the quantum state, e.g. performed by means of an intense field. Although this idea has been revived only recently (Mihokova, Pascazio and Schulman [1997]; Schulman [1998]; Pascazio and Facchi [1999]), it is contained, in embryo, in earlier papers (Kraus [1981]; Peres [1980a]; Plenio, Knight and Thompson [1996]). This idea will lead us to formulate a theorem which is somewhat complementary to Misra and Sudarshan's and a novel definition of QZE (Facchi and Pascazio [2001]).

The *leitmotif* of this chapter and, in fact, of the whole second part of this work is that the quantum Zeno effect is a dynamical phenomenon, that can be explained in terms of the Schrödinger equation, without making use of projection operators. We will implicitly assume, throughout our discussion, that a projection operators is just a shorthand notation, that summarizes the effects of a much more complicated underlying dynamical process, involving a huge number of elementary quantum mechanical systems (Namiki, Pascazio and Nakazato [1997]).

7.2 Pulsed observation

Let us introduce the fundamental features of the quantum Zeno effect. We shall follow the "historical" approach (von Neumann [1932]; Beskow and Nilsson [1967]; Khalfin [1968]; Misra and Sudarshan [1977]), by considering "pulsed" measurements. The alternative notion of continuous measurement will be discussed in Sec. 7.4.

7.2.1 Survival probability under pulsed measurements

We have seen in the first part of this work that, under general conditions, the undisturbed survival probability

$$P(t) = |\mathcal{A}(t)|^2 = |\langle a|e^{-iHt}|a\rangle|^2 \tag{7.1}$$

exhibits at short times a quadratic behavior

$$P(t) = 1 - t^2/\tau_{\rm Z}^2 + \cdots, \qquad \tau_{\rm Z}^{-2} \equiv \langle a|H^2|a\rangle - \langle a|H|a\rangle^2. \tag{7.2}$$

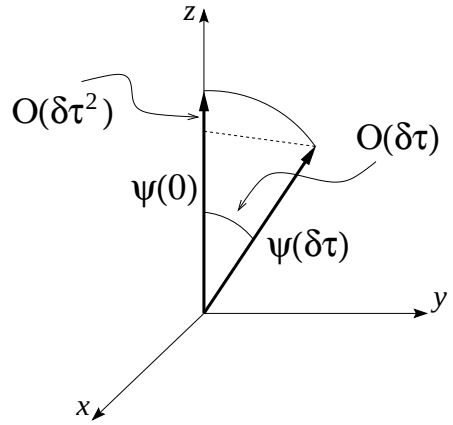

Figure 7.2: Short-time evolution of phase and probability.

For instance, with the two-level Hamiltonian (3.1), when $\omega_a = \omega_b = 0$, one finds

$$\mathcal{A}(t) = \cos \lambda t, \tag{7.3}$$
$$P(t) = \cos^2 \lambda t, \tag{7.4}$$
$$\tau_{\rm Z} = \lambda^{-1}. \tag{7.5}$$

Let us now perform N measurements at time intervals τ, in order to check whether the system is still in its initial state. The survival probability after the measurements reads

$$P^{(N)}(t) = P(\tau)^N = P(t/N)^N \sim \left[1 - (t/N\tau_{\rm Z})^2\right]^N \sim \exp(-t^2/N\tau_{\rm Z}^2) \stackrel{N\to\infty}{\longrightarrow} 1, \tag{7.6}$$

where $t = N\tau$ is the total duration of the experiment. The $N \to \infty$ limit was originally named limit of "continuous observation" and regarded as a paradoxical result (Misra and Sudarshan [1977]): Infinitely frequent measurements halt the quantum mechanical evolution and "freeze" the system in its initial state. Zeno's quantum mechanical arrow (the wave function), sped by the Hamiltonian, does not move, if it is continuously observed. The investigation of the last few years has shown that the QZE is not paradoxical: although the $N \to \infty$ limit must be considered as a mathematical abstraction (Ghirardi, Omero, Weber and Rimini [1979]; Nakazato, Namiki, Pascazio and Rauch [1995]; Venugopalan and Ghosh [1995]; Pati [1996]; Hradil, Nakazato, Namiki, Pascazio and Rauch [1998]), the evolution of a quantum system can indeed be slowed down for sufficiently large N (Itano, Heinzen, Bollinger and Wineland [1990]; Petrosky, Tasaki and Prigogine [1990]; Petrosky, Tasaki and Prigogine [1991]; Peres and Ron [1990]; Ballentine [1991]; Itano, Heinzen, Bollinger and Wineland [1991]; Frerichs and Schenzle [1992]; Inagaki, Namiki and Tajiri [1992]; Home and Whitaker [1992]; Pascazio, Namiki, Badurek and Rauch [1993]; Home and Whitaker [1993]; Blanchard and Jadczyk [1993]; Altenmuller and Schenzle [1994]; Pascazio and Namiki [1994]; Schulman, Ranfagni and Mugnai [1994]; Berry [1995]; Beige and Hegerfeldt [1996]; Schulman [1997]; Thun and Peřina [1998]). The Zeno evolution is shown in Fig. 7.1.

In a few words, the QZE is ascribable to the following mathematical properties of the Schrödinger equation: in a short time $\delta\tau \sim 1/N$, the phase of the wave function evolves like $\mathrm{O}(\delta\tau)$, while the probability changes by $\mathrm{O}(\delta\tau^2)$, so that

$$P^{(N)}(t) \simeq \left[1 - \mathrm{O}(1/N^2)\right]^N \stackrel{N\to\infty}{\longrightarrow} 1. \tag{7.7}$$

This is sketched in Fig. 7.2 and is a very general feature of the Schrödinger equation.

7.2.2 Misra and Sudarshan's theorem

We consider here the derivation of the quantum Zeno paradox given by Misra and Sudarshan [1977]. The proof makes use of von Neumann's projections and therefore assumes that the measurement is instantaneous. Consider a quantum system Q, whose states belong to the Hilbert space $\mathcal{H}$ and whose evolution is described by the unitary operator $U(t) = \exp(-iHt)$, where H is a time-independent semi-bounded Hamiltonian. Let E be a projection operator that does not commute with the Hamiltonian, $[E, H] \neq 0$, and $E\mathcal{H}E = \mathcal{H}_E$ the subspace spanned by its eigenstates. The initial density matrix ρ_0 of system Q is taken to belong to $\mathcal{H}_E$. If Q is let to follow its "undisturbed" evolution, under the action of the Hamiltonian H (i.e., no measurements are performed in order to get information about its quantum state), the final state at time T reads

$$\rho(T) = U(T)\rho_0 U^\dagger(T) \tag{7.8}$$

and the probability that the system is still in $\mathcal{H}_E$ at time T is

$$P(T) = \mathrm{Tr}\left[U(T)\rho_0 U^\dagger(T)E\right]. \tag{7.9}$$

This is the survival probability: it is in general smaller than 1, since the Hamiltonian H induces transitions out of $\mathcal{H}_E$. We shall say that the quantum system has "survived" if it is found to be in $\mathcal{H}_E$ by means of a suitable measurement process. We stress that we do not distinguish between one- and many-dimensional projections.

Assume that we perform a measurement at time t, in order to check whether Q has survived. Such a measurement is formally represented by the projection operator E. By definition,

$$\rho_0 = E\rho_0 E, \qquad \mathrm{Tr}[\rho_0 E] = 1. \tag{7.10}$$

After the measurement, the state of Q changes into

$$\rho_0 \to \rho(t) = EU(t)\rho_0 U^\dagger(t)E, \tag{7.11}$$

with probability

$$P(t) = \mathrm{Tr}\left[U(t)\rho_0 U^\dagger(t)E\right] = \mathrm{Tr}\left[EU(t)E\rho_0 EU^\dagger(t)E\right] = \mathrm{Tr}\left[V(t)\rho_0 V^\dagger(t)\right], \quad \text{where} \quad V(t) \equiv EU(t)E. \tag{7.12}$$

This is the probability that the system has "survived" in $\mathcal{H}_E$. There is, of course, a probability $1-P$ that the system has not survived (i.e., it has made a transition outside $\mathcal{H}_E$) and its state has changed into $\rho'(t) = (1-E)U(t)\rho_0 U^\dagger(t)(1-E)$. The states ρ and ρ' together make up a block diagonal matrix: The initial density matrix is reduced to a mixture and any possibility of interference between "survived" and "not survived" states is destroyed (complete decoherence).

We shall concentrate henceforth our attention on the measurement outcome (7.11)-(7.12). We observe that the evolution just described is time-translation invariant and the dynamics is *not* reversible (not only not time-reversal invariant).

The above is the Copenhagen interpretation: the measurement is considered to be instantaneous. The *quantum Zeno paradox* is the following. We prepare Q in the initial state ρ_0 at time 0 and perform a series of E-observations at times $t_j = jT/N$ $(j = 1, \cdots, N)$. The state of Q after the above-mentioned N measurements reads

$$\rho^{(N)}(T) = V_N(T)\rho_0 V_N^\dagger(T), \qquad V_N(T) \equiv [EU(T/N)E]^N \tag{7.13}$$

and the probability to find the system in $\mathcal{H}_E$ (survival probability) is given by

$$P^{(N)}(T) = \mathrm{Tr}\left[V_N(T)\rho_0 V_N^\dagger(T)\right]. \tag{7.14}$$

Equations (7.13)-(7.14) display the "quantum Zeno effect:" repeated observations in succession modify the dynamics of the quantum system; under general conditions, if N is sufficiently large, all transitions outside $\mathcal{H}_E$ are inhibited. Notice again that the dynamics (7.13)-(7.14) is not reversible.

In order to consider the $N \to \infty$ limit ("continuous observation"), one needs some mathematical requirements: assume that the limit

$$\mathcal{V}(T) \equiv \lim_{N\to\infty} V_N(T) \tag{7.15}$$

exists in the strong sense for $T \geq 0$. The final state of Q is then

$$\rho(T) = \mathcal{V}(T)\rho_0\mathcal{V}^\dagger(T) \tag{7.16}$$

and the probability to find the system in $\mathcal{H}_E$ is

$$\mathcal{P}(T) \equiv \lim_{N\to\infty} P^{(N)}(T) = \mathrm{Tr}\left[\mathcal{V}(T)\rho_0\mathcal{V}^\dagger(T)\right]. \tag{7.17}$$

One should carefully notice that nothing is said about the final state $\rho(T)$, which depends on the characteristics of the model investigated and on the *very measurement performed* (i.e. on the projection operator E, by means of which V_N is defined). By assuming the strong continuity of $\mathcal{V}(t)$

$$\lim_{t\to 0^+} \mathcal{V}(t) = E, \tag{7.18}$$

one can prove that, under general conditions, the operators

$$\mathcal{V}(T) \quad \text{exist for all real } T \text{ and form a semigroup.} \tag{7.19}$$

Moreover, by time-reversal invariance

$$\mathcal{V}^\dagger(T) = \mathcal{V}(-T), \tag{7.20}$$

so that $\mathcal{V}^\dagger(T)\mathcal{V}(T) = E$. This implies, by (7.10), that

$$\mathcal{P}(T) = \mathrm{Tr}\left[\rho_0\mathcal{V}^\dagger(T)\mathcal{V}(T)\right] = \mathrm{Tr}\left[\rho_0 E\right] = 1. \tag{7.21}$$

If the particle is "continuously" observed, in order to check whether it has survived inside $\mathcal{H}_E$, it will never make a transition to $\mathcal{H}_E^\perp$. This was named *quantum Zeno paradox* (Misra and Sudarshan [1977]). The expression *quantum Zeno effect* seems more appropriate, nowadays, in particular when one considers the evolution for large, but not infinite, values of N.

Two important remarks are now in order: first, it is not clear whether the dynamics in the $N \to \infty$ limit is time reversible. Although one ends up, in general, with a semigroup, there are concrete elements of reversibility in the above equations. Second, the theorem just summarized *does not* state that the system *remains* in its initial state, after the series of very frequent measurements. Rather, the system is left in the subspace $\mathcal{H}_E$, instead of evolving "naturally" in the total Hilbert space $\mathcal{H}$. This subtle point, implied by Eqs. (7.16)-(7.21), is not duely stressed in the literature (a concrete example is considered by Machida, Nakazato, Pascazio, Rauch and Yu [1999]).

We also emphasize that there is a conceptual gap between Eqs. (7.14) and (7.17): to perform an experiment with N finite is only a practical problem, from the physical point of view. On the other hand, the $N \to \infty$ case is physically unattainable, and is rather to be regarded as a mathematical limit (although a very interesting one).

7.2.3 Quantum Zeno and Inverse quantum Zeno effects

It is convenient to rewrite (7.6) in the following way ($t = N\tau$)

$$P^{(N)}(t) = P(\tau)^N = \exp(N \log P(\tau)) = \exp(-\gamma_{\text{eff}}(\tau)t), \tag{7.22}$$

where we introduced an effective decay rate

$$\gamma_{\text{eff}}(\tau) \equiv -\frac{1}{\tau} \log P(\tau) \geq 0 \, . \tag{7.23}$$

For instance, for times τ such that $P(\tau) \sim \exp(-\tau^2/\tau_{\text{Z}}^2)$ with good approximation, one easily checks that γ_{eff} is a linear function of τ

$$\gamma_{\text{eff}}(\tau) \sim \tau/\tau_{\text{Z}}^2, \qquad \text{for} \quad \tau \to 0. \tag{7.24}$$

Notice that $\gamma_{\text{eff}}(\tau)$ in (7.23) represents the effective decay rate of a system that evolves freely up to time τ and is measured at time τ. One expects to recover the "natural" decay rate γ (if it exists), in agreement with the Fermi Golden Rule, for sufficiently long times, i.e., after the initial quadratic region is over

$$\gamma_{\text{eff}}(\tau) \overset{\text{"long"}\tau}{\longrightarrow} \gamma. \tag{7.25}$$

The *quantitative* meaning of the expression "long" in the above equation represents an interesting conceptual problem and has been tackled in chapter 5, where we found that τ_{Z} is not the right time scale, for the quadratic behavior is in general valid at times much shorter (proportional to the inverse bandwidth).

We now concentrate our attention on a truly unstable system, with decay rate γ. We ask whether it is possible to find a finite time τ^* such that

$$\gamma_{\text{eff}}(\tau^*) = \gamma. \tag{7.26}$$

If such a time exists, then by performing measurements at time intervals τ^* the system decays according to its "natural" lifetime, as if no measurements were performed. By Eqs. (7.26) and (7.23) one gets

$$P(\tau^*) = e^{-\gamma\tau^*}, \tag{7.27}$$

i.e., τ^* is the intersection between the curves $P(t)$ and $e^{-\gamma t}$. Figure 7.3 illustrates an example in which such a time τ^* exists. By looking at this figure, it is evident that if $\tau = \tau_1 < \tau^*$ one obtains a QZE. *Vice versa*, if $\tau = \tau_2 > \tau^*$, one obtains an *inverse* Zeno effect (IZE). In this sense, τ^* can be viewed as a *transition time* from a quantum Zeno to an inverse Zeno effect. Paraphrasing Misra and Sudarshan [1977] we can say that τ^* determines the transition from Zeno (who argued that a sped arrow, if observed, does not move) to Heraclitus (who replied that everything flows). We shall see that in general it is not always possible to determine τ^*: Eq. (7.26) may have no finite solutions. This will be thoroughly discussed in the following, but it is interesting to anticipate some general conclusions. As we have seen in the first part of this work, at intermediate times the survival probability of a truly unstable system is dominated by the pole contribution and reads with very good approximation

$$P(t) = |\mathcal{A}(t)|^2 \simeq \mathcal{Z} e^{-\gamma t}, \tag{7.28}$$

where $\mathcal{Z}$, the intersection of the asymptotic exponential with the $t = 0$ axis, is the wave function renormalization, given by the square modulus of the residue of the pole of the propagator.

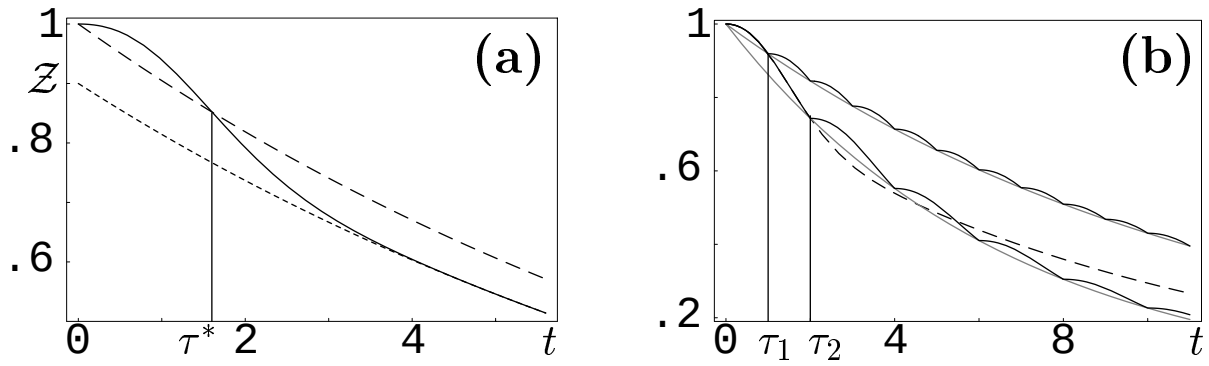

Figure 7.3: (a) Determination of τ^*. The full line is the survival probability, the dashed line the exponential $e^{-\gamma t}$ and the dotted line the asymptotic exponential $\mathcal{Z}e^{-\gamma t}$ in (7.28). (b) Quantum Zeno vs inverse Zeno ("Heraclitus") effect. The dashed line represents a typical behavior of the survival probability $P(t)$ when no measurement is performed: the short-time Zeno region is followed by an approximately exponential decay with a natural decay rate γ. When measurements are performed at time intervals τ, we get the effective decay rate $\gamma_{\rm eff}(\tau)$. The full lines represent the survival probabilities and the dotted lines their exponential interpolations, according to (7.22). For $\tau_1 < \tau^* < \tau_2$ the effective decay rate $\gamma_{\rm eff}(\tau_1)$ [$\gamma_{\rm eff}(\tau_2)$] is smaller (QZE) [larger (IZE)] than the "natural" decay rate γ. When $\tau = \tau^*$ one recovers the natural lifetime, according to (7.26).

We claim that a sufficient condition for the existence of a solution τ^* of Eq. (7.26) is that

$$\mathcal{Z} < 1. \tag{7.29}$$

This is easily proved by graphical inspection. The case $\mathcal{Z} < 1$ is shown in Fig. 7.3(a): $P(t)$ and $e^{-\gamma t}$ must intersect, since according to (7.28) $P(t) \sim \mathcal{Z}e^{-\gamma t}$ for large t, and a finite solution τ^* can always be found. The other case, $\mathcal{Z} > 1$, is shown in Fig. 7.4: a solution may or may not exist, depending on the features of the model investigated. We shall come back to the Zeno-Heraclitus transition many times in the following. The occurrence of an inverse Zeno effect has been discussed by several authors, in different contexts (Pascazio [1996]; Schulman [1997]; Pascazio and Facchi [1999]; Kofman and Kurizki [1999]; Facchi and Pascazio [2000a]; Kofman and Kurizki [2000]; Facchi, Nakazato and Pascazio [2000]; Facchi and Pascazio [2001]).

There are situations (e.g., oscillatory systems, whose Poincaré time is finite) where γ and $\mathcal{Z}$ cannot be defined. As we shall see, these cases require a different treatment, for the very definition of Zeno effect becomes somewhat delicate. This will be discussed later.

7.2.4 Pitfalls: "repopulation" and conceptual difficulties

The quantum Zeno effect has become very popular during the last decade, mainly because of an interesting idea due to Cook [1988], who proposed to test the QZE with a two-level system, and the subsequent experiment performed by Itano, Heinzen, Bollinger and Wineland [1990]. This experiment provoked a very lively debate and was discussed by many authors (Petrosky, Tasaki and Prigogine [1990]; Peres and Ron [1990]; Petrosky, Tasaki and Prigogine [1991]; Ballentine [1991]; Itano, Heinzen, Bollinger and Wineland [1991]; Frerichs and Schenzle [1992]; Inagaki, Namiki and Tajiri [1992]; Home and Whitaker [1992]; Home and Whitaker [1993]; Blanchard and Jadczyk [1993]; Pascazio, Namiki, Badurek and Rauch [1993]; Altenmuller and Schenzle [1994]; Pascazio and Namiki [1994]; Schulman, Ranfagni and Mugnai [1994]; Berry

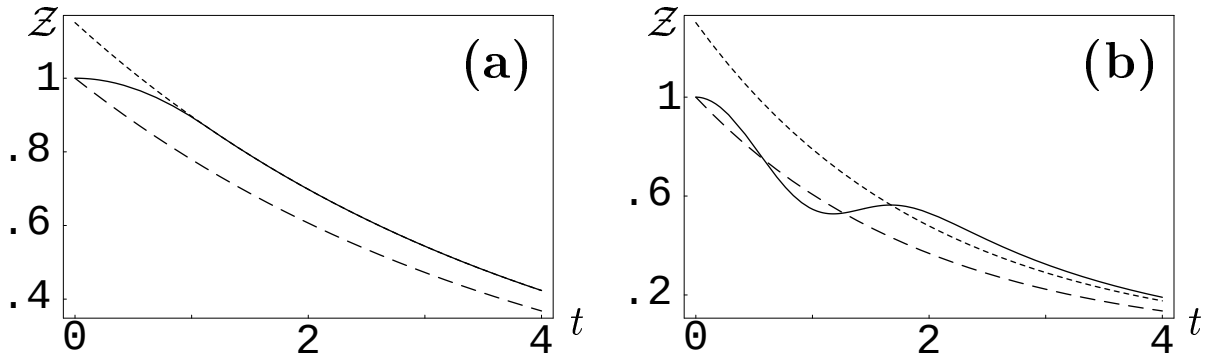

Figure 7.4: Study of the case $\mathcal{Z} > 1$. The full line is the survival probability, the dashed line the renormalized exponential $e^{-\gamma t}$ and the dotted line the asymptotic exponential $\mathcal{Z}e^{-\gamma t}$. (a) If $P(t)$ and $e^{-\gamma t}$ do not intersect, a finite solution τ^* does not exist. (b) If $P(t)$ and $e^{-\gamma t}$ intersect, a finite solution τ^* exists. (In this case there are always at least two intersections.)

[1995]; Beige and Hegerfeldt [1996]; Schulman [1997]; Thun and Peřina [1998]). However, we shall follow here a different route: rather than analyzing Cook's proposal and the related experiment, we shall consider a physically equivalent situation that suits better our discussion and can be easily compared to the analysis of the following sections.

The central mathematical quantity considered by Misra and Sudarshan [1977] is "the probability $\mathcal{P}(0, T; \rho_0)$ that no decay is found *throughout the interval* $\Delta = [0, T]$ when the initial state of the system was known to be ρ_0." (Italics in the original. Some symbols have been changed.) In the notation of Sec. 7.2.1, this reads

$$\mathcal{P}(0, T; \rho_0) \equiv \lim_{N\to\infty} P^{(N)}(T). \tag{7.30}$$

Notice that the above-mentioned "survival probability" is the probability of finding the system in its initial state ρ_0 at *every* measurement, during the interval Δ. This is a subtle point, as we shall see.

Consider a three-level (atomic) system, shined by an rf field of frequency Ω, that provokes Rabi oscillations between levels $|a\rangle$ and $|b\rangle$. The two-level Hamiltonian (3.1), when $\omega_a = \omega_b = 0$, reads

$$H_{\rm I} = \Omega\sigma_1 = \Omega(|a\rangle\langle b| + |b\rangle\langle a|), \tag{7.31}$$

with the Rabi frequency $\Omega = \lambda$. The equations of motion (3.16)-(3.17), with initial condition $\boldsymbol{R}(0) \equiv (0, 0, 1)$ (only level $|a\rangle$ is initially populated) yield

$$\boldsymbol{R}(t) = (0, \sin 2\Omega t, \cos 2\Omega t). \tag{7.32}$$

If the transition between the two levels is driven by an on-resonant $\pi/2$ pulse, of duration

$$T = \pi/2\Omega, \tag{7.33}$$

one gets $\boldsymbol{R}(T) \equiv (0, 0, -1)$, so that only level $|b\rangle$ is populated at time T.

Perform a measurement at time $\tau = T/N = \pi/2N\Omega$, by shining on the system a very short "measurement" pulse, that provokes transitions from level $|b\rangle$ to a third level $|M\rangle$, followed by the rapid spontaneous emission of a photon. The measurement pulse "projects" the atom onto level $|b\rangle$ or $|a\rangle$ and "kills" the off-diagonal terms ρ_{ab}, ρ_{ba} of the density matrix, while leaving unaltered its diagonal terms ρ_{aa}, ρ_{bb}, so that, from Eq. (3.20),

$$\boldsymbol{R}(\pi/2N\Omega) = \left(0, \sin\frac{\pi}{N}, \cos\frac{\pi}{N}\right) \stackrel{\text{measurement}}{\longrightarrow} \left(0, 0, \cos\frac{\pi}{N}\right) \equiv \boldsymbol{R}^{(1)}. \tag{7.34}$$

Then the evolution restarts, always governed by Eq. (3.16), but with the new initial condition $\boldsymbol{R}^{(1)}$. After N measurements, at time $T = N\tau = \pi/2\Omega$,

$$\boldsymbol{R}(T) = \left(0, 0, \cos^N \frac{\pi}{N}\right) \equiv \boldsymbol{R}^{(N)} \tag{7.35}$$

and the probabilities that the atom is in level $|a\rangle$ or $|b\rangle$ read [see Eq. (3.19)]

$$\mathcal{P}_a^{(N)}(T) = \frac{1}{2}\left(1 + R_3^{(N)}\right) = \frac{1}{2}\left(1 + \cos^N \frac{\pi}{N}\right), \tag{7.36}$$

$$\mathcal{P}_b^{(N)}(T) = \frac{1}{2}\left(1 - R_3^{(N)}\right) = \frac{1}{2}\left(1 - \cos^N \frac{\pi}{N}\right), \tag{7.37}$$

respectively. Since $\mathcal{P}_a^{(N)}(T) \to 1$ and $\mathcal{P}_b^{(N)}(T) \to 0$ as $N \to \infty$, this looks like a quantum Zeno effect. However, it is *not* the quantum Zeno effect *à la* Misra and Sudarshan: equation (7.36) [(7.37)] expresses only the probability that the atom is in level $|a\rangle$ [$|b\rangle$] at time T, after N measurements, *independently* of its past history. In particular, Eqs. (7.36)-(7.37) take into account the *possibility that one level gets repopulated after the atom has made transitions to the other level*. In order to shed light on this rather subtle point, let us look explicitly at the first two measurements.

After the first measurement, by Eq. (7.34),

$$R_3^{(1)} = \cos\frac{\pi}{N} = \cos^2\frac{\pi}{2N} - \sin^2\frac{\pi}{2N} = \mathcal{P}_a^{(1)} - \mathcal{P}_b^{(1)}, \tag{7.38}$$

where $\mathcal{P}_a^{(1)}$ and $\mathcal{P}_b^{(1)}$ are the occupation probabilities of levels $|a\rangle$ and $|b\rangle$ at time $\tau = \pi/2N\Omega$, after the first measurement pulse, respectively. After the second measurement, one obtains

$$R_3^{(2)} = \cos^2\frac{\pi}{N} = \mathcal{P}_a^{(2)} - \mathcal{P}_b^{(2)}, \tag{7.39}$$

where the occupation probabilities at time $2\tau = \pi/N\Omega$ read

$$\mathcal{P}_a^{(2)} = \frac{1}{2}\left(1 + R_3^{(2)}\right) = \cos^4\frac{\pi}{2N} + \sin^4\frac{\pi}{2N}. \tag{7.40}$$

$$\mathcal{P}_b^{(2)} = \frac{1}{2}\left(1 - R_3^{(2)}\right) = 2\sin^2\frac{\pi}{2N}\cos^2\frac{\pi}{2N}, \tag{7.41}$$

It is then obvious that $\mathcal{P}_a^{(2)}$, in Eq. (7.40), is *not the survival probability* of level $|a\rangle$, according to definition (7.30). It is just the probability that level $|a\rangle$ is populated at time $t = \pi/N\Omega$, including the possibility that the transition $|a\rangle \to |b\rangle \to |a\rangle$ took place, with probability $\sin^2(\pi/2N) \cdot \sin^2(\pi/2N) = \sin^4(\pi/2N)$. By contrast, the *survival* probability, namely the probability that the atom is found in level $|a\rangle$ *both* at the first and second measurements, is given by $\mathcal{P}_a^{(1,2)} = \cos^2(\pi/2N) \cdot \cos^2(\pi/2N) = \cos^4(\pi/2N)$. Figure 7.5 shows what happens during the first two measurements.

After N measurements, the probability that level $|a\rangle$ is populated at time T, independently of its "history", is given by (7.36), and includes the possibility that transitions to level $|b\rangle$ took place. As a matter of fact, it is not difficult to realize that (7.36)-(7.37) conceal a binomial

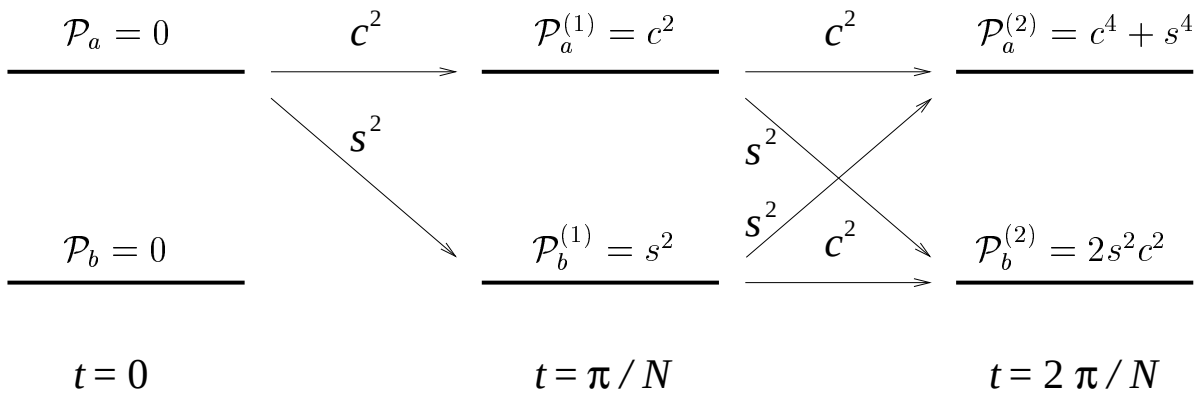

Figure 7.5: Transition probabilities after the first two measurements for an oscillating system $[s = \sin(\pi/2N)$ and $c = \cos(\pi/2N)]$.

distribution:

$$\begin{aligned}
\sum_{n\ \text{even}} \left(\begin{array}{c} N \\ n \end{array} \right) s^{2n} c^{2(N-n)} &= c^{2N} \sum_{n\ \text{even}} \left(\begin{array}{c} N \\ n \end{array} \right) (s/c)^{2n} \\
&= \frac{c^{2N}}{2} \sum_{n=0}^{N} \left[\left(\begin{array}{c} N \\ n \end{array} \right) \left(\frac{s}{c}\right)^{2n} + \left(\begin{array}{c} N \\ n \end{array} \right) (-1)^n \left(\frac{s}{c}\right)^{2n} \right] \\
&= \frac{c^{2N}}{2} \left[(1 + (s/c)^2)^N + (1 - (s/c)^2)^N \right] \\
&= \frac{1}{2} \left[1 + \cos^N(\pi/N) \right] \\
&= \mathcal{P}_a^{(N)}(T), \qquad (7.42)
\end{aligned}$$

where $\sum_{n\ \text{even}}$ is a sum over all even values of n between 0 and N, $s = \sin(\pi/2N)$ and $c = \cos(\pi/2N)$. Clearly, Eq. (7.36) includes all possible transitions between levels $|a\rangle$ and $|b\rangle$ and is conceptually very different from Misra and Sudarshan's survival probability (7.30). The correct formula for the survival probability, in the present case, is obtained by considering *only* the $n = 0$ term in (7.42):

$$P_a^{(N)}(T) = \cos^{2N} \frac{\pi}{2N}. \qquad (7.43)$$

This is a *bona fide* "survival probability", namely the probability that level $|a\rangle$ is populated at every measurement, at times $n\tau = nT/N$ $(n = 1, \ldots, N)$.

The conclusions drawn in this section are always valid when the temporal behavior of the system under investigation is of the oscillatory type and no precautions are taken in order to prevent repopulation of the initial state (Nakazato, Namiki, Pascazio and Rauch [1996]). For instance, this problematic feature is present in the interesting proposal by Cook [1988] and the beautiful experiment by Itano, Heinzen, Bollinger and Wineland [1990]. On the other hand, no repopulation of the initial state takes place in other experiments involving neutron spin (Pascazio, Namiki, Badurek and Rauch [1993]) or photon polarization (Kwiat, Weinfurter, Herzog, Zeilinger and Kasevich [1995]).

We have seen that $P_a^{(N)}(T)$, in Eq. (7.43), is a *bona fide* survival probability, but $\mathcal{P}_a^{(N)}(T)$, in Eq. (7.36) is not (at least not according to Misra and Sudarshan's definition). However, both quantities tend to the same limiting value 1 as $N \to \infty$ and for large N the evolution is, in fact, hindered. We are therefore led to wonder whether it would not be meaningful to extend

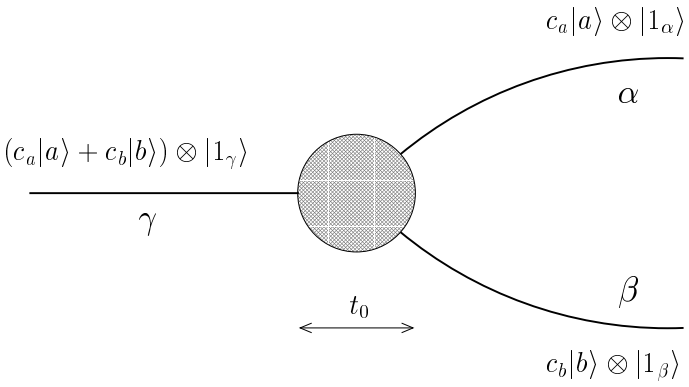

Figure 7.6: The generalized spectral decomposition.

the notion of QZE beyond Misra and Sudarshan's definition of survival probability. This will be the subject of Sec. 7.6.

7.3 Dynamical quantum Zeno effect

In the usual formulation of QZE the measurement process is schematized by making use of projection operators *à la* von Neumann (Copenhagen interpretation), without endeavoring to shed light on the underlying dynamics. However, a quantum mechanical measurement is a very complicated physical process, taking place in a finite time and involving complex (macroscopic) physical systems.

It is possible to give a dynamical explanation of the Zeno effect (Pascazio and Namiki [1994]; Pascazio [1997]), that involves only the Schrödinger equation and makes no use of projection operators. Let us briefly sketch how this is accomplished by introducing the notion of "generalized spectral decomposition" (GSD).

Consider again a two level system, prepared in a superposed state. A GSD is a dynamical (Hamiltonian) process by which different states of the system become associated (entangled) with different external "channels" (e.g., different degrees of freedom of a larger system). See Fig. 7.6. One can think, for example, of a two-level atomic system getting entangled with different photon states of the electromagnetic field. The notion of "spectral decomposition" was introduced by Wigner [1963], who considered the Stern-Gerlach decomposition of an initial spin state, where each component of the spin becomes associated with a different wave packet. It is worth observing that the external channels the system gets entangled with need not be "external:" for example, different wave packets of the system itself can act as "external" degrees of freedom.

A GSD is realized by the following Hamiltonian

$$H_{\rm GSD}(t) = g(t)\left[|a\rangle\langle a|\sigma_\alpha + |b\rangle\langle b|\sigma_\beta\right]\sigma_\gamma = g(t)H', \qquad \int_0^{t_0} g(t)dt = \frac{\pi}{2}, \tag{7.44}$$

where the interaction is switched on during the time interval $[0, t_0]$, g is a real function, $\sigma_\mu^\dagger = \sigma_\mu$ (the index $\mu = \alpha, \beta, \gamma$ labels the channel in Fig. 7.6) and the effect of σ_μ is defined by

$$\sigma_\mu|0_\mu\rangle = |1_\mu\rangle, \qquad \sigma_\mu|1_\mu\rangle = |0_\mu\rangle, \tag{7.45}$$

so that if there is a "particle" in channel μ the operator σ_μ destroys it, while if there is no particle, σ_μ creates one. The effect of σ_μ ($\forall\mu$) is therefore identical to that of the first Pauli

matrix. We set

$$[\sigma_\mu, \sigma_\nu] = 0. \tag{7.46}$$

The action of the Hamiltonian $H_{\rm GSD}$ is

$$H_{\rm GSD}\left(c_a|a\rangle + c_b|b\rangle\right) \otimes |1_\gamma, 0_\alpha, 0_\beta\rangle \propto \left(c_a|a\rangle \otimes |0_\gamma, 1_\alpha, 0_\beta\rangle + c_b|b\rangle \otimes |0_\gamma, 0_\alpha, 1_\beta\rangle\right)$$

and consists in sending the $|a\rangle$ ($|b\rangle$) state of the system in the upper (lower) channel in Fig. 7.6, performing in this way a GSD.

In general, the only effect of a GSD is to set up a perfect correlation between the two states of the system and different external channels (namely, a univocal and unambiguous correspondence between different states of the system and different external channels). This is easily accomplished: the evolution engendered by $H_{\rm GSD}$ can be explicitly calculated (Pascazio and Namiki [1994]) and the result is

$$e^{-i\int_0^{t_0} H_{\rm GSD}(t')dt'}\left(c_a|a\rangle + c_b|b\rangle\right) \otimes |1_\gamma\rangle = -i\left(c_a|a\rangle \otimes |1_\alpha\rangle + c_b|b\rangle \otimes |1_\beta\rangle\right), \qquad (t > t_0) \tag{7.47}$$

where we suppressed all 0's for simplicity.

A projection operator represents an *instantaneous* measurement. This is clearly a very idealized situation that cannot correspond to a real physical process, taking place at a microscopic level. The problem is therefore to understand how we can simulate such an instantaneous and unphysical process in our analysis, that makes use *only* of unitary evolutions. We observe that, in general, a GSD must take place in a very short time. Obviously, the term "very short time" must be understood at a macroscopic level of description, because the time microscopically required to efficaciously perform a GSD is very long. Therefore, if we restrict our analysis to a macroscopic level of description, we can describe an (almost) instantaneous GSD by means of the so-called impulse approximation

$$\int_0^{t_0} g(t)dt = \pi/2, \qquad t_0 \to 0^+ \ . \tag{7.48}$$

which roughly amounts to setting $g(t) \to (\pi/2)\delta(t)$ as $t_0 \to 0$, where δ is the Dirac function $\int_0^{t_0} \delta(t) = 1$. This is our alternative description of a von Neumann-like instantaneous projection. It is a good approximation of the physical situation whenever t_0 is much shorter than the characteristic time of the free evolution of the system under observation.

By making repeated use of GSDs it is very simple to get a quantum Zeno dynamics. A general proof is given by Pascazio and Namiki [1994] (a somewhat simpler version can be found in Pascazio [1997]), but here let us only sketch the main idea by looking at the example (7.31). The initial state (3.4), that we rewrite by including the external channel (wave packet) in the description

$$|\Psi_0\rangle = |a\rangle \otimes |1_\gamma\rangle, \tag{7.49}$$

evolves after a short time τ into (3.5):

$$|\Psi_\tau\rangle = e^{-iH_{\rm I}\tau}|\Psi_0\rangle = [\cos(\Omega\tau)|a\rangle - i\sin(\Omega\tau)|b\rangle] \otimes |1_\gamma\rangle. \tag{7.50}$$

The GSD yields then (for $t_0 \ll \Omega^{-1}$)

$$|\Psi_{\tau+t_0}\rangle = e^{-i\int_0^{t_0} H_{\rm GSD}(t')dt'}|\Psi_\tau\rangle \propto \cos(\Omega\tau)|a\rangle \otimes |1_\alpha\rangle - i\sin(\Omega\tau)|b\rangle \otimes |1_\beta\rangle, \tag{7.51}$$

apart from a phase factor. Observe that the quantum coherence is perfectly preserved, during this evolution. At the next "step" of the evolution, channels α and β become new incoming

channels and the system evolves again under the action of $H_{\rm I}$ for a time τ and $H_{\rm GSD}$ for a time t_0. After N steps the final wave function reads

$$|\Psi_{N(\tau+t_0)}\rangle = \prod_{n=1}^{N}\left[e^{-i\int_0^{t_0}H_{\rm GSD}^{(n)}(t')dt'}e^{-iH_{\rm I}\tau}\right]|\Psi_0\rangle \propto \cos^N(\Omega\tau)|a\rangle\otimes|1_\alpha^{(N)}\rangle + {\rm O}(N^{-1}), \quad (7.52)$$

where $H_{\rm GSD}^{(n)}$ is the Hamiltonian that performs a generalized spectral decomposition at the nth step and $|1_\alpha^{(N)}\rangle$ (all 0's were suppressed) represent the wave packet traveling in channel α at step N. Note that $N(\tau+t_0)$ is kept finite.

The contribution of all the other channels is ${\rm O}(N^{-1})$: a QZE is obtained because the particle, initially in state (7.49), ends up with probability

$$[1-{\rm O}(1/N^2)]^N \sim 1-{\rm O}(1/N) \quad (7.53)$$

in state $|a\rangle\otimes|1_\alpha^{(N)}\rangle$. The "external" degrees of freedom are irrelevant and can be traced out (or recombined with the initial one).

We would like to emphasize that the very dynamical mechanism leading to QZE is curious: QZE is obtained via repeated use of generalized spectral decompositions $H_{\rm GSD}$'s, even though the interaction Hamiltonian $H_{\rm I}$ "attempts" to drive $|a\rangle$ into $|b\rangle$ for a finite time $N\tau$. This is probably the reason why QZE is often considered a counterintuitive phenomenon.

7.4 Continuous observation

A projection *à la* von Neumann (von Neumann [1932]) is a handy way to "summarize" the complicated physical processes that take place during a quantum measurement. A measurement process is performed by an external (macroscopic) apparatus and involves dissipative effects, that imply an exchange of energy with and often a flow of probability towards the environment. The external system performing the observation need not be a *bona fide* detection system, namely a system that "clicks" or is endowed with a pointer. It is enough that the information on the state of the observed system be encoded in the state of the apparatus. For instance, a spontaneous emission process is often a very effective measurement process, for it is irreversible and leads to an entanglement of the state of the system (the emitting atom or molecule) with the state of the apparatus (the electromagnetic field). The von Neumann rules arise when one traces away the photonic state and is left with an incoherent superposition of atomic states.

We shall now introduce several alternative descriptions of a measurement process and discuss the notion of continuous measurement. This is to be contrasted with the idea of pulsed measurements, discussed in Sec. 7.2. Both formulations lead to QZE.

7.4.1 Mimicking the projection with a non-Hermitian Hamiltonian

It is useful for our discussion on the QZE and probably interesting on general grounds to see how the action of an external apparatus can be mimicked by a non Hermitian Hamiltonian. Let us consider the following Hamiltonian

$$H_{\rm I} = \begin{pmatrix} 0 & \Omega \\ \Omega & -i2V \end{pmatrix} = -iV\mathbf{1} + \boldsymbol{h}\cdot\boldsymbol{\sigma}, \qquad \boldsymbol{h} = (\Omega, 0, iV)^T, \quad (7.54)$$

that yields Rabi oscillations of frequency Ω, but at the same time absorbs away the $|b\rangle$ component of the Hilbert space, performing in this way a "measurement." Due to the non Hermitian

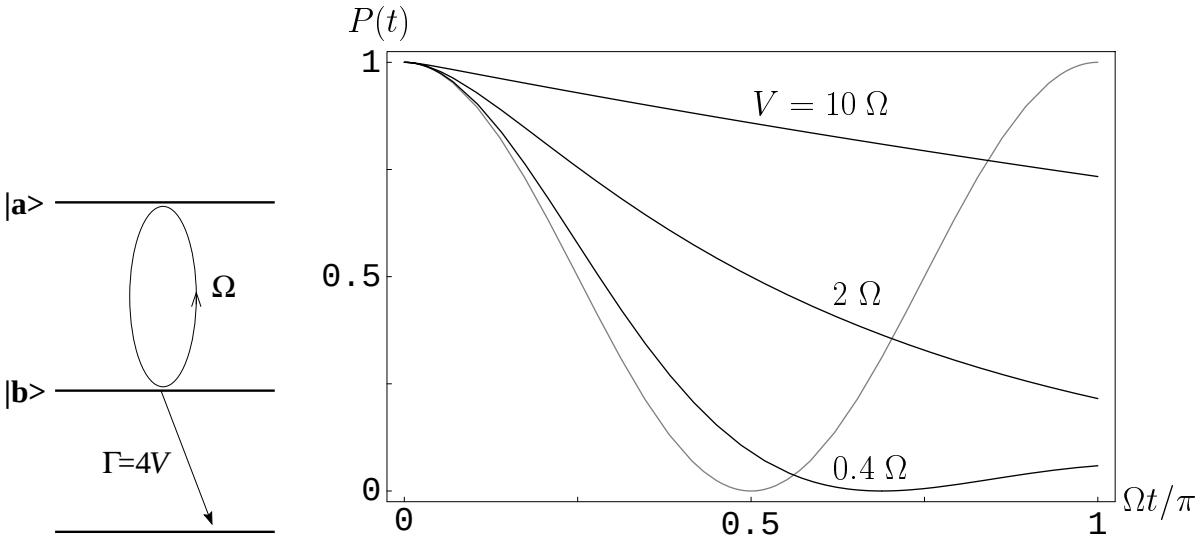

Figure 7.7: Survival probability for a system undergoing Rabi oscillations in presence of absorption ($V = 0.4, 2, 10\Omega$). The gray line is the undisturbed evolution ($V = 0$).

features of this description, probabilities are not conserved: we are concentrating our attention only on the $|a\rangle$ component.

An elementary SU(2) manipulation yields the following evolution operator

$$e^{-iH_{\rm I}t} = e^{-Vt}\left[\cosh(ht) - i\frac{\boldsymbol{h}\cdot\boldsymbol{\sigma}}{h}\sinh(ht)\right], \tag{7.55}$$

where $h = \sqrt{V^2-\Omega^2}$ and we supposed $V > \Omega$. Let the system be initially prepared in the state $|a\rangle$: the survival amplitude reads

$$\begin{aligned}\mathcal{A}(t) &= \langle a|e^{-iH_{\rm I}t}|a\rangle = e^{-Vt}\left[\cosh(\sqrt{V^2-\Omega^2}t) + \frac{V}{\sqrt{V^2-\Omega^2}}\sinh(\sqrt{V^2-\Omega^2}t)\right] \\ &= \frac{1}{2}\left(1+\frac{V}{\sqrt{V^2-\Omega^2}}\right)e^{-(V-\sqrt{V^2-\Omega^2})t} + \frac{1}{2}\left(1-\frac{V}{\sqrt{V^2-\Omega^2}}\right)e^{-(V+\sqrt{V^2-\Omega^2})t}. \end{aligned}\tag{7.56}$$

The above results are exact and display some interesting and very general aspects of the quantum Zeno dynamics. The survival probability $P(t) = |\mathcal{A}(t)|^2$ is shown in Fig. 7.7 for $V = 0.4, 2, 10\Omega$. As expected, probability is (exponentially) absorbed away as $t \to \infty$. However, as V increases, by using Eq. (7.56), the survival probability reads

$$P(t) \sim \left(1+\frac{\Omega^2}{2V}\right)\exp\left(-\frac{\Omega^2}{V}t\right), \tag{7.57}$$

and the effective decay rate $\gamma_{\rm eff}(V) = \Omega^2/V$ becomes smaller, eventually halting the "decay" (absorption) of the initial state and yielding an interesting example of QZE: a larger V entails a more "effective" measurement of the initial state. We emphasize that the expansion (7.57) becomes valid very quickly, on a time scale of order V^{-1}. Notice that this example is not affected by the repopulation drawback described in Sec. 7.2.4 (once the probability is absorbed away, it does not flow back to the initial state).

7.4.2 Coupling with a flat continuum

We now show that the non Hermitian Hamiltonian (7.54) can be obtained by considering the evolution engendered by a Hermitian Hamiltonian acting on a larger Hilbert space and then restricting the attention to the subspace spanned by $\{|a\rangle, |b\rangle\}$. Consider the Hamiltonian

$$H = \Omega(|a\rangle\langle b| + |b\rangle\langle a|) + \int d\omega\ \omega|\omega\rangle\langle\omega| + \sqrt{\frac{\Gamma}{2\pi}} \int d\omega\ (|b\rangle\langle\omega| + |\omega\rangle\langle b|), \tag{7.58}$$

which describes a two level system coupled to the photon field in the rotating-wave approximation. The state of the system at time t can be written as

$$|\psi_t\rangle = x(t)|a\rangle + y(t)|b\rangle + \int d\omega\ z(\omega, t)|\omega\rangle \tag{7.59}$$

and the Schrödinger equation reads

$$\begin{aligned} i\dot{x}(t) &= \Omega y(t), \\ i\dot{y}(t) &= \Omega x(t) + \sqrt{\frac{\Gamma}{2\pi}} \int d\omega\ z(\omega, t), \\ i\dot{z}(\omega, t) &= \omega z(\omega, t) + \sqrt{\frac{\Gamma}{2\pi}} y(t). \end{aligned} \tag{7.60}$$

By using the initial condition $x(0) = 1$ and $y(0) = z(\omega, 0) = 0$ one obtains

$$z(\omega, t) = -i\sqrt{\frac{\Gamma}{2\pi}} \int_0^t d\tau\ e^{-i\omega(t-\tau)} y(\tau) \tag{7.61}$$

and

$$i\dot{y}(t) = \Omega x(t) - i\frac{\Gamma}{2\pi} \int d\omega \int_0^t d\tau\ e^{-i\omega(t-\tau)} y(\tau) = \Omega x(t) - i\frac{\Gamma}{2} y(t). \tag{7.62}$$

Therefore $z(\omega, t)$ disappears from the equations and we get two first order differential equation for x and y. The only effect of the continuum is the appearance of the imaginary frequency $-i\Gamma/2$. Incidentally, this is ascribable to the "flatness" of the continuum [there is no form factor or frequency cutoff in the last term of Eq. (7.58)], which yields a purely exponential (Markovian) decay of $y(t)$.

In conclusion, the dynamics in the subspace spanned by $|a\rangle$ and $|b\rangle$ reads

$$\begin{aligned} i\dot{x}(t) &= \Omega y(t), \\ i\dot{y}(t) &= -i\frac{\Gamma}{2} y + \Omega x(t). \end{aligned} \tag{7.63}$$

Of course, this dynamics is not unitary, for probability flows out of the subspace, and is generated by the non Hermitian Hamiltonian

$$H = \Omega(|a\rangle\langle b| + |b\rangle\langle a|) - i\frac{\Gamma}{2}|b\rangle\langle b|. \tag{7.64}$$

This Hamiltonian is the same as (7.54) when one sets $\Gamma = 4V$. QZE is obtained by increasing Γ: a larger coupling to the environment leads to a more effective "continuous" observation on the system (quicker response of the apparatus), and as a consequence to a slower decay (QZE).

The processes described in this section and the previous one can therefore be viewed as "continuous" measurements performed on the initial state. The non Hermitian term $-2iV$

is proportional to the decay rate Γ of state $|b\rangle$, quantitatively $\Gamma = 4V$. Therefore, state $|b\rangle$ is continuously monitored with a response time $1/\Gamma$: as soon as it becomes populated, it is detected within a time $1/\Gamma$. The "strength" $\Gamma = 4V$ of the observation can be compared to the frequency $\tau^{-1} = (t/N)^{-1}$ of measurements in the "pulsed" formulation. Indeed, for large values of Γ one gets from Eq. (7.57)

$$\gamma_{\text{eff}}(\Gamma) \sim \frac{4\Omega^2}{\Gamma} = \frac{4}{\tau_{\text{Z}}^2 \Gamma}, \qquad \text{for} \quad \Gamma \to \infty, \tag{7.65}$$

which, compared with Eq. (7.24), yields an interesting relation between continuous and pulsed measurements (Schulman [1998])

$$\Gamma \simeq 4/\tau = 4N/t. \tag{7.66}$$

7.4.3 Continuous Rabi observation

The two previous examples might lead the reader to think that absorption and/or probability leakage to the environment (or in general to other degrees of freedom) are fundamental requisites to obtain QZE. This expectation would be incorrect. Let us analyze a somewhat different situation, by coupling one of the two levels of the system to a third one, that will play the role of measuring apparatus. The (Hermitian) Hamiltonian is

$$H_{\text{I}} = \Omega(|a\rangle\langle b| + |b\rangle\langle a|) + K(|b\rangle\langle M| + |M\rangle\langle b|) = \begin{pmatrix} 0 & \Omega & 0 \\ \Omega & 0 & K \\ 0 & K & 0 \end{pmatrix}, \tag{7.67}$$

where $K \in \mathbb{R}$ is the strength of the coupling to the new level M and

$$\langle a| = (1,0,0), \quad \langle b| = (0,1,0), \quad \langle M| = (0,0,1). \tag{7.68}$$

This is probably the simplest way to include an "external" apparatus in our description: as soon as the system is in $|b\rangle$ it undergoes Rabi oscillations to $|M\rangle$. Similar examples were considered by Peres [1980a] and Kraus [1981]. We expect level $|M\rangle$ to perform better as a measuring apparatus when the strength K of the coupling becomes larger.

The above Hamiltonian is easily diagonalized. Its eigenvalues and eigenvectors are

$$\begin{aligned} &\lambda_0 = 0, \qquad |u_0\rangle = \frac{1}{\sqrt{K^2+\Omega^2}} \begin{pmatrix} K \\ 0 \\ -\Omega \end{pmatrix}, \\ &\lambda_\pm = \pm\sqrt{K^2+\Omega^2}, \qquad |u_\pm\rangle = \frac{1}{\sqrt{2(K^2+\Omega^2)}} \begin{pmatrix} \Omega \\ \pm\sqrt{K^2+\Omega^2} \\ K \end{pmatrix}. \end{aligned} \tag{7.69}$$

Let the initial state be, as usual,

$$|a\rangle = \frac{1}{\sqrt{K^2+\Omega^2}} \left(K|u_0\rangle + \frac{\Omega}{\sqrt{2}}|u_-\rangle + \frac{\Omega}{\sqrt{2}}|u_-\rangle \right). \tag{7.70}$$

The evolution is easily computed

$$|\psi_t\rangle = e^{-iH_{\text{I}}t}|a\rangle = \frac{1}{\sqrt{K^2+\Omega^2}} \left(K|u_0\rangle + \frac{\Omega}{\sqrt{2}} e^{-i\lambda_+ t}|u_-\rangle + \frac{\Omega}{\sqrt{2}} e^{-i\lambda_- t}|u_-\rangle \right) \tag{7.71}$$

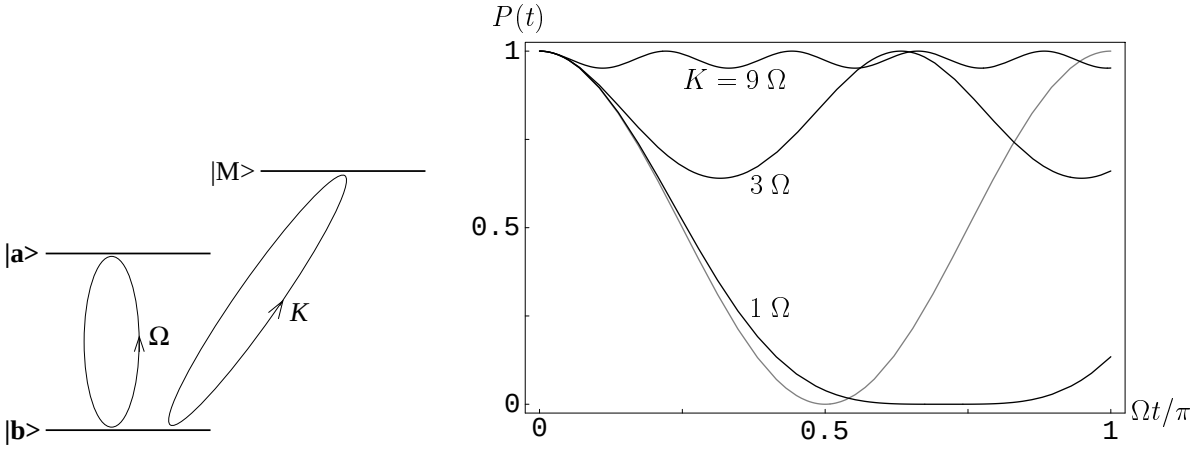

Figure 7.8: Survival probability for a continuous Rabi "measurement" with $K = 1, 3, 9\Omega$: quantum Zeno effect.

and the survival probability reads

$$P(t) = \frac{1}{(K^2+\Omega^2)^2}\left[K^2 + \Omega^2\cos(\sqrt{K^2+\Omega^2}t)\right]^2. \tag{7.72}$$

This is shown in Fig. 7.8 for $K = 1, 3, 9\Omega$. We notice that for large K the state of the system does not change much: as K is increased, level $|M\rangle$ performs a better "observation" of the state of the system, hindering transitions from $|a\rangle$ to $|b\rangle$. This can be viewed as a QZE due to a "continuous," yet Hermitian observation performed by level $|M\rangle$.

This simple example triggers also another remarkable observation. The Zeno time is easily computed and turns out to be much longer than the Poincaré time (we are assuming $K \gg \Omega$)

$$\tau_{\rm Z} = \Omega^{-1} \gg T_{\rm P} = {\rm O}(K^{-1}). \tag{7.73}$$

As a matter of fact, the Zeno time yields only the convexity of the survival probability in the origin.

A few more comments are necessary. First of all, the example considered in this section is not free from repopulation effects like those considered in Sec. 7.2.4. As a matter of facts, the situation here is even worse: unlike the case studied in Sec. 7.2.4, where there was a probability repopulation of the initial state, in the present case there is a (coherent) amplitude repopulation phenomenon. However, even if these cases are at variance with Misra and Sudarshan's definition [see (7.30) and paragraph preceding it], they call, in our opinion, for a broader formulation of QZE. This will be proposed in the following sections.

Let us see how "effective" the Rabi "measurement" is, compared to the case of pulsed measurements. Notice that by performing pulsed observations on system (7.31) one gets from Eq. (7.4)

$$P^{(N)}(t) = P(t/N)^N = \left(\cos\frac{\Omega t}{N}\right)^{2N} \sim \left(1 - \frac{\Omega^2 t^2}{N^2}\right)^N \sim 1 - \frac{\Omega^2 t^2}{N}, \tag{7.74}$$

for large values of N. On the other hand, in the present case of continuous observation, for large values of K, Eq (7.72) reads

$$P^{(K)}(t) \sim \left(1 - 2\frac{\Omega^2}{K^2}\right)\left(1 + 2\frac{\Omega^2}{K^2}\cos(\sqrt{K^2+\Omega^2}t)\right) \sim 1 - 4\frac{\Omega^2}{K^2}\sin^2\left(\frac{\sqrt{K^2+\Omega^2}}{2}t\right), \tag{7.75}$$

whence, by taking the average over a very short time of order $1/K$,

$$\overline{P^{(K)}(t)} \sim 1 - 2\frac{\Omega^2}{K^2}. \tag{7.76}$$

By comparing Eq. (7.74) and Eq. (7.76), one sees that the evolution is hindered (QZE) for

$$\frac{\Omega^2 t^2}{N} \simeq \frac{2\Omega^2}{K^2} (\ll 1), \tag{7.77}$$

namely

$$K \simeq \frac{\sqrt{2N}}{t}. \tag{7.78}$$

This relation is similar to (7.66): strong coupling is equivalent to frequent measurements.

A final comment is in order. All the situations analyzed in Sec. 7.4 lead to QZE but never to IZE. The reason for this is profound and lies in the absence of the form factors of the interactions. The importance of form factors and the role they play in this context will be discussed later.

7.5 A quantum Zeno theorem

We now prove a theorem, which is the exact analog of Misra and Sudarshan's theorem valid for a dynamical evolution.

Consider the Hamiltonian

$$H_K = H_{\rm sys} + K H_{\rm meas}, \tag{7.79}$$

where $H_{\rm sys}$ represents the Hamiltonian of the system under observation (which can include the free Hamiltonian of the apparatus too) and $H_{\rm meas}$ is the interaction Hamiltonian between the system and the apparatus, K being the strength of the measurement. Let us look at the time evolution operator in the $H_{\rm meas}$ interaction picture

$$U_K(t) = \exp(iKH_{\rm meas}t)\, U(t) = \exp(iKH_{\rm meas}t)\exp(-iH_K t). \tag{7.80}$$

The theorem states that in the infinitely strong measurement limit ($K \to \infty$) the evolution operator becomes diagonal in the $H_{\rm meas}$ representation, namely

$$\lim_{K\to\infty} U_K(t) = \exp(-iH_{\rm sys}^{\rm diag} t), \tag{7.81}$$

where

$$H_{\rm sys}^{\rm diag} = \sum_n P_n H_{\rm sys} P_n \tag{7.82}$$

is the diagonal part of the system Hamiltonian $H_{\rm sys}$ with respect to the interaction Hamiltonian $H_{\rm meas}$

$$H_{\rm meas} P_n = \eta_n P_n, \tag{7.83}$$

P_n being the orthogonal projection onto the eigenspace of $H_{\rm meas}$ belonging the the eigenvalue η_n. Note that in Eqs. (7.82) and (7.83) one has to consider distinct eigenvalues, i.e., $\eta_n \neq \eta_m$ for $n \neq m$, whence the P_n are not necessarily unidimensional.

The physical implications of the theorem (7.81) are straightforward: in the $K \to \infty$ limit, the time evolution operator becomes diagonal with respect to $H_{\rm meas}$, namely

$$[U_\infty(t), H_{\rm meas}] = 0, \tag{7.84}$$

a superselection rule arises and the total Hilbert space is split into subspaces which are invariant under the evolution. These subspaces are simply defined by the P_n's, i.e., they are eigenspaces belonging to distinct eigenvalues η_n: in other words, eigenspaces that the apparatus can distinguish. As a consequence, if the initial state of the system belongs to a specific sector, it will be forced to remain there forever (QZE).

Here is the proof. Rewrite the time evolution operator in the form

$$U(t) = \exp(-iH_K t) = \exp(-iH_\lambda \tau) \tag{7.85}$$

where

$$\lambda = 1/K, \qquad \tau = Kt = t/\lambda, \qquad H_\lambda = \lambda H_K = H_{\rm meas} + \lambda H_{\rm sys}, \tag{7.86}$$

and apply the perturbation theory to the Hamiltonian H_λ for small λ. To this end choose the unperturbed degenerate projections $P_{n\alpha}$

$$H_{\rm meas} P_{n\alpha} = \eta_n P_{n\alpha}, \tag{7.87}$$

whose degeneration α is resolved at some order in the coupling constant λ. This means that by denoting with $\widetilde{E}_{n\alpha}$ and $\widetilde{P}_{n\alpha}$ the eigenvalues and the orthogonal projections of the total Hamiltonian H_λ

$$H_\lambda \widetilde{P}_{n\alpha} = \widetilde{E}_{n\alpha} \widetilde{P}_{n\alpha}, \tag{7.88}$$

they reduce to the unperturbed ones when the perturbation vanishes

$$\widetilde{P}_{n\alpha} \stackrel{\lambda\to 0}{\longrightarrow} P_{n\alpha}, \qquad \widetilde{E}_{n\alpha} \stackrel{\lambda\to 0}{\longrightarrow} \eta_n. \tag{7.89}$$

Therefore, by applying the standard perturbation theory we get the eigenvectors

$$\begin{aligned} \widetilde{P}_{n\alpha} &= P_{n\alpha} + \lambda P^{(1)}_{n\alpha} + {\rm O}(\lambda^2) \\ &= P_{n\alpha} + \lambda \left(\frac{Q_n}{a_n} H_{\rm sys} P_{n\alpha} + P_{n\alpha} H_{\rm sys} \frac{Q_n}{a_n} \right) + {\rm O}(\lambda^2) \end{aligned} \tag{7.90}$$

and the eigenvalues

$$\begin{aligned} \widetilde{E}_{n\alpha} &= \eta_n + \lambda E^{(1)}_{n\alpha} + \lambda^2 E^{(2)}_{n\alpha} + {\rm O}(\lambda^3) \\ &= \eta_n + \lambda \langle n\alpha | H_{\rm sys} | n\alpha \rangle + \lambda^2 \langle n\alpha | H_{\rm sys} \frac{Q_n}{a_n} H_{\rm sys} | n\alpha \rangle + {\rm O}(\lambda^3), \end{aligned} \tag{7.91}$$

where

$$P_n = \sum_\alpha P_{n\alpha}, \qquad Q_n = 1 - P_n = \sum_{m\neq n} P_m, \qquad \frac{Q_n}{a_n} = \frac{Q_n}{\eta_n - H_{\rm meas}} = \sum_{m\neq n} \frac{P_m}{\eta_n - \eta_m} \tag{7.92}$$

and $P_{n\alpha} = |n\alpha\rangle\langle n\alpha|$. Write now the spectral decomposition of the evolution operator (7.85) in terms of the projections $\widetilde{P}_{n\alpha}$

$$U(t) = \exp(-iH_\lambda \tau) \sum_{n,\alpha} \widetilde{P}_{n\alpha} = \sum_{n,\alpha} \exp(-i\widetilde{E}_{n\alpha}\tau) \widetilde{P}_{n\alpha} \tag{7.93}$$

and plug in the perturbation expansions (7.90), to obtain

$$U(t) = \sum_{n,\alpha} e^{-i\widetilde{E}_{n\alpha}\tau} P_{n\alpha} + \lambda \sum_{n,\alpha} \left(\frac{Q_n}{a_n} H_{\rm sys} P_{n\alpha} e^{-i\widetilde{E}_{n\alpha}\tau} + e^{-i\widetilde{E}_{n\alpha}\tau} P_{n\alpha} H_{\rm sys} \frac{Q_n}{a_n} \right) + {\rm O}(\lambda^2). \tag{7.94}$$

Let us define a new operator $\widetilde{H}_\lambda$ as

$$\begin{aligned}\widetilde{H}_\lambda &= \sum_{n,\alpha} \widetilde{E}_{n\alpha} P_{n\alpha} \\ &= H_{\rm meas} + \lambda \sum_n P_n H_{\rm sys} P_n + \lambda^2 \sum_n P_n H_{\rm sys} \frac{Q_n}{a_n} H_{\rm sys} P_n + {\rm O}(\lambda^3),\end{aligned} \tag{7.95}$$

where Eq. (7.91) was used. By plugging Eq. (7.95) into Eq. (7.94) we finally obtain

$$U(t) = \exp(-i\widetilde{H}_\lambda \tau) + \lambda \sum_n \left(\frac{Q_n}{a_n} H_{\rm sys} P_n e^{-i\widetilde{H}_\lambda \tau} - e^{-i\widetilde{H}_\lambda \tau} \frac{Q_n}{a_n} H_{\rm sys} P_n \right) + {\rm O}(\lambda^2). \tag{7.96}$$

Multiplying Eq. (7.96) to the left by $\exp(iKH_{\rm meas}t)$ and by using the definition (7.86) we can write the time evolution operator $U_K(t)$ as the sum of two terms

$$U_K(t) = U_{\rm ad}(t) + \frac{1}{K} U_{\rm na}(t), \tag{7.97}$$

where

$$U_{\rm ad}(t) = \exp\left[-i \left(\sum_n P_n H_{\rm sys} P_n + \frac{1}{K} \sum_n P_n H_{\rm sys} \frac{Q_n}{a_n} H_{\rm sys} P_n + {\rm O}\left(\frac{1}{K^2}\right) \right) t \right] + {\rm O}\left(\frac{1}{K^2}\right) \tag{7.98}$$

is a diagonal, "adiabatic" evolution and

$$U_{\rm na}(t) = \left[e^{iKH_{\rm meas}t} \sum_n \frac{Q_n}{a_n} H_{\rm sys} P_n,\ e^{-iKH_{\rm meas}t} U_{\rm ad}(t) \right] + {\rm O}\left(\frac{1}{K}\right) \tag{7.99}$$

is the nondiagonal, "nonadiabatic" correction. In the $K \to \infty$ limit only the adiabatic term survives and one obtains

$$\lim_{K\to\infty} U_K(t) = U_{\rm ad}(t) = \exp\left(-i \sum_n P_n H_{\rm sys} P_n\ t \right), \tag{7.100}$$

which is formula (7.81). The proof is complete. As a byproduct we get the corrections to the exact limit, valid for large, but finite, values of K.

7.6 Novel definition of quantum Zeno effect

The diverse examples considered in the previous sections and the theorem just proved motivate us to look for a broader definition of Zeno effect, that includes "continuous" observations as well as somewhat delicate situations in which repopulation effects (in amplitude or probability) take place.

Let us consider a quantum system whose evolution is described by a Hamiltonian H. Let the initial state be ρ_0 (not necessarily a pure state) and the survival probability $P(t)$. Consider the evolution of the system under the effect of an additional interaction, so that the total Hamiltonian reads

$$H_K = H + H_{\rm meas}(K), \tag{7.101}$$

where K is a set of parameters and $H_{\rm meas}(K = 0) = 0$. This Hamiltonian includes also as a particular case the GSD described in Sec. 7.3; moreover, since a GSD is basically equivalent

to a *bona fide* measurement, the above Hamiltonian includes, for all practical purposes, the usual formulation of quantum Zeno effect in terms of projection operators. Notice that H is not necessarily the free Hamiltonian; rather, one should think of H as a full Hamiltonian, containing interaction terms, and $H_{\rm meas}(K)$ should be viewed as an additional interaction Hamiltonian performing the measurement. We have considered plenty of examples in our analysis: all of them fit in the scheme (7.101).

We shall say that the system displays a QZE if there exists an interval $I^{(K)} = [t_1^{(K)}, t_2^{(K)}]$ such that

$$P^{(K)}(t) > P(t), \qquad \forall t \in I^{(K)}, \tag{7.102}$$

where $P^{(K)}(t)$ and $P(t)$ are the survival probabilities under the action of the Hamiltonians H_K and H, respectively. We shall say that the system displays an *inverse* QZE if there exists an interval $I^{(K)}$ such that

$$P^{(K)}(t) < P(t), \qquad \forall t \in I^{(K)}. \tag{7.103}$$

The time interval $I^{(K)}$ must be evaluated case by case. However,

$$t_2^{(K)} \leq T_{\rm P}, \tag{7.104}$$

where $T_{\rm P}$ is the Poincaré time. Obviously, for the definition (7.102)-(7.103) to be meaningful from a physical point of view, the length of the interval $I^{(K)}$ must be of order $T_{\rm P}$. The above one is a very broad definition, for it includes a huge class of systems (even trivial cases like time translations $P(t) \to P(t - t_0)$ are included). We have not succeeded in finding a more restrictive definition and we do not think it would be meaningful. This is in line with our general philosophy: the Zeno effects are very common phenomena.

In order to elucidate the meaning of the above definition, let us look at some particular cases considered in this paper. The situations considered in Figs. 7.7 and 7.8 are both QZEs, according to this definition: one has $t_1^{(K)} = 0$ and $t_2^{(K)} \leq T_{\rm P} = \pi/\Omega$ [and $(t_2^{(K)} - t_1^{(K)}) = {\rm O}(T_{\rm P})$]. The case outlined in Fig. 7.1 is also a QZE, with $t_1^{(K)} = 0$ and $t_2^{(K)} \leq T_{\rm P}$ (notice that $T_{\rm P}$ may even be infinite).

If we deal with an unstable system, the definition of Zeno effect can be made more stringent, by simply generalizing the results of Sec. 7.2.3 to a broader class of measurements. Indeed, in such a case, one need not refer to an interval $I^{(K)}$ and can consider the *global* behavior of the survival probability. By introducing the lifetime γ, one can define the occurrence of a QZE or an IZE if

$$\gamma_{\rm eff}(K) \lesseqgtr \gamma, \tag{7.105}$$

respectively, where $\gamma_{\rm eff}(K)$ is the new (effective) lifetime under the action of H_K. Notice that this case is in agreement with the definitions (7.102)-(7.103). Moreover, $t_2^{(K)} \to \infty$ for IZE, while $t_2^{(K)} \leq t_{\rm pow}$ for QZE, where $t_{\rm pow}$ is the time at which a transition from an exponential to a power law takes place. [As we have seen in Chap. 6, such a time is of order $\log(1/\lambda)$.] The definition (7.105) includes all the cases considered in Sec. 7.2.3. See for example Fig. 7.3(b). Notice that when a Zeno effect is obtained by repeated use of projection operators (at equal time intervals τ), one always gets an exponential behavior, with a well defined $\gamma_{\rm eff}(\tau)$ (see Sec. 7.2.3). A problem arises with oscillating systems (or in general with systems whose Poincaré time is finite), because of the impossibility of defining the "natural" decay rate γ (see, for instance, Fig. 7.7). From this perspective, we cannot help feeling that the very concept of QZE is somewhat less meaningful for purely oscillating systems, exhibiting no *bona fide* instability.

We shall adopt these new definitions of Zeno effects in the following (Facchi and Pascazio [2001]). They work in all the cases considered in this work and also comprise, in a more

general theoretical scheme, all the examples of Zeno effects considered in the literature. These definitions should be kept in mind while considering the examples proposed in the following chapters.

Chapter 8

Zeno effects in down-conversion processes

8.1 Introduction

The differences and analogies between pulsed and continuous observations analyzed in the previous chapter will now be discussed by considering a quantum optical example. A down-conversion process in a nonlinear crystal can be thought of as the decay of a pump photon into a pair of signal and idler photons of lower frequency. If the pumping is sufficiently strong and there is phase matching, the energy of the spontaneously down-converted light monotonously increases and that of the pump beam monotonously decreases. In this sense, the down-conversion process may be looked at as the decay process of an unstable system.

Let us first discuss the case of "pulsed" observation. There are similar ideas in the literature (Pascazio, Namiki, Badurek and Rauch [1993]; Kwiat, Weinfurter, Herzog, Zeilinger and Kasevich [1995]; Facchi, Klein, Pascazio and Schulman [1999]), but here we shall discuss an interesting example first proposed by Luis and Peřina [1996]. A pump beam illuminates a nonlinear crystal, that is transversely cut in N pieces which are then carefully aligned so that the signal and pump photons leaving a given slice become the input signal and pump photons for the next slice of the crystal, while the idler photons are taken out at each step (see Fig. 8.2 in the following). By increasing the number N of slices, the probability of emission of the down-converted pair decreases: this is QZE. However, if the phase matching condition is not fulfilled in the process of down-conversion (Luis and Sánchez–Soto [1998]; Thun and Peřina [1998]), the observation may, on the contrary, *enhance* the emission for a properly chosen N: this is an IZE.

We shall see that such a behaviour occurs also when, instead of cutting the crystal into N pieces, the idler beam is coupled to an auxiliary mode (see Fig. 8.3 in the following). The continuous interaction with the auxiliary mode is a sort of "steady gaze" at the system and performs a continuous observation.

The Zeno–inverse Zeno interplay that takes place in this model can be easily understood in the light of the theoretical scheme outlined in Sec. 7.2.3 and will be the object study of this chapter.

8.2 The system

Consider a nonlinear crystal through which three modes, pump p, signal s and idler i propagate in the same direction. The nonlinear waveguide is filled with a second-order nonlinear medium

in which ultra–violet pump photons are down-converted into signal and idler photons of lower frequency.

We will assume that all modes are monochromatic and their frequencies fixed, e.g. by placing narrow interference filters in front of the detectors. Provided the amplitudes of the fields vary little during an optical period (SVEA approximation), the effective Hamiltonian reads ($\hbar = 1$)

$$H = \omega_p a_p^\dagger a_p + \omega_s a_s^\dagger a_s + \omega_i a_i^\dagger a_i + \Gamma \left[a_p a_s^\dagger a_i^\dagger e^{i\Delta t} + a_p^\dagger a_s a_i e^{-i\Delta t} \right], \tag{8.1}$$

where ω_α is the frequency of mode α, $\Delta = (\boldsymbol{k}_p - \boldsymbol{k}_s - \boldsymbol{k}_i)_z$ is the nonlinear phase mismatch and the propagation variable z has been replaced with the evolution parameter t. The nonlinear coupling constant Γ is proportional to the second order nonlinear susceptibility $\chi(2)$ (Hong and Mandel [1985]). We suppose that the incident pump field is intense and that the pump mode a_p can be treated classically, as a field of complex amplitude $a_p = \xi \exp(-i\omega_p t)$, where ξ and ω_p denote the complex amplitude and the frequency of the classical pump wave, respectively. In this approximation the Hamiltonian (8.1) has only two quantized field modes and reads

$$H = \omega_s a_s^\dagger a_s + \omega_i a_i^\dagger a_i + \Gamma \left[a_s^\dagger a_i^\dagger e^{-i(\omega_p - \Delta)t} + a_s a_i e^{i(\omega_p - \Delta)t} \right], \tag{8.2}$$

where the amplitude ξ has been absorbed in the coupling constant Γ (taken real for simplicity). Notice that the strong pump wave approximation will cease to be valid once appreciable depletion of the pump field occurs. Therefore the solution of Eq. (8.2) properly describes the process of parametric down-conversion under the restriction $\langle n_{s,i}(t) \rangle \ll |\xi|^2$, where n is the number operator, i.e., for sufficiently strong pumping and sufficiently weak nonlinear interaction.

By introducing the slowly varying operators

$$a_s' = e^{i(\omega_s - \Delta/2)t} a_s, \qquad a_i' = e^{i(\omega_i - \Delta/2)t} a_i, \tag{8.3}$$

which obey the same commutation rules as the a's, the Heisenberg equations of motions take the form

$$\dot{a}_s' = -i[a_s', H'], \qquad \dot{a}_i' = -i[a_i', H'], \tag{8.4}$$

with the time-independent Hamiltonian

$$H' = \frac{\Delta}{2} a_s'^\dagger a_s' + \frac{\Delta}{2} a_i'^\dagger a_i' + \Gamma \left[a_s'^\dagger a_i'^\dagger + a_s' a_i' \right], \tag{8.5}$$

where the frequency matching condition $\omega_p = \omega_s + \omega_i$ was used.

The state of the field at time $t = 0$ is taken to be the vacuum for the signal and idler modes

$$|\psi_0\rangle = |0_s, 0_i\rangle. \tag{8.6}$$

Under the action of the Hamiltonian (8.5) this state is unstable and spontaneously decays, continuously generating photon pairs. For example, when $\Delta = 0$ the average number of signal and idler photons originating in the crystal of length t,

$$\langle a_s^\dagger(t) a_s(t) \rangle \equiv \langle \psi_0 | a_s^\dagger(t) a_s(t) | \psi_0 \rangle = \langle \psi_0 | a_i^\dagger(t) a_i(t) | \psi_0 \rangle = \sinh^2(\Gamma t), \tag{8.7}$$

is an exponentially increasing function of t. In Eq. (8.7) and henceforth all (slowly varying) operators are written without primes to simplify the notation.

Our interest is focused on the survival amplitude of the vacuum state under the action of the Hamiltonian (8.5). It is somewhat more convenient to consider the evolution of the following linear combinations

$$a = \frac{a_i + a_s}{\sqrt{2}}, \qquad b = \frac{a_i - a_s}{\sqrt{2}}. \tag{8.8}$$

In terms of these two modes the Hamiltonian (8.5) reads

$$H = \frac{\Delta}{2}a^\dagger a + \frac{\Gamma}{2}\left[a^{\dagger 2} + a^2\right] + \frac{\Delta}{2}b^\dagger b - \frac{\Gamma}{2}\left[b^{\dagger 2} + b^2\right] \tag{8.9}$$

and the modes a and b are completely decoupled.

It is now straightforward to evaluate the time evolution of $|\psi_0\rangle$ by considering the properties of the generalized two-photon coherent states (Mandel and Wolf [1995]). Remember that by letting $U(\mu,\nu)$ be a unitary transformation that generates the pseudo-annihilation operator

$$A(\mu,\nu) = U(\mu,\nu)\; a\; U^\dagger(\mu,\nu) = \mu a + \nu a^\dagger, \quad \text{with} \quad |\mu|^2 - |\nu|^2 = 1, \tag{8.10}$$

for two complex numbers μ, ν, the generalized two-photon coherent state $|[\mu,\nu;v]\rangle$ is defined by operating $U(\mu,\nu)$ on the coherent state $|v\rangle$, i.e.

$$|[\mu,\nu;v]\rangle = U(\mu,\nu)|v\rangle. \tag{8.11}$$

The scalar product between this state and a coherent state has the following form

$$\langle v|[\mu,\nu;w]\rangle = \frac{1}{\sqrt{\mu}}\exp\left[-\frac{1}{2}|v|^2 - \frac{1}{2}|w|^2 - \frac{1}{2}\frac{\nu}{\mu}v^{*2} + \frac{w}{\mu}v^* + \frac{1}{2}\frac{\nu^*}{\mu}w^2\right], \tag{8.12}$$

and the most general unitary transformation that has the property (8.10) is

$$U(\mu,\nu) = \exp[-i(Ka^\dagger a + ka^2 + k^*a^{\dagger 2})], \tag{8.13}$$

where K is real and k a constant. The complex numbers μ and ν are related to the parameters K and k by the relation

$$\begin{cases} \mu = \cosh(\triangle k) + i\frac{K}{\triangle k}\sinh(\triangle k) \\ \nu = i\frac{2k}{\triangle k}\sinh(\triangle k) \end{cases}, \quad \text{with} \quad \triangle k = \sqrt{4k^2 - K^2}, \tag{8.14}$$

where we considered, for simplicity, k real.

Let us look at the survival amplitude of the vacuum state under the action of the quadratic Hamiltonian (8.9), corresponding to a two-photon interaction with a classical pump for the two independent modes a and b. By using Eq. (8.12) this reads

$$\mathcal{A}(t) = \langle 0_a, 0_b|e^{-iHt}|0_a, 0_b\rangle = \langle 0_a, 0_b|[\mu_a(t), \nu_a(t); 0_a], [\mu_b(t), \nu_b(t); 0_b]\rangle = \frac{1}{\sqrt{\mu_a(t)\mu_b(t)}}. \tag{8.15}$$

In our case

$$\mu_a(t) = \mu_b(t) = \cosh(\triangle\Gamma t) + i\frac{\Delta}{2\triangle\Gamma}\sinh(\triangle\Gamma t), \quad \text{with} \quad \triangle\Gamma = \sqrt{\Gamma^2 - \frac{\Delta^2}{4}}, \tag{8.16}$$

whence one gets the survival probability

$$P(t) = |\mathcal{A}(t)|^2 = \frac{1}{|\mu_a(t)|^2} = \left[\cosh^2(\triangle\Gamma t) + \frac{\Delta^2}{4\triangle\Gamma^2}\sinh^2(\triangle\Gamma t)\right]^{-1}. \tag{8.17}$$

We can now look at the features of this system.

At short times

$$P(t) \sim 1 - \triangle\Gamma^2 t^2 - \frac{\Delta^2}{4}t^2 = 1 - \Gamma^2 t^2, \tag{8.18}$$

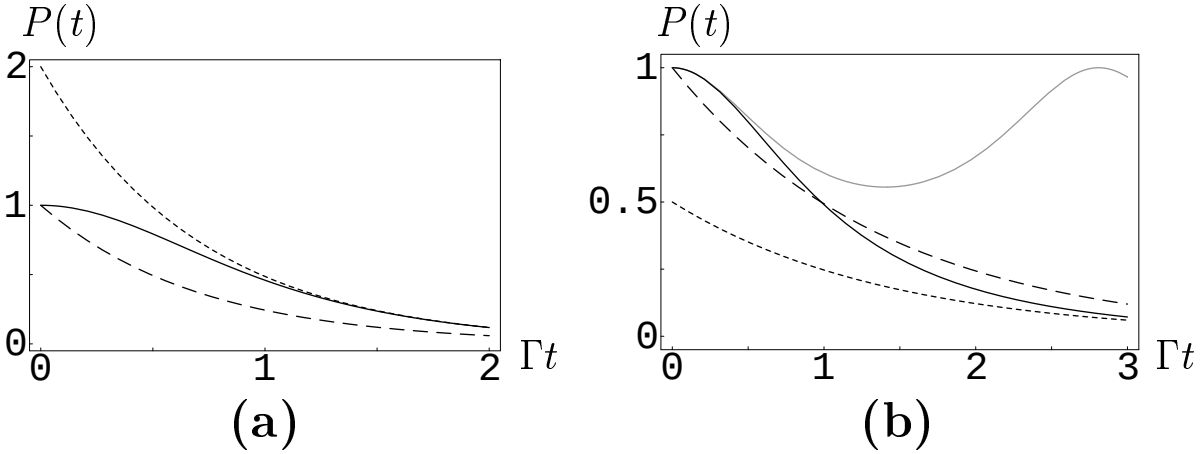

Figure 8.1: Survival probability of the initial (vacuum) state. (a) $\Delta = \sqrt{2}\Gamma (< \sqrt{3}\Gamma)$ and $\mathcal{Z} = 2$; the full line is the survival probability (8.17), the dotted line the asymptotic exponential (8.21) and the dashed line the renormalized exponential $\exp(-\gamma t)$. $P(t)$ and $\exp(-\gamma t)$ do not intersect, τ^* does not exist and only a QZE is possible. (b) $\Delta = \sqrt{7/2}\Gamma$ ($\sqrt{3}\Gamma < \Delta < 2\Gamma$) and $\mathcal{Z} = .5$; the full line is the survival probability (8.17), the dotted line the asymptotic exponential (8.21) and the dashed line the renormalized exponential $\exp(-\gamma t)$. $P(t)$ and $\exp(-\gamma t)$ intersect, τ^* exists and a Zeno–inverse Zeno transition is possible. The gray line is the survival probability (8.22) for $\Delta = 3\Gamma (> 2\Gamma)$: in this case one gets an oscillatory behavior and $\mathcal{Z}$ cannot be defined.

so that the Zeno time reads

$$\tau_{\rm Z}^{-2} = \langle H^2 \rangle = \frac{\Gamma^2}{4} \langle 0_a, 0_b | (a^2 a^{\dagger 2} + b^2 b^{\dagger 2}) | 0_a, 0_b \rangle = \Gamma^2. \tag{8.19}$$

The long-time behavior depends on the value of $\triangle\Gamma^2$ in (8.16): if $\Delta < 2\Gamma$, at long times,

$$P(t) \sim \left[\frac{1}{4} e^{2\triangle\Gamma t} + \frac{\Delta^2}{16\triangle\Gamma^2} e^{2\triangle\Gamma t} \right]^{-1} = \frac{4\triangle\Gamma^2}{\Gamma^2} e^{-2\triangle\Gamma t} \tag{8.20}$$

so that

$$P(t) \sim \mathcal{Z} e^{-\gamma t}, \quad \text{where} \quad \gamma = \sqrt{4\Gamma^2 - \Delta^2} \quad \text{and} \quad \mathcal{Z} = \frac{4\Gamma^2 - \Delta^2}{\Gamma^2}. \tag{8.21}$$

This formula, as already emphasized in Sec. 7.2.3, is an excellent approximation at long times and enables us to discuss the Zeno–inverse Zeno transition. Notice also that in this model the Hamiltonian (8.9) is not lower bounded and indeed the asymptotic behavior at large times is exactly exponential, with no inverse power law tails. The condition $\mathcal{Z} < 1$ reads $\Delta > \sqrt{3}\Gamma$. In Fig. 8.1 the vacuum survival probability (8.17) is shown for different values of the parameters.

As we have seen, when $\Delta < 2\Gamma$ the survival probability decreases exponentially; on the other hand, when $\Delta > 2\Gamma$ the behavior is oscillatory

$$P(t) = |\mathcal{A}(t)|^2 = \frac{1}{|\mu_a(t)|^2} = \left[\cos^2(|\triangle\Gamma| t) + \frac{\Delta^2}{4|\triangle\Gamma|^2} \sin^2(|\triangle\Gamma| t) \right]^{-1}, \tag{8.22}$$

with $4|\triangle\Gamma|^2/\Delta^2 < P(t) < 1$. In this case a decay rate γ and, as a consequence, $\mathcal{Z}$ cannot be defined. We note that the vacuum state never decays completely. We can now discuss pulsed and continuous observation.

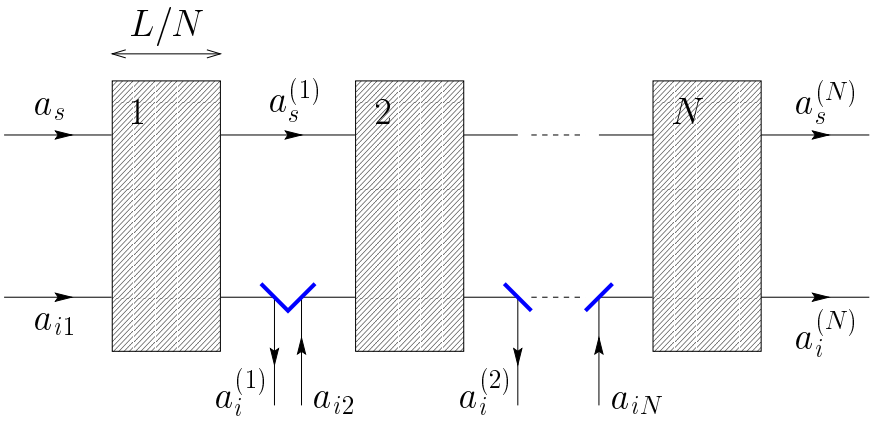

Figure 8.2: Outline of a "sliced" parametric down-conversion scheme. The down-converter is cut into N crystals of length L/N. After each slice, the output idler beams $a_i^{(k)}$ are removed by means of mirrors inserted in the idler path and replaced by different input idler fields a_{ik} in vacuum.

8.3 Pulsed observation

Let us first consider pulsed observations performed at time intervals $\tau = t/N$ (Luis and Peřina [1996]). The nonlinear crystal is divided into N equal parts of length L/N, corresponding to an interaction time $\tau = t/N$, as shown in Fig. 8.2. Assume that the signal beams at each slice are perfectly superimposed and aligned and that reflection at each step is made negligible, for instance by embedding the N pieces in a linear medium with exactly the same refractive index. On the other hand, the idler path is interrupted after each slice, for instance by means of mirrors. At each step the output idler beam is completely removed and replaced by a new input idler beam in the vacuum state. With this modification it is possible to detect the emission of the idler photons, for instance, by means of N photodetectors.

By using the definition (8.8) and the evolution law (8.10) or, alternatively, by directly solving the Heisenberg equations (8.4) for the Hamiltonian (8.5) one gets for a single slice

$$\begin{cases} a_s(\tau) = \mu(\tau) a_s + \nu(\tau) a_i^\dagger \\ a_i(\tau) = \mu(\tau) a_i + \nu(\tau) a_s^\dagger \end{cases} , \tag{8.23}$$

where $\mu(t) = \mu_a(t)$ is defined by Eq. (8.16) and $\nu(t) = \nu_a(t) = i\Gamma \sinh(\triangle\Gamma t)/\triangle\Gamma$. Remember that unitarity requires $|\mu(t)|^2 - |\nu(t)|^2 = 1$.

We study how the survival probability of the vacuum state is modified by frequent interruptions of the idler path. To this end we will look at the modified evolution of the signal mode, following Luis and Peřina [1996]; Luis and Sánchez–Soto [1998] and Thun and Peřina [1998]. By using (8.23) we can express the signal annihilation operator after the Nth slice $a_s^{(N)}$ in terms of the annihilation (creation) operator of the signal (idler) mode before it

$$a_s^{(N)} = \mu(\tau) a_s^{(N-1)} + \nu(\tau) a_{iN}^\dagger, \tag{8.24}$$

where we used the fact that a different vacuum mode a_{ik}, $k = 1, \ldots, N$, is at the idler input of each of the N crystals. By iterating Eq. (8.24) we obtain

$$a_s^{(N)} = \mu^N a_s + \nu \sum_{k=1}^{N} \mu^{N-k} a_{ik}^\dagger. \tag{8.25}$$

The mean value of the number of signal photons reads

$$\langle a_s^{(N)\dagger} a_s^{(N)} \rangle = |\nu|^2 \sum_{k=1}^{N} |\mu|^{2(N-k)} = |\nu|^2 \frac{|\mu|^{2N} - 1}{|\mu|^2 - 1} = |\mu|^{2N} - 1, \tag{8.26}$$

where the unitarity condition was used. For large values of N, by making use of Eq. (8.17) we get

$$\langle a_s^{(N)\dagger} a_s^{(N)} \rangle = |\mu(t/N)|^{2N} - 1 = P(t/N)^{-N} - 1 \sim 1 - P(t/N)^N = 1 - P^{(N)}(t) \tag{8.27}$$

and the mean number of photons coincides with the probability of emitting one signal photon (for the probability of emission of more than one photon is negligible), i.e. with the (modified) decay probability of the vacuum state.

By using the short times expansion of the survival probability (8.18) we get

$$P^{(N)}(t) \sim \exp(-\Gamma^2 \tau t), \tag{8.28}$$

i.e. an effective decay rate

$$\gamma_{\text{eff}}(\tau) = \Gamma^2 \tau \ , \tag{8.29}$$

which is in accord with Eq. (7.24), because $\tau_{\text{Z}} = 1/\Gamma$ [as shown by Eq. (8.19)]. In the $N \to \infty$ limit the effective decay rate approaches zero and the decay is completely frozen, i.e. no photons are emitted (QZE).

If, in (8.21),

$$\mathcal{Z} > 1 \Leftrightarrow \Delta < \sqrt{3}\Gamma, \tag{8.30}$$

we are in the situation outlined in Figs. 7.4(a) and 8.1(a) and according to the analysis of Section 7.2.3 only a QZE can occur. On the other hand, if

$$\mathcal{Z} < 1, \tag{8.31}$$

then, according to the analysis of Sec. 7.2.3 (See figures 7.3 and 7.4), a transition time τ^* exists and by decreasing the frequency of measurements one observes the transition from a Zeno to an inverse Zeno (Heraclitus) regime. By using Eq. (8.21), the condition (8.31) reads

$$\Delta > \sqrt{3}\Gamma. \tag{8.32}$$

In particular, if the phase mismatch Δ is close to the value $\Delta = 2\Gamma$, the linear approximation (8.29) is valid up to τ^*, because γ in Eq. (8.21) approaches zero, and we get

$$\tau^* = \frac{t}{N^*} \simeq \frac{\gamma}{\Gamma^2} = \frac{\sqrt{4\Gamma^2 - \Delta^2}}{\Gamma^2} = \frac{2\triangle\Gamma}{\Gamma^2}, \tag{8.33}$$

whence for $N^* < \Gamma^2 t / 2\triangle\Gamma$ the photon production is enhanced (IZE).

So far, we supposed $\Delta < 2\Gamma$. The effect becomes more spectacular for $\Delta > 2\Gamma$ [see Eqs. (8.22)]. Indeed, in this case the phase mismatch is so large that the down conversion process is no longer exponential, but has an oscillatory behavior

$$\langle a_s^\dagger(t) a_s(t) \rangle = |\mu(t)|^2 - 1 = \cos^2(|\triangle\Gamma|t) + \frac{\Delta^2}{4|\triangle\Gamma|^2} \sin^2(|\triangle\Gamma|t) - 1 = \frac{\Gamma^2}{|\triangle\Gamma|^2} \sin^2(|\triangle\Gamma|t), \tag{8.34}$$

which is bounded by

$$\langle a_s^\dagger(t) a_s(t) \rangle_{\text{MAX}} = \frac{\Gamma^2}{|\triangle\Gamma|^2}. \tag{8.35}$$

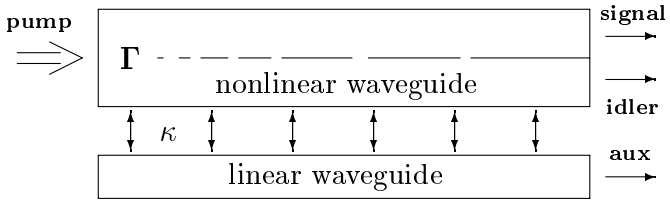

Figure 8.3: Outline of the nonlinear coupler

On the other hand, by cutting the crystal and removing the idler path, one gets

$$\langle a_s^{(N)\dagger} a_s^{(N)} \rangle = \left(1 + \frac{\Gamma^2 t^2}{N^2}\right)^N - 1 \sim \exp(\Gamma^2 \tau t) - 1, \tag{8.36}$$

and an explosive exponential behavior is recovered (IZE). It is easy to check that $\tau^* = 0$, a quite remarkable situation: Independently of the frequency of measurements N, one always obtains an IZE: see Fig. 8.1(b) (a QZE is recovered only in the $N \to \infty$ limit). Remember also that $\mathcal{Z}$ cannot be defined, in this case. We will rigorously justify this interpretation in Chap. 10, by considering complete and incomplete Rabi oscillations as the limiting case of a truly unstable system with a finite-width form factor.

We notice that the process described is always unitary and it actually makes no difference whether any measurements on the idler modes are actually carried out or not. It is sufficient that such measurements could *in principle* be made, as stressed in Sec. 7.3. We also emphasize that the situation just analyzed is affected by (probability) repopulation effects like those described in Sec. 7.2.4.

8.4 The nonlinear coupler: continuous observation

We now modify the system considered in the previous subsections and discuss continuous observation. Consider a nonlinear coupler made up of two waveguides, through which four modes, pump p, signal s, idler i, and auxiliary mode b propagate in the same direction, see Fig. 8.3. The nonlinear waveguide is again filled with a second-order nonlinear medium in which ultra–violet pump photons are down-converted to signal and idler photons of lower frequency, but in addition, the idler mode is allowed to exchange energy, e.g. by means of evanescent waves, with the auxiliary mode b propagating through a linear medium (Řeháček, Peřina, Facchi, Pascazio, and Mišta [2000]).

We assume again the validity of the SVEA approximation and we consider the linear coupling weak enough so that it can be described by the coupled modes theory (Born approximation) (Stich and Bass [1985], Chap. 4; Yariv and Yeh [1984]; Saleh and Teich [1991], Sec. 7.4.B). With the help of the strong pump wave approximation the Hamiltonian of our problem is simplified as follows

$$H_\kappa = H + H_{\rm meas}(\kappa), \quad \text{with} \quad H_{\rm meas}(\kappa) = \kappa(a_i^\dagger b + a_i b^\dagger) + \omega_b b^\dagger b, \tag{8.37}$$

where H is the down-converter Hamiltonian (8.2) and κ the linear coupling constant. By introducing the slowly varying operators (with a slightly different choice for a_s' and a_i', which is somewhat more convenient for the following discussion)

$$a_s' = e^{i\omega_s t} a_s, \qquad a_i' = e^{i(\omega_i - \Delta)t} a_i, \qquad b' = e^{i(\omega_b - \Delta)t} b, \tag{8.38}$$

we get, instead of (8.5), the new time-independent Hamiltonian

$$H_\kappa = \Delta a_i^\dagger a_i + \Gamma(a_s^\dagger a_i^\dagger + a_s a_i) + \Delta b^\dagger b + \kappa(a_i^\dagger b + a_i b^\dagger), \tag{8.39}$$

where we assumed again that the frequency matching conditions, $\omega_p - \omega_s - \omega_i = 0$ and $\omega_b = \omega_i$, hold and we suppressed all primes.

The dynamics of the nonlinear coupler (8.39) reduces to the dynamics of the spontaneous down-conversion process (8.5) provided that $\kappa = 0$. In the case of phase matching $\Delta = 0$, the average number of signal and idler photons originating in the crystal of length t, Eq. (8.7), is an exponentially increasing function of t.

The behaviour of the down-conversion process changes completely when one of the two down-converted modes (say, the idler mode) is coupled to an auxiliary mode via the linear interaction, performing the continuous observation. The Hamiltonian (8.39) yields, when $\Delta = 0$ (phase matching),

$$\begin{aligned} \dot{a}_s &= -i\Gamma a_i^\dagger, \\ \dot{a}_i &= -i\Gamma a_s^\dagger - i\kappa b, \qquad (\Delta = 0) \\ \dot{b} &= -i\kappa a_i \end{aligned} \tag{8.40}$$

and we are interested in the regime of weak nonlinearity, expressed by the condition $\kappa > \Gamma$. Notice that two opposite tendencies compete in Eqs. (8.40): an elliptic structure, leading to oscillatory behavior, governed by the coupling parameter κ,

$$\ddot{a}_i = -\kappa^2 a_i, \qquad \ddot{b} = -\kappa^2 b \tag{8.41}$$

and a hyperbolic structure, yielding exponential behavior, governed by the nonlinear parameter Γ,

$$\ddot{a}_s = \Gamma^2 a_s, \qquad \ddot{a}_i = \Gamma^2 a_i. \tag{8.42}$$

The threshold between these two regimes occurs for $\Gamma \simeq \kappa$.

The system of equations (8.40) is easily solved and the number of output signal photons, which is the same as the number of pump photons decays, reads

$$\langle a_s^\dagger(t) a_s(t)\rangle = \frac{\Gamma^2}{\chi^2}\sin^2\chi t + \frac{\kappa^2\Gamma^2}{\chi^4}(1-\cos\chi t)^2, \tag{8.43}$$

where $\chi = \sqrt{\kappa^2 - \Gamma^2}$. Unlike the case of phase matched down-conversion (8.7), the exchange of energy between all modes now becomes periodical when $\kappa > \Gamma$. As the linear coupling becomes stronger, the period of the oscillations gets shorter and the amplitude of the oscillations decreases as κ^{-2}, namely

$$\langle a_s^\dagger(t) a_s(t)\rangle \sim \frac{\Gamma^2}{\kappa^2}\sin^2\kappa t + \frac{\Gamma^2}{\kappa^2}(1-\cos\kappa t)^2 = \frac{4\Gamma^2}{\kappa^2}\sin^2\frac{\kappa t}{2} \qquad (\kappa \gg \Gamma). \tag{8.44}$$

For strong coupling the down-conversion process is completely frozen, the medium becomes effectively linear and the pump photons propagate through it without "decay." (In the regime of very large κ, however, the coupled modes theory breaks down and some other experimental realization of the Hamiltonian (8.39) should be found.) Notice that in this situation, even if t is increased, the number of down-converted photons is bounded [compare with the opposite case (8.7)]. This is QZE in the following sense: by increasing the coupling with the auxiliary mode, a better "observation" of the idler mode (and therefore of the decay of the pump) is

performed and the evolution is hindered. There is an intuitive explanation of this behavior: since the linear coupling changes the phases of the amplitudes of the interacting modes, the constructive interference yielding exponential increase of the converted energy (8.7) is destroyed and down-conversion is frozen (see Sec. 8.4.2 in the following).

In agreement with the final part of Sec. 7.4.3, by comparing Eq. (8.44) with Eqs. (8.27)-(8.29), we find that the linear coupling is effective as the square root of the number of pulsed measurements, namely

$$\kappa = \frac{\sqrt{2N}}{t}. \tag{8.45}$$

Consider now the Hamiltonian (8.39) when $\kappa = 0$, describing down-conversion with phase mismatch Δ. It is apparent that the coupling and the phase mismatch influence the down-conversion process in the same way. Indeed for large values of the phase mismatch Δ it is easy to find from Eq. (8.34) that

$$\langle a_s^\dagger(t) a_s(t)\rangle \sim \frac{4\Gamma^2}{\Delta^2}\sin^2\frac{\Delta t}{2} \qquad (\Delta \gg \Gamma), \tag{8.46}$$

which is to be compared with Eq. (8.44). The interesting interplay between coupling κ and mismatch Δ will be investigated in the following subsection.

8.4.1 Competition between the coupling and the mismatch

In the previous section we saw that the nonlinear interaction was affected by both linear coupling and phase mismatch in the same way: the effectiveness of the nonlinear process drops down under their action. In this section we show that when both disturbing elements are present in the dynamics of the down-conversion process, the linear coupling can compensate for the phase mismatch and vice versa, so that the probability of emission of the signal and idler photons can almost return back to its undisturbed value.

We start from the equations of motion generated by the full interaction Hamiltonian (8.39)

$$\begin{aligned} \dot{a}_s &= -i\Gamma a_i^\dagger, \\ \dot{a}_i &= -i\Delta a_i - i\Gamma a_s^\dagger - i\kappa b, \qquad (\Delta \neq 0, \kappa \neq 0) \\ \dot{b} &= -i\Delta b - i\kappa a_i. \end{aligned} \tag{8.47}$$

Although it is easy to write down the explicit solution of the system (8.47), we shall provide only a qualitative discussion of the solution. The main features are then best demonstrated with the help of a figure. Eliminating idler and auxiliary mode variables from Eq. (8.47) we get a differential equation of the third order for the annihilation operator of the signal mode. Its characteristic polynomial (upon substitution $a_s(t)=\xi\exp(-i\lambda t)$)

$$\lambda^3 + 2\Delta\lambda^2 + (\Delta^2 - \kappa^2 + \Gamma^2)\lambda + \Gamma^2\Delta, \quad \kappa \neq 0 \tag{8.48}$$

is a cubic polynomial in λ with real coefficients. An oscillatory behaviour of the signal mode occurs only provided the polynomial (8.48) has three real roots (*causus irreducibilis*), i.e. if its determinant D obeys the condition $D < 0$. Expanding the determinant in the small nonlinear coupling parameter Γ and keeping terms up to the second order in Γ we obtain

$$D \sim -\frac{\kappa^2}{27}\left[(\kappa^2 - \Delta^2)^2 - (5\Delta^2 + 3\kappa^2)\Gamma^2\right], \quad \Gamma \ll \Delta, \kappa. \tag{8.49}$$

It is seen that a mismatched down-conversion behaves in either an oscillatory or a hyperbolic way, depending on the strength of the coupling with the auxiliary mode. The values of κ lying

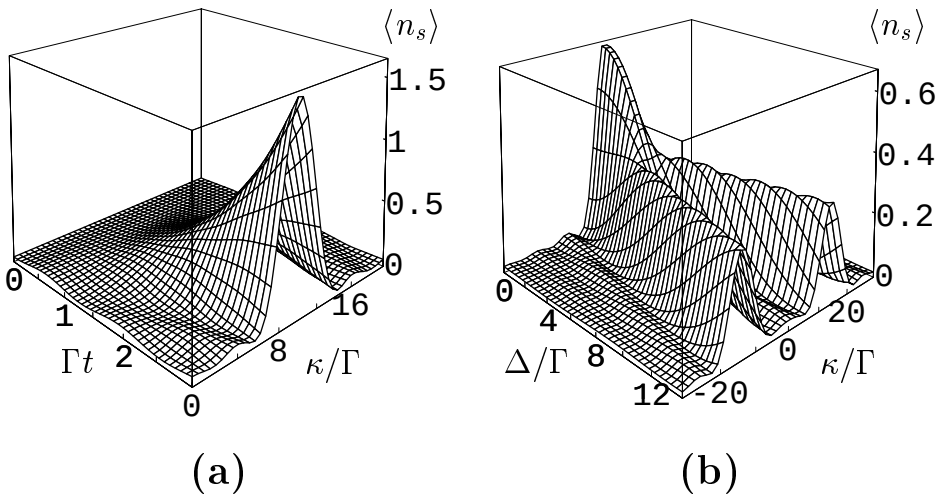

Figure 8.4: (a) Mean number of signal photons $\langle n_s \rangle$ behind the nonlinear medium as a function of interaction length t and strength κ of the linear coupling. The nonlinear mismatch is Δ=10Γ. (b) Interplay between linear coupling and phase mismatch. The mean number of signal photons $\langle n_s \rangle$ behind the nonlinear medium of length $\Gamma t = 1.5$ is shown vs the strength κ of the linear coupling and the nonlinear mismatch Δ. A significant production of signal photons, viewed as a "decay" of the initial state (vacuum), is a clear manifestation of an inverse Zeno effect.

at the boundary between these two types of dynamics are determined by solving the equation $D = 0$. The only two nontrivial solutions are

$$\kappa_{1,2} = \sqrt{\Delta^2 + \frac{3}{2}\Gamma^2 \pm \sqrt{8}\Delta\Gamma}. \tag{8.50}$$

The case $\Delta \gg \Gamma$ is of main interest here. Hence we can, eventually, drop Γ^2 in Eq. (8.50). The resulting intervals are

$$\begin{array}{ll} \text{hyperbolic behaviour:} & \kappa \in \langle \Delta - \sqrt{2}\Gamma, \Delta + \sqrt{2}\Gamma \rangle \\ \text{oscillatory behaviour:} & \kappa \in \langle 0, \Delta - \sqrt{2}\Gamma) \cup (\Delta + \sqrt{2}\Gamma, \infty). \end{array} \tag{8.51}$$

The behaviour of the mismatched down-conversion process is shown in Fig. 8.4(a) for a particular choice of Δ. In absence of linear coupling the down-converted light shows oscillations and the overall effectiveness of the nonlinear process is small due to the presence of phase mismatch Δ. However, as we switch on the coupling between the idler and auxiliary mode, the situation changes. By increasing the strength κ of the coupling the period of the oscillations gets longer and their amplitude larger. When κ becomes larger than $\Delta - \sqrt{2}\Gamma$ the oscillations are no longer seen and the intensity of the signal beam starts to grow monotonously. We can say that in this regime the initial nonlinear mismatch has been compensated by the coupling.

The interplay between nonlinear mismatch and linear coupling is illustrated in Fig. 8.4(b). A significant production of signal photons is a clear manifestation of IZE. In accord with the observations of Luis and Sánchez–Soto [1998] and Thun and Peřina [1998], such an IZE occurs only provided a substantial phase mismatch is introduced in the process of down-conversion. This is the condition (8.32) for having $\mathcal{Z} < 1$ in the decay of the vacuum state. It is worth comparing the interesting behavior seen in Fig. 8.4(b) with the Zeno and inverse Zeno effects in a sliced nonlinear crystal discussed in Section 8.4. The coupling parameter κ here plays a role similar to the number of slices N, so that one can state again that $\kappa \sim \sqrt{N}$ in the sense of Section 7.4.

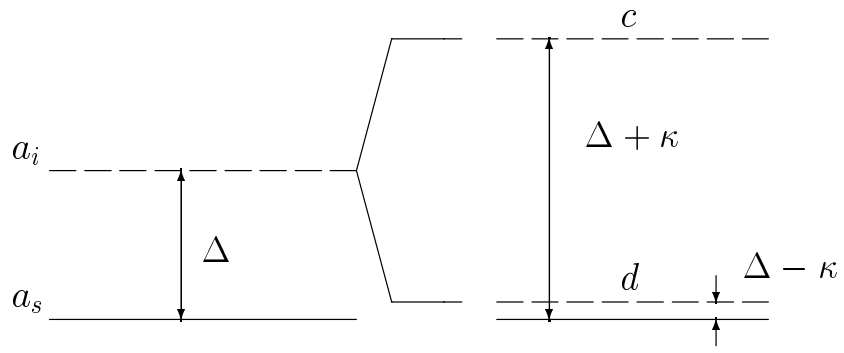

Figure 8.5: Energy scheme of a mismatched down-conversion process subject to linear coupling. The bottom solid lines denote a resonant process.

8.4.2 Dressed modes

We now look for the modes dressed by the interaction κ. This will provide an alternative interpretation and a more rigorous explanation of the result obtained above. Let us diagonalize the Hamiltonian (8.39) with respect to the linear coupling. It is easy to see that in terms of the dressed modes

$$\begin{aligned} c &= (a_i + b)/\sqrt{2}, \\ d &= (a_i - b)/\sqrt{2}, \end{aligned} \tag{8.52}$$

the Hamiltonian (8.39) reads

$$H_\kappa = \omega_c c^\dagger c + \omega_d d^\dagger d + \frac{\Gamma}{\sqrt{2}}(a_s^\dagger c^\dagger + a_s c) + \frac{\Gamma}{\sqrt{2}}(a_s^\dagger d^\dagger + a_s d), \tag{8.53}$$

where the dressed energies are

$$\begin{aligned} \omega_c &= \Delta + \kappa, \\ \omega_d &= \Delta - \kappa. \end{aligned} \tag{8.54}$$

The coupling of the idler mode a_i with the auxiliary mode b yields two dressed modes c and d the pump photon can decay to. They are completely decoupled and due to their energy shift (8.54), exhibit a phase mismatch $\Delta \pm \kappa$. Since the phase mismatch effectively shortens the time during which a fixed phase relation holds between the interacting beams, the amount of converted energy is smaller than in the ideal case of perfectly phase matched interaction, $\Delta = 0$. A strong linear coupling then makes the subsequent emissions of converted photons interfere destructively and the nonlinear interaction is frozen. In this respect the disturbances caused by the coupling and by frequently repeated measurements are similar and we can interpret the phenomenon as a QZE. The energy scheme implied by the Hamiltonian (8.53) is shown in Fig. 8.5. Under the influence of the coupling with the auxiliary mode b the mismatched down-conversion splits into two dressed energy–shifted interactions. It is apparent that when $\kappa = \pm\Delta$ one of the two interactions becomes resonant. The other one is "counter-rotating" and acquires a phase mismatch 2Δ, yielding oscillations. Also, the amplitude of such oscillations decreases as Δ^{-2} and the mode output becomes negligible compared to the other one. The use of the rotating wave approximation in Eq. (8.53) is fully justified in this case and the system is easily solved. The output signal intensity reads

$$\langle a_s^\dagger(t) a_s(t)\rangle = \sinh^2\left(\frac{\Gamma}{\sqrt{2}}t\right), \quad (\kappa = \pm\Delta) \quad (\Delta t \gg 1) \tag{8.55}$$

[compare with Eq. (8.7)]. The linear coupling to an auxiliary mode compensates for the phase mismatch up to a change in the effective nonlinear coupling strength $\Gamma \to \Gamma/\sqrt{2}$.

As a matter of fact, the condition $\kappa = \pm\Delta$ can also be interpreted as a condition for achieving the so–called quasi–phase–matching in the nonlinear process. A quasi–phase–matched regime of generation (Armstrong, Bloembergen, Ducuing and Pershan [1962]; Fejer, Magel, Jundt and Byer [1992]; Chirkin and Volkov [1998]) is usually forced by creating an artificial lattice inside a nonlinear medium, e.g. by periodic modulation of the nonlinear coupling coefficient. A periodic change of sign of Γ (rectangular modulation) yields the effective coupling strength $\Gamma \to 2\Gamma/\pi$, where, as before, Γ is the coupling strength of the phase–matched interaction. Thus the continuous observation of the idler mode even gives a slightly better enhancement of the decay rate than the most common quasi–phase–matching technique.

To summarize, the statement "the down-conversion process is mismatched" means that the nonlinear process is out of resonance in the sense that the momentum of the decay products (signal and idler photons) differs from the momentum carried by the pump photon before the decay took place. When the linear interaction is switched on the system gets dressed and the energy spectrum changes. A careful adjustment of the coupling strength κ makes then possible to tune the nonlinear interaction back to resonance. In this way the probability of pump photon decay can be greatly enhanced. This occurs when $\kappa \simeq \pm\Delta$ and explains why the inverse Zeno effect takes place along the lines $\kappa = \pm\Delta$ in Fig. 8.4(b).

In some sense, on very general grounds, the Zeno effect is a consequence of the new dynamical features introduced by the coupling with an external agent that (through its interaction) "looks closely" at the system. When this interaction can be effectively described as a projection operator *à la* von Neumann, we obtain the usual formulation of the quantum Zeno effect in the limit of very frequent measurements. In general, the description in terms of projection operators may not apply, but the dynamics can be modified in such a way that an interpretation in terms of Zeno or inverse Zeno effect is appealing and intuitive. This is the main reason why we think that examples of the type analyzed in this work call for a broader definition of Zeno effects.

Chapter 9

Classical stabilization and quantum Zeno effect

9.1 Introduction

An inverted pendulum is an ordinary classical pendulum initially prepared in the vertical upright position (Stephenson [1908]; Kapitza [1965], Vol. 2, p. 714; Arnold [1989], p. 121; Arnold [1992], p. 263; Fenn, Bayne and Sinclair [1998], and references therein). This is normally an unstable system, but can be made stable by imposing a vertical oscillatory motion to the pivot. In a few words, when the pivot is accelerated upwards the motion is unstable, while when it is accelerated downwards the motion can be stable: the periodic switch between these two situations can be globally stable or unstable depending on the values of some physical parameters. In particular, when the frequency of the oscillation is higher than a certain threshold, the system becomes stable. This result is a bit surprising at first sight, but can be given an interesting explanation in terms of the so-called parametric resonance (Arnold [1989], p. 121; Arnold [1992], p. 263).

In this chapter we shall study a system (Facchi, Nakazato, Pascazio, Peřina and Řeháček [2000]) that can be viewed as a quantum version of the inverted pendulum. The system to be considered makes use of down-conversion processes interspersed with zones where a linear coupling takes place between the down-converted photon modes. It is similar to the examples analyzed in the previous chapter and, in a certain sense, it combines the pulsed measurement scheme of Sec. 8.3 with the scheme analyzed in Sec. 8.4, by letting a mode of the field perform the "measurement" on another mode. When the coupling between the two modes is large enough, the measurement becomes more effective and the dynamics gets stable: this is just a manifestation of the quantum Zeno effect, which consists in the hindrance of the quantum evolution caused by measurements. The very method of stabilization of the quantum system analyzed here is one of its most interesting features and the configuration we discuss is experimentally realizable in an optical laboratory. It is therefore of interest both for the investigation of the stable/unstable borderline for classical and quantum mechanical systems and their links with the quantum Zeno effect.

9.2 The system

We consider a laser field (pump) of frequency ω_p, propagating through a nonlinear coupler. The field is considered to be classical and the signal and idler modes are denoted by a and b, respectively. As in the previous chapter, we will assume that all modes are monochromatic

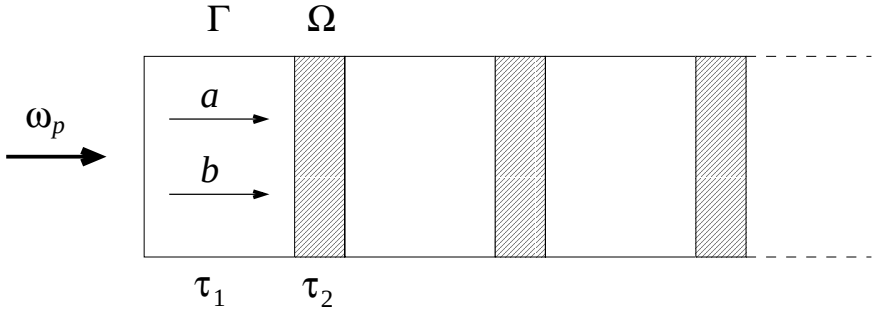

Figure 9.1: The system

and the amplitudes of the fields inside the coupler vary little during an optical period (SVEA approximation). The effective (time-dependent) Hamiltonian reads ($\hbar$=1)

$$H(t) = \omega_a a^\dagger a + \omega_b b^\dagger b + H_{\rm int}(t), \tag{9.1}$$

where the interaction Hamiltonian is given by

$$H_{\rm int}(t) = \begin{cases} \Gamma(a^\dagger b^\dagger e^{-i\omega_p t} + abe^{i\omega_p t}) & \text{if } 0 < t < \tau_1, \\ \Omega(a^\dagger b + ab^\dagger) & \text{if } \tau_1 < t < \tau_1 + \tau_2 \end{cases} \tag{9.2}$$

and $H_{\rm int}(t + nT) = H_{\rm int}(t)$, with a period $T = \tau_1 + \tau_2$. The nonlinear coupling constant Γ is proportional to the second-order nonlinear susceptibility of the medium $\chi(2)$ (Hong and Mandel [1985]), Ω to the overlap between the two modes (Stich and Bass [1985], Chapter 4; Saleh and Teich [1991], Section 7.4.B) and $n = 0, 1, \cdots, N$ is an integer.

We require the matching conditions $\omega_p = \omega_a + \omega_b$ and $\omega_a = \omega_b$ [1]. The above Hamiltonian describes phase-matched down-conversion processes, for $nT < t < nT + \tau_1$, interspersed with linear interactions between signal and idler modes, for $nT + \tau_1 < t < (n + 1)T$. Since time is equivalent, within our approximations, to propagation length, our system can be thought of as a nonlinear crystal cut into N pieces, in each of which a, b photons are created in a down-conversion process. Between these pieces, no new photons are created by the laser beam, but the idler and signal modes (linearly) interact with each other, for instance via evanescent waves. See Fig. 9.1. By introducing the slowly varying operators $a' = e^{i\omega_a t}a$, $b' = e^{i\omega_b t}b$, the free part of the Hamiltonian (9.1) is transformed away and the Hamiltonian becomes (suppressing all primes for simplicity)

$$H(t) = \begin{cases} H_{\rm u} \equiv \Gamma(a^\dagger b^\dagger + ab) & \text{if } 0 < t < \tau_1, \\ H_{\rm s} \equiv \Omega(a^\dagger b + ab^\dagger) & \text{if } \tau_1 < t < \tau_1 + \tau_2, \end{cases} \tag{9.3}$$

with $H(t + nT) = H(t)$, yielding the equations of motion

$$\dot{a} = -i[a, H], \qquad \dot{b} = -i[b, H]. \tag{9.4}$$

9.3 Quantum and classical maps

In terms of the variables

$$x_\pm = \frac{1}{2}[(a + a^\dagger) \mp (b + b^\dagger)], \qquad p_\pm = -\frac{i}{2}[(a - a^\dagger) \mp (b - b^\dagger)], \tag{9.5}$$

[1] The latter matching condition can be relaxed at the cost of introducing a second classical pump wave of frequency $\omega'_p = \omega_a - \omega_b$ and the Hamiltonian $\Omega(a^\dagger b e^{-i\omega'_p t} + ab^\dagger e^{i\omega'_p t})$, for $\tau_1 < t < \tau_1 + \tau_2$, in (9.2). Physically, this corresponds to replacing the linear exchange between modes a and b with the nonlinear process of difference frequency generation.

which satisfy the equal-time commutation relations $[x_+, p_+] = [x_-, p_-] = i$, others $= 0$, the Hamiltonians become

$$H_{\rm u} = \frac{\Gamma}{2}[(p_+^2 - x_+^2) - (p_-^2 - x_-^2)], \qquad H_{\rm s} = \frac{\Omega}{2}[(p_+^2 + x_+^2) - (p_-^2 + x_-^2)]. \tag{9.6}$$

They describe two uncoupled oscillators, whose equations of motion are

$$\begin{cases} \dot{x}_\pm = -i[x_\pm, H_{\rm u}] = \pm\Gamma p_\pm \\ \dot{p}_\pm = -i[p_\pm, H_{\rm u}] = \pm\Gamma x_\pm \end{cases} \iff \begin{cases} \ddot{x}_\pm - \Gamma^2 x_\pm = 0 \\ \ddot{p}_\pm - \Gamma^2 p_\pm = 0 \end{cases},$$

$$\begin{cases} \dot{x}_\pm = -i[x_\pm, H_{\rm s}] = \pm\Omega p_\pm \\ \dot{p}_\pm = -i[p_\pm, H_{\rm s}] = \mp\Omega x_\pm \end{cases} \iff \begin{cases} \ddot{x}_\pm + \Omega^2 x_\pm = 0 \\ \ddot{p}_\pm + \Omega^2 p_\pm = 0 \end{cases}. \tag{9.7}$$

The first set of equations describes an *unstable* motion, the second set a *stable* one, around the equilibrium point $x = p = 0$. Notice that the motion of (x_-, p_-) is the time-reversed version of that of (x_+, p_+). This is due to the fact that the two motions are governed by Hamiltonians with opposite sign in Eq. (9.6). Henceforth, we shall concentrate on the variables (x_+, p_+) [the stability condition for (x_-, p_-) is identical]. The solutions are

$$\begin{pmatrix} x_+(\tau_1) \\ p_+(\tau_1) \end{pmatrix} = A_{\rm u} \begin{pmatrix} x_+(0) \\ p_+(0) \end{pmatrix}, \qquad A_{\rm u} \equiv \begin{pmatrix} \cosh(\Gamma\tau_1) & \sinh(\Gamma\tau_1) \\ \sinh(\Gamma\tau_1) & \cosh(\Gamma\tau_1) \end{pmatrix}, \tag{9.8}$$

for the period governed by $H_{\rm u}$ and

$$\begin{pmatrix} x_+(\tau_2) \\ p_+(\tau_2) \end{pmatrix} = A_{\rm s} \begin{pmatrix} x_+(0) \\ p_+(0) \end{pmatrix}, \qquad A_{\rm s} \equiv \begin{pmatrix} \cos(\Omega\tau_2) & \sin(\Omega\tau_2) \\ -\sin(\Omega\tau_2) & \cos(\Omega\tau_2) \end{pmatrix}, \tag{9.9}$$

for that governed by $H_{\rm s}$. Remember that $T = \tau_1 + \tau_2$ is the period of the Hamiltonian $H(t)$ in (9.3).

The dynamics engendered by (9.3) at time $t = NT$ (remember that $n = 1, \ldots, N$) yields therefore

$$\begin{pmatrix} x_+(NT) \\ p_+(NT) \end{pmatrix} = A^N \begin{pmatrix} x_+(0) \\ p_+(0) \end{pmatrix}, \qquad A \equiv A_{\rm s} A_{\rm u}. \tag{9.10}$$

These equations of motion have the same structure of a classical inverted pendulum with a vertically oscillating point of suspension (Arnold [1989], p. 121; Arnold [1992], p. 263), whose classical map is given by the product of two matrices $A_{\rm cl} \equiv A_2 A_1$, with

$$A_1 \equiv \begin{pmatrix} \cosh(k_1\tau) & k_1^{-1}\sinh(k_1\tau) \\ k_1\sinh(k_1\tau) & \cosh(k_1\tau) \end{pmatrix}, \qquad A_2 \equiv \begin{pmatrix} \cos(k_2\tau) & k_2^{-1}\sin(k_2\tau) \\ -k_2\sin(k_2\tau) & \cos(k_2\tau) \end{pmatrix}, \tag{9.11}$$

where the parameters k_1 and k_2 are subject to the physical condition $k_1 > k_2 > 0$. Observe that our system has more freedoms: τ_1 and τ_2 are in general different and the parameters Ω and Γ do not have to obey any additional constraint.

9.4 Stability vs Zeno

The global motion is stable or unstable, according to the value of $|{\rm Tr}A| \lesseqgtr 2$ (Arnold [1989], p. 121; Arnold [1992], p. 263). The stability condition $|{\rm Tr}A| < 2$ reads

$$|{\rm Tr}A|/2 = |\cos(\Omega\tau_2)\cosh(\Gamma\tau_1)| < 1. \tag{9.12}$$

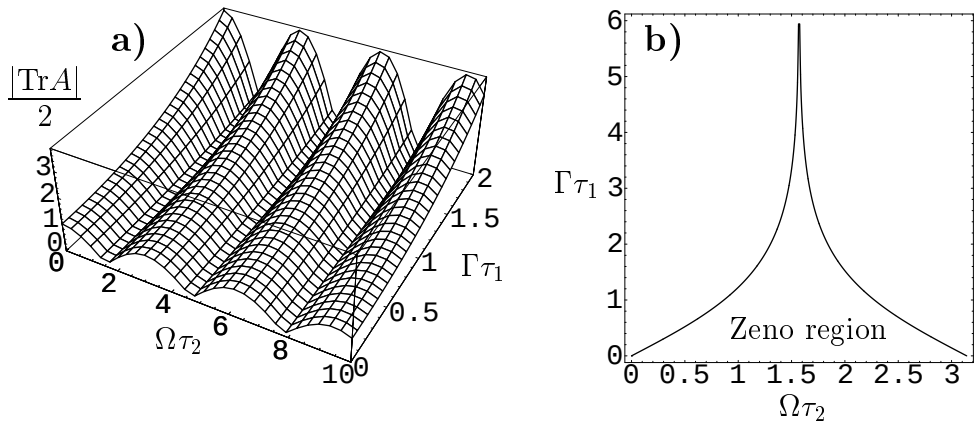

Figure 9.2: Stability condition (9.12) in parameter space. a) $|\mathrm{Tr}A|/2$ vs $\Omega\tau_2$ and $\Gamma\tau_1$; b) Stability (Zeno) region.

This relation is of general validity and holds for any value of the parameters Ω, Γ and τ_i. The value of $|\mathrm{Tr}A|/2$ is shown in Fig. 9.2a). A small-τ expansion (the physically relevant regime: see final discussion) yields

$$1 - (\Omega^2\tau_2^2 - \Gamma^2\tau_1^2)/2 + O(\tau^4) < 1, \tag{9.13}$$

so that the system is stable for $\Omega\tau_2 > \Gamma\tau_1$ when $\tau_2 \to 0$.

It is interesting to discuss the stability condition just obtained for the (x, p) variables in terms of the number of down-converted photons. To this end, let us look at some limiting cases. [Needless to say, the analysis could be done from the outset in terms of n_a and n_b and would yield an identical stability condition (9.12).] When $\Omega = 0$ in (9.3) and following equations, only the down-conversion process takes place and both $n_a = a^\dagger a$ and $n_b = b^\dagger b$ grow exponentially with time. There is an exponential energy transfer from the pump to the a, b modes. On the other hand, if $\Gamma = 0$ and the system is prepared in any initial state (except vacuum, whose evolution is trivial), n_a and n_b oscillate in such a way that their sum is conserved (this is due to the property $[n_a + n_b, H_\mathrm{s}] = 0$). If both Ω and Γ are nonvanishing, these two opposite tendencies (exponential photon production and bounded oscillations) compete in an interesting way. When $\Gamma\tau_1 > \Omega\tau_2$, in the limit $\tau_1 \to 0$, the exponential photon production dominates and there is no way of halting (or even hindering) this process: the (external) pump transmits energy to the a, b modes. In terms of the (x, p) variables, the stability condition (9.13) *cannot* be fulfilled and the oscillator variables move exponentially away from the origin. The opposite situation $\Omega\tau_2 > \Gamma\tau_1$ is very interesting and displays some quite nontrivial aspects: The motion becomes stable and the pump does not transmit energy to the a, b modes anymore (the two modes oscillate).

For arbitrary values of all parameters, the action of H_s can be framed in our theoretical scheme as a measurement, in the following sense[2]: the a mode performs an observation on the b mode and *vice versa*, the photonic states get entangled and information on one mode is encoded in the state of the other one. For example, the condition $\Omega\tau_2 = \pi/2$ yields an "ideal measurement" of one mode on the other one, for in such a case the states $|1_a, 0_b\rangle \leftrightarrow |0_a, 1_b\rangle$ evolve into each other. From this viewpoint, the stabilization regime just investigated is a

[2]It is interesting to notice that for infinitesimal τ_1, τ_2 the effective Hamiltonian of the system becomes just the sum of the unstable and stable Hamiltonians (9.3). Such Hamiltonians are well known in the field of quantum nondemolition measurements: (Milburn, Lane and Walls [1983]).

manifestation of QZE, in that the measurements essentially affect and change the original dynamics. In fact, if one considers $\Omega\tau_2$ as the "strength" of the measurement, by increasing (at fixed $\Omega\tau_2$) the frequency of measurements, i.e. by letting $\tau_1 \to 0$, the system moves down along a vertical line in Fig. 9.2b) and enters a region of stability (Zeno region) from a region of instability. (Notice that it is not necessary to consider the $\tau_1 = 0$ limit ("continuous measurement") in order to stabilize the dynamics; there is a threshold, given by the curve in Fig. 9.2 b), at which stability and instability interchange.) Analogously, at fixed $\Gamma\tau_1$, by moving along a horizontal line $\Omega\tau_2 \to \pi/2$ the system enters a region of stability because the measurement becomes more "effective:" indeed, as emphasized before, $\Omega\tau_2 = \pi/2$ is a π-pulse condition and leads to a very effective measurement of one mode on the other one. It is worth stressing that even an instantaneous measurement (projection) can be obtained by letting $\tau_2 \to 0$, while keeping $\Omega\tau_2$ finite (the so-called impulse approximation in quantum mechanics), and in this case our system yields the standard formulation of QZE.

A final comment is in order. Notice that, as we have seen in the previous chapter, a quantum Zeno effect is obtained when the down-conversion behavior is still explosive and is manifested in the reduction of the down-conversion rate. On the other hand, when the coupling with the measuring apparatus is increased enough, it can happen that the dynamics becomes oscillatory, and this strictly corresponds to the classical stabilization we found here. In other words, the real Zeno region of the system is larger and contains the region shown in Fig. 9.2 b). Therefore we can say that, rather surprisingly, the core of the Zeno region consists of a region of operator stability with a purely classical origin. It would be very interesting to understand how general is this surprising property.

9.5 Single-mode version

It is interesting (and convenient from an experimental perspective) to consider a single-mode version of the Hamiltonian (9.3), in which the down-conversion process is replaced by a subharmonic generation process (degenerated parametric down conversion). The single-mode effective Hamiltonian reads

$$H(t) = \omega a^\dagger a + H_{\rm int}(t), \tag{9.14}$$

where the interaction Hamiltonians describing the unstable and stable part of the device are

$$H_{\rm int} = \begin{cases} (\Gamma/2)(a^{\dagger 2}e^{-2i\omega t} + a^2 e^{2i\omega t}) & \text{if } 0 < t < \tau_1, \\ (\Omega/2)(a^\dagger a + a a^\dagger) & \text{if } \tau_1 < t < \tau_1 + \tau_2, \end{cases} \tag{9.15}$$

respectively and $H_{\rm int}(t+nT) = H_{\rm int}(t)$. By introducing the slowly varying operator $a' = e^{i\omega_a t}a$, the free part of the Hamiltonian (9.14) is transformed away and the Hamiltonian becomes (suppressing again all primes)

$$H(t) = \begin{cases} H_{\rm u} \equiv (\Gamma/2)(a^{\dagger 2} + a^2) & \text{if } 0 < t < \tau_1, \\ H_{\rm s} \equiv (\Omega/2)(a^\dagger a + a a^\dagger) & \text{if } \tau_1 < t < \tau_1 + \tau_2, \end{cases} \tag{9.16}$$

under which the equation of motion $\dot{a} = -i[a, H]$ follows.

In terms of the variables $x = (a + a^\dagger)/\sqrt{2}, p = -i(a - a^\dagger)/\sqrt{2}$ the Hamiltonians read

$$H_{\rm u} = \frac{\Gamma}{2}(x^2 - p^2), \quad H_{\rm s} = \frac{\Omega}{2}(x^2 + p^2). \tag{9.17}$$

These Hamiltonians are identical to the two-mode versions (9.6) describing the decoupled mode (x_+, p_+), apart from the substitution $\Gamma \to -\Gamma$. Hence, the stability condition is given again by Eq. (9.12), which is even in Γ. Also in this case one can talk of quantum Zeno, but the "measurement" is performed by the single mode on itself.

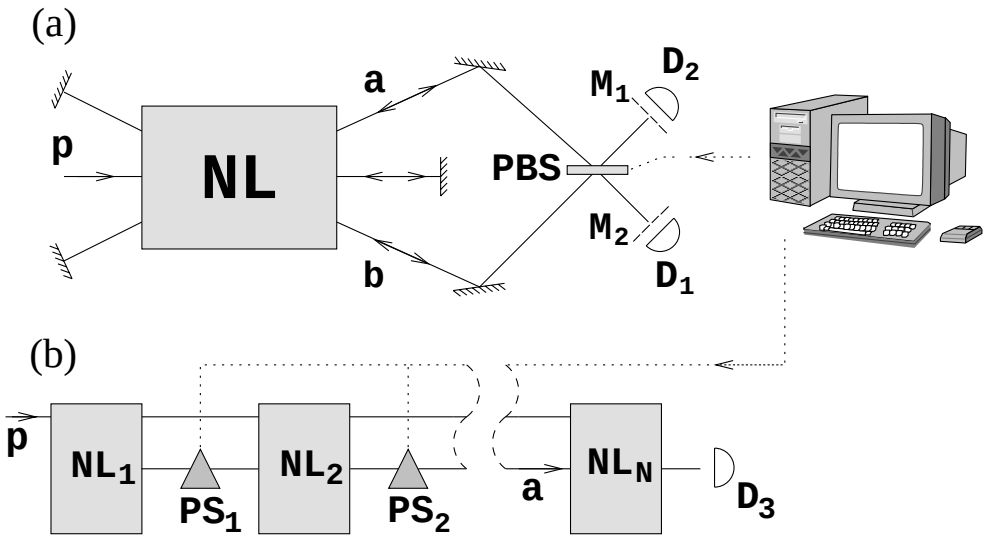

Figure 9.3: Experimental setup. (a) Possible experimental realization of the Hamiltonian (9.1)-(9.2). NL, nonlinear crystal; $\mathrm{M}_i, (i = 1, 2)$, semitransparent mirrors; D_i, detectors; PBS, polarizing beamsplitter. (b) Possible experimental realization of the Hamiltonian (9.14)-(9.15). $\mathrm{NL}_i (i = 1, \ldots, N)$, nonlinear crystals; PS_i, phase shifters; D_3, detector. The dotted lines indicate which elements are computer controllable.

9.6 Experimental setup

It is interesting to discuss a possible experimental realization of the two situations considered in this Letter. The experimental arrangement sketched in Fig. 9.3(a) corresponds to the two-mode (nondegenerate) case, whereas that sketched in Fig. 9.3(b) to the single-mode (degenerate) case. In Fig. 9.3(a) a type II down-conversion process generates two orthogonally polarized beams of down-converted light of the same frequency. The two beams are mixed using a polarizing beamsplitter PBS. The stable part of the evolution of the system is realized by two successive passes of the beams through the beamsplitter. Its reflection coefficient, and hence $\Omega\tau_2$, is adjusted by rotating it. Mirrors and semitransparent mirrors keep sending the beams through the crystal many times. A successful stabilization of the unstable system is manifested in the decrease of the rate of photon registrations at detectors D_1, D_2 at a certain position of the beamsplitter PBS. A different setup is sketched in Fig. 9.3(b), where N processes of subharmonic generation take place in N nonlinear crystals with controlled phase shifters in between them. For appropriately chosen phase shifts $\theta_i = (\Omega\tau_2 + C_i) \bmod 2\pi$, where C_i are $N-1$ phase shifts intrinsic to the actual experimental arrangement (given by distances between crystals, etc.), the generation of the subharmonic wave is suppressed.

In order to give a reasonable estimate of the value of the coupling constant Γ, consider that, due to the correspondence principle, the gain of classical and quantum parametric amplifiers must be the same; therefore one can use the well-known classical formula for the nonlinear coupling parameter Γ_c governing the space evolution inside the nonlinear medium, which in MKS units reads

$$\Gamma_c^2 = \frac{\eta^3}{2}\chi(2)^2\omega_a\omega_b I_p. \tag{9.18}$$

Here η is the impedance of the medium, $\chi(2)$ is the second-order susceptibility, ω_a and ω_b are the frequencies of modes a and b, respectively, and I_p is the intensity of the pump beam. The following numerical values could be typical for a performed experiment: $\eta \approx 220\Omega$, $\chi(2) \approx$

2×10^{-23} CV^{-2}, $\omega_a = \omega_b \approx 3 \times 10^{15}\mathrm{s}^{-1}$ and $I_p \approx 10^5 \mathrm{Wm}^{-2}$. Hence the nonlinear coupling parameter is of the order of $\Gamma_c \approx 0.1\mathrm{m}^{-1}$. Reasonable lengths of nonlinear crystals are of the order of $l \approx 10^{-2}$m, so that the dimensionless product of interest can be estimated to be about

$$\Gamma\tau_1 = \Gamma_c l \approx 0.001. \tag{9.19}$$

This means that the down-converted beam(s) ought to pass the nonlinear region many times in order to show an explosive increase of its (their) intensity(ies). This could be achieved by placing the nonlinear crystal in a resonator as shown in Fig. 9.3(a). However, in order to observe a significant change of the dynamics of the process in question due to the performed stabilization, a few passes might already turn out to be sufficient.

In conclusion, we have discussed a striking quantum-optical analogue of a well-known classical unstable system. By interspersing the nonlinear regions with regions of suitably chosen linear evolution, the global dynamics of our system can become stable and the generation of down-converted light can be strongly suppressed. This is a manifestation of the quantum Zeno effect: by increasing the strength of the observation performed by the a mode on the b mode and *vice versa* the evolution is frozen and the system tends to remain in its initial state. As all Zeno effects, this phenomenon is somewhat counterintuitive: in the setups in Fig. 9.3, even though the beams are forced to go through the crystal many times, no exponential photon production takes place. The experiment seems feasible and its realization would illustrate an interesting aspect related to the stabilization of a seemingly explosive behavior. Moreover, from the theoretical point of view, we found that, at the least in this particular model, the core of the quantum Zeno region in parameter space is of purely classical origin. This is another unexpected feature of the Zeno effects.

Chapter 10

The role of the form factor

10.1 Introduction

We consider the QZE and IZE for *bona fide* unstable systems. This is a more complicated problem, because it requires the use of quantum field theoretical techniques. The study of a solvable (but significant) example will enable us to better understand the role played by the Weisskopf-Wigner approximation introduced in Sec. 4.6.3. Moreover, we shall see that for an unstable system the form factors of the interaction play a fundamental role and determine the occurrence of a Zeno or an inverse Zeno regime, depending of the physical parameters describing the system. We finally investigate the intriguing possibility that the lifetime of an unstable quantum system be modified by the presence of a very intense electromagnetic field. We shall look at the temporal behavior of a three-level system (such as an atom or a molecule) shined by an intense laser field (Pascazio and Facchi [1999]; Facchi and Pascazio [2000a]) and see that, for physically sensible values of the intensity of the laser, the decay can be *enhanced*. This will be interpreted as an inverse quantum Zeno effect.

10.2 Zeno–inverse Zeno transition

We will now study the Zeno–inverse Zeno transition in greater detail, by making use of a quantum field theoretical framework, and discuss the primary role played by the form factors of the interaction. The reader should refer to the discussion of Sec. 7.2.3, where we introduced the effective decay rate

$$\gamma_{\rm eff}(\tau) \equiv -\frac{1}{\tau}\log P(\tau) = -\frac{2}{\tau}\log|\mathcal{A}(\tau)| = -\frac{2}{\tau}{\rm Re}\Big[\log\mathcal{A}(\tau)\Big], \tag{10.1}$$

which is a linear function of τ for sufficiently small values of τ (inside the Zeno region)

$$\gamma_{\rm eff}(\tau) \sim \frac{\tau}{\tau_{\rm Z}^2}, \qquad \text{for} \quad \tau \lesssim 1/\Lambda, \tag{10.2}$$

with $\tau_{\rm Z}^{-2} \equiv \langle a|H_{\rm int}^2|a\rangle$, and becomes, with good approximation, a constant equal to the natural decay rate at intermediate times

$$\gamma_{\rm eff}(\tau) \simeq \gamma \qquad \text{for} \quad \tau \gg 1/\Lambda. \tag{10.3}$$

The transition between Zeno and inverse Zeno occurs at the geometrical intersection τ^* between the curves $P(t)$ and $e^{-\gamma t}$, solution of the equation

$$\gamma_{\rm eff}(\tau^*) = \gamma\ , \tag{10.4}$$

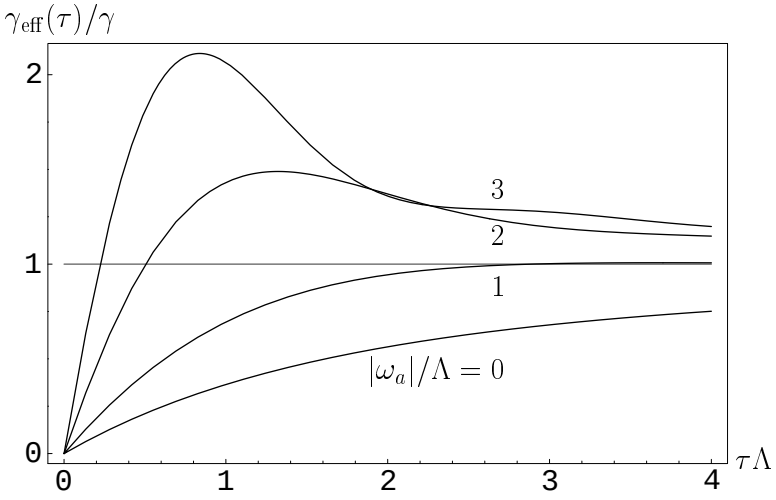

Figure 10.1: Effective decay rate $\gamma_{\rm eff}(\tau)$ for the two-pole model (10.5), for $\lambda = 0.1$ and different values of the ratio $|\omega_a|/\Lambda$ (indicated). The horizontal line shows the "natural" decay rate γ: its intersection with $\gamma_{\rm eff}(\tau)$ yields the solution τ^* of Eq. (10.4). The asymptotic value of all curves is γ, as expected. A Zeno (inverse Zeno) effect is obtained for $\tau < \tau^*$ ($\tau > \tau^*$). Notice the presence of a linear region for small values of τ and observe that τ^* does not belong to such linear region as the ratio $|\omega_a|/\Lambda$ decreases. Above a certain threshold, given by Eq. (10.7) in the weak coupling limit of the model (and in general by the condition $\mathcal{Z} = 1$), Eq. (10.4) has no finite solutions: only a Zeno effect is realizable in such a case.

as shown in Fig. 7.3.

Consider for example the two-pole model studied in detail in Sec. 5.3, whose survival amplitude is given by Eq. (5.19)

$$\mathcal{A}(t) = \frac{\omega_a + \Delta + i(\Lambda - \gamma/2)}{\omega_a + 2\Delta + i(\Lambda - \gamma)} e^{-i(\omega_a + \Delta)t} e^{-\gamma t/2} + \frac{\Delta - i\gamma/2}{\omega_a + 2\Delta + i(\Lambda - \gamma)} e^{i\Delta t} e^{-(\Lambda - \gamma/2)t}, \quad (10.5)$$

with Δ and γ given by Eq. (5.17). By plugging (10.5) into (10.1) one obtains the effective decay rate, whose behavior is displayed in Fig. 10.1 for different values of the ratio $|\omega_a|/\Lambda$. These curves show that for large values of $|\omega_a|$ (in units Λ) there is indeed a transition from a Zeno to an inverse Zeno (Heraclitus) behavior: such a transition occurs at $\tau = \tau^*$, solution of Eq. (10.4). However, for small values of $|\omega_a|$, such a solution ceases to exist.

The determination of the critical value of $|\omega_a|$ for which the Zeno–inverse Zeno transition ceases to take place discloses an interesting aspect of this issue. The problem can be discussed in general, but for the sake of simplicity we consider the weak coupling limit (small λ) considered in Eqs. (5.24)-(5.25). According to the geometrical theorem proved in Sec. 7.2.3, a sufficient condition for the system to exhibit an Zeno–inverse Zeno transition is $\mathcal{Z} < 1$, with $\mathcal{Z}$ the wave function renormalization. In our case, by making use of Eq. (5.25), this condition reads

$$\mathcal{Z} = |1 - \mathcal{R}|^2 = 1 - 2\frac{\lambda^2}{\omega_a^2 + \Lambda^2} \mathrm{Re}\left[\frac{\omega_0 - i\Lambda}{\omega_a + i\Lambda}\right] + \mathrm{O}(\lambda^4) = 1 - 2\frac{\lambda^2}{\omega_a^2 + \Lambda^2}\frac{\omega_a^2 - \Lambda^2}{\omega_a^2 + \Lambda^2} + \mathrm{O}(\lambda^4) < 1, \quad (10.6)$$

namely

$$\omega_a^2 > \Lambda^2 + \mathrm{O}(\lambda^2). \quad (10.7)$$

The meaning of this relation is the following: a sufficient condition to obtain a Zeno–inverse Zeno transition is that the energy of the decaying state be placed asymetrically with respect

to the peak of the form factor (bandwidth) (see Fig. 5.1). If, on the other hand, $\omega_a \simeq 0$ (center of the bandwidth), no transition time τ^* exists (see Fig. 10.1) and only a QZE is possible: this is the case analyzed in Fig. 7.4(a).

There is more: Equation (10.5) yields a time scale. Indeed, from the definitions of the quantities in (5.17) one gets $\gamma/2 < \Lambda - \gamma/2$, so that the second exponential in (10.5) vanishes more quickly than the first one [1]. If the coupling is weak, since $\gamma = \mathrm{O}(\lambda^2)$, the second term is very rapidly damped so that, after a short initial quadratic region of duration Λ^{-1}, the decay becomes purely exponential with decay rate γ. For $\tau \lesssim 1/\Lambda$ (which is, by definition, the extension of the quadratic Zeno region), we can use the linear approximation (10.2). When it applies up to the intersection (i.e., $|\omega_a| \gg \Lambda$) one gets

$$\tau^* \simeq \gamma\tau_{\mathrm{Z}}^2. \tag{10.8}$$

When ω_a gets closer to the peak of the form factor, the linear approximation does not hold and the r.h.s. of the above expression yields a lower bound to the transition time τ^*. In this case the solution τ^* of the equation (10.4) becomes larger than the approximation (10.8), eventually going to infinity when the condition (10.7) is no longer valid. In such a case, only a QZE is possible. The quantity $\gamma\tau_{\mathrm{Z}}^2$ is also relevant in different contexts and has been called "jump time" by Schulman [1998].

The conclusions obtained for the two-pole model (10.5) are of general validity. In general, in the Lee Hamiltonian (5.9), for any $g(\omega)$, we assume that $\omega_a > \omega_g$, in order to get an unstable system. The matrix elements of the interaction Hamiltonian depend of course on the physical model considered. However, for physically relevant situations, the interaction smoothly vanishes for small values of $\omega - \omega_g$ and quickly drops to zero for $\omega > \Lambda$, a frequency cutoff related to the size of the decaying system and the characteristics of the environment. This is true both for cavities, as well as for typical EM decay processes in vacuum, where the bandwidth $\Lambda \simeq 10^{14} - 10^{18}\mathrm{s}^{-1}$ is given by an inverse characteristic length (say, of the order of Bohr radius) and is much larger than the natural decay rate $\gamma \simeq 10^7 - 10^9\mathrm{s}^{-1}$, as we have seen in Sec. 5.5. (See also Fig. 5.2.)

For roughly bell-shaped form factors all the conclusions drawn for the Lorentzian model remain valid. The main role is played by the ratio ω_{ag}/Λ, with $\omega_{ag} = \omega_a - \omega_g$ the available energy. In general, the asymmetry condition $\omega_{ag} < \Lambda$ is satisfied if the energy ω_a of the unstable state is sufficiently close to the threshold. In fact, from the definition of the Zeno time τ_{Z} one has

$$\frac{1}{\tau_{\mathrm{Z}}^2} = \int d\omega\; g^2(\omega) = g^2(\bar{\omega})\Lambda, \tag{10.9}$$

where $\bar{\omega}$ is defined by this relation and is of order $\omega_{\max}$, the energy at which $g(\omega)$ takes the maximum value. For ω_a sufficiently close to the threshold ω_g one has $g(\bar{\omega}) \gg g(\omega_a)$, the time scale $\gamma\tau_{\mathrm{Z}}^2$ is well within the short-time regime, namely

$$\gamma\tau_{\mathrm{Z}}^2 = \frac{2\pi g^2(\omega_a)}{g^2(\bar{\omega})\Lambda} \ll \frac{1}{\Lambda}, \tag{10.10}$$

where the Fermi golden rule $\gamma = 2\pi g^2(\omega_a)$ has been used, and therefore the estimate (10.8) is valid.

On the other hand, for a system such that $\omega_{ag} \simeq \Lambda$ (or, better, $\omega_a \simeq$ center of the bandwidth), τ^* does not necessarily exist and usually *only* a Zeno effect can occur. In this context, it is useful and interesting to remember that the Lorentzian form factor (5.13) yields, in the

[1] The two time scales become comparable only in the strong coupling regime: $\gamma \to \Lambda$ as $\lambda \to \infty$.

limit $g^2(\omega) = \lambda^2\delta(\omega - \omega_a)$, the physics of a two level system. This is also true in the general case, for a roughly symmetric form factor, when the bandwidth $\Lambda \to 0$. In such a case, if $\omega_a = 0$ (initial state energy at the center of the form factor), the survival probability oscillates between 1 and 0 and only a QZE is possible. On the other hand, if $\omega_a \neq 0$ (initial state energy strongly asymmetric with respect to the form factor of "width" $\Lambda = 0$) the initial state never decays completely. By measuring the system, the survival probability will vanish exponentially, independently of the strength of observation, whence only an IZE is possible. This is what we found for a down-conversion process with a sufficiently large phase mismatch at the end of Sec. 8.3.

If one consider the large bandwidth limit of the two-pole model, which is equivalent to a Weisskopf-Wigner approximation, the propagator (5.27) has only a simple pole and the survival probability (5.28) is purely exponential. Therefore measurements cannot modify the free behavior. Indeed, the conditions for occurrence of a Zeno effect are always ascribable to the presence of an initial non-exponential behavior of the survival probability, which is caused by a propagator exhibiting a richer structure than a simple pole in the complex energy plane.

Some final comments are in order. The present analysis has been performed in terms of instantaneous measurements, according to the Copenhagen prescription. Our starting point was indeed Eq. (7.22). We can consider, instead, a continuous measurement process. This is accomplished, for instance, by adding to (5.9) the following Hamiltonian

$$H_{\rm meas}(\Gamma) = \sqrt{\frac{\Gamma}{2\pi}} \int d\omega d\omega' \, (|\omega\rangle\langle\omega,\omega'| + |\omega,\omega'\rangle\langle\omega|) + \int d\omega' \, |\omega'\rangle\langle\omega'| : \tag{10.11}$$

as soon as a photon is emitted, it is coupled to another boson of frequency ω' (notice that the coupling has no form factor). By following a reasoning identical to that of Section 7.4.2, one can show that the dynamics of the Hamitonian (5.9) and (10.11), in the relevant subspace, is generated by

$$H = \omega_a|a\rangle\langle a| + \int d\omega \, (\omega - i\Gamma/2)|\omega\rangle\langle\omega| + \int d\omega \, g(\omega)(|a\rangle\langle\omega| + |\omega\rangle\langle a|), \tag{10.12}$$

and an effective continuous observation on the system is obtained by increasing Γ. Indeed it is easy to see that the only effect due to Γ in Eq. (10.12) is the substitution of $\Sigma_a(E)$ with $\Sigma_a(E + i\Gamma/2)$ in Eq. (5.6), namely,

$$G_a(E) = \frac{1}{E - \omega_a - \Sigma_a(E + i\Gamma/2)}. \tag{10.13}$$

For large values of Γ, i.e., for very quick response of the apparatus, the self-energy function (5.11) has the asymptotic behavior

$$\Sigma_a\left(E + i\frac{\Gamma}{2}\right) \sim -i\frac{2}{\Gamma}\int d\omega \, g^2(\omega) = -i\frac{2}{\Gamma\tau_{\rm Z}^2}, \quad \text{for} \quad \Gamma \to \infty. \tag{10.14}$$

[Notice that $\Gamma \to \infty$ in (10.14) means $\Gamma \gg \Lambda$, the frequency cutoff of the form factor.] In this case the propagator (10.13) reads

$$G_a(E) \sim \frac{1}{E - \omega_a + i\gamma_{\rm eff}(\Gamma)/2}, \qquad \text{for} \quad \Gamma \to \infty \tag{10.15}$$

and the survival probability decays with the effective exponential rate (valid for $\Gamma \gg \Lambda$)

$$\gamma_{\rm eff}(\Gamma) = \frac{4}{\tau_{\rm Z}^2\Gamma}. \tag{10.16}$$

The effective rate (10.16) is the same result (7.65) we found for the particular model considered in Sec. 7.4.2. We see that it is a general result. The equivalence (7.66) is therefore of general validity. More to this, we have here a scale for the validity of the linear approximation (10.2) for $\gamma_{\rm eff}$: the linear term in the asymptotic expansion (10.14) approximates well the self-energy function only for values of Γ that are larger than the bandwidth Λ. For smaller values of Γ one has to take into account the nonlinearities arising from the successive terms in the expansion.

Note that the flat-band case (5.27), yielding a purely exponential decay, is unaffected also by the continuous measurement. Indeed in that case $\Sigma_a(E) = -i\gamma/2$ is a constant independent of E, whence $\Sigma_a(E + i\Gamma/2) = \Sigma_a(E)$ is independent of Γ. The same happens if one considers the Weisskopf-Wigner approximation (4.84): in this case one neglects the whole structure of the propagator in the complex energy plane and retains only the dominant pole near the real axis. This yields, as we have seen, a self-energy function which does not depends on energy and a purely exponential decay (without any deviations), that cannot be modified by any observations.

Notice that the very existence of a QZE is related to the existence of an initial quadratic behavior of the survival probability, i.e. to a finite value of $\tau_{\rm Z}$. As Eq. (5.38) shows, this is related to the convergence of the integral of the form factor. In general, in a quantum field theoretical framework, the Zeno time $\tau_{\rm Z}$ (the inverse of the second moment of the Hamiltonian) cannot be defined, because it vanishes for pointlike particles. It becomes necessary to introduce form factors and cutoffs and use more sophisticated techniques. These problems will not be discussed here. See Bernardini, Maiani and Testa [1993]; Facchi and Pascazio [1998]; Joichi, Matsumoto and Yoshimura [1998]; Maiani and Testa [1998]; Alvarez-Estrada and Sánchez-Gómez [1999] and Facchi and Pascazio [1999b].

10.3 Three-level system in a laser field

We shall now investigate a realistic situation in which a continuous observation performed by a laser field leads to an inverse Zeno effect, in a way very similar to that outlined in Sec. 7.4. We shall look at the temporal behavior of a three-level system (such as an atom or a molecule), where level $|1\rangle$ is the ground state and levels $|2\rangle$, $|3\rangle$ are two excited states. (See fig. 10.2.) The system is initially prepared in level $|2\rangle$ and if it follows its natural evolution, it will decay to level $|1\rangle$. The decay will be (approximately) exponential and characterized by a certain lifetime, that can be calculated from the Fermi Golden Rule. But if one shines on the system an intense laser field, tuned at the transition frequency 3-1, the evolution can be different. This problem was investigated by Mihokova, Pascazio and Schulman [1997], who found that the lifetime of the initial state depends on the intensity of the laser field. We shall see that for physically sensible values of the intensity of the laser, the decay is *enhanced*. This can be viewed as an inverse quantum Zeno effect (Facchi and Pascazio [2000a]; Pascazio and Facchi [1999]). An important role will be played by the form factor of the interaction Hamiltonian.

10.3.1 The system

We consider the Hamiltonian ($\hbar = c = 1$)

$$\begin{aligned} H &= H_0 + H_{\rm int} \\ &= \omega_0 |2\rangle\langle 2| + \Omega_0 |3\rangle\langle 3| + \sum_{\boldsymbol{k},\lambda} \omega_k a^\dagger_{\boldsymbol{k}\lambda} a_{\boldsymbol{k}\lambda} \\ &\quad + \sum_{\boldsymbol{k},\lambda} \Big(\phi_{\boldsymbol{k}\lambda} a^\dagger_{\boldsymbol{k}\lambda} |1\rangle\langle 2| + \phi^*_{\boldsymbol{k}\lambda} a_{\boldsymbol{k}\lambda} |2\rangle\langle 1| \Big) + \sum_{\boldsymbol{k},\lambda} \Big(\Phi_{\boldsymbol{k}\lambda} a^\dagger_{\boldsymbol{k}\lambda} |1\rangle\langle 3| + \Phi^*_{\boldsymbol{k}\lambda} a_{\boldsymbol{k}\lambda} |3\rangle\langle 1| \Big) \end{aligned} \tag{10.17}$$

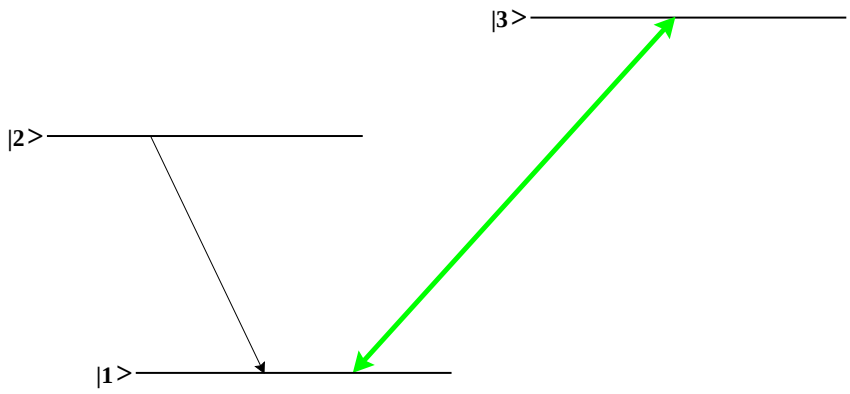

Figure 10.2: Level configuration

where the first two terms are the free Hamiltonian of the 3-level atom (whose states $|i\rangle$ ($i = 1, 2, 3$) have energies $E_1 = 0$, $\omega_0 = E_2 - E_1 > 0$, $\Omega_0 = E_3 - E_1 > 0$), the third term is the free Hamiltonian of the EM field and the last two terms describe the $1 \leftrightarrow 2$ and $1 \leftrightarrow 3$ transitions in the rotating wave approximation, respectively. (See Fig. 10.2.) States $|2\rangle$ and $|3\rangle$ are chosen so that no transition between them is possible (e.g., because of selection rules). The matrix elements of the interaction Hamiltonian read

$$\phi_{\boldsymbol{k}\lambda} = \frac{e}{\sqrt{2\epsilon_0 V\omega}} \int d^3x\, e^{-i\boldsymbol{k}\cdot\boldsymbol{x}} \boldsymbol{\epsilon}^*_{\boldsymbol{k}\lambda} \cdot \boldsymbol{j}_{12}(\boldsymbol{x}), \qquad \Phi_{\boldsymbol{k}\lambda} = \frac{e}{\sqrt{2\epsilon_0 V\omega}} \int d^3x\, e^{-i\boldsymbol{k}\cdot\boldsymbol{x}} \boldsymbol{\epsilon}^*_{\boldsymbol{k}\lambda} \cdot \boldsymbol{j}_{13}(\boldsymbol{x}), \tag{10.18}$$

where $-e$ is the electron charge, ϵ_0 the vacuum permittivity, V the volume of the box, $\omega = |\boldsymbol{k}|$, $\boldsymbol{\epsilon}_{\boldsymbol{k}\lambda}$ the photon polarization and $\boldsymbol{j}_{\rm fi}$ the transition current of the radiating system. For example, in the case of an electron in an external field, we have $\boldsymbol{j}_{\rm fi} = \psi^\dagger_{\rm f}\boldsymbol{\alpha}\psi_{\rm i}$ where $\psi_{\rm i}$ and $\psi_{\rm f}$ are the wavefunctions of the initial and final state, respectively, and $\boldsymbol{\alpha}$ is the vector of Dirac matrices. For the sake of generality we are using relativistic matrix elements, but our analysis can also be performed with nonrelativistic ones $\boldsymbol{j}_{\rm fi} = \psi^*_{\rm f}\boldsymbol{p}\psi_{\rm i}/m_e$, where $\boldsymbol{p}/m_e$ is the electron velocity.

We shall concentrate our attention on a 3-level system bathed in a continuous laser beam, whose photons have momentum $\boldsymbol{k}_0$ ($|\boldsymbol{k}_0| = \Omega_0$) and polarization λ_0, and assume, throughout this paper, that

$$\phi_{\boldsymbol{k}_0\lambda_0} = 0, \tag{10.19}$$

i.e., the laser does not interact with state $|2\rangle$. The laser is in a coherent state $|\alpha_0\rangle$ with a very large average number $\bar{N}_0 = |\alpha_0|^2$ of $\boldsymbol{k}_0$-photons in volume V [we will eventually consider the thermodynamical limit; see Eq. (10.37)]. In the picture defined by the unitary operator

$$T(t) = \exp\left(\alpha^*_0 e^{i\Omega_0 t} a_{\boldsymbol{k}_0\lambda_0} - \alpha_0 e^{-i\Omega_0 t} a^\dagger_{\boldsymbol{k}_0\lambda_0}\right), \tag{10.20}$$

the $\boldsymbol{k}_0$ mode is initially in the vacuum state (Mollow [1975]; Cohen-Tannoudji, Dupont-Roc and Grynberg [1998]) and the Hamiltonian becomes ($\bar{N}_0 \gg 1$)

$$\begin{aligned} H \;\simeq\; & \omega_0|2\rangle\langle 2| + \Omega_0|3\rangle\langle 3| + \sum_{\boldsymbol{k},\lambda} \omega_k a^\dagger_{\boldsymbol{k}\lambda} a_{\boldsymbol{k}\lambda} + {\sum_{\boldsymbol{k},\lambda}}' \left(\phi_{\boldsymbol{k}\lambda} a^\dagger_{\boldsymbol{k}\lambda}|1\rangle\langle 2| + \phi^*_{\boldsymbol{k}\lambda} a_{\boldsymbol{k}\lambda}|2\rangle\langle 1|\right) \\ & + \left(\Phi_{\boldsymbol{k}_0\lambda_0}\alpha^*_0 e^{i\Omega_0 t}|1\rangle\langle 3| + \Phi^*_{\boldsymbol{k}_0\lambda_0}\alpha_0 e^{-i\Omega_0 t}|3\rangle\langle 1|\right), \end{aligned} \tag{10.21}$$

where a prime means that the summation does not include $(\boldsymbol{k}_0, \lambda_0)$ [due to hypothesis (10.19)]. In the above equations and henceforth, the vector $|i; n_{\boldsymbol{k}\lambda}\rangle$ represents a state in which the atom is in state $|i\rangle$ and the electromagnetic field in a state with $n_{\boldsymbol{k}\lambda}$ $(\boldsymbol{k}, \lambda)$-photons. We shall analyze

the behavior of the system under the action of a continuous laser beam of high intensity. Under these conditions, level configurations similar to that of Fig. 10.2 give rise to the phenomenon of induced transparency (Tewari and Agarwal [1986]; Harris, Field and Imamoğlu [1990]; Boller, Imamoğlu and Harris [1991]; Field, Hahn and Harris [1991]; Zhu, Narducci and Scully [1995]; Zhu and Scully [1996]; Huang, Zhu, Zubairy and Scully [1996]), for laser beams of sufficiently high intensities. Our interest, however, will be focused on *unstable* initial states: we shall study the temporal behavior of level $|2\rangle$ when the system is shined by a continuous laser of intensity comparable to those used to obtain induced transparency.

Note that the excitation number operator

$$\mathcal{N} = |2\rangle\langle 2| + {\sum_{\boldsymbol{k},\lambda}}' a^\dagger_{\boldsymbol{k}\lambda} a_{\boldsymbol{k}\lambda}, \tag{10.22}$$

commutes with the Hamiltonian

$$[H, \mathcal{N}] = 0. \tag{10.23}$$

As we have seen Sec. 5.5.2, the Hilbert space splits into Tamm-Dancoff sectors that are invariant under the action of the Hamiltonian: in our case, the system evolves in the subspace labeled by the eigenvalue $\mathcal{N} = 1$ and the analysis can be restricted to this sector.

10.3.2 Schrödinger equation and temporal evolution

We will study the temporal evolution by solving the time-dependent Schrödinger equation

$$i\frac{d}{dt}|\psi(t)\rangle = H(t)|\psi(t)\rangle, \tag{10.24}$$

where the states of the total system in the sector $\mathcal{N} = 1$ read

$$|\psi(t)\rangle = \mathcal{A}(t)|2;0\rangle + {\sum_{\boldsymbol{k},\lambda}}' y_{\boldsymbol{k}\lambda}(t)|1;1_{\boldsymbol{k}\lambda}\rangle + {\sum_{\boldsymbol{k},\lambda}}' z_{\boldsymbol{k}\lambda}(t)e^{-i\Omega_0 t}|3;1_{\boldsymbol{k}\lambda}\rangle \tag{10.25}$$

and are normalized:

$$\langle\psi(t)|\psi(t)\rangle = |\mathcal{A}(t)|^2 + {\sum_{\boldsymbol{k},\lambda}}' |y_{\boldsymbol{k},\lambda}(t)|^2 + {\sum_{\boldsymbol{k},\lambda}}' |z_{\boldsymbol{k},\lambda}(t)|^2 = 1. \qquad (\forall t) \tag{10.26}$$

By inserting (10.25) in (10.24) one obtains the equations of motion

$$\begin{aligned} i\,\dot{\mathcal{A}}(t) &= \omega_0\mathcal{A}(t) + {\sum_{\boldsymbol{k},\lambda}}' \phi^*_{\boldsymbol{k}\lambda} y_{\boldsymbol{k}\lambda}(t), \\ i\,\dot{y}_{\boldsymbol{k}\lambda}(t) &= \phi_{\boldsymbol{k}\lambda}\mathcal{A}(t) + \omega_k y_{\boldsymbol{k}\lambda}(t) + \alpha_0^*\Phi_{\boldsymbol{k}_0\lambda_0} z_{\boldsymbol{k}\lambda}(t), \\ i\,\dot{z}_{\boldsymbol{k}\lambda}(t) &= \alpha_0\Phi^*_{\boldsymbol{k}_0\lambda_0} y_{\boldsymbol{k}\lambda}(t) + \omega_k z_{\boldsymbol{k}\lambda}(t), \end{aligned} \tag{10.27}$$

where a dot denotes time derivative. At time $t = 0$ we prepare our system in the state

$$|\psi(0)\rangle = |2;0\rangle \quad \Leftrightarrow \quad \mathcal{A}(0) = 1,\ y_{\boldsymbol{k}\lambda}(0) = 0,\ z_{\boldsymbol{k}\lambda}(0) = 0. \tag{10.28}$$

By Fourier-Laplace transforming the system of differential equations (10.27) and incorporating the initial conditions (10.28) the solution reads

$$G_a(E) = \widetilde{\mathcal{A}}(E) = \frac{1}{E - \omega_0 - \Sigma(B,E)}, \tag{10.29}$$

$$\widetilde{y}_{\boldsymbol{k}\lambda}(E) = \frac{\phi_{\boldsymbol{k}\lambda}(E-\omega_k)}{(E-\omega_k)^2 - B^2}\, G_a(E), \tag{10.30}$$

$$\widetilde{z}_{\boldsymbol{k}\lambda}(E) = \frac{\sqrt{\bar{N}_0}\Phi^*_{\boldsymbol{k}_0\lambda_0}\phi_{\boldsymbol{k}\lambda}}{(E-\omega_k)^2 - B^2}\, G_a(E), \tag{10.31}$$

with

$$\Sigma(B,E)=\sum_{\boldsymbol{k},\lambda}|\phi_{\boldsymbol{k}\lambda}|^2\frac{E-\omega_k}{(E-\omega_k)^2-B^2} \tag{10.32}$$

and where

$$B^2=\bar{N}_0\,|\Phi_{\boldsymbol{k}_0\lambda_0}|^2 \tag{10.33}$$

is proportional to the intensity of the laser field and can be viewed as the strength of the observation performed by the laser beam on level $|2\rangle$ (in the sense of Sec. 7.4). Note that the coupling B is related to the Rabi frequency by the simple relation $B=\Omega_{\rm Rabi}/2$.

In the continuum limit ($V\to\infty$), the matrix elements scale as follows

$$\lim_{V\to\infty}\frac{V\omega^2}{(2\pi)^3}\sum_{\lambda}\int d\Omega|\phi_{\boldsymbol{k}\lambda}|^2\equiv g^2\omega_0\chi^2(\omega), \tag{10.34}$$

where Ω is the solid angle. The (dimensionless) function $\chi(\omega)$ and coupling constant g have the following general properties (Facchi and Pascazio [2000a])

$$\chi^2(\omega)\;\propto\;\begin{cases}\omega^{2j\mp1} & \text{if } \omega\ll\Lambda\\ \omega^{-\beta} & \text{if } \omega\gg\Lambda\end{cases}, \tag{10.35}$$

$$g^2\;=\;\alpha(\omega_0/\Lambda)^{2j+1\mp1}, \tag{10.36}$$

where j is the total angular momentum of the photon emitted in the $2\to1$ transition, $\mp$ represent electric and magnetic transitions, respectively, $\beta(>1)$ is a constant, α the fine structure constant and Λ a natural cutoff (of the order of the inverse size of the emitting system, e.g. the Bohr radius for an atom), that can be explicitly evaluated and determines the range of the atomic or molecular form factor (Berestetskii, Lifshits and Pitaevskii [1982]; Moses [1972a]; Moses [1972b]; Moses [1973]; Seke [1994a]; Seke [1994b]).

In order to scale the quantity B, we take the limit of very large cavity, by keeping the density of Ω_0-photons in the cavity constant:

$$V\to\infty,\qquad \bar{N}_0\to\infty,\quad\text{with}\quad\frac{\bar{N}_0}{V}=n_0=\text{const} \tag{10.37}$$

and obtain from (10.33)

$$B^2=n_0V|\Phi_{\boldsymbol{k}_0\lambda_0}|^2=(2\pi)^3n_0|\varphi_{\lambda_0}(\boldsymbol{k}_0)|^2, \tag{10.38}$$

where $\varphi\equiv\Phi V^{1/2}/(2\pi)^{3/2}$ is the scaled matrix element of the 1-3 transition. If the 1-3 transition is of the dipole type, the above formula reads

$$B^2=2\pi\alpha\Omega_0|\boldsymbol{\epsilon}^*_{\boldsymbol{k_0}\lambda_0}\cdot\boldsymbol{x}_{13}|^2n_0, \tag{10.39}$$

where $\boldsymbol{x}_{13}$ is the dipole matrix element.

In terms of laser power P and laser spot area A, Eq. (10.39) reads

$$B^2=\frac{P}{cA}\frac{\lambda_L^3}{16\pi^2}(\hbar\Gamma_{13})=132\frac{P\lambda_L^3}{A}(\hbar\Gamma_{13})\ \text{eV}^2, \tag{10.40}$$

where P is expressed in Watt, λ_L (laser wavelength) in μm, A in μm^2 and $\hbar\Gamma$ in eV. In Eq. (10.40) the quantity B is expressed in suitable units and can be easily compared to ω_0 [the ratio B/ω_0 being the relevant quantity, as we shall see]. For laser intensities that are routinely used in the study of electromagnetic induced transparency, the inverse quantum Zeno effect should be experimentally observable. For a quick comparison remember that B is just half the Rabi frequency of the resonant transition $1-3$.

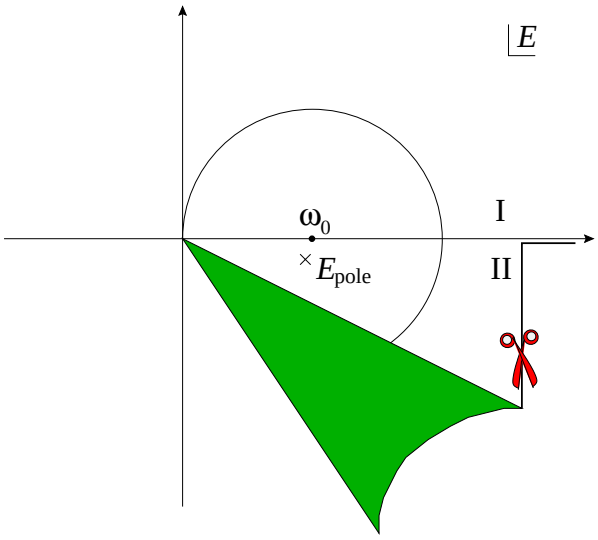

Figure 10.3: Cut and pole in the E-plane ($B = 0$) and convergence circle for the expansion of $\Sigma(E)$ around $E = \omega_0$. I and II are the first and second Riemann sheets, respectively. The pole is on the second Riemann sheet, at a distance $\mathrm{O}(g^2)$ from ω_0.

10.3.3 Laser off

Let us first look at the case $B = 0$. The laser is off and we expect to recover the well-known physics of the spontaneous emission a two-level system prepared in an excited state and coupled to the vacuum of the radiation field, studied in Sec. 5.5. In this case the self-energy function $\Sigma(0, E)$ reads, in the continuum limit, [see Eq. (5.11)]

$$\Sigma(E) \equiv g^2\omega_0 q(E) \equiv g^2\omega_0 \int_0^\infty d\omega \frac{\chi^2(\omega)}{E-\omega}, \tag{10.41}$$

where χ is defined in (10.34). The propagator $G_a(E)$ in Eq. (10.29) (with $B = 0$) has a logarithmic branch cut, extending from 0 to $+\infty$, and no singularities on the first Riemann sheet (physical sheet). On the other hand, it has a simple pole on the second Riemann sheet, that is the solution of the equation

$$E - \omega_0 - g^2\omega_0 q_{\mathrm{II}}(E) = 0, \tag{10.42}$$

where

$$q_{\mathrm{II}}(E) = q(Ee^{-2\pi i}) = q(E) - 2\pi i\chi^2(E) \tag{10.43}$$

is the determination of $q(E)$ on the second Riemann sheet. We note that $g^2q(E)$ is $\mathrm{O}(g^2)$, so that the pole can be found perturbatively, with the procedure outlined in Sec. 4.6.2: by expanding $q_{\mathrm{II}}(E)$ around ω_0 we get a power series, whose radius of convergence is $R_c = \omega_0$ because of the branch point at the origin. The circle of convergence lies half on the first Riemann sheet and half on the second sheet (Fig. 10.3). The pole is well inside the convergence circle and by setting

$$E_{\mathrm{pole}} = \omega_0 + \Delta - i\frac{\gamma}{2}, \tag{10.44}$$

one perturbatively obtains from Eq. (10.41) the Fermi Golden Rule and the second order correction to the energy of level $|2\rangle$

$$\gamma = 2\pi g^2\omega_0\chi^2(\omega_0) + \mathrm{O}(g^4), \qquad \Delta = g^2\omega_0 P\int_0^\infty d\omega\, \frac{\chi^2(\omega)}{\omega_0-\omega} + \mathrm{O}(g^4) \tag{10.45}$$

[see Eqs. (4.73)-(4.74)].

The Weisskopf-Wigner approximation (4.84) consists in neglecting all branch cut contributions and approximating the self-energy function with a constant (its value in the pole), that is

$$G_a^{\rm WW}(E) = \frac{1}{E - \omega_0 - \Sigma_{\rm II}(E_{\rm pole})} = \frac{1}{E - E_{\rm pole}}. \tag{10.46}$$

10.3.4 Laser on

We turn now our attention to the situation with the laser switched on ($B \neq 0$) and tuned at the 1-3 transition frequency Ω_0. The self-energy function $\Sigma(B, E)$ in (10.32) depends on B and can be written in terms of the self-energy function $\Sigma(E)$ in absence of laser field [Eq. (10.41)], by making use of the following remarkable property:

$$\Sigma(B, E) = \frac{1}{2} \sum_{\boldsymbol{k},\lambda} |\phi_{\boldsymbol{k}\lambda}|^2 \left(\frac{1}{E - \omega_k - B} + \frac{1}{E - \omega_k + B} \right) = \frac{1}{2} \left[\Sigma(E - B) + \Sigma(E + B) \right]. \tag{10.47}$$

Notice, incidentally, that in the continuum limit ($V \to \infty$), due to the above formula, $\Sigma(B, E)$ scales just like $\Sigma(E)$. The position of the pole $E_{\rm pole}$ (and as a consequence the decay rate $\gamma = -2{\rm Im}E_{\rm pole}$) depends on the value of B. There are now two branch cuts in the complex E plane, due to the two terms in (10.47). They lie over the real axis, along $[-B, +\infty)$ and $[+B, +\infty)$.

The pole satisfies the equation

$$E - \omega_0 - \Sigma(B, E) = 0, \tag{10.48}$$

where $\Sigma(B, E)$ is of order g^2, as before, and can again be expanded in power series around $E = \omega_0$, in order to find the pole perturbatively. However, this time one has to choose the right determination of the function $\Sigma(B, E)$. Two cases are possible: a) The branch point $+B$ is situated at the left of ω_0, so that ω_0 lies on both cuts. See Fig. 10.4(a); b) The branch point $+B$ is situated at the right of ω_0, so that ω_0 lies only on the upper branch cut. See Fig. 10.4(b). We notice that in the latter case ($B > \omega_0$) a number of additional effects should be considered: multi-photon processes would take place, the other atomic levels would start to play an important role and our approach (3-level atom in the rotating wave approximation) would no longer be completely justified. Notice also that our approximation still apply for values of B that are of the same order of magnitude as those utilized in electromagnetic induced transparency: in this case the influence of the other atomic levels can be taken into account and does not modify the main conclusions (Facchi and Pascazio [2000a]).

In case a), i.e. for $B < \omega_0$, the pole is on the third Riemann sheet (under both cuts) and the power series converges in a circle lying half on the first and half on the third Riemann sheet, within a convergence radius $R_c = \omega_0 - B$, which decreases as B increases [Fig. 10.4(a)]. On the other hand, in case b), i.e. for $B > \omega_0$, the pole is on the second Riemann sheet (under the upper cut only) and the power series converges in a circle lying half on the first and half on the second Riemann sheet, within a convergence radius $R_c = B - \omega_0$, which increases with B [Fig. 10.4(b)].

In either cases we obtain, for $|E_{\rm pole} - \omega_0| < R_c = |B - \omega_0|$,

$$\begin{aligned} E_{\rm pole} &= \omega_0 + \frac{1}{2} \left[\Sigma(\omega_0 + B + i0^+) + \Sigma(\omega_0 - B + i0^+) \right] + {\rm O}(g^4) \\ &= \omega_0 + \frac{1}{2} g^2 \omega_0 \left[q(\omega_0 + B + i0^+) + q(\omega_0 - B + i0^+) \right] + {\rm O}(g^4). \end{aligned} \tag{10.49}$$

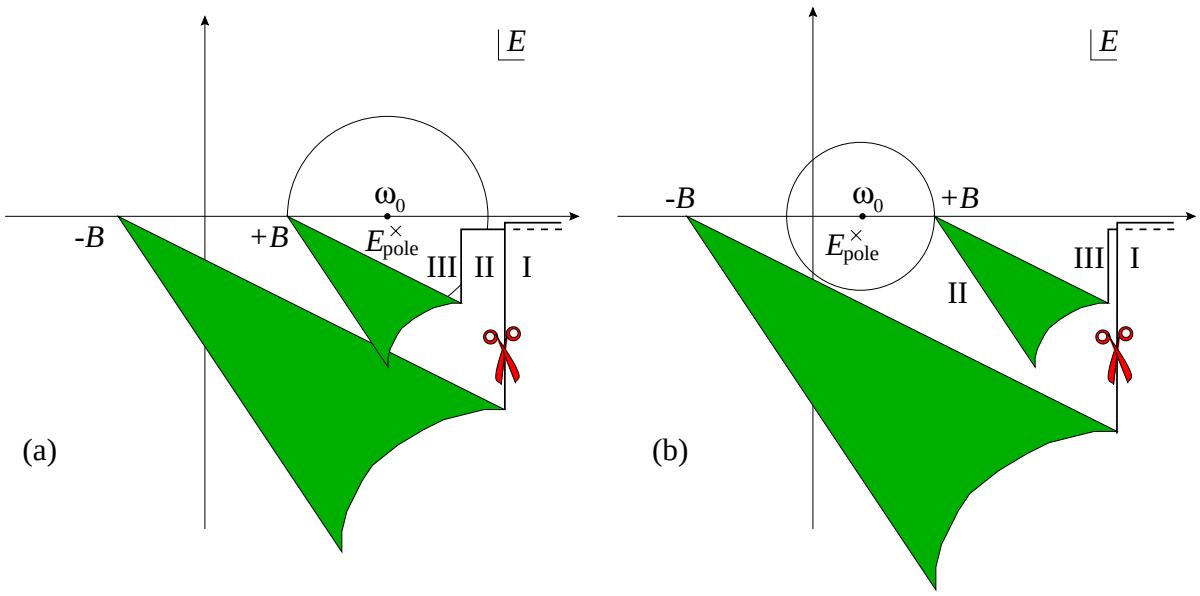

Figure 10.4: Cuts and pole in the E-plane ($B \neq 0$) and convergence circle for the expansion of $\Sigma(B, E)$ around $E = \omega_0$. I , II and III are the first, second and third Riemann sheets, respectively. (a) $B < \omega_0$. (b) $B > \omega_0$. In both cases, the pole is at a distance $\mathrm{O}(g^2)$ from ω_0.

We write, as in (10.44),

$$E_{\text{pole}} = \omega_0 + \Delta(B) - i\frac{\gamma_{\text{eff}}(B)}{2}. \tag{10.50}$$

Substituting (10.41) into (10.49) and taking the imaginary part, one obtains the following expression for the decay rate

$$\gamma_{\text{eff}}(B) = \pi g^2 \omega_0 \left[\chi^2(\omega_0 + B) + \chi^2(\omega_0 - B)\theta(\omega_0 - B)\right] + \mathrm{O}(g^4), \tag{10.51}$$

which yields, by (10.45),

$$\gamma_{\text{eff}}(B) = \gamma\, \frac{\chi^2(\omega_0 + B) + \chi^2(\omega_0 - B)\theta(\omega_0 - B)}{2\chi^2(\omega_0)} + \mathrm{O}(g^4). \tag{10.52}$$

Equation (10.52) expresses the "new" decay rate $\gamma_{\text{eff}}(B)$, when the system is bathed in an intense laser field B, in terms of the "natural" decay rate γ, when there is no laser field. By taking into account the general behavior (10.35) of the matrix elements $\chi^2(\omega)$ and substituting into (10.52), one gets to $\mathrm{O}(g^4)$

$$\gamma_{\text{eff}}(B) \simeq \frac{\gamma}{2}\left[\left(1 + \frac{B}{\omega_0}\right)^{2j\mp 1} + \left(1 - \frac{B}{\omega_0}\right)^{2j\mp 1}\theta(\omega_0 - B)\right], \qquad (B \ll \Lambda) \tag{10.53}$$

where $\mp$ refers to 1-2 transitions of electric and magnetic type, respectively. Observe that, since $\Lambda \simeq$ inverse Bohr radius, the case $B < \omega_0 \ll \Lambda$ is the physically most relevant one. The decay rate is profoundly modified by the presence of the laser field. Its behavior is shown in Fig. 10.5 for a few values of j. In general, for $j > 1$ (1-2 transitions of electric quadrupole, magnetic dipole or higher), the decay rate $\gamma_{\text{eff}}(B)$ increases with B, so that the lifetime $\gamma_{\text{eff}}(B)^{-1}$ decreases as B is increased. Since B is the strength of the observation performed by the laser beam on level $|2\rangle$, this is an IZE, for decay is *enhanced* by observation.

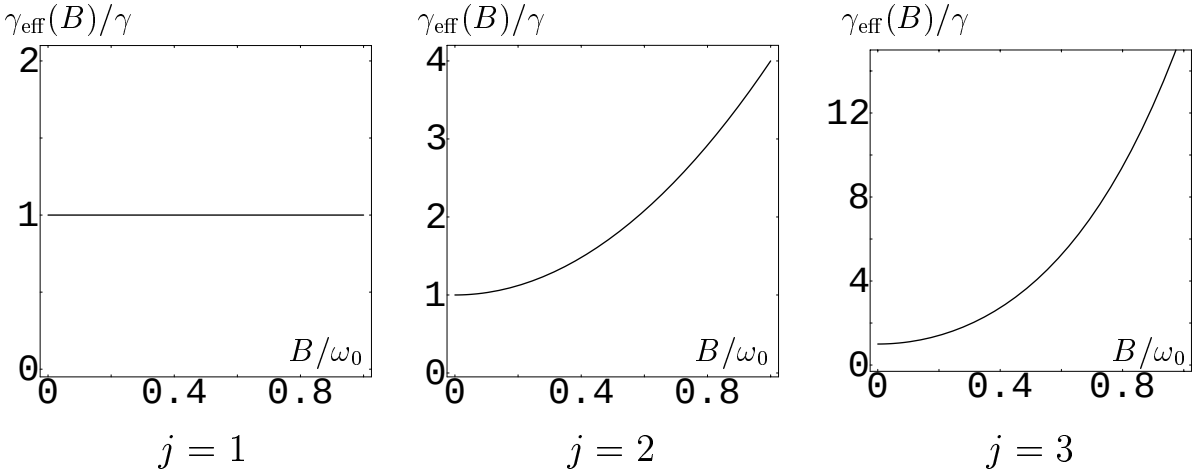

Figure 10.5: The decay rate $\gamma_{\rm eff}(B)$ vs B, for electric transitions with $j = 1, 2, 3$; $\gamma_{\rm eff}(B)$ is in units γ and B in units ω_0. Notice the different scales on the vertical axis.

As already emphasized, Eq. (10.53) is valid for $B \ll \Lambda$. In the opposite case $B \gg \Lambda$, by (10.35) and (10.52), one gets to $\mathrm{O}(g^4)$

$$\gamma_{\rm eff}(B) \simeq \frac{\gamma}{2}\,\frac{\chi^2(B)}{\chi^2(\omega_0)} \propto (B/\Lambda)^{-\beta}. \qquad (B \gg \Lambda) \tag{10.54}$$

This result is similar to that obtained by Mihokova, Pascazio and Schulman [1997]. If such high values of B were experimentally obtainable, the decay would be considerably hindered (QZE).

A final remark is now in order. If one would use the Weisskopf-Wigner approximation (10.46) in Eq. (10.47), in order to evaluate the new lifetime, by setting $\Sigma(E) = \Sigma(E_{\rm pole}) =$ const, one would obtain $\Sigma(B, E) = \Sigma(E) = \Sigma(E_{\rm pole})$, i.e. no B-dependence. Therefore, the effect we are discussing is ultimately due to the nonexponential contributions arising from the cut. In particular, viewed from the perspective of the time domain, this effect is ascribable to the quadratic short-time behavior of the $|2\rangle \to |1\rangle$ decay.

10.3.5 Photon spectrum, dressed states and induced transparency

It is interesting to look at the spectrum of the emitted photons. It is easy to check that, in the Weisskopf-Wigner approximation, the survival probability $|\mathcal{A}(t)|^2$ decreases exponentially with time. In this approximation, for any value of B, the spectrum of the emitted photons is Lorentzian. The proof is straightforward and is given by Facchi and Pascazio [2000a]. One finds that, for $B = 0$, the probability to emit a photon in the range $(\omega, \omega + d\omega)$ reads

$$dP_{B=0} = g^2\omega_0\chi^2(\omega) f_L(\omega - \bar{\omega}_0; \gamma) d\omega, \tag{10.55}$$

where $\bar{\omega}_0 = \omega_0 + \Delta(B)$ and

$$f_L(\omega; \gamma) = \frac{1}{\omega^2 + \gamma^2/4}. \tag{10.56}$$

On the other hand, when $B \neq 0$ one gets:

$$dP_B = g^2\omega_0\chi^2(\omega)\frac{1}{2}\left[f_L(\omega - \bar{\omega}_0 - B; \gamma_{\rm eff}(B)) + f_L(\omega - \bar{\omega}_0 + B; \gamma_{\rm eff}(B))\right] d\omega. \tag{10.57}$$

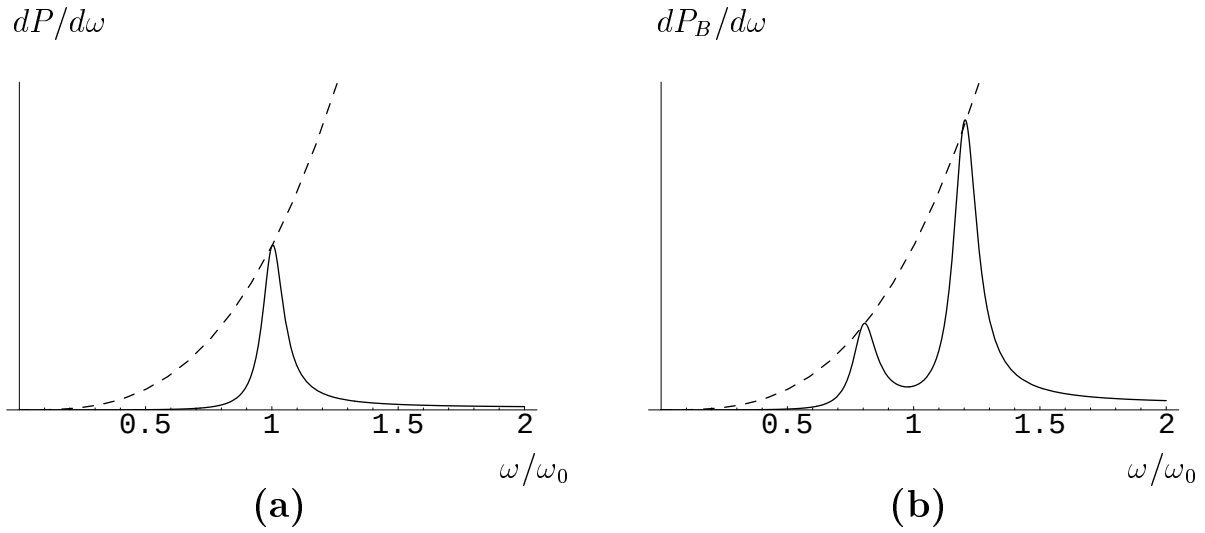

Figure 10.6: The spectrum (10.57) of the emitted photons. The height of the Lorentzians is proportional to the matrix element $\chi^2(\omega)$ (dashed line). We chose an electric quadrupole transition, with $j = 2$ and $\gamma = 10^{-1}\bar{\omega}_0$, and used arbitrary units on the vertical axis. a) B=0; b) $B = \bar{\omega}_0/5$; note that from (10.53) $\gamma_{\rm eff}(B) = (28/25)\gamma$.

The emission probability is given by the sum of two Lorentzians, centered in $\bar{\omega}_0 \pm B$. We see that the emission probability of a photon of frequency $\bar{\omega}_0 + B$ ($\bar{\omega}_0 - B$) increases (decreases) with B (Fig. 10.6). The linewidths are modified according to Eq. (10.53). When B reaches the "threshold" value $\bar{\omega}_0$, only the photon of higher frequency ($\bar{\omega}_0 + B$) is emitted (with increasing probability vs B).

Photons of different frequencies are therefore emitted at different rates. In order to understand better the features of the emission, let us look at the dressed states of the system. For simplicity, since the average number $\bar{N}_0$ of $\boldsymbol{k}_0$-photons in the total volume V can be considered very large, we consider number (rather than coherent) states of the electromagnetic field. Henceforth, the vector $|i; n_{\boldsymbol{k}\lambda}, M_0\rangle$ represents an atom in state $|i\rangle$, with $n_{\boldsymbol{k}\lambda}$ $(\boldsymbol{k}, \lambda)$-photons and M_0 laser photons.

The Hamiltonian (10.17) becomes

$$\begin{aligned} H \;\simeq\; & \omega_0|2\rangle\langle 2| + \Omega_0|3\rangle\langle 3| + \sum_{\boldsymbol{k},\lambda} \omega_k a^\dagger_{\boldsymbol{k}\lambda} a_{\boldsymbol{k}\lambda} + {\sum_{\boldsymbol{k},\lambda}}' \left(\phi_{\boldsymbol{k}\lambda} a^\dagger_{\boldsymbol{k}\lambda} |1\rangle\langle 2| + \phi^*_{\boldsymbol{k}\lambda} a_{\boldsymbol{k}\lambda} |2\rangle\langle 1| \right) \\ & + \left(\Phi_{\boldsymbol{k}_0\lambda_0} a^\dagger_{\boldsymbol{k}_0\lambda_0} |1\rangle\langle 3| + \Phi^*_{\boldsymbol{k}_0\lambda_0} a_{\boldsymbol{k}_0\lambda_0} |3\rangle\langle 1| \right), \end{aligned} \tag{10.58}$$

where a prime means that the summation does not include $(\boldsymbol{k}_0, \lambda_0)$ [due to hypothesis (10.19)]. Besides (10.22), there is now another conserved quantity: indeed the operator

$$\mathcal{N}_0 = |3\rangle\langle 3| + a^\dagger_{\boldsymbol{k}_0\lambda_0} a_{\boldsymbol{k}_0\lambda_0} \tag{10.59}$$

satisfies

$$[H, \mathcal{N}_0] = [\mathcal{N}_0, \mathcal{N}] = 0. \tag{10.60}$$

In this case, the system evolves in the subspace labeled by the two eigenvalues $\mathcal{N} = 1$ and $\mathcal{N}_0 = N_0$, whose states read

$$|\psi(t)\rangle = \mathcal{A}(t)|2; 0, N_0\rangle + {\sum_{\boldsymbol{k},\lambda}}' y_{\boldsymbol{k}\lambda}(t)|1; 1_{\boldsymbol{k}\lambda}, N_0\rangle + {\sum_{\boldsymbol{k},\lambda}}' z_{\boldsymbol{k}\lambda}(t)|3; 1_{\boldsymbol{k}\lambda}, N_0 - 1\rangle. \tag{10.61}$$

By using the Hamiltonian (10.58) and the states (10.61) and identifying N_0 with $\bar{N}_0 = |\alpha_0|^2$ of Sec. 10.3.1, the Schrödinger equation yields again the equations of motion (10.27), obtained by assuming a coherent state for the laser mode. Our analysis is therefore independent of the statistics of the driving field, provided it is sufficiently intense, and the (convenient) use of number states is completely justified.

Energy conservation implies that if there are two emitted photons with different energies [see (10.57)], there are two levels of different energies to which the atom can decay. This can be seen by considering the laser-dressed atomic states (Cohen-Tannoudji and Reynaud [1977a]; Cohen-Tannoudji and Reynaud [1977b]; Cohen-Tannoudji and Reynaud [1977c]; Yoo and Eberly [1985]). The shift of the dressed states can be obtained directly from the Hamiltonian (10.58). In the sector $\mathcal{N}_0 = N_0$, the operator $\mathcal{N}_0$ is proportional to the unit operator, the constant of proportionality being its eigenvalue. Hence one can write the Hamiltonian in the following form

$$H = H - \Omega_0 \mathcal{N}_0 + \Omega_0 N_0, \tag{10.62}$$

which, by the setting $E_1 + N_0\Omega_0 = 0$, reads

$$\begin{aligned} H &= H_0 + H_{\rm int} \\ &= \omega_0 |2\rangle\langle 2| + {\sum_{\boldsymbol{k},\lambda}}' \omega_k a^\dagger_{\boldsymbol{k}\lambda} a_{\boldsymbol{k}\lambda} + {\sum_{\boldsymbol{k},\lambda}}' \left(\phi_{\boldsymbol{k}\lambda} a^\dagger_{\boldsymbol{k}\lambda} |1\rangle\langle 2| + \phi^*_{\boldsymbol{k}\lambda} a_{\boldsymbol{k}\lambda} |2\rangle\langle 1| \right) \\ &\quad + \left(\Phi_{\boldsymbol{k}_0\lambda_0} a^\dagger_{\boldsymbol{k}_0\lambda_0} |1\rangle\langle 3| + \Phi^*_{\boldsymbol{k}_0\lambda_0} a_{\boldsymbol{k}_0\lambda_0} |3\rangle\langle 1| \right). \end{aligned} \tag{10.63}$$

On the other hand, in the sector $\mathcal{H}_{\mathcal{N}\mathcal{N}_0}$ with $\mathcal{N} = 1$ and $\mathcal{N}_0 = N_0$, the last term becomes

$$\left(\Phi_{\boldsymbol{k}_0\lambda_0} a^\dagger_{\boldsymbol{k}_0\lambda_0} |1\rangle\langle 3| + \Phi^*_{\boldsymbol{k}_0\lambda_0} a_{\boldsymbol{k}_0\lambda_0} |3\rangle\langle 1| \right) = \left(\Phi_{\boldsymbol{k}_0\lambda_0} \sqrt{N_0} |1\rangle\langle 3| + \Phi^*_{\boldsymbol{k}_0\lambda_0} \sqrt{N_0} |3\rangle\langle 1| \right). \tag{10.64}$$

This operator is easily diagonalized in terms of the (orthonormal) non-interacting states

$$|\pm\rangle = \frac{1}{\sqrt{2}} \left(|1\rangle + |3\rangle \right) \tag{10.65}$$

[this is the simplest choice (Facchi and Pascazio [2000a])]. A simple manipulation yields

$$H = H'_0 + H'_{\rm int}, \tag{10.66}$$

where the primed free and interaction Hamiltonians read respectively

$$\begin{aligned} H'_0 &= \omega_0 |2\rangle\langle 2| + B|+\rangle\langle +| - B|-\rangle\langle -| + {\sum_{\boldsymbol{k},\lambda}}' \omega_k a^\dagger_{\boldsymbol{k}\lambda} a_{\boldsymbol{k}\lambda}, \\ H'_{\rm int} &= {\sum_{\boldsymbol{k},\lambda}}' \left[\left(\frac{\phi_{\boldsymbol{k}\lambda}}{\sqrt{2}} a^\dagger_{\boldsymbol{k}\lambda} |+\rangle\langle 2| + \frac{\phi^*_{\boldsymbol{k}\lambda}}{\sqrt{2}} a_{\boldsymbol{k}\lambda} |2\rangle\langle +| \right) \right. \\ &\quad \left. + \left(\frac{\phi_{\boldsymbol{k}\lambda}}{\sqrt{2}} a^\dagger_{\boldsymbol{k}\lambda} |-\rangle\langle 2| + \frac{\phi^*_{\boldsymbol{k}\lambda}}{\sqrt{2}} a_{\boldsymbol{k}\lambda} |2\rangle\langle -| \right) \right] \end{aligned} \tag{10.67}$$

and $B^2 = |\Phi_{\boldsymbol{k}_0\lambda_0}|^2 N_0$. The dressed states $|+\rangle$ and $|-\rangle$ have energies $+B$ and $-B$ and interact with state $|2\rangle$ with a coupling $\phi_{\boldsymbol{k}\lambda}/\sqrt{2}$. Since $2B = \Omega_{\rm Rabi}$ this is the well-known Autler-Townes doublet (Autler and Townes [1955]; Townes and Schawlow [1975]).

Therefore, by applying the Fermi golden rule, the decay rates into the dressed states read

$$\gamma_+ = 2\pi g^2 \omega_0 \frac{\chi^2(\omega_0 - B)}{2} \qquad \gamma_- = 2\pi g^2 \omega_0 \frac{\chi^2(\omega_0 + B)}{2} \tag{10.68}$$

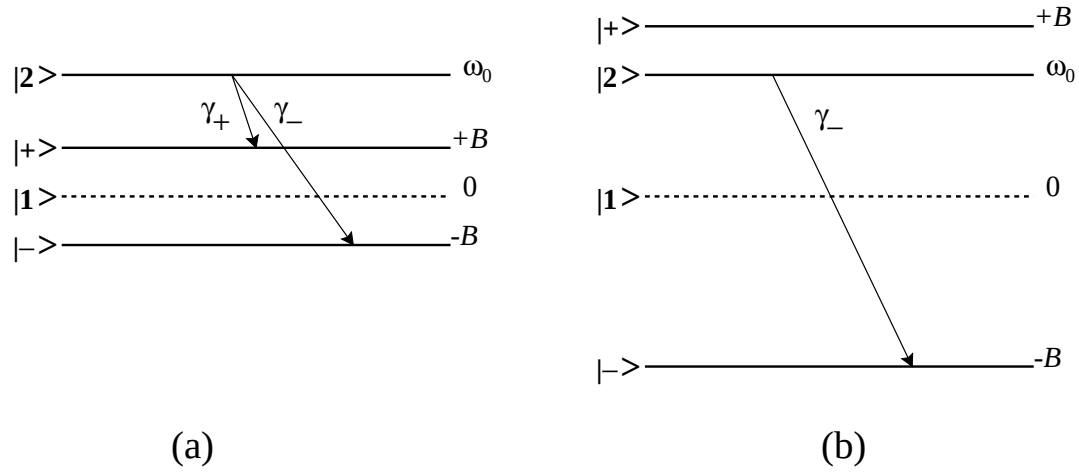

Figure 10.7: Shift of the dressed states $|+\rangle$ and $|-\rangle$ vs B. (a) For $B < \omega_0$ there are two decay channels, with $\gamma_- > \gamma_+$. (b) For $B > \omega_0$ level $|+\rangle$ is above level $|2\rangle$ and only the γ_- decay channel remains.

and the total decay rate of state $|2\rangle$ is given by their sum

$$\gamma_{\text{eff}}(B) = \gamma_+ + \gamma_-, \tag{10.69}$$

which yields (10.51). One sees why there is a threshold at $B = \omega_0$: For $B < \omega_0$, the energies of both dressed states $|\pm\rangle$ is lower than that of the initial state $|2\rangle$ [Fig. 10.7(a)]. The decay rate γ_- increases with B, whereas γ_+ decreases with B; their sum γ increases with B. These two decays (and their lifetimes) could be easily distinguished by selecting the frequencies of the emitted photons, e.g. by means of filters. On the other hand, when $B > \omega_0$, the energy of the dressed state $|+\rangle$ is larger than that of state $|2\rangle$ and this decay channel disappears [Fig. 10.7(b)].

Finally, let us emphasize that if state $|2\rangle$ were *below* state $|1\rangle$, our system would become a three-level system in a ladder configuration, and the shift of the dressed states would give rise to electromagnetically induced transparency (Tewari and Agarwal [1986]; Harris, Field and Imamoğlu [1990]; Boller, Imamoğlu and Harris [1991]; Field, Hahn and Harris [1991]). The situation we consider and the laser power required to bring these effects to light are therefore similar to those used in induced transparency.

Summarizing, for physically sensible values of the intensity of the laser field, the decay of level $|2\rangle$ is *faster* when the laser is present. Equations (10.52)-(10.53) (valid to 4th order in the coupling constant) express the new lifetime as a function of the natural one and other parameters characterizing the physical system. The initial state decays to the laser-dressed states with different lifetimes, yielding an IZE.

Chapter 11

Measurement-induced quantum chaos

11.1 Introduction

The "kicked" rotator is a pendulum that evolves under the action of a gravitational field that is "switched on" at periodic time intervals. It is a very useful system, that enables one to elucidate many different features between the classical and the quantum case. In the classical case, when the coupling constant exceeds some critical value, there appear regions of stochasticity in the phase space, yielding a diffusive behavior of the action variable (Lichtenberg and Lieberman [1992]). On the other hand, in the quantum version, a peculiar phenomenon takes place, essentially ascribable to quantum coherence. The evolution of the wave function is more regular than the complicated evolution of classical trajectories and indeed, as shown in the seminal paper by Casati, Chirikov, Shepelyansky and Guarneri [1987], the wave function exhibits quantum localization in momentum space and a consequent quantum suppression of the chaotic behavior after a sufficiently long time.

We show in this chapter that these coherence effects are completely destroyed and diffusion is restored if the momentum variable is measured after each kick. We call this phenomenon, which is a clear manifestation of an inverse quantum Zeno effect, "measurement-induced quantum chaos" (Facchi, Pascazio and Scardicchio [1999a]). This is a model in which IZE is manifested in the modified large-time behavior of the wave function and has some relevance in the "problem" of quantum chaos. Indeed, we find a diffusive behavior for a large class of Hamiltonians, even when the dynamics of the classical counterpart is not chaotic. Moreover, this results in a completely randomized classical map in the semiclassical limit (Facchi, Pascazio and Scardicchio [1999b]).

11.2 The kicked system

We consider the Hamiltonian

$$H = H_0(p) + \lambda V(x)\delta_T(t), \tag{11.1}$$

where p and $x \in [-\pi, \pi]$ are the action and angle variable, respectively, and

$$\delta_T(t) = \sum_{k=-\infty}^{\infty} \delta(t - kT), \tag{11.2}$$

T being the period of the perturbation. We impose periodic boundary conditions on the interaction $V(x)$. This Hamiltonian gives rise to the so-called radial twisting map, that describes the local behavior of a perturbed integrable map near resonance (Arnold and Avez [1968]; Lichtenberg and Lieberman [1992]). The free Hamiltonian H_0 has a discrete spectrum and a countable complete set of eigenstates $\{|m\rangle\}$:

$$\langle x|m\rangle = \frac{1}{\sqrt{2\pi}} \exp\left(imx\right), \qquad m = 0, \pm 1, \pm 2, \dots \ . \tag{11.3}$$

The classical and quantum dynamics of these systems under the action of periodic "kicks" are in general very different. Classical systems can follow very complicated trajectories in phase space, while the evolution of the wave function in the quantum case is more regular. In the classical case, in those regions of the phase space that are stochastic, the evolution of the system can be well described in terms of the action variable alone and one of the most distinctive features of an underlying chaotic behavior is just the diffusion of the action variable in phase space. On the other hand, in the quantum case, such a diffusion is always suppressed after a sufficiently long time (Casati, Chirikov, Ford and Izrailev [1979]; Berry, Balazs, Tabor and Voros [1979]). This phenomenon, known as the quantum mechanical suppression of classical chaos, can be framed in a proper context in terms of the semiclassical approximation $\hbar \to 0$ (Casati, Chirikov, Shepelyansky and Guarneri [1987]; Izrailev [1990]; Berry and Balazs [1979]; Tabor [1989]; Haake [1991]).

In particular, the "kicked" rotator is a pendulum that evolves under the action of a gravitational field that is "switched on" at periodic time intervals. In this case the Hamiltonian (11.1) is specialized to

$$H_0(p) = \frac{p^2}{2}, \qquad V(x) = \cos x. \tag{11.4}$$

This is a very useful system, able to elucidate many different features between the classical and the quantum case and was studied by Casati, Chirikov, Ford and Izrailev [1979] in their seminal work on quantum chaos. Rather recently, by studying this model, Kaulakys and Gontis [1997] showed that a diffusive behavior of the action variable takes place even in the quantum case, yielding an IZE, if a quantum measurement is performed after every kick.

11.3 Kicks interspersed with quantum measurements

We investigate in some detail the dynamics of a measured kicked system and prove that quantum mechanical measurements of the action variable provoke diffusion in a very large class of kicked systems, even when the corresponding classical dynamics is regular. Consider the evolution engendered by the Hamiltonian (11.1) interspersed with quantum measurements, in the following sense: the system evolves under the action of the free Hamiltonian for $(N-1)T + \tau < t < NT \ \ (0 < \tau < T)$, undergoes a "kick" at $t = NT$, evolves again freely and then undergoes a "measurement" of p at $t = NT + \tau$. The evolution of the system is best described in terms of the density matrix: between successive measurements one has

$$\rho_{NT+\tau} = U_{\rm free}(\tau) U_{\rm kick} U_{\rm free}(T-\tau) \rho_{(N-1)T+\tau} U^\dagger_{\rm free}(T-\tau) U^\dagger_{\rm kick} U^\dagger_{\rm free}(\tau), \tag{11.5}$$

$$U_{\rm kick} = \exp\left(-i\lambda V/\hbar\right), \quad U_{\rm free}(t) = \exp\left(-iH_0 t/\hbar\right). \tag{11.6}$$

At each measurement, the wave function is "projected" onto the nth eigenstate of p with probability $P_n(NT+\tau) = {\rm Tr}(|n\rangle\langle n|\rho_{NT+\tau})$ and the off-diagonal terms of the density matrix

disappear. The occupation probabilities $P_n(t)$ change discontinuously at times NT and their evolution is governed by the master equation

$$P_n(N) = \sum_m W_{nm} P_m(N-1), \tag{11.7}$$

where

$$W_{nm} \equiv |\langle n|U_{\rm free}(\tau)U_{\rm kick}U_{\rm free}(T-\tau)|m\rangle|^2 = |\langle n|U_{\rm kick}|m\rangle|^2 \tag{11.8}$$

are the transition probabilities and we defined, with a little abuse of notation,

$$P_n(N) \equiv P_n(NT+\tau). \tag{11.9}$$

The map (11.7) depends on λ, V, H_0 in a complicated way. However, interestingly, very general conclusions can be drawn about the average value of a generic regular function of momentum $g(p)$ (Facchi, Pascazio and Scardicchio [1999a]). Let

$$\langle g(p)\rangle_t \equiv {\rm Tr}(g(p)\rho(t)) = \sum_n g(p_n)P_n(t), \tag{11.10}$$

where $p|n\rangle = p_n|n\rangle$ ($p_n = n\hbar$), and consider the average value of g after N kicks

$$\langle g(p)\rangle_N \equiv \langle g(p)\rangle_{NT+\tau} = \sum_n g(p_n)P_n(N) = \sum_{n,m} g(p_n)W_{nm}P_m(N-1). \tag{11.11}$$

Substituting W_{nm} from (11.8) one obtains

$$\begin{aligned} \langle g(p)\rangle_N &= \sum_{n,m} g(p_n)\langle m|U^\dagger_{\rm kick}|n\rangle\langle n|U_{\rm kick}|m\rangle P_m(N-1) \\ &= \sum_m \langle m|U^\dagger_{\rm kick}g(p)U_{\rm kick}|m\rangle P_m(N-1), \end{aligned} \tag{11.12}$$

where we used $g(p)|n\rangle = g(p_n)|n\rangle$. We are mostly interested in the evolution of the quantities p and p^2 (momentum and kinetic energy). By the Baker-Hausdorff lemma

$$U^\dagger_{\rm kick}g(p)U_{\rm kick} = g(p) + i\frac{\lambda}{\hbar}[V,g(p)] + \frac{1}{2!}\left(\frac{i\lambda}{\hbar}\right)^2[V,[V,g(p)]] + ..., \tag{11.13}$$

we obtain the exact expressions

$$U^\dagger_{\rm kick}pU_{\rm kick} = p + i\frac{\lambda}{\hbar}[V,p], \tag{11.14}$$

$$U^\dagger_{\rm kick}p^2U_{\rm kick} = p^2 + i\frac{\lambda}{\hbar}[V,p^2] + \lambda^2\left(V'\right)^2, \tag{11.15}$$

where prime denotes derivative. We observe, incidentally, that in general, for polynomial $g(p)$, the highest order of λ appearing in (11.13) is the degree of the polynomium.

Substituting (11.14) and (11.15) in (11.12) and then iterating on the number of kicks we obtain

$$\langle p\rangle_N = \langle p\rangle_{N-1} = \langle p\rangle_0, \tag{11.16}$$

$$\langle p^2\rangle_N = \langle p^2\rangle_{N-1} + \lambda^2\langle f^2\rangle = \langle p^2\rangle_0 + \lambda^2\langle f^2\rangle N, \tag{11.17}$$

where $f = -V'(x)$ is the force and

$$\langle f^2 \rangle = \mathrm{Tr}\left(f^2 \rho_{NT+\tau}\right) = \sum_n \langle n|f^2|n\rangle P_n(N) = \frac{1}{2\pi}\int_{-\pi}^{\pi} dx\ f^2(x) \tag{11.18}$$

is a constant that does not depend on N: Indeed $\langle n|f^2|n\rangle$ is independent of the state $|n\rangle$ [see (11.3)] and $\sum P_n = 1$. In particular, the kynetic energy $K = p^2/2m$ grows at a constant rate: $\langle K\rangle_N = \langle K\rangle_0 + \lambda^2\langle f^2\rangle N/2m$. By using (11.16)-(11.17) we obtain the friction (F) and the diffusion (D) coefficients

$$F = \frac{\langle p\rangle_N - \langle p\rangle_0}{NT} = 0, \tag{11.19}$$

$$D = \frac{\langle \Delta p^2\rangle_N - \langle \Delta p^2\rangle_0}{NT} = \frac{\lambda^2\langle f^2\rangle}{T}, \tag{11.20}$$

where $\langle \Delta p^2\rangle_N = \langle p^2\rangle_N - \langle p\rangle_N^2$. We stress that the above results are *exact*: their derivation involves no approximation. This shows that Hamiltonian systems of the type (11.1) (radial twisting maps), in the quantum case, if measured after every kick, have a constant diffusion rate in momentum with no friction, for *any* perturbation $V = V(x)$. In particular, the seminal kicked-rotator model $H_0 = p^2/2I, V = \cos x$ has the diffusion coefficient

$$D = \frac{\lambda^2}{2T}, \tag{11.21}$$

which is nothing but the result obtained in the classical case (Casati, Chirikov, Ford and Izrailev [1979]; Kaulakys and Gontis [1997]).

The above results are somewhat puzzling, essentially because one finds that in the quantum case, when repeated measurements of momentum (action variable) are performed on the system, a chaotic behavior is obtained for *every* value of λ and for *any* potential $V(x)$. On the other hand, in the classical case, diffusion occurs only for some $V(x)$, when λ exceeds some critical value λ_{crit}. (For instance, the kicked rotator displays diffusion for $\lambda \geq \lambda_{\mathrm{crit}} \simeq 0.972$ (Casati, Chirikov, Ford and Izrailev [1979]; Lichtenberg and Lieberman [1992]).) It appears, therefore, that quantum measurements not only yield a chaotic behavior in a quantum context, they even produce chaos when the classical motion is regular. This is a clear manifestation of the "effectiveness" of the inverse quantum Zeno effect. In order to bring to light the causes of this peculiar situation, one has to look at the classical case. The classical map for the Hamiltonian (11.1) reads

$$\begin{aligned} x_N &= x_{N-1} + H_0'(p_{N-1})T, \\ p_N &= p_{N-1} - \lambda V'(x_N). \end{aligned} \tag{11.22}$$

A quantum measurement of p yields an exact determination of momentum p and, as a consequence, makes position x completely undetermined (uncertainty principle). This situation has no classical analog: it is inherently quantal. However, the classical "map" that best mymics this physical picture is obtained by assuming that position x_N at time τ after each kick (i.e. when the quantum counterpart undergoes a measurement) behaves like a random variable ξ_N uniformly distributed over $[-\pi, \pi]$:

$$\begin{aligned} x_N &= \xi_N, \\ p_N &= p_{N-1} - \lambda V'(x_N). \end{aligned} \tag{11.23}$$

Introducing the ensemble average $\langle\langle \cdots \rangle\rangle$ over the stochastic process (i.e. over the set of independent random variables $\{\xi_k\}_{k\leq N}$), we obtain

$$\langle\langle p_N \rangle\rangle = \langle\langle p_{N-1} \rangle\rangle - \lambda \langle V'(\xi_N) \rangle, \tag{11.24}$$

where

$$\langle g(\xi) \rangle \equiv \frac{1}{2\pi} \int_{-\pi}^{\pi} g(\xi) d\xi \tag{11.25}$$

is the average over the single random variable ξ [this coincides with the quantum average: see for instance the last term of (11.18)]. The average of $V'(\xi_N)$ in (11.24) vanishes due to the periodic boundary conditions on V, so that

$$\langle\langle p_N \rangle\rangle = \langle\langle p_{N-1} \rangle\rangle, \tag{11.26}$$

which is the same as Eq. (11.16). Moreover, using (11.23) and (11.26) we get

$$\langle\langle \Delta p_N^2 \rangle\rangle = \langle\langle p_N^2 \rangle\rangle - \langle\langle p_N \rangle\rangle^2 = \langle\langle \Delta p_{N-1}^2 \rangle\rangle + \lambda^2 \langle V'(\xi_N)^2 \rangle - 2\lambda \langle\langle p_{N-1} \rangle\rangle \langle V'(\xi_N) \rangle. \tag{11.27}$$

In writing (11.27), the average of $V'(\xi_N) p_{N-1}$ has been factorized because p_{N-1} depends only on $\{\xi_k\}_{k\leq N-1}$, as can be evinced from (11.23). Using again the periodic boundary condition on V, one finally gets

$$\langle\langle \Delta p_N^2 \rangle\rangle = \langle\langle \Delta p_{N-1}^2 \rangle\rangle + \lambda^2 \langle f^2 \rangle \tag{11.28}$$

and the momentum diffuses at the rate (11.20), as in the quantum case with measurements. We obtain in this case a diffusion taking place in the whole phase space, without effects due to the presence of adiabatic islands.

It is interesting to compare the different cases analyzed: (A) a classical system, under the action of a suitable kicked perturbation, displays a diffusive behavior if the coupling constant exceeds a certain threshold (KAM theorem); (B) on the other hand, in its quantum counterpart, this diffusion is always suppressed. (C) The introduction of measurements between kicks encompasses this limitation, yielding diffusion in the quantum case. More so, diffusion takes place for any potential and all values of the coupling constant (namely, even when the classical motion is regular). (D) The same behavior is displayed by a "randomized classical map," in the sense explained above. These conclusions are sketched in Table 1.

Table 1: Classical vs quantum diffusion

A	classical	diffusion for $\lambda > \lambda_{\text{crit}}$
B	quantum	no diffusion
C	quantum + measurements	diffusion $\forall\lambda$
D	classical + random	diffusion $\forall\lambda$

11.4 Semiclassical limit

As we have seen, the effect of quantum measurements is basically equivalent to a complete randomization of the classical angle variable x, at least if one's attention is limited to the calculation of the diffusion coefficient in the chaotic regime. One might therefore naively think that the randomized classical map (11.23) and the quantum map with measurements (11.7),

(11.16)-(11.20) are identical. This expectation would be wrong: there are in fact corrections in $\hbar$. It is indeed straightforward, using Eqs. (11.12)-(11.13), to obtain in the quantum case

$$\begin{aligned}\langle p^3\rangle_N &= \langle p^3\rangle_{N-1} + 3\lambda^2\langle f^2\rangle\langle p\rangle_{N-1} + \lambda^3\langle f^3\rangle,\\ \langle p^4\rangle_N &= \langle p^4\rangle_{N-1} + 6\lambda^2\langle f^2\rangle\langle p^2\rangle_{N-1} + 4\lambda^3\langle f^3\rangle\langle p\rangle_{N-1} + \lambda^4\langle f^4\rangle + \lambda^2\hbar^2\langle (f')^2\rangle.\end{aligned} \tag{11.29}$$

On the other hand, using (11.23) and the periodic boundary conditions, one gets for the randomized classical map

$$\begin{aligned}\langle\langle p_N^3\rangle\rangle &= \langle\langle p_{N-1}^3\rangle\rangle + 3\lambda^2\langle f^2\rangle\langle\langle p_{N-1}\rangle\rangle + \lambda^3\langle f^3\rangle,\\ \langle\langle p_N^4\rangle\rangle &= \langle\langle p_{N-1}^4\rangle\rangle + 6\lambda^2\langle f^2\rangle\langle\langle p_{N-1}^2\rangle\rangle + 4\lambda^3\langle f^3\rangle\langle\langle p_{N-1}\rangle\rangle + \lambda^4\langle f^4\rangle.\end{aligned} \tag{11.30}$$

Hence the two maps have equal moments up to third order, while the fourth moment displays a difference of order $O(\hbar^2)$:

$$\langle p^4\rangle_N - \langle p^4\rangle_{N-1} = \langle\langle p_N^4\rangle\rangle - \langle\langle p_{N-1}^4\rangle\rangle + \lambda^2\hbar^2\langle (f')^2\rangle. \tag{11.31}$$

In order to understand better the similarities and differences between the two maps, as well as the quantum mechanical corrections, we focus our attention on the particular case of the kicked rotator $H_0 = p^2/2$, $V(x) = \cos x$, which gives rise to the so-called standard map

$$\begin{aligned}x_N &= x_{N-1} + p_{N-1}T,\\ p_N &= p_{N-1} + \lambda\sin x_N.\end{aligned} \tag{11.32}$$

The conditional probability density $W_{\rm cl}$ that an initial state (p', x') evolves after one step into the final state (p, x) is, from (11.32),

$$\begin{aligned}W_{\rm cl}(p,x|p',x') &= \delta(p - p' - \lambda\sin x)\;\delta(x - x' - p'T)\\ &= \delta(p - p' - \lambda\sin[x' + p'T])\;\delta(x - x' - p'T).\end{aligned} \tag{11.33}$$

This is a completely deterministic evolution. On the other hand, if one randomizes the standard map, as in (11.23),

$$\begin{aligned}x_N &= \xi_N,\\ p_N &= p_{N-1} + \lambda\sin x_N,\end{aligned} \tag{11.34}$$

the conditional probability density becomes

$$W_{\rm cl}(p,x|p',x') = W_{\rm cl}(p,x|p') = P(x)\;\delta(p - p' - \lambda\sin x) = \frac{1}{2\pi}\delta(p - p' - \lambda\sin x) \tag{11.35}$$

and is independent of the initial position x'. It is therefore possible to describe the dynamics by considering only the momentum distribution

$$\begin{aligned}W_{\rm cl}(p|p') &= \frac{1}{2\pi}\int_{-\pi}^{\pi} dx\;\delta(p - p' - \lambda\sin x) = \frac{1}{\lambda\pi}\int_{-1}^{+1}\frac{dy}{\sqrt{1-y^2}}\;\delta\left(y - \frac{p-p'}{\lambda}\right)\\ &= \frac{1}{\pi}\frac{1}{\sqrt{\lambda^2 - (p-p')^2}}\;\theta(\lambda - |p-p'|).\end{aligned} \tag{11.36}$$

Notice that $W_{\rm cl}(p|p')$ is a function of the momentum transfer $|\Delta p| = |p - p'|$ and vanishes for $|\Delta p| > \lambda$.

Consider now the kicked quantum rotator with measurements. From Eq. (11.8), the transition probability reads

$$W_{\rm q}(p=\hbar n|p'=\hbar n') = \frac{1}{\hbar}W_{nn'} = \frac{1}{\hbar}\left|\langle n|e^{-i\lambda\cos x/\hbar}|n'\rangle\right|^2 \tag{11.37}$$

and by using the definition (11.3) one obtains

$$\begin{aligned}\langle n|e^{-i\lambda\cos x/\hbar}|n'\rangle &= \int_{-\pi}^{\pi} dx\langle n|x\rangle e^{-i\lambda\cos x/\hbar}\langle x|n'\rangle \\ &= \frac{1}{2\pi}\int_{-\pi}^{\pi} dx\; e^{-i(n-n')x}e^{-i\lambda\cos x/\hbar} = i^{n-n'}J_{n-n'}\left(\frac{\lambda}{\hbar}\right),\end{aligned} \tag{11.38}$$

where $J_m(z)$ is the Bessel function of order m. Therefore, in the quantum case, from (11.37) and (11.38), we can write

$$W_{\rm q}(p=\hbar n|p'=\hbar n') = \frac{1}{\hbar}J_\nu\left(\frac{\lambda}{\hbar}\right)^2 \qquad (\Delta p = p-p' = \hbar\nu;\;\; \nu\equiv n-n'). \tag{11.39}$$

There are two important differences between the classical case (11.36) and its quantum counterpart (11.39): i) the quantum mechanical transition probability $W_{\rm q}$ admits only quantized values of momentum $\hbar n$, while the classical one $W_{\rm cl}$ is defined on the real line; ii) momentum can change by any value in the quantum case (notice however that this occurs with very small probability for $|\Delta p| = \hbar|\nu| \gg \lambda$ (Casati, Chirikov, Ford and Izrailev [1979])), while in the classical case this change is strictly constrained by $|\Delta p| \le \lambda$. These features have an interesting physical meaning: see Fig. 11.1. The transition probability of classical momentum appears as an "average" of its quantum counterpart, which explains the strong analogy discussed in Section 11.3. At the same time, the quantum mechanical transition probability has a small nonvanishing tail for $|\Delta p| = \hbar|\nu| > \lambda$: this is at the origin of the difference (11.31).

Finally, let us show how one recovers the transition probability $W_{\rm cl}$ starting from $W_{\rm q}$, in the semiclassical limit. We look at the limit $\hbar \to 0$, while keeping $\Delta p = \hbar\nu$ finite:

$$\hbar\to 0, \quad \nu\to\infty \quad \text{with} \quad \Delta p = \hbar\nu = \text{const.} \tag{11.40}$$

In this limit, the argument and the order of the Bessel function in (11.39) are infinities of the same order. For $|\Delta p| \le \lambda$, setting $\Delta p/\lambda \equiv \cos\beta$, one gets

$$\frac{\lambda}{\hbar} = \frac{\lambda}{\Delta p}\frac{\Delta p}{\hbar} = \nu\sec\beta. \tag{11.41}$$

Hence, by using the asymptotic limit of the Bessel function (Gradshteyn and Ryzhik [1994], §8.45)

$$J_\nu(\nu\sec\beta) \overset{\nu\ \text{large}}{\sim} \sqrt{\frac{2}{\nu\pi\tan\beta}}\left[\cos\left(\nu\tan\beta - \nu\beta - \frac{\pi}{4}\right) + \mathrm{O}(\nu^{-1})\right], \tag{11.42}$$

Eq. (11.39) becomes, in the limit (11.40),

$$\begin{aligned}W_{\rm q}(p|p') &= \frac{1}{\hbar}J_{\frac{\Delta p}{\hbar}}\left(\frac{\lambda}{\hbar}\right)^2 = \frac{1}{\hbar}J_\nu\left(\nu\sec\beta\right)^2 \\ &\sim \frac{1}{\hbar}\frac{2}{\frac{\Delta p}{\hbar}\pi\sqrt{\frac{\lambda^2}{\Delta p^2}-1}}\left[\cos^2\left(\frac{\Delta p}{\hbar}\sqrt{\frac{\lambda^2}{\Delta p^2}-1} - \frac{\Delta p}{\hbar}\arccos\frac{\Delta p}{\lambda} - \frac{\pi}{4}\right) + \mathrm{O}\left(\frac{\hbar}{\Delta p}\right)\right] \\ &\sim W_{\rm cl}(p|p')\left[1+\sin\left(\frac{2\sqrt{\lambda^2-\Delta p^2}}{\hbar} - \frac{2\Delta p}{\hbar}\arccos\frac{\Delta p}{\lambda}\right) + \mathrm{O}\left(\frac{\hbar}{\Delta p}\right)\right], \\ &\qquad\qquad (|\Delta p|\le\lambda)\end{aligned} \tag{11.43}$$

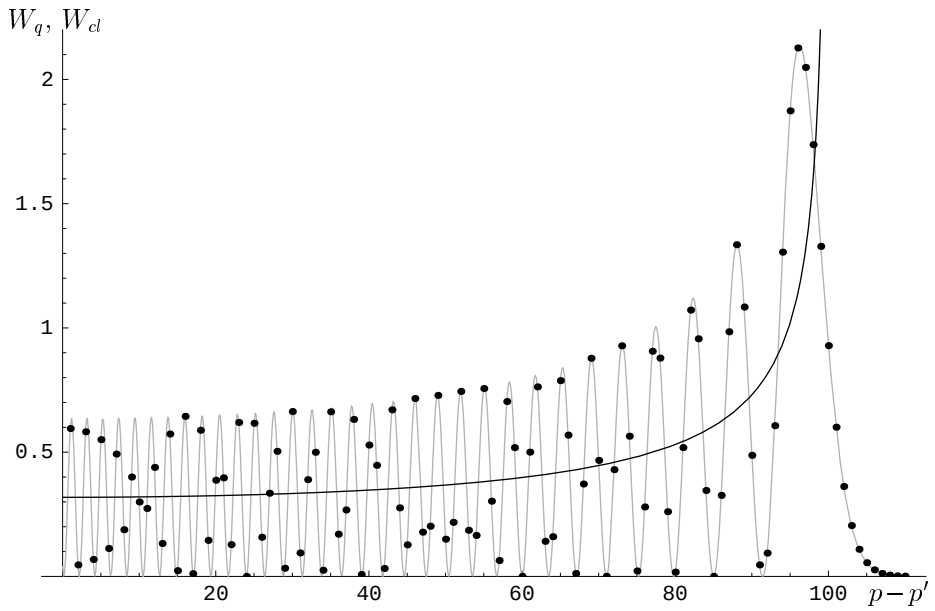

Figure 11.1: Momentum transition probabilities for the kicked rotator ($\lambda = 100\hbar$ and the momentum transfer $p - p'$ is expressed in units $\hbar$). The thick line is the classical expression (11.36): it diverges for $p-p' = \lambda$ and vanishes for $p-p' > \lambda$. The quantum mechanical transition probability (11.39) is defined only for integer values of $p - p'$ (dots). The interpolating line (obtained by treating the order of the Bessel function as a continuos variable) oscillates around its classical counterpart and is nonvanishing (although very small) outside the classical range, i.e. for $p - p' > \lambda$.

that, due to Riemann-Lebesgue lemma, tends to $W_{\rm cl}$ in the sense of distributions.

On the other hand, for $|\Delta p| > \lambda$, setting $\Delta p/\lambda \equiv \cosh\alpha$ and using the asymptotic formula (Gradshteyn and Ryzhik [1994], §8.45)

$$J_\nu\left(\frac{\nu}{\cosh\alpha}\right) \overset{\nu \text{ large}}{\sim} \frac{\exp(\nu\tanh\alpha - \nu\alpha)}{\sqrt{2\nu\pi\tan\beta}}\left[1 + \mathrm{O}(\nu^{-1})\right], \tag{11.44}$$

we get

$$W_{\rm q}(p|p') \sim \frac{1}{2\pi\sqrt{\Delta p^2 - \lambda^2}} \exp\left\{-\frac{2\Delta p}{\hbar}\left[\arccos\frac{\Delta p}{\lambda} - \sqrt{1 - \left(\frac{\lambda}{\Delta p}\right)^2}\right]\right\}\left[1 + \mathrm{O}\left(\frac{\hbar}{\Delta p}\right)\right], \quad (|\Delta p| > \lambda) \tag{11.45}$$

which vanishes exponentially with Δp (remember that $\tanh\alpha < \alpha$). Equations (11.43) and (11.45) corroborate the results of Section 11.3 and enable us to conclude that the "randomized" classical kicked rotator is just the semiclassical limit of the "measured" quantum kicked rotator.

11.5 Dynamical model of measurement

Needless to say, the very same results can be obtained by making only use of a purely unitary evolution (albeit, as we will see, of a larger system). To this end, we must give a model for measurement, by looking more closely at the physics of such a process. This is easily accomplished by following a strategy analogous to that outlined in Sec. 7.3 and using a generalized

spectral decomposition. Let us add the following decomposition Hamiltonian to (11.1)

$$H_{\rm dec} = \frac{\pi}{2} \sum_{n,k} |n\rangle\langle n| \otimes \sigma^{(n,k)} \delta(t - kT - \tau), \tag{11.46}$$

where $|n\rangle$ is an eigenstate of p and $\sigma^{(n,k)} \ \ \forall (n,k)$ is the first Pauli matrix, whose action is given by

$$\sigma^{(n,k)} |\pm\rangle_{(n,k)} = |\mp\rangle_{(n,k)}, \tag{11.47}$$

where $|+\rangle_{(n,k)}, |-\rangle_{(n,k)}$ denote spin up, down, respectively, in "channel" (n,k). This Hamiltonian "measures" each p-eigenstate by entangling it with a spin state. Let us prepare the total (rotator + spins) system in the initial ($t = 0^+$) state

$$|\Psi_{\rm in}\rangle = \sum_m c_m |m\rangle \bigotimes_{k,n} |-\rangle_{(n,k)} \tag{11.48}$$

(all "spins" down). For the sake of simplicity, we shall concentrate our attention on the first two kicks. In the same notation as in (11.9), the evolution of the state $|\Psi(N)\rangle \equiv |\Psi(NT + \tau^+)\rangle$ reads

$$|\Psi(0)\rangle = -i \sum_m c'_m |m\rangle \otimes |+\rangle_{(m,0)} \bigotimes_{k\geq 1,n} |-\rangle_{(n,k)} \ , \tag{11.49}$$

$$|\Psi(1)\rangle = (-i)^2 \sum_{\ell,m} |\ell\rangle \otimes |+\rangle_{(\ell,1)} \otimes A_{\ell m} c'_m |+\rangle_{(m,0)} \bigotimes_{k\geq 2,n} |-\rangle_{(n,k)} \ , \tag{11.50}$$

$$|\Psi(2)\rangle = (-i)^3 \sum_{j,\ell,m} |j\rangle \otimes |+\rangle_{(j,2)} \otimes A_{j\ell} |+\rangle_{(\ell,1)} \otimes A_{\ell m} c'_m |+\rangle_{(m,0)} \bigotimes_{k\geq 3,n} |-\rangle_{(n,k)} \ , \tag{11.51}$$

where $c'_m = c_m \exp[-iH_0(p_m)\tau]$ and

$$A_{\ell m} \equiv \langle \ell | U_{\rm free}(\tau) U_{\rm kick} U_{\rm free}(T - \tau) | m \rangle \tag{11.52}$$

is the transition amplitude (the transition probability beeing $W_{\ell m} = |A_{\ell m}|^2$). We see that at time τ after the kth kick, the nth eigenstate of the system becomes associated with spin up in channel (n,k). By using (11.50)-(11.51) one readily shows that the occupation probabilities evolve according to

$$P_n(2) \equiv \langle \Psi(2) | \Big(|n\rangle\langle n| \otimes \mathbf{1}_{\rm spins} \Big) |\Psi(2)\rangle = \sum_m W_{nm} P_m(1). \tag{11.53}$$

The generalization to N kicks is straightforward and it is very easy to obtain the same master equation (11.7). The observables of the quantum particle evolve therefore like in (11.11): in particular, the average value of the quantum observable $\tilde{p} = p \otimes \mathbf{1}_{\rm spins}$ displays diffusion with coefficients (11.19)-(11.20). This shows that the *unitary* dynamics engendered by (11.1) and (11.46) yields the same quantal diffusive behavior that is obtained by making use of projections. We notice indeed that, although the combined system (rotator + spins) evolves unitarily, if one chooses to "look" only at the rotator, by tracing away the spin degrees of freedom, the resulting dynamics (11.53) is non-unitary.

Note that the conclusion drawn in the previous section for the kicked rotator can be generalized to an arbitrary radial twisting map. The calculation and the techniques utilized are more involved and will not be considered here. There are also a number of related problems that deserve attention and a careful investigation. Among these, we just mention the case of imperfect quantum measurements, yielding a partial loss of quantum mechanical coherence, the relation to disordered systems, the Anderson localization (Flores [1999]) and finally the extension to a different class of Hamiltonians (Casati, Guarneri and Mantica [1994]; Frasca [1997]; Gardiner, Cirac and Zoller [1997]).

Chapter 12

Berry phase from a quantum Zeno effect

12.1 Introduction

In all the previous chapters we dealt with what might be called the "static" version of the quantum Zeno effect. However, the most striking action of the observer is not only to stop time evolution (e.g., by repeatedly checking if a system has decayed), but to *guide* it. In this last chapter we will be concerned with a "dynamical" version of the phenomenon: we will show how guiding a system through a closed loop in its state space (projective Hilbert space) leads to a geometrical phase (Pancharatnam [1956]; Berry [1984]; Berry [1985]; Shapere and Wilczek [1989]; Wagh, Rakhecha, Summhammer, Badurek, Weinfurter, Allman, Kaiser, Hamacher, Jacobson and Werner [1997]). This was predicted on general grounds (Aharonov and Anandan [1987]; Anandan and Aharonov [1988]), but here we use a specific implementation on a spin system (Facchi, Klein, Pascazio and Schulman [1999]) and propose a particular experimental context in which to see this effect. To this end we study the case of neutron spin, examine the practical aspects of realizing the "projections," and estimate the difference between the idealized projections and the experimental implementation. It is remarkable that the Berry phase that is discussed below is due to measurements only: no Hamiltonian is needed.

12.2 Forcing the pot to boil

We summarize again the main features of the quantum Zeno effect. Prepare a quantum system in some initial state $\psi(0)$. In time dt, by the Schrödinger equation, its phase changes by $\mathrm{O}(dt)$ while the absolute value of its scalar product with the initial state changes by $\mathrm{O}(dt^2)$. See Fig. 7.2.

The *dynamical* quantum Zeno effect exploits the above features and forces the evolution in an arbitrary direction by a series of repeated measurements: Let ψ evolve with the Hamiltonian H, so that in the absence of observations its evolution would be $\psi(T) = \exp(-iHT)\psi(0)$ (we take $\hbar = 1$ throughout). Let there be a family of states ϕ_k, $k = 0, 1, \ldots, N$, such that $\phi_0 = \psi(0)$, and such that successive states differ little from one another (i.e., $|\langle\phi_{k+1}|\phi_k\rangle|$ is nearly 1). Now let $\delta T = T/N$ and at $T_k = k\delta T$ project the evolving wave function on ϕ_k. Then for sufficiently large N, $\psi(T) \approx \phi_N$. [The usual QZE is the special case $\phi_k = \phi_0 (= \psi(0))\ \forall\ k$.]

In the following we consider an experiment involving a neutron spin. It should be clear, however, that our proposal is valid for any system with the same two-level structure.

12.2.1 Evolution with no Hamiltonian

Assume first that there is *no* Hamiltonian acting on the system: one can think, for instance, of a neutron crossing a region where no magnetic field is present. The time-evolution is due to measurement only.

The system starts with spin up along the z-axis and is projected on the family of states

$$\phi_k \equiv \exp(-i\theta_k \boldsymbol{\sigma}\cdot\boldsymbol{n}) \begin{pmatrix} 1 \\ 0 \end{pmatrix} \qquad \text{with } \theta_k \equiv \frac{ak}{N}\,, \qquad k = 0, \ldots, N\,, \tag{12.1}$$

where $\boldsymbol{\sigma}$ is the vector of the Pauli matrices and $\boldsymbol{n} = (n_x, n_y, n_z)$ a unit vector (independent of k).

We assume that the system evolves for a time T with projections at times $T_k = k\delta T$ ($k = 1, \ldots, N$ and $\delta T = T/N$). The final state is $\left[\phi_0 = \binom{1}{0}\right]$

$$\begin{aligned} |\psi(T)\rangle &= |\phi_N\rangle\langle\phi_N|\phi_{N-1}\rangle \cdots \langle\phi_2|\phi_1\rangle\langle\phi_1|\phi_0\rangle \\ &= |\phi_N\rangle \left(\cos\frac{a}{N} + in_z \sin\frac{a}{N}\right)^N \\ &= \cos^N\left(\frac{a}{N}\right)\left(1 + in_z \tan\frac{a}{N}\right)^N |\phi_N\rangle \\ &\overset{N\to\infty}{\longrightarrow} \exp(ian_z)|\phi_N\rangle \\ &= \exp(ian_z)\exp(-ia\boldsymbol{\sigma}\cdot\boldsymbol{n})|\phi_0\rangle. \end{aligned} \tag{12.2}$$

Therefore, as $N \to \infty$, $\psi(T)$ is an eigenfunction of the final projection operator P_N, with unit norm. If $\cos\Theta \equiv n_z$ and $a = \pi$,

$$\psi(T) = \exp(i\pi\cos\Theta)(-1)\phi_0 = \exp[-i\pi(1-\cos\Theta)]\phi_0 = \exp(-i\Omega/2)\phi_0, \tag{12.3}$$

where Ω is the solid angle subtended by the curve traced by the spin during its evolution. The factor $\exp(-i\Omega/2)$ is a Berry phase (Berry [1984]) and it is due only to measurements (the Hamiltonian is zero). Notice that no Berry phase appears in the usual quantum Zeno context, namely when $\phi_k \propto \phi_0\ \forall\ k$, because in that case $a = 0$ in (12.2).

To provide experimental implementation of the mathematical process just described, one could (in principle) let a neutron spin evolve in a field-free region of space. With no further tinkering, the spin state would not change. However, suppose we place spin filters sequentially projecting the neutron spin onto the states of (12.1), for $k = 0, \ldots, N$. Thus the neutron spin is forced to follow another trajectory in spin space. The essence of the mathematical demonstration just provided is that while N measurements are performed, the norm of wave function that is absorbed by the filters is $N\cdot\mathrm{O}(1/N^2) = \mathrm{O}(1/N)$. For $N \to \infty$, this loss is negligible. Meanwhile, as a result of these projections, the trajectory of the spin (in its space) is a cone whose symmetry axis is $\boldsymbol{n}$. By suitably matching the parameters, the spin state can be forced back to its initial state after time T (Schulman [1998]; Facchi, Klein, Pascazio and Schulman [1999]).

It is interesting to look at the process (12.2) for N finite. The spin goes back to its initial state after describing a regular polygon on the Poincaré sphere, as in Fig. 12.2.1a. After $N(< \infty)$ projections the final state is

$$|\psi(T)\rangle = \left(\cos\frac{a}{N} + in_z \sin\frac{a}{N}\right)^N \exp(-ia\boldsymbol{\sigma}\cdot\boldsymbol{n})|\phi_0\rangle. \tag{12.4}$$

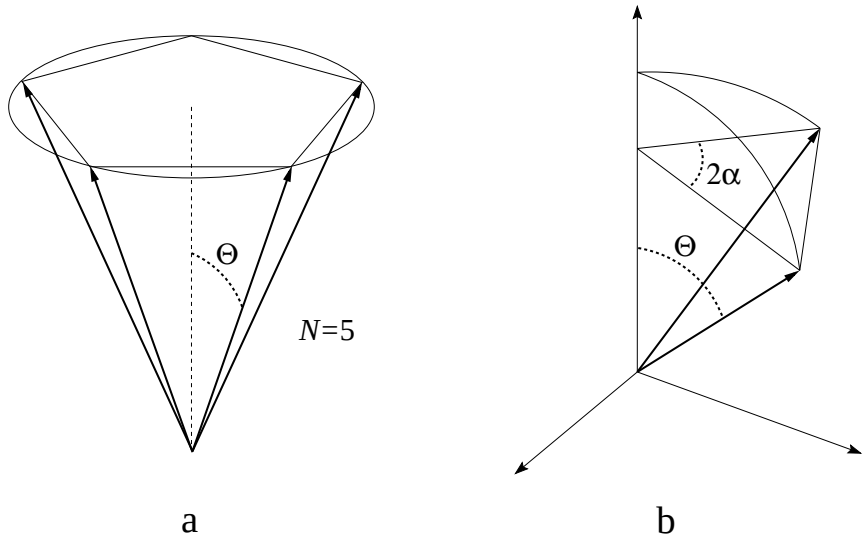

Figure 12.1: a) Spin evolution due to $N = 5$ measurements. b) Solid angles.

For $a = \pi$ the spin describes a closed path and

$$\begin{aligned} |\psi(T)\rangle &= \left(\cos\frac{\pi}{N} + in_z \sin\frac{\pi}{N}\right)^N \exp(-i\pi)|\phi_0\rangle \\ &= \left(\cos^2\frac{\pi}{N} + n_z^2 \sin^2\frac{\pi}{N}\right)^{\frac{N}{2}} \exp\left(iN \arctan\left(n_z \tan\frac{\pi}{N}\right)\right) \exp(-i\pi)|\phi_0\rangle. \end{aligned} \tag{12.5}$$

The first factor in the far r.h.s. accounts for the probability loss (N is finite and there is no QZE). We can rewrite (12.5) in the following form

$$|\psi(T)\rangle = \rho_N \exp(-i\beta_N)|\phi_0\rangle, \tag{12.6}$$

where

$$\rho_N = \left(\cos^2\frac{\pi}{N} + n_z^2 \sin^2\frac{\pi}{N}\right)^{\frac{N}{2}}, \tag{12.7}$$

$$\beta_N = \pi - N \arctan\left(\cos\Theta \tan\frac{\pi}{N}\right). \tag{12.8}$$

In the "continuous measurement" limit (QZE), we have

$$\begin{aligned} \rho &= \lim_{N\to\infty} \rho_N = 1, \\ \beta &= \lim_{N\to\infty} \beta_N = \pi(1 - \cos\Theta) = \frac{\Omega}{2}, \end{aligned} \tag{12.9}$$

where Ω is the solid angle subtended by the circular path, viewed at an angle Θ (see Fig. 12.2.1a). We recover therefore the result (12.3).

The relation between the solid angle and the geometrical phase is valid also with a finite number of polarizers N. Indeed, it is straightforward to show that the solid angle subtended by an isosceles triangle with vertex angle equal to 2α (Fig. 12.2.1b) has the value

$$\Omega_{2\alpha} = 2\alpha - 2\arctan(\cos\Theta \tan\alpha). \tag{12.10}$$

Hence if the polarizers are equally rotated of an angle $2\pi/N$, the spin describes a regular N-sided polygon, whose solid angle is

$$\Omega_{(N)} = N\Omega_{2\pi/N} = 2\pi - 2N \arctan\left(\cos\Theta \tan\frac{\pi}{N}\right) = 2\beta_N, \tag{12.11}$$

where we used the definition (12.8). This result is of course in agreement with other analyses (Bhandari and Samuel [1988]; Samuel and R. Bhandari [1988]; Mukunda and Simon [1993]) based on the Pancharatnam connection (Pancharatnam [1956]).

The above conclusion can be further generalized to the general case of an arbitrary (not necessarily regular) polygon. Indeed, if the polarizers are rotated at (relative) angles α_n with $n = 0, \ldots, N$, so that

$$\sum_{n=1}^{N} 2\alpha_n = 2\pi, \tag{12.12}$$

the solid angle is

$$\Omega'_{(N)} = \sum_{n=1}^{N} \Omega_{2\alpha_n} = 2\pi - 2\sum_{n=1}^{N} \arctan(\cos\Theta \tan\alpha_n). \tag{12.13}$$

This is also twice the Berry phase. Notice that if all $\alpha_n \to 0$ as $N \to \infty$ one again obtains the limit (12.3):

$$\Omega' = \lim_{N\to\infty} \Omega'_N = 2\pi - 2 \lim_{N\to\infty} \sum_{n=1}^{N} \alpha_n \cos\Theta = \Omega. \tag{12.14}$$

We emphasize that these predictions for the $N < \infty$ case are not trivial from the physical point of view. The above phases are computed by assuming that, during a "projection" *à la* von Neumann, the spin follows a geodesics on the Poincaré sphere. The mathematics of the projection has no such assumptions. The "postulate's" only job is to relate all this projection formalism to measurements.

12.2.2 Evolution with a non-zero Hamiltonian

Let us now consider the effect of a non-zero Hamiltonian

$$H = \mu\boldsymbol{\sigma}\cdot\boldsymbol{b}, \tag{12.15}$$

where $\boldsymbol{b} = (b_x, b_y, b_z)$ is a unit vector, in general different from $\boldsymbol{n}$. One can think of a neutron spin in a magnetic field. See Fig. 12.2.2.

If the system starts with spin up it would have the following—undisturbed—evolution:

$$\psi(t) = \exp(-i\mu t\boldsymbol{\sigma}\cdot\boldsymbol{b}) \begin{pmatrix} 1 \\ 0 \end{pmatrix}. \tag{12.16}$$

Now let the system evolve for a time T with projections at times $T_k = k\delta T$ ($k = 1, \ldots, N$ and $\delta T = T/N$) and Hamiltonian evolution in between. Defining $P_0 \equiv |\phi_0\rangle\langle\phi_0| = \begin{pmatrix} 1 & 0 \\ 0 & 0 \end{pmatrix}$, the 2×2 projection operator at stage-k is

$$P_k = |\phi_k\rangle\langle\phi_k| = \exp(-i\theta_k\boldsymbol{\sigma}\cdot\boldsymbol{n}) P_0 \exp(i\theta_k\boldsymbol{\sigma}\cdot\boldsymbol{n}) \tag{12.17}$$

and the state evolves to

$$\psi(T) = \left[\prod_{k=1}^{N} [P_k \exp(-i\mu\delta T\boldsymbol{\sigma}\cdot\boldsymbol{b})]\right] \begin{pmatrix} 1 \\ 0 \end{pmatrix}, \tag{12.18}$$

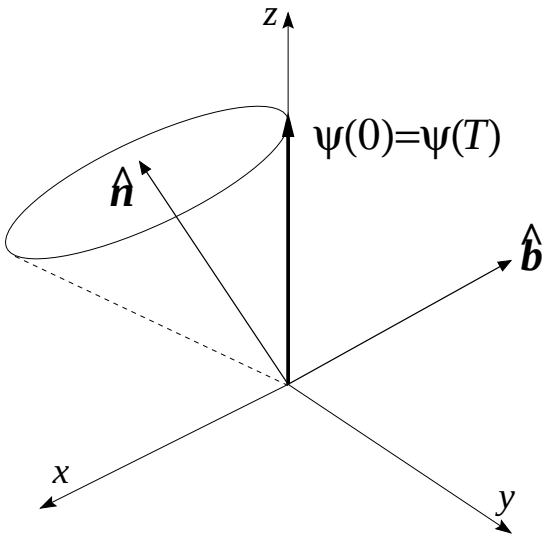

Figure 12.2: Spin evolution with measurements and non-zero Hamiltonian.

where here and in subsequent expressions a time-ordered product is understood [with earlier times (lower k) to the right]. Using $P_0^2 = P_0$, Eq. (12.18) can be rewritten

$$\psi(T) = \exp(-ia\boldsymbol{\sigma}\cdot\boldsymbol{n})\left[\prod_{k=1}^{N} B_k\right]\begin{pmatrix}1\\0\end{pmatrix}, \tag{12.19}$$

with

$$B_k \equiv P_0 \exp(i\theta_k\boldsymbol{\sigma}\cdot\boldsymbol{n})\exp(-i\mu\delta T\boldsymbol{\sigma}\cdot\boldsymbol{b})\exp(-i\theta_{k-1}\boldsymbol{\sigma}\cdot\boldsymbol{n})P_0 \tag{12.20}$$

($\theta_0 \equiv 0$). The computation of B_k requires a bit of SU(2) manipulation. One gets

$$\exp(i\theta\boldsymbol{\sigma}\cdot\boldsymbol{n})\boldsymbol{\sigma}\cdot\boldsymbol{b}\exp(-i\theta\boldsymbol{\sigma}\cdot\boldsymbol{n}) = \boldsymbol{\sigma}\cdot\widetilde{\boldsymbol{b}}, \tag{12.21}$$

with

$$\widetilde{\boldsymbol{b}}(\theta) \equiv \boldsymbol{b}\cos 2\theta + \boldsymbol{n}(\boldsymbol{b}\cdot\boldsymbol{n})(1-\cos 2\theta) + \boldsymbol{b}\times\boldsymbol{n}\sin 2\theta, \tag{12.22}$$

which is the vector $\boldsymbol{b}$ rotated by 2θ about the $\boldsymbol{n}$-axis. The calculation of B_k is now straightforward:

$$\begin{aligned} B_k &= P_0\exp(i\delta\theta\boldsymbol{\sigma}\cdot\boldsymbol{n})\exp(-i\mu\delta T\boldsymbol{\sigma}\cdot\widetilde{\boldsymbol{b}}(\theta_{k-1}))P_0 \\ &= P_0\left(1 + i\delta\theta\boldsymbol{\sigma}\cdot\boldsymbol{n} - i\mu\delta T\boldsymbol{\sigma}\cdot\widetilde{\boldsymbol{b}}(\theta_k)\right)P_0 + O(1/N^2), \end{aligned} \tag{12.23}$$

where $\delta\theta = \theta_{k+1} - \theta_k$ is k-independent. Second order terms in $1/N$ drop out when the product

(12.19) is computed for $N \to \infty$, so that

$$\begin{aligned}
\prod_{k=1}^{N} B_k &= \prod_{k=1}^{N} P_0(1 + i\delta\theta\boldsymbol{\sigma}\cdot\boldsymbol{n} - i\mu\delta T\boldsymbol{\sigma}\cdot\widetilde{\boldsymbol{b}}(\theta_k))P_0 \\
&= \prod_{k=1}^{N}\left\{P_0 + iP_0(\delta\theta\boldsymbol{\sigma}\cdot\boldsymbol{n} - \mu\delta T\boldsymbol{\sigma}\cdot\widetilde{\boldsymbol{b}}(\theta_k))P_0\right\} \\
&= \prod_{k=1}^{N} P_0\left\{1 + i[\delta\theta n_z - \mu\delta T\widetilde{b}_z(\theta_k)]\right\} \\
&= P_0\exp\left\{i\sum_{k=1}^{N}\left(\delta\theta n_z - \mu\delta T\widetilde{b}_z(\theta_k)\right)\right\} \qquad (12.24)
\end{aligned}$$

where we have used $P_0\sigma_x P_0 = P_0\sigma_y P_0 = 0$ and $P_0\sigma_z P_0 = P_0$. The continuum limit can be computed by letting the summations in (12.24) become integrals in dT and $d\theta$. Moreover, $\frac{dT}{d\theta} = \frac{T}{a}$, which enables one to change integration variable and get for the "(1,1)" component of $\prod_{k=1}^{N} B_k$ (all other components being zero)

$$\begin{aligned}
&\exp\left(in_z\int_0^a d\theta - i\mu\frac{T}{a}\int_0^a [b_z\cos 2\theta + (\boldsymbol{b}\cdot\boldsymbol{n})n_z(1-\cos 2\theta) + (\boldsymbol{b}\times\boldsymbol{n})_z\sin 2\theta]\,d\theta\right) \\
&= \exp\left(in_z a - i\mu\frac{T}{a}\left[b_z\frac{\sin 2a}{2} + (\boldsymbol{b}\cdot\boldsymbol{n})n_z\left(a - \frac{\sin 2a}{2}\right) + (\boldsymbol{b}\times\boldsymbol{n})_z\frac{1-\cos 2a}{2}\right]\right), \qquad (12.25)
\end{aligned}$$

The final state is an eigenstate of P_N with unit norm, *independent* of the Hamiltonian H:

$$\begin{aligned}
\psi(T) &= \exp\left(-i\mu\frac{T}{a}\left[b_z\frac{\sin 2a}{2} + (\boldsymbol{b}\cdot\boldsymbol{n})n_z\left(a - \frac{\sin 2a}{2}\right) + (\boldsymbol{b}\times\boldsymbol{n})_z\frac{1-\cos 2a}{2}\right]\right) \\
&\quad\times\exp\left(ian_z - ia\boldsymbol{\sigma}\cdot\boldsymbol{n}\right)\begin{pmatrix}1\\0\end{pmatrix}. \qquad (12.26)
\end{aligned}$$

The first factor in (12.26) is obviously the "dynamical phase." Note that up to a phase, $\psi(t)$ is just ϕ_k, with $k = tN/T$. Therefore

$$\begin{aligned}
\int_0^T \langle\psi(t)|H|\psi(t)\rangle dt &= \frac{T}{a}\int_0^a \langle\phi_0|\exp(i\theta\boldsymbol{\sigma}\cdot\boldsymbol{n})\mu\boldsymbol{\sigma}\cdot\boldsymbol{b}\exp(-i\theta\boldsymbol{\sigma}\cdot\boldsymbol{n})|\phi_0\rangle d\theta \\
&= \mu T\left[b_z\frac{\sin 2a}{2a} + (\boldsymbol{b}\cdot\boldsymbol{n})n_z\left(1 - \frac{\sin 2a}{2a}\right) + (\boldsymbol{b}\times\boldsymbol{n})_z\frac{1-\cos 2a}{2a}\right], \qquad (12.27)
\end{aligned}$$

because the phases drop out in the above sandwich. It follows that the remaining phase in (12.26), when the spin goes back to its initial state, is the geometrical phase. When $a = \pi$

$$\psi(T) = \exp\left(-i\Omega/2\right)\exp\left(-i\mu T(\boldsymbol{b}\cdot\boldsymbol{n})n_z\right)\begin{pmatrix}1\\0\end{pmatrix}, \qquad (12.28)$$

where Ω is the solid angle subtended by the curve traced out by the spin, as in (12.3), and $\mu T(\boldsymbol{b}\cdot\boldsymbol{n})n_z$ yields the dynamical phase, as can also be seen by direct computation of (12.27). We remark that if time ordered products are looked upon as path integrals (Hamilton and Schulman [1971]; Schulman [1981]; Kuratsuji [1988]), then our above demonstration is effectively a path integral derivation of the geometrical phase.

A practical implementation of the process just described would involve an experimental setup similar to the one described after (12.3), but with a magnetic field whose action on the spin is described by the Hamiltonian (12.15). If the neutron were to evolve *only* under the action of the Hamiltonian, its spin would precess around the magnetic field. However, the sequence of spin filters, which project the neutron spin onto the states (12.1), compel the spin to follow the same trajectory as in the previous case [Eq. (12.2)], i.e. a cone whose symmetry axis is $\boldsymbol{n}$. As above, the spin acquires a geometrical phase, but now there is a dynamical phase as well.

12.2.3 A particular case

It is instructive to look at a particular case of (12.26)-(12.28). We first note that if $\mu = 0$ in (12.26) we recover (12.2). Now let $\boldsymbol{b} = \boldsymbol{n}$. In this situation the projectors and the Hamiltonian yield the same trajectory in spin space (although, as will be seen, at different rates). If $\mu = 0$ (so that $H = 0$), the spin evolution is only due to the projectors and the final result was computed in (12.3)

$$\psi(T) = \exp(-i\Omega/2)\phi_0. \tag{12.29}$$

If, on the other hand, there is a nonvanishing Hamiltonian (12.15), but *no* projectors are present, a cyclic evolution of the spin is obtained for $\mu T = \pi$. The calculation is elementary and yields

$$\psi(T) = \exp(-i\pi)\phi_0. \tag{12.30}$$

Observe that the dynamical phase in this case is [$\mu T = \pi, \boldsymbol{b} = \boldsymbol{n}$ and $a = \pi$ in Eq. (12.27)]

$$\int_0^T \langle\psi(t)|H|\psi(t)\rangle dt = \pi n_z = \pi[1 - (1 - n_z)] = \pi - \Omega/2. \tag{12.31}$$

Therefore, the "π" phase in (12.30) can be viewed, *à la* Aharonov and Anandan (Aharonov and Anandan [1987]; Anandan and Aharonov [1988]), as the sum of a geometrical ($\Omega/2$) and a dynamical ($\pi - \Omega/2$) contribution.

Now let both the Hamiltonian and the projectors be present. From Eq. (12.28), one gets

$$\psi(T) = \exp\left(-i\Omega/2\right) \exp\left(-i\mu T n_z\right) \begin{pmatrix} 1 \\ 0 \end{pmatrix}, \tag{12.32}$$

Notice that the value of μ is now arbitrary, so that μT is not necessarily equal to π (the cyclic evolution of the spin is due to the projectors, not to the Hamiltonian). When $\mu T < \pi$, the projections are too "fast" and do not yield (12.30). On the other hand, when $\mu T > \pi$, the projections are too slow and supply less phase, in comparison with Eq. (12.30). Only in the case $\mu T = \pi$ do the projections yield the right phase in (12.30). Their presence is superfluous in this case: one would obtain exactly the same vector and the same phase without them. Our conclusions are summarized in Table 1. In some sense, one may say that the Hamiltonian dynamics provides a "natural clock" for the phase of the wave function.

Table 1: Phases for cyclic spin evolutions

	$H = 0$ and projections	$H = \mu\boldsymbol{\sigma} \cdot \boldsymbol{b}$ no projections	$H = \mu\boldsymbol{\sigma} \cdot \boldsymbol{b}$ and projections
ϕ_{geom}	$\Omega/2$	$\Omega/2$	$\Omega/2$
ϕ_{dyn}	0	$\pi - \Omega/2$	$\mu T n_z$
$\phi_{\text{tot}} = \phi_{\text{geom}} + \phi_{\text{dyn}}$	$\Omega/2$	$\pi(= \mu T)$	$\Omega/2 + \mu T n_z$
	cyclic evolution due to projections	cyclic evolution due to field	cyclic evolution due to projections

12.3 A Gedanken Experiment

An experimental implementation with neutrons would be difficult because it would involve putting a QZE set-up inside an interferometer in order to measure phase. We therefore restrict ourselves to a gedanken experiment (Facchi, Klein, Pascazio and Schulman [1999]) based on the use of ^{3}He as a neutron polarization filter (Heil, Andersen, Hofmann, Humblot, Kulda, Lelievre-Berna, Schärpf and Tasset [1998]). It is well known (Passel and Schermer [1966]) that Helium 3 is "black" to neutrons but *polarized* ^{3}He only absorbs one spin state of a neutron beam—hence acts as a 50% absorber of a beam; the rest of it emerges fully polarized. In practice an external magnetic field is used to maintain the polarization axis of the ^{3}He. If this external bias field were to be given a slow twist along a longitudinal axis, the state of polarization of the ^{3}He should follow the direction of the twist. A neutron beam propagating through a cell of high-pressure polarized ^{3}He along an axis aligned with the direction of twist will become fully polarized and should develop a Berry phase according to the argument of the previous section.

From an experimental perspective a significant problem is that we so far lack a notion of slowness (as when we speak of "slow twist" of the B field). In the previous calculation, it is implicitly assumed that θ changes more slowly than t (time): in other words, the relaxation processes in the ^{3}He are given enough time (are fast enough) to function as a polarizer. A full treatment of this problem should therefore describe the physics of the projection process. We now tackle this issue and see that the notion of slowness can be given quantitative meaning in terms of a condition for adiabaticity.

In practice, the absorption of the non-selected spin state occurs over a finite distance, of the order of one or two centimeters. This situation can be modeled via the following family of effective (nonhermitian) Hamiltonians [which are the straightforward generalization of the "static" Hamiltonian (7.54)]:

$$H_k = -iV|\phi_k^\perp\rangle\langle\phi_k^\perp|, \tag{12.33}$$

where V is a real constant and

$$\phi_k^\perp \equiv \exp(-i\theta_k \boldsymbol{\sigma}\cdot\boldsymbol{n}) \begin{pmatrix} 0 \\ 1 \end{pmatrix} \qquad \text{with} \quad \theta_k \equiv \frac{ak}{N}\,, \qquad k = 0, \ldots, N\,. \tag{12.34}$$

Note that $\langle\phi_k|\phi_k^\perp\rangle = 0$ [see Eq. (12.1)]. We first assume, for simplicity, that no external (^{3}He aligning) magnetic field is present. We define

$$P_k^\perp \equiv |\phi_k^\perp\rangle\langle\phi_k^\perp| = \exp(-i\theta_k\boldsymbol{\sigma}\cdot\boldsymbol{n}) P_0^\perp \exp(i\theta_k\boldsymbol{\sigma}\cdot\boldsymbol{n}) \qquad (P_0^\perp = |\phi_0^\perp\rangle\langle\phi_0^\perp|)\,. \tag{12.35}$$

Obviously $P_k^\perp = 1 - P_k$, where P_k was defined in (12.17). The evolution engendered by the above Hamiltonian reads

$$e^{-iH_k\tau} = P_k + \epsilon P_k^\perp = \exp(-i\theta_k\boldsymbol{\sigma}\cdot\boldsymbol{n}) \begin{pmatrix} 1 & 0 \\ 0 & \epsilon \end{pmatrix} \exp(i\theta_k\boldsymbol{\sigma}\cdot\boldsymbol{n}) \equiv P_k', \tag{12.36}$$

where (inserting $\hbar$)

$$\epsilon \equiv e^{-V\tau/\hbar} \tag{12.37}$$

is a parameter yielding an estimate of the efficiency of the polarizer. One can estimate a minimal value for V: for a thermal neutron (speed $v \simeq 2000$m/s) and an absorption length ℓ on the order of 1 cm for the wrong-spin component, one gets $\tau = \ell/v \simeq 5\mu$s and one obtains a good polarizer for $V > \hbar/\tau \simeq 10^{-29}$ J $\simeq 10^{-7}$ meV.

The evolution can be computed by using the technique of Section 12.2 ($\sqrt{P_0'} = P_0 + \epsilon^{1/2} P_0^{\perp}$):

$$\psi'(T) = \exp(-ia\boldsymbol{\sigma}\cdot\boldsymbol{n})\sqrt{P_0'}\left[\prod_{k=1}^{N} B_k'\right]\begin{pmatrix}1\\0\end{pmatrix}, \tag{12.38}$$

with $T = N\tau$ and

$$\begin{aligned}\prod_{k=1}^{N} B_k' &= \prod_{k=1}^{N}\sqrt{P_0'}(1+i\delta\theta\boldsymbol{\sigma}\cdot\boldsymbol{n})\sqrt{P_0'} = \prod_{k=1}^{N} P_0' + i\sqrt{P_0'}(\delta\theta\boldsymbol{\sigma}\cdot\boldsymbol{n})\sqrt{P_0'}\\ &= \begin{pmatrix}1+i\delta\theta n_z & i\delta\theta\epsilon^{1/2}n_-\\ i\delta\theta\epsilon^{1/2}n_+ & \epsilon(1-i\delta\theta n_z)\end{pmatrix}^N,\end{aligned} \tag{12.39}$$

where $n_\pm \equiv n_x \pm i n_y$. The evaluation of the above matrix product when $N \to \infty$ is lengthy but straightforward and is given in Appendix A. One gets

$$\psi'(T) = \exp(-ia\boldsymbol{\sigma}\cdot\boldsymbol{n})\mathcal{M}\phi_0, \tag{12.40}$$

where

$$\mathcal{M} = \frac{e^{-ab}}{\Delta}\begin{pmatrix}\Delta\,\mathrm{ch}(a\Delta) + (b+in_z)\,\mathrm{sh}(a\Delta) & in_-\,\mathrm{sh}(a\Delta)\\ in_+\,\mathrm{sh}(a\Delta) & \Delta\,\mathrm{ch}(a\Delta) - (b+in_z)\,\mathrm{sh}(a\Delta)\end{pmatrix}, \tag{12.41}$$

with

$$b = \frac{VT}{2a\hbar}, \qquad \Delta = \sqrt{b^2 + 2ibn_z - 1}. \tag{12.42}$$

We are interested in the limit of large $b = VT/2a\hbar$. Indeed, larger values of b correspond to more ideal polarizers. In fact $\gamma = V/\hbar$ represents the absorption rate of the wrong component of the spin, while $\omega = 2a/T$ is the angular velocity of precession (the spin describes an angle of $2a$ in time T). The parameter $b = \gamma/\omega$ is the ratio of these two quantities. Large values of b imply

$$\gamma \gg \omega, \tag{12.43}$$

i.e., an absorption rate much larger than the velocity of precession. In other words, the spin rotation must be sufficiently slow to allow the absorption of the wrong component of the spin. By introducing the neutron speed v, one can define the absorption length $\ell = v/\gamma = v\hbar/V$ and the length covered by the neutron while rotating for 1 rad, $L = v/\omega = vT/2a$. Hence (12.43) reads

$$L \gg \ell. \tag{12.44}$$

These are all conditions of adiabaticity.

In the large b limit, using the definition (12.42), (12.41) becomes

$$\begin{aligned}\mathcal{M} &= \frac{e^{a(\Delta-b)}}{2\Delta}\begin{pmatrix}\Delta+b+in_z & in_-\\ in_+ & \Delta-b-in_z\end{pmatrix} + \mathrm{O}(e^{-2ab})\\ &= \exp(ian_z)\begin{pmatrix}1-a\frac{1-n_z^2}{2b} & i\frac{n_-}{2b}\\ i\frac{n_+}{2b} & 0\end{pmatrix} + \mathrm{O}\left(\frac{1}{b^2}\right).\end{aligned} \tag{12.45}$$

Remembering the definition of b in (12.42), one gets

$$\begin{aligned}\mathcal{M} &= \exp(ian_z)\begin{pmatrix}1+\frac{\hbar a^2(n_z^2-1)}{VT} & i\frac{\hbar a n_-}{VT}\\ i\frac{\hbar a n_+}{VT} & 0\end{pmatrix} + \mathrm{O}\left(\left(\frac{2a\hbar}{VT}\right)^2\right)\\ &\longrightarrow \exp(ian_z)P_0, \quad \text{when} \quad \frac{VT}{2a\hbar} \to \infty.\end{aligned} \tag{12.46}$$

The above formula yields the first corrections to an ideal, purely adiabatic evolution. Basically, the system is projected on slightly different directions, thereby rotating in spin space. But if the system "on its own" (i.e., through its dynamics) manages to rotate significantly between projections, then more will be absorbed on the next projection and it will not follow the rotating field, at least not without loss of probability (or intensity).

It is interesting to note that the same result can be obtained by considering a continuous version of the effective Hamiltonian (12.33)

$$H(t) = -iVP^{\perp}(t) = -iVU^{\dagger}(t)P_0^{\perp}U(t), \tag{12.47}$$

where

$$U(t) = \exp\left(i\frac{a}{T}t\,\boldsymbol{\sigma}\cdot\boldsymbol{n}\right) \tag{12.48}$$

is a unitary operator (rotation). The state vector $\psi(t)$ satisfies the Schrödinger equation

$$i\partial_t\psi(t) = H(t)\psi(t). \tag{12.49}$$

Consider now the following rotated vector

$$\widetilde{\psi}(t) = U(t)\psi(t). \tag{12.50}$$

It is easy to prove that it satisfies the equation

$$i\partial_t\widetilde{\psi}(t) = \widetilde{H}\widetilde{\psi}(t), \tag{12.51}$$

where

$$\widetilde{H} = i\dot{U}(t)U^{\dagger}(t) + U(t)H(t)U^{\dagger}(t) = -\frac{a}{T}\boldsymbol{\sigma}\cdot\boldsymbol{n} - iVP_0^{\perp} \tag{12.52}$$

is independent of t. One then gets

$$\psi(t) = U^{\dagger}(t)\widetilde{\psi}(t) = \exp\left(-i\frac{a}{T}t\,\boldsymbol{\sigma}\cdot\boldsymbol{n}\right)\exp(-i\widetilde{H}t)\psi(0), \tag{12.53}$$

where

$$\widetilde{H}T = -a\boldsymbol{\sigma}\cdot\boldsymbol{n} - iVTP_0^{\perp} = -aM, \quad M = \begin{pmatrix} n_z & n_- \\ n_+ & -n_z + i2b \end{pmatrix}, \tag{12.54}$$

b being defined in (12.42). Hence one obtains

$$\exp(-i\widetilde{H}T) = \exp(iaM) = \mathcal{M} \tag{12.55}$$

and (12.53) yields (12.40). Observe that

$$\widetilde{H} = -\omega\frac{\boldsymbol{\sigma}\cdot\boldsymbol{n}}{2} - i\gamma P_0^{\perp}, \tag{12.56}$$

from which it is apparent the previous interpretation of the coefficients ω and γ.

The above calculation was performed by assuming that no external field is present. However, we do need an external B field, in order to align ^{3}He. Its effect can be readily taken into account by noticing that, when the neutron crosses the region containing polarized ^{3}He, if the conditions for adiabaticity are satisfied, the neutron spin will always be (almost) parallel to the direction of ^{3}He and therefore to the direction of the magnetic field. The resulting dynamical phase is therefore trivial to compute and reads $\phi_{\rm dyn} \simeq \mu BT/\hbar$. In order to obtain the geometric phase in a realistic experiment, such a dynamical phase should be subtracted from the total phase acquired by the neutron during its interaction with ^{3}He. Incidentally, notice that this

is experimentally feasible: one can take into account the contribution of a large dynamical phase due to the magnetic field and neatly extract a small Berry phase (Bitter and Dubbers [1987]; Wagh, Rakhecha, Fischer and Ioffe [1998]). The novelty of our proposal consists in the introduction of polarizing ^{3}He to force the neutron spin to follow a given trajectory in spin space.

An alternative realization relies on a set of discrete ^{3}He polarization filters with progressively tilted polarization axes, as a finite-difference approximation to the system discussed above. Such a system would be a neutron analog of a set of polaroid filters with progressively tilted axes through which a photon beam propagates with little or no loss (in the limit of small angles) as proposed by Peres [1980a]. However, in the case discussed above, the axes of the neutron polarizers need not belong to a single plane and the neutron can acquire a Berry phase as well as change in polarization direction.

The extension of this last property to photons, by making use of polarizers and mirrors, is not straightforward, because of "cancellation" effects (Facchi and Pascazio [1999a]), ultimately due to the transversality of photon polarization, and indeed would deserve to be studied in greater detail.

Conclusions and outlook

In this thesis we have discussed the features of quantum time evolution, concentrating our attention on the form factor of the interaction and the analytical properties of the propagator in the complex energy plane. We have seen that the exponential decay is given by a simple pole on the second Riemann sheet and that all corrections at short and long times are given by the contribution of other singularities in the energy plane.

Moreover, we have seen that all interesting effects are ultimately ascribable to this richer analytical structure of the propagator. The whole collection of phenomena known as quantum Zeno effects is only due to the presence of such a structure. A simple pole propagator, yielding a purely exponential decay, would be completely "transparent" to Zeno effects.

We have extended the traditional formulation in terms of projections to a more general framework, which include the latter as a particular case. According to this theoretical scheme, these effects are obtained if the (Hamiltonian) dynamics is such that the interaction takes a sort of "close look" at the system. When such an interaction can be effectively described as a projection operator *à la* von Neumann, we obtain the usual formulation of the quantum Zeno effect in the limit of very frequent measurements. Otherwise, if the description in terms of projection operators does not apply, but one can still properly think in terms of a "continuous gaze" at the system, an intuitive explanation in terms of Zeno can still be very appealing and intuitive.

We believe that this approach is prolific. Not only it often yields a simple intuitive picture of the dynamical features of the system, it also enables one to look at these dynamical features from a different, new perspective: the very concept of inverse Zeno effect is a good example.

Somewhat surprisingly, we have seen that quantum Zeno effects are not an exotic property of quantum theory, manifesting itself in rather peculiar situations. By contrast, they are very common phenomena! We have found links with instability (Chap. 9), chaos (Chap. 11) and geometrical phases (Chap. 12). Further possible links with new neutron interferometric experiments (Facchi, Mariano and Pascazio [1999]; Facchi, Mariano and Pascazio [2000a]; Facchi, Mariano and Pascazio [2000b]), decoherence (Namiki, Pascazio and Nakazato [1997]) and mesoscopic physics (Facchi and Pascazio [2000b]) have not been considered here, but deserve a further investigation. The very fact that these links may not always be obvious is in itself a motivation to pursue the investigation in this direction.

There is another open problem to be investigated in the future. It is the description of unstable particles in relativistic quantum field theory (Schwinger [1960]). In particle physics, from the perspective outlined in this work, there are two "kinds" of unstable particle: elementary particles such as μ and τ leptons, which decay through weak interaction, and composite particles such as all hadronic resonances and neutrons (and maybe protons). The latter ones are particles with a finite size, i.e. with a finite form factor. Therefore, according to our analysis, they exhibit an initial quadratic Zeno region. On the other hand, the first ones are pointlike particles with a constant form factor and the Zeno region seems to be absent. Therefore their decay law seems to be very different, from the theoretical point of view (Bernardini, Maiani

and Testa [1993]; Facchi and Pascazio [1998]; Joichi, Matsumoto and Yoshimura [1998]; Facchi and Pascazio [1999b]). Furthermore, this property could be used to distinguish between these two classes. The resolution of this problem could have unexpected byproducts: indeed the decay of finite-size particles could be modified in sufficiently strong fields, arising in particular situations such as the early universe, yielding relevant cosmological effects. There is probably more to come, in the context of the quantum Zeno effects: maybe, additional surprises will show up in the next future.

Appendix A

We compute here the matrix product (12.39) and its $N \to \infty$ limit (12.41).

Let $\tau = T/N$ in (12.37). For large values of N

$$\epsilon = \exp\left(-\frac{VT}{N}\right) = 1 - \frac{VT}{N} + \mathrm{O}\left(\frac{1}{N^2}\right). \tag{A.1}$$

Notice that $\epsilon \to 1$ when $N \to \infty$.

For an infinitesimal time interval the matrix in (12.39) reads

$$\begin{aligned} A &\equiv \begin{pmatrix} 1 + i\delta\theta n_z & i\delta\theta\epsilon^{1/2} n_- \\ i\delta\theta\epsilon^{1/2} n_+ & \epsilon(1 - i\delta\theta n_z) \end{pmatrix} \\ &= \begin{pmatrix} 1 + i\frac{an_z}{N} & i\frac{an_-}{N} \\ i\frac{an_+}{N} & 1 - i\frac{an_z}{N} - \frac{VT}{N} \end{pmatrix} + \mathrm{O}\left(\frac{1}{N^2}\right) \\ &= 1 + i\frac{a}{N} M + \mathrm{O}\left(\frac{1}{N^2}\right), \end{aligned} \tag{A.2}$$

where we have defined

$$M = \begin{pmatrix} n_z & n_- \\ n_+ & -n_z + i2b \end{pmatrix}, \qquad b = \frac{VT}{2a}. \tag{A.3}$$

We are interested in the $N \to \infty$ limit

$$\mathcal{M} = \lim_{N\to\infty} \sqrt{P_0'} A^N \lim_{N\to\infty} A^N = \lim_{N\to\infty} \left(1 + i\frac{a}{N} M\right)^N = \exp(iaM), \tag{A.4}$$

where one gets

$$\psi'(T) = \exp(-ia\boldsymbol{\sigma}\cdot\boldsymbol{n})\mathcal{M}\phi_0. \tag{A.5}$$

We need to compute the matrix $\mathcal{M}$. To this purpose we have to diagonalize M. The eigenvalue equation, $\det(M - \lambda I) = 0$, reads

$$\lambda^2 - i2b\lambda + i2bn_z - 1 = 0 \tag{A.6}$$

and has the solutions

$$\lambda_{1/2} = i(b \mp \Delta), \qquad \Delta = \sqrt{b^2 + 2ibn_z - 1}. \tag{A.7}$$

The matrix that diagonalizes M is

$$S = \begin{pmatrix} n_- & n_- \\ -n_z + ib - i\Delta & -n_z + ib + i\Delta \end{pmatrix} \tag{A.8}$$

and its inverse is

$$S^{-1} = \frac{1}{2in_-\Delta} \begin{pmatrix} -n_z + ib + i\Delta & -n_- \\ -n_z + ib - i\Delta & n_- \end{pmatrix}. \tag{A.9}$$

Hence we have

$$S^{-1}MS = D = \begin{pmatrix} \lambda_1 & 0 \\ 0 & \lambda_2 \end{pmatrix} = i \begin{pmatrix} b-\Delta & 0 \\ 0 & b+\Delta \end{pmatrix}, \tag{A.10}$$

and finally

$$\mathcal{M} = \exp(iaM) = S\exp(iaD)S^{-1} = Se^{-ab}\begin{pmatrix} e^{a\Delta} & 0 \\ 0 & e^{-a\Delta} \end{pmatrix} S^{-1}. \tag{A.11}$$

Evaluating the matrix product (A.11), after some algebra, one obtains

$$\mathcal{M} = \frac{e^{-ab}}{\Delta}\begin{pmatrix} \Delta\ \mathrm{ch}(a\Delta) + (b+in_z)\ \mathrm{sh}(a\Delta) & in_-\ \mathrm{sh}(a\Delta) \\ in_+\ \mathrm{sh}(a\Delta) & \Delta\ \mathrm{ch}(a\Delta) - (b+in_z)\ \mathrm{sh}(a\Delta) \end{pmatrix}, \tag{A.12}$$

which is Eq. (12.41) of the text.

Bibliography

Accardi, L., S. V. Kozyrev and I. V. Volovich, 1997, *Dynamics of dissipative two-level systems in the stochastic approximation,* Phys. Rev. **A56**, 2557

Accardi, L., Y.G. Lu and I. V. Volovich, 2000, Quantum Theory and Its Stochastic Limit (Springer-Verlag, New York).

Aharonov, Y., and J. Anandan, 1987, *Phase Change during a Cyclic Quantum Evolution,* Phys. Rev. Lett. **58**, 1593.

Akhiezer, A.I., and V.B. Berestetskii, 1965, Quantum electrodynamics (Interscience Publ., New York).

Altenmuller, T.P., and A. Schenzle, 1994, *Quantum Zeno effect in a double-well potential: A model of a physical measurement,* Phys. Rev. **A49**, 2016.

Alvarez-Estrada, R.F., and J.L. Sánchez-Gómez, 1999, *On the absence of the Zeno effect in relativistic quantum field theory,* Phys. Lett. **A253**, 252.

Anandan, J., and Y. Aharonov, 1988, *Geometric quantum phase and angles,* Phys. Rev. **D38**, 1863.

Araki, H., Y. Munakata, M. Kawaguchi and T. Goto, 1957, *Quantum Field Theory of Unstable Particles,* Progress of Theoretical Physics **17**, 419.

Armstrong, L.A., N. Bloembergen, J. Ducuing and P.S. Pershan, 1962, *Interaction between Light Waves in a Nonlinear Dielectric,* Phys. Rev. **127**, 1918.

Arnold, V.I., 1989, Mathematical Methods of Classical Mechanics (Springer-Verlag, Berlin).

Arnold, V.I., 1992, Ordinary Differential Equations (Springer-Verlag, Berlin).

Arnold, V.I., and A. Avez, 1968, Ergodic Problems of Classical Mechanics (Benjamin, New York).

Autler, S.H., and C.H. Townes, 1955, *Stark Effect in Rapidly Varying Fields,* Phys. Rev. **100**, 703.

Ballentine, L.E., 1991, *Comment on "Quantum Zeno effect",* Phys. Rev. **A43**, 5165.

Beige, A., and G. Hegerfeldt, 1996, *Projection postulate and atomic quantum Zeno effect,* Phys. Rev. **A53**, 53.

Berestetskii, V.B., E.M. Lifshits and L.P. Pitaevskii, 1982, Quantum electrodynamics (Pergamon Press, Oxford), Chapter 5.

Bernardini, C., L. Maiani and M. Testa, 1993, *Short-time behavior of unstable systems in field theory and proton decay,* Phys. Rev. Lett. **71**, 2687.

Berry, M.V., 1984, *Quantal phase factors accompanying adiabatic changes,* Proc. Roy. Soc. London **A392**, 45.

Berry, M.V., 1985, *Classical adiabatic angles and quantal adiabatic phase,* J. Phys. **A18**, 15.

Berry, M., 1995, *Two-State Quantum Asymptotics,* in: Fundamental Problems in Quantum Theory, eds D.M. Greenberger and A. Zeilinger (Ann. N.Y. Acad. Sci. **Vol. 755**, New York), p. 303.

Berry, M.V., and N.L. Balazs, 1979, *Evolution of semiclassical quantum states in phase space,* J. Phys. **A12**, 625.

Berry, M.V., N.L. Balazs, M. Tabor and A. Voros, 1979, *Quantum Maps,* Ann. Phys. **122**, 26.

Berry, M.V., and S. Klein, 1996, *Geometric phases from stacks of crystal plates,* J. Mod. Optics **43**, 165.

Beskow, A., and J. Nilsson, 1967, Arkiv für Fysik **34**, 561.

Bhandari, R., and J. Samuel, 1988, *Observation of topological phase by use of a laser interferometer,* Phys. Rev. Lett. **60**, 1211.

Bitter, T., and D. Dubbers, 1987, *Manifestation of Berry's topological phase in neutron spin rotation,* Phys. Rev. Lett. **59**, 251.

Bjorken, J.D., and S.D. Drell, 1964, Relativistic Quantum Mechanics (McGraw-Hill, New York).

Blanchard, Ph., and A. Jadczyk, 1993, *Strongly coupled quantum and classical systems and Zeno's effect,* Phys. Lett. **A183**, 272.

Block, F., 1946, *Nuclear Induction,* Phys. Rev. **70**, 460.

Bocchieri, F., and L. Loinger, 1957, *Quantum Recurrence Theorem,* Phys. Rev. **107**, 337.

Bohr, H., 1932, Fastperiodische Funktionen (Verlag Julius Springer, Berlin).

Boller, K.J., A. Imamoğlu and S.E. Harris, 1991, *Observation of electromagnetically induced transparency,* Phys. Rev. Lett. **66**, 2593.

Breit, G., and E.P. Wigner, 1936, *Capture of Slow Neutrons,* Phys. Rev. **49**, 519.

Brown, L.S., 1992, Quantum field theory (Cambridge University Press, Bristol).

Casati, G., B.V. Chirikov, J. Ford and F.M. Izrailev, 1979, *Stochastic behavior of a quantum pendulum under a periodic perturbation,* in: Stochastic behaviour in classical and quantum Hamiltonian systems, edited by G. Casati and J. Ford, Lecture Notes in Physics (Springer-Verlag, Berlin) **93**, 334.

Casati, G., B.V. Chirikov, D.L. Shepelyansky and I. Guarneri, 1987, *Relevance of classical chaos in quantum mechanics: the hydrogen atom in a monochromatic field,* Phys. Rep. **154**, 77.

Casati, G., I. Guarneri and G. Mantica, 1994, *Classical stabilization of periodically kicked hydrogen atoms,* Phys. Rev. **A50**, 5018.

Chirkin, A.S., and V.V. Volkov, 1998, *Consecutive quasi-phase-matched interactions of light waves in periodically poled nonlinear optical crystals,* J. Russian Laser Research **19**, 409.

Chiu, C.B., E.C.G. Sudarshan and B. Misra, 1977, *Time evolution of unstable quantum states and a resolution of Zeno's paradox,* Phys. Rev. **D16**, 520.

Cho, G.-C., H. Kasari and Y. Yamaguchi, 1993, *The Time Evolution of Unstable Particles,* Prog. Theor. Phys. **90**, 803.

Cohen-Tannoudji, C., J. Dupont-Roc and G. Grynberg, 1988, Atom-Photon Interactions: Basic Processes and Applications (Wiley, New York).

Cohen-Tannoudji, C., and S. Reynaud, 1977, *Dressed-atom description of resonance fluorescence and absorption spectra of a multi-level atom in an intense laser beam,* J. Phys. **B10**, 345.

Cohen-Tannoudji, C., and S. Reynaud, 1977, *Modification of resonance Raman scattering in very intense laser fields,* J. Phys. **B10**, 365.

Cohen-Tannoudji, C., and S. Reynaud, 1977, J. Phys. **B10**, 2311.

Cook, R.J., 1988, *What are quantum jumps?,* Phys. Scr. **T21**, 49.

Dancoff, S., 1950, *Non-Adiabatic Meson Theory of Nuclear Forces,* Phys. Rev. **78**, 382.

Davidovich, L., and H.M. Nussenzveig, 1980, *Theory of Natural Line Shape,* in: Foundations of radiation theory and quantum electrodynamics, ed. A.O. Barut (Plenum, New York), p.83.

Dirac, P.A.M., 1958, The principles of quantum mechanics (Oxford University Press, London).

Enaki, N.A., 1996, *The dynamics of spontaneous decay on short and long time scales,* Zh. Eksp. Teor. Fiz. **109**, 1130 [Sov. Phys. JETP **82**, 607 (1996)].

Ersak,I. , 1969, Yad. Fiz. **9**, 458 [Sov. Journ. Nucl. Phys. **9**, 263].

Facchi,P., 2000, *Van Hove's limit in relativistic quantum field theory,* BA-TH/00-385.

Facchi, P., A. G. Klein, S. Pascazio and L.S. Schulman, *Berry phase from a quantum Zeno effect,* 1999, Phys. Lett. **A257**, 232.

Facchi, P., A. Mariano and S. Pascazio, 1999, *Wigner function and coherence properties of cold and thermal neutrons,* Acta Phys. Slov. **49**, 677.

Facchi, P., A. Mariano and S. Pascazio, 2000, *Decoherence in neutron interferometry,* Physica **B276-278**, 970.

Facchi, P., A. Mariano and S. Pascazio, *Decoherence vs entropy in neutron interferometry,* quant-ph/9906118.

Facchi, P., H. Nakazato and S. Pascazio, 2000, *From the quantum Zeno to the inverse quantum Zeno effect,* quant-ph/0006094.

Facchi, P., H. Nakazato, S. Pascazio, J. Peřina and J. Řeháček, 2000, *Stability and instability in parametric resonance and quantum Zeno effect,* quant-ph/0004039.

Facchi, P., and S. Pascazio, 1998, *Temporal behavior and quantum Zeno time of an excited state of the hydrogen atom,* Phys. Lett. **A241**, 139.

Facchi, P., and S. Pascazio, 1999, *Berry phase due to quantum measurements,* Acta Phys. Slov. **49**, 671.

Facchi, P., and S. Pascazio, 1999, La regola d'oro di Fermi (Bibliopolis, Napoli). [In Italian]

Facchi, P., and S. Pascazio, 1999, *Deviations from exponential law and Van Hove's "$\lambda^2 t$" limit,* Physica **A271**, 133.

Facchi, P., and S. Pascazio, 1999, *Van Hove's "$\lambda^2 t$" limit in nonrelativistic and relativistic field-theoretical models,* quant-ph/9910111.

Facchi, P., and S. Pascazio, 2000, *Spontaneous emission and lifetime modification caused by an intense electromagnetic field,* Phys. Rev. **A62**, 023804.

Facchi, P., and S. Pascazio, 2000, *Mesoscopic interference,* BA-TH/00-386.

Facchi, P., and S. Pascazio, 2001, *Quantum Zeno and Inverse Quantum Zeno Effects,* to appear in: Progress in Optics.

Facchi, P., S. Pascazio and A. Scardicchio, 1999, *Measurement-Induced Quantum Diffusion,* Phys. Rev. Lett. **83**, 61.

Facchi, P., S. Pascazio and A. Scardicchio, 1999, *Quantum chaos induced by measurements,* quant-ph/9906060, in: Proceedings of the Symposium on "Mathematical Aspects of Quantum Information and Quantum Chaos", (Kyoto, Japan).

Fano, U., 1961, *Effects of Configuration Interaction on Intensities and Phase Shifts,* Phys. Rev. **124**, 1866.

Fejer, M.M., G.A. Magel, D.H. Jundt and R.L. Byer, 1992, *Quasi-phase-matched second harmonic generation: tuning and tolerances,* IEEE J. Quant. Electron. **28**, 2631.

Fenn, J.G., D.A. Bayne and B.D. Sinclair, 1998, *Experimental investigation of the "effective potential" pf an inverted pendulum,* Am. J. Phys. **66**, 981.

Fermi, E., 1932, *Quantum Theory of Radiation,* Rev. Mod. Phys. **4**, 87.

Fermi, E., 1950, Nuclear Physics (University of Chicago, Chicago) pp. 136, 148.

Fermi, E., 1960, Notes on Quantum Mechanics. A Course Given at the University of Chicago in 1954, edited by E Segré (University of Chicago, Chicago) Lec. 23.

Feynman, R.P., F.L. Vernon, Jr. and R.W. Hellwarth, 1957, *Geometrical Representation of the Schrödinger Equation for Solving Maser Problems,* J. Appl. Phys. **28**, 49.

Field, J.E., K.H. Hahn and S.E. Harris, 1991, *Observation of electromagnetically induced transparency in collisionally broadened lead vapor,* Phys. Rev. Lett. **67**, 3062.

Fleming, G.N., 1973, *A unitary Bound on the Evolution of Nonstationary States,* Nuovo Cim. **A16**, 232.

Flores, J.C., 1999, *Diffusion in disordered systems under iterative measurement,* Phys. Rev. **B60**, 30.

Fock, V., and N. Krylov, 1947, J. Phys. **11**, 112.

Fonda, L., G.C. Ghirardi and A. Rimini, 1978, *Decay theory of unstable quantum systems,* Rep. Prog. Phys. **41**, 587.

Fonda, L., G.C. Ghirardi, A. Rimini and T. Weber, 1973, *On the Quantum Foundations of the Exponential Decay Law,* Nuovo Cim. **A15**, 689.

Fonda, L., G.C. Ghirardi, A. Rimini and T. Weber, 1973, *On the Quantum Foundations of the Exponential Decay Law,* Nuovo Cim. **A18**, 805.

Frasca, M., 1997, *Quantum kicked dynamics and classical diffusion,* Phys. Lett. **A231**, 344.

Frerichs, V., and A. Schenzle, 1992, in: Foundations of Quantum Mechanics, eds T.D. Black, M.M. Nieto, H.S. Pilloff, M.O. Scully and R.M. Sinclair (World Scientific, Singapore).

Gamow, G., 1928, *Zur Quantentheorie des Atomkernes,* Z. Phys. **51**, 204.

Gardiner, C.W., 1990, Handbook of Stochastic Methods (Springer-Verlag, Berlin).

Gardiner, S.A., J.I. Cirac and P. Zoller, 1997, *Quantum Chaos in an Ion Trap: The Delta-Kicked Harmonic Oscillator,* Phys. Rev. Lett. **79**, 4790 (1997) [Erratum: *ibid.* **80**, 2968 (1998)].

Gaveau, B., and L.S. Schulman, 1995, *Limited quantum decay,* Journ. of Phys. **A28**, 7359.

Gea-Banacloche, J., N. Lu, L.M. Pedrotti, S. Prasad, M.O. Scully, and K. Wodkiewicz, 1990, *Treatment of the spectrum of squeezing based on the modes of the universe. II. Applications,* Phys. Rev. **A41**, 381.

Ghirardi, G.C., C. Omero, T. Weber and A. Rimini, 1979, *Small-Time Behavior of Quantum Nondecay Probability and Zeno's Paradox in Quantum Mechanics,* Nuovo Cim. **A52**, 421.

Goldberger, M.L., and K.M. Watson, 1964, Collision Theory (John Wiley, New York).

Gradshteyn, I.S., and I.M. Ryzhik, 1994, Table of Integrals, Series, and Products (Academic Press, San Diego).

Haake, F., 1991, Quantum Signatures of Chaos (Springer-Verlag, Berlin).

Hamilton Jr., J.F., and L.S. Schulman, 1971, *Path Integrals and Product Integrals,* J. Math. Phys. **12**, 160.

Harris, S.E., J.E. Field and A. Imamoğlu, 1990, *Nonlinear optical processes using electromagnetically induced transparency,* Phys. Rev. Lett. **64**, 1107.

Heil, W., K. Andersen, D. Hofmann, H. Humblot, J. Kulda, E. Lelievre-Berna, O. Schärpf and F. Tasset, 1998, ^{3}*He neutron spin filter at ILL,* Physica **B56**, 241.

Heitler, W., 1936, Proc. Cambridge Phil. Soc. **32**, 112.

Hellund, E.J., 1953, *The Decay of Resonance Radiation by Spontaneous Emission,* Phys. Rev. **89**, 919.

Hillery, M., 1981, *Fermi's golden rule and exponential decay in two-level systems,* Phys. Rev. **A24**, 933.

Home, D., and M.A.B. Whitaker, 1992, *A critical re-examination of the quantum Zeno paradox,* J. Phys. **A25**, 657.

Home, D., and M.A.B. Whitaker, 1993, *A unified framework for quantum Zeno processes,* Phys. Lett. **A173**, 327.

Home, D., and M.A.B. Whitaker, 1997, *A Conceptual Analysis of Quantum Zeno; Paradox, Measurement, and Experiment,* Ann. Phys. **258**, 237.

Hong, C.K., and L. Mandel, 1985, *Theory of parametric frequency down conversion of light,* Phys. Rev. A **31**, 2409.

Horwitz, L.P., 1995, *The Unstable System in Relativistic Quantum Mechanics,* Found. Phys. **25**, 39.

Hradil, Z., H. Nakazato, M. Namiki, S. Pascazio and H. Rauch, 1998, *Infinitely frequent measurements and quantum Zeno effect,* Phys. Lett. **A239**, 333.

Huang, H., S.-Y. Zhu, M.S. Zubairy and M.O. Scully, 1996, *Two-time intensity correlation in a driven three-level system,* Phys. Rev. **A53**, 1834.

Inagaki, S., M. Namiki and T. Tajiri, 1992, *Possible observation of the quantum Zeno effect by means of neutron spin-flipping,* Phys. Lett. **A166**, 5.

Itano, W.H., D.J. Heinzen, J.J. Bollinger and D.J. Wineland, 1990, *Quantum Zeno effect,* Phys. Rev. **A41**, 2295.

Itano, W.H., D.J. Heinzen, J.J. Bollinger and D.J. Wineland, 1991, *Reply to "Comment on 'Quantum Zeno effect"',* Phys. Rev. **A43**, 5168.

Izrailev, F.M., 1990, *Simple models of quantum chaos: spectrum and eigenfunctions,* Phys. Rep. **196**, 299.

Joichi, I., Sh. Matsumoto and M. Yoshimura, 1998, *Time evolution of unstable particle decay seen with finite resolution,* Phys. Rev. **D58**, 045004.

Kapitza, P.L., 1965, Collected papers, ed. by Ter Haar (Pergamon Press, London).

Kato, T., 1949, Progress of Theoretical Physics **4**, 154.

Khalfin, L.A., 1957, Dokl. Acad. Nauk USSR **115**, 277 [Sov. Phys. Dokl. **2**, 340 (1957)];

Khalfin, L.A., 1958, Zh. Eksp. Teor. Fiz. **33**, 1371 [Sov. Phys. JET **6**, 1053 (1958)].

Khalfin, L.A., 1968, Zh. Eksp. Teor. Fiz. Pis. Red. **8**, 106 [JETP Letters **8**, 65 (1968)].

Kaulakys, B., and V. Gontis, 1997, *Quantum anti-Zeno effect,* Phys. Rev. **A56**, 1131.

Knight, P.L., and M.A. Lauder, *Laser-induced continuum structure,* 1990, Phys. Rep. **190**, 1.

Knight, P.L., and P.W. Milonni, 1976, *Long-time deviations from exponential decay in atomic spontaneous emission theory,* Phys. Lett. **56A**, 275.

Kofman, A.G., and G. Kurizki, 1996, *Quantum Zeno effect on atomic excitation decay in resonators,* Phys. Rev. **A54**, R3750.

Kofman, A.G., and G. Kurizki, 1999, *Decay control in dissipative quantum systems,* Acta Physica Slovaca **49**, 541.

Kofman, A.G., and G. Kurizki, 2000, *Acceleration of quantum decay processes by frequent observations,* Nature **405**, 546.

Kraus, K., 1981, *Measuring Processes in Quantum Mechanics. Continuous Observation and the Watchdog Effect,* Found. Phys. **11**, 547.

Kuratsuji, H., 1988, *Geometric Canonical Phase factors and Path Integrals,* Phys. Rev. Lett. **61**, 1687.

Kwiat, P., H. Weinfurter, T. Herzog, A. Zeilinger and M. Kasevich, 1995, *Interaction-free measurement,* Phys. Rev. Lett. **74**, 4763.

Lang, R., M.O. Scully, and W.E. Lamb, Jr., 1973, *Why is the Laser Line so Narrow? A Theory of Single-Quasimode Laser Operation,* Phys Rev. **A7**, 1788.

Lee, T.D., 1954, *Some Special Examples in Renormalizable Field Theory,* Phys Rev. **95**, 1329.

Ley, M., and R. Loudon, 1987, *Quantum theory of high-resolution length measurement with a Fabry-Perot interferometer,* J. Mod. Opt. **34**, 227.

Lichtenberg, A.J., and M.A. Lieberman, 1992, Regular and Chaotic Dynamics (Springer-Verlag, New York).

Loudon, R., 1984, The quantum theory of light (Oxford University Press, New York).

Luis, A., and J. Peřina, 1996, *Zeno Effect in Parametric Down-Conversion,* Phys. Rev. Lett. **76**, 4340.

Luis, A., and L.L. Sánchez–Soto, 1998, *Anti-Zeno effect in parametric down-conversion,* Phys. Rev. **A57**, 781.

Machida, K., H. Nakazato, S. Pascazio, H. Rauch and S. Yu, 1999, *Reflection and transmission in a neutron-spin test of the quantum Zeno effect,* Phys. Rev. **A60**, 3448.

Maiani, L., and M. Testa, 1998, *Unstable Systems in Relativistic Quantum Field Theory,* Ann. Phys. (NY) **263**, 353.

Mandel, L., and E. Wolf, 1995, Optical coherence and quantum optics (Cambridge University Press, Cambridge).

Mandelstam, L., and I. Tamm, 1945, J. Phys. **9**, 249.

Merzbacher, E., 1961, Quantum mechanics (John Wiley and Sons, New York).

Messiah, A., 1961, Quantum mechanics (Interscience, New York).

Mihokova, E., S. Pascazio and L.S. Schulman, 1997, *Hindered decay: Quantum zeno effect through electromagnetic field domination,* Phys. Rev. **A56**, 25.

Milburn, G.J., A.S. Lane and D.F. Walls, 1983, *Quantum nondemolition measurements on coupled harmonic oscillators,* Phys. Rev. **A27**, 2804.

Misra, B., and E.C.G. Sudarshan, 1977, *The Zeno's paradox in quantum theory,* J. Math. Phys. **18**, 756.

Mollow, B.R., 1975, *Pure-state analysis of resonant light-scattering: Radiative damping, saturation, and multiphoton effects,* Phys. Rev. **A12**, 1919.

Moses, H.E., 1972, *Exact Electromagnetic Matrix elements and Exact Selection Rules for Hydrogenic Atoms,* Lett. Nuovo Cimento **4**, 51.

Moses, H.E., 1972, *The Ultraviolet Convergence of the Electromagnetic Correction to the Ground-State Energy of Hydrogen,* Lett. Nuovo Cimento **4**, 54.

Moses, H.E., 1973, *Photon Wave Functions and the Exact Electromagnetic Matrix Elements for Hydrogenic Atoms,* Phys. Rev. **A8**, 1710.

Mukunda, N., and R. Simon, 1993, *Quantum Kinematic Approach to the Geometric Phase,* Ann. Phys. (N.Y.) **228**, 205.

Nakazato, H., M. Namiki and S. Pascazio, 1996, *Temporal behavior of quantum mechanical systems,* Int. J. Mod. Phys. **B10**, 247.

Nakazato, H., M. Namiki, S. Pascazio and H. Rauch, 1995, *On the quantum Zeno effect,* Phys. Lett. **A199**, 27.

Nakazato, H., M. Namiki, S. Pascazio and H. Rauch, 1996, *Understanding the quantum Zeno effect,* Phys. Lett. **A217**, 203.

Nakazato, H., and S. Pascazio, 1995, *On the short-time behavior of quantum mechanical systems,* Mod. Phys. Lett. **A10**, 3103.

Namiki, M., and N. Mugibayashi, 1953, Prog. Theor. Phys. **10**, 474.

Namiki, M., S. Pascazio and H. Nakazato, 1997, Decoherence and Quantum Measurements (World Scientific, Singapore).

Norman, E.B., S.B. Gazes, S.G. Crane and D.A. Bennett, 1966, *Tests of the Exponential Decay Law at Short and Long Times,* Phys. Rev. Lett. **60**, 2246.

Paley, R.E.A.C., and N. Wiener, 1934, Fourier Transforms in the Complex Domain (American Mathematical Society Colloquium Publications Vol. XIX, New York).

Pancharatnam, S., 1956, Proc. Indian Acad. Sci. **A44**, 247, reprinted in: Collected Works of S. Pancharatnam (Oxford University Press, London, 1975).

Pascazio, S., 1996, *Quantum Zeno effect and inverse Zeno effect,* in: Quantum Interferometry, eds F. De Martini, G. Denardo and Y. Shih (VCH, Weinheim) p. 525.

Pascazio, S., 1997, *Dynamical Origin of the Quantum Zeno Effect,* Found. Phys. **27**, 1655.

Pascazio, S., and P. Facchi, 1998, *Duration of the quantum "Zeno" region for an excited state of the hydrogen atom,* in: Proceedings of the 5th Wigner Symposium, edited by P. Kasperkovitz and D. Grau (World Scientific, Singapore), p. 512.

Pascazio, S., and P. Facchi, 1999, *Modifying the lifetime of an unstable system by an intense electromagnetic field,* Acta Phys. Slov. **49**, 557.

Pascazio, S., and M. Namiki, 1994, *Dynamical quantum Zeno effect,* Phys. Rev. **A50**, 4582.

Pascazio, S., M. Namiki, G. Badurek and H. Rauch, 1993, *Quantum Zeno effect with neutron spin,* Phys. Lett. **A179**, 155.

Passel, L., and R.I. Schermer, 1966, *Measurement of the Spin Dependence of the $He^3(n,p)T$ Reaction and of the Nuclear Susceptibility of Adsorbed He^3,* Phys. Rev. **150**, 146.

Pati, A., 1996, *Limit on the frequency of measurements in the quantum Zeno effect,* Phys. Lett. **A215**, 7.

Pauli, W., 1928, Festschrift zum 60. Geburtstage A. Sommerfelds, (Hirzel, Leipzig).

Peierls, R., 1991, More Surprises in Theoretical Physics (Princeton University Press, Princeton).

Peres, A., 1980, *Zeno paradox in quantum theory,* Am. J. Phys. **48**, 931.

Peres, A., 1980, *Nonexponential Decay Law,* Ann. Phys. **129**, 33.

Peres, A., and A. Ron, 1990, *Incomplete "collapse" and partial quantum Zeno effect,* Phys. Rev. **A42**, 5720.

Petrosky, T., S. Tasaki and I. Prigogine, 1990, *Quantum Zeno effect,* Phys. Lett. **A151**, 109.

Petrosky, T., S. Tasaki and I. Prigogine, 1991, *Quantum Zeno effect,* Physica **A170**, 306.

Plenio, M.B., P.L. Knight and R.C. Thompson, 1996, *Inhibition of spontaneous decay by continuous measurements. Proposal for realizable experiment,* Opt. Comm. **123**, 278.

Prigogine, I., 1980, From being to becoming (Freeman, New York).

Rabi, I.I., N.F. Ramsey and J. Schwinger, 1954, *Use of Rotating Coordinates in Magnetic Resonance Problems,* Rev. Mod. Phys. **26**, 167.

Radmore, P.M., and P.L. Knight, 1982, *Population trapping and dispersion in a three-level system,* J. Phys. **B15**, 561.

Řeháček, J., J. Peřina, P. Facchi, S. Pascazio, and L. Mišta, 2000, *Quantum Zeno effect in a probed down-conversion process,* Phys. Rev. **A62**, 013804.

Sakurai, J.J., 1994, Modern quantum mechanics (Addison-Wesley, Reading, Massachusetts).

Saleh, B.E.A., and M.C. Teich, 1991, Fundamentals of Photonics (J. Wiley, New–York).

Samuel, J., and R. Bhandari, 1988, *General setting for Berry's phase,* Phys. Rev. Lett. **60**, 2339.

Schulman, L.S., 1981, Techniques and Applications of Path Integration (Wiley, New York).

Schulman, L.S., 1997, *Observational line broadening and the duration of a quantum jump,* J. Phys. **A30**, L293.

Schulman, L.S., 1998, *Continuous and pulsed observations in the quantum Zeno effect,* Phys. Rev. **A57**, 1509.

Schulman, L.S., A. Ranfagni and D. Mugnai, 1994, *Characteristic Scales for Dominated Time Evolution,* Phys. Scr. **49**, 536.

Schwinger, J., 1960, *Field Theory of Unstable Particles,* Annals of Physics **9**, 169.

Seke, J., 1992, *Finite-time deviations from exponential decay for the Lyman-α radiation in the Dirac hydrogen atom without ignoring virtual transitions,* Phys. Rev. **A45**, 542.

Seke, J., 1994, *Analytic evaluation of exact transition matrix elements in nonrelativistic hydrogenic atoms,* Physica **A203**, 269.

Seke, J., 1994, *Calculation of the discrete-spectrum Lamb-shift contribution in atomic hydrogen,* Physica **A203**, 284.

Seke, J., and W. Herfort, 1989, *Finite-time deviations from exponential decay in the case of spontaneous emission from a two-level hydrogenic atom,* Phys. Rev. **A40**, 1926.

Shapere, A., and F. Wilczek, 1989, Geometric Phases in Physics (World Scientific, Singapore).

Stephenson, A., 1908, Philos. Mag. **15**, 233.

Stich, M.L., and M. Bass, 1985, Laser Handbook (North–Holland, Amsterdam).

Tabor, M., 1989 Chaos and Integrability in Nonlinear Dynamics (Wiley, New York).

Tamm, I., 1945, J. Phys. (USSR) **9**, 449.

Tewari, S.P., and G.S.Agarwal, 1986, *Control of Phase Matching and Nonlinear Generation in Dense Media by Resonant Fields,* Phys. Rev. Lett. **56**, 1811.

Thun, K., and J. Peřina, 1998, *Zeno effect in optical parametric process with quantum pumping,* Phys. Lett. A **249**, 363.

Townes, C.H., and A.L. Schawlow, 1975, Microwave Spectroscopy (Dover, New York).

Van Hove, L., 1955, *Quantum-mechanical perturbations giving rise to a statistical transport equation,* Physica **21**, 517.

van Kampen, N.G., 1992, Stochastic Processes in Physics and Chemistry (North-Holland, Amsterdam).

Venugopalan, A., and R. Ghosh, 1995, *Decoherence and the quantum Zeno effect,* Phys. Lett. **A204**, 11.

von Neumann, J., 1932, Die Mathematische Grundlagen der Quantenmechanik (Springer, Berlin). [English translation by E. T. Beyer: Mathematical Foundation of Quantum

Mechanics (Princeton University Press, Princeton, 1955)]. For the QZE, see in particular p. 195 of the German edition (p. 366 of the English translation).

Yariv and Yeh, 1984, Optical Waves in Crystals (J. Wiley, New York);

Yoo, H.-I., and J.H. Eberly, 1985, *Dynamical theory of an atom with two or three levels interacting with quantized cavity fields,* Phys. Rep. **118**, 239.

Wagh, A.G., V.C. Rakhecha, P. Fischer and A. Ioffe, 1998, *Neutron Interferometric Observation of Noncyclic Phase,* Phys. Rev. Lett. **81**, 1992.

Wagh, A.G., V.C. Rakhecha, J. Summhammer, G. Badurek, H. Weinfurter, B.E. Allman, H. Kaiser, K. Hamacher, D.L. Jacobson and S.A. Werner, 1997, *Experimental Separation of Geometric and Dynamical Phases Using Neutron Interferometry,* Phys. Rev. Lett. **78**, 755.

Weinberg, S., 1996, The quantum theory of fields (Cambridge University Press, Cambridge).

Weisskopf, V., and E.P. Wigner, 1930, Z. Phys. **63**, 54.

Weisskopf, V., and E.P. Wigner, 1930, Z. Phys. **65**, 18.

Whitaker, M.A.B., 2000, *Theory and experiment in the foundations of quantum theory,* Progress in Quantum Electronics **24**, 1.

Wigner, E.P., 1963, *The Problem of Measurement,* Am. J. Phys. **31**, 6.

Wilkinson, S.R., C.F. Bharucha, M.C. Fischer, K.W. Madison, P.R. Morrow, Q. Niu, B. Sundaram and M.G. Raizen, 1997, *Experimental evidence for non-exponential decay in quantum tunnelling,* Nature **387**, 575.

Zhu, S.-Y., L.M. Narducci and M.O. Scully, 1995, *Quantum-mechanical interference effects in the spontaneous-emission spectrum of a driven atom,* Phys. Rev. **A52**, 4791.

Zhu, S.-Y., and M.O. Scully, 1996, *Spectral Line Elimination and Spontaneous Emission Cancellation via Quantum Interference,* Phys. Rev. Lett. **76**, 388.

Acknowledgments

I would like to express my gratitude to S. Pascazio, who had been supervising carefully and patiently my work. He is both a friend and a teacher to me. My debt to him is enormous; above all from him I learned the "method".

It is also a pleasure to thank all of them I was lucky enough to collaborate with during my doctoral years. I would like to mention in particular A. G. Klein, A. Mariano, H. Nakazato, J. Peřina, J. Řeháček, A. Scardicchio and L. S. Schulman. I owe them much of my own comprehension of the diverse phenomena discussed in this thesis.